EXPERIMENTAL INVESTIGATION OF THE EFFECT OF BROKEN ORE PROPERTIES ON SECONDARY FRAGMENTATION DURING BLOCK CAVING

by

Leonardo Dorador

M.Sc, University of Chile, Chile, 2010

A THESIS SUBMITTED IN PARTIAL FULFILLMENT OF

THE REQUIREMENTS FOR THE DEGREE OF

DOCTOR OF PHILOSOPHY

in

The Faculty of Graduate and Postdoctoral Studies

(Geological Engineering)

THE UNIVERSITY OF BRITISH COLUMBIA

(Vancouver)

October, 2016

Abstract

Block cave mining is experiencing a global growth in importance as new large, lower grade and deeper ore bodies favouring underground mass mining methods are developed. With block caving, the rock mass fragmentation process is decisive in the design and success of the operation. The last stage of this fragmentation process known as secondary fragmentation, plays a major role in the design and success of a caving operation. Despite this, it is the least understood fragmentation stage due in part to the complex mechanisms and the numerous variables involved in this phenomenon.

The broken ore density (BOD) and the inter-block friction angle (ϕ') are comprehensively investigated here. A conceptual framework describing the BOD distribution and a procedure to evaluate this parameter under both an isolated movement zone and interactive flow are proposed, and an approach to evaluate ϕ' under different broken ore properties and draw column conditions is developed to be applied to early stage feasibility studies and design.

A comprehensive laboratory testing program was carried out using concrete cuboids, controlling their size, shape and compressive strength. These are used as a proxy for broken ore fragments. These results were used to develop empirical design charts for assessing secondary fragmentation and hang-ups potential.

Several factors influencing the secondary fragmentation for feasibility and advanced engineering assessments have been investigated including: air gap thickness, BOD, segregation of large blocks due to draw column surface topology, broken ore strength

heterogeneity, block strength damage and crushing under high confining stresses, water within draw columns, and cushioning by fines. This new knowledge will contribute to more accurate secondary fragmentation predictions at the drawpoints.

Finally, a new empirical approach to predict secondary fragmentation and drawpoint block size distribution (BSD) directed at early-stage conceptual and feasibility engineering design studies is developed. This methodology, built with relevant data from related fields and supplemented by generated data, was tested against field data from the El Teniente mine, Chile, confirming satisfactory predictions for stronger rocks and mixtures of strong and weak broken ore materials. The results were not as reliable for predicting drawpoint BSD for weak rocks.

Preface

Chapter 2 "Broken Ore Density Distribution within a Draw Column during Block Caving" was co-authored by Leonardo Dorador, Dr. Erik Eberhardt and Dr. Davide Elmo. As the lead author, Leonardo Dorador conducted the data analysis, based on information available in the public domain, and prepared the manuscript. Dr. Eberhardt provided guidance and reviewed the manuscript. Dr. Elmo reviewed the manuscript.

Chapter 3 "Inter-block Friction Angle of Broken Ore Applied to Gravitational Flow in Block Caving" was co-authored by Leonardo Dorador, Dr. Davide Elmo and Dr. Erik Eberhardt. As the lead author, Leonardo Dorador conducted the data analysis, based on information available in the public domain, and prepared the manuscript. Dr. Elmo and Dr. Eberhardt provided guidance and reviewed the manuscript.

Chapter 4 "Experimental Investigation of Secondary Fragmentation and Hang-Up Potential in the Compression Zone of a Draw Column during Block Cave Mining" was co-authored by Leonardo Dorador, Dr. Erik Eberhardt and Dr. Davide Elmo. As the lead author, Leonardo Dorador conducted the laboratory testing program, carried out the data analysis, and prepared the manuscript. Dr. Eberhardt provided guidance in the development of the manuscript and reviewed the manuscript. Dr. Elmo reviewed the manuscript.

Chapter 5 "Factors Affecting Secondary Fragmentation during Block Caving" was co-authored by Leonardo Dorador, Dr. Davide Elmo and Dr. Erik Eberhardt. As the lead author, Leonardo Dorador conducted the laboratory testing program, employing these results as well as information available in thepublic domain for data analysis, and prepared the manuscript. Dr. Elmo and Dr. Eberhardt provided guidance and reviewed the manuscript.

Chapter 6 “Evolution of Broken Ore Size Distribution in a Draw Column during Block Cave Mining” was co-authored by Leonardo Dorador, Dr. Erik Eberhardt and Dr. Davide Elmo. As the lead author, Leonardo Dorador generated a methodology to evaluate secondary fragmentation on block caving, validated on data from El Teniente Mine, and prepared the manuscript. Dr. Eberhardt provided guidance in the development of the manuscript and reviewed the manuscript. Dr. Elmo reviewed the manuscript.

Table of Contents

List of Tables

List of Figures

Acknowledgements

I owe my deepest gratitude to my advisor Dr. Erik Eberhardt for his invaluable encourage, guidance and support throughout my PhD study. My sincere thanks also goes to my co-advisor Dr. Davide Elmo for his great support on this research. I also thank Dr. Oldrich Hungr, Dr. Bern Klein and Dr. Greg Smith for their valuable feedback, and Dr. Dharma Wijewickreme for providing me laboratory facilities.

I am deeply grateful to my wife Pamela, my parents Wilfredo and Milena, my brothers and sister Ivan, Claudio and Cristina, my parents-in-law Anamaria and Gregorio, my sister-in-law Carolina and my entire family for their invaluable support during my doctoral study.

I am indebted to Augusto Aguayo (Codelco - PMCHS) for his support on this research. I also thank to F. Ramirez, D. Villegas, D. Harrison, N. Montecinos, D. Antillo, and S. Valencia. In addition, I am grateful to: V. Encina, A. Russo, M. Didyk, A. Brzovic, E. Arancibia and R. Vergara for their valuable feedback related to block caving. I thank to Chris Harrod for his great help and friends: Masoud, Geidy, Karen, Karem, Kathy, Cristian, Maria.

Sincere thanks also go to Golder Associates for their support on this PhD. Deepest gratitude to Terry Eldridge and Richard Beddoes. I also thank: M. Monroy, R. Hammett, S. Rogers, A. Haynes, J. Cunning, B. Wickland, H. Puebla, B. Weeks, K. Moena, C. Fossey, G. Pizarro, M. Sanin, J. Steele and colleagues at the Burnaby laboratory.

Finally, this PhD would not have been possible without the funding by Codelco (PMCHS) and the Natural Sciences and Engineering Research Council of Canada (NSERC).

Dedication

Wilfredo and Milena: Thank you for teaching me the value of life

Pamela: Thank you for all your love

Chapter 1: Introduction

1.1 Problem Statement

As the rate of discovering new near-surface deposits declines, large copper producers like Codelco, Rio Tinto, and Freeport-McMoRan have begun to transition their large open pits to underground block caving operations to extend mine life and continue mining deeper resources. The block caving method has several advantages over others mining methods, including: high production, reduced production costs, and high productivity; furthermore, the process can be automatized (Brown 2007). This method can be used preferentially in kimberlite pipes, porphyry copper, and other large, massive deposits with low grades involving rock masses weak enough to start caving but strong enough maintain production rates (Laubscher 1994).

Despite the potential benefits associated with this mining method, the use of block caving at increasing depths and scales has introduced a number of serious technological and environmental challenges (Rashidi-Nejad et al. 2014, Eberhardt et al. 2015). This has led to several international research programs as well as symposiums and conferences focussed on improving block caving practices. These include: International Caving Study I and II (1997-2000; 2000-2004), Mass Mining Technology MMT I, II and III (2006-2010; 2009-2012; 2012-2016), MassMin conference (1992, 2000, 2004, 2008, 2012), International Symposium on Block and Sublevel Caving (2007, 2010, 2014), and International Conference on Deep and High Stress Mining 2006, 2010) among others. Despite the significant advances in block caving practices, improvements in knowledge regarding *fragmentation* and *gravitational flow* are still required (Chitombo 2010).

As noted by Moss (2011), *fragmentation is the key*, while Brown (2007) added that fragmentation controls layout design. *Block caving fragmentation* takes place when the rock mass fractures and breaks into smaller fragments after it has been undercut and allowed to collapse (Fig. 1.1). This primary fragmentation further reduces block size through secondary fragmentation within the draw column (Laubscher 1994, Eadie 2003).

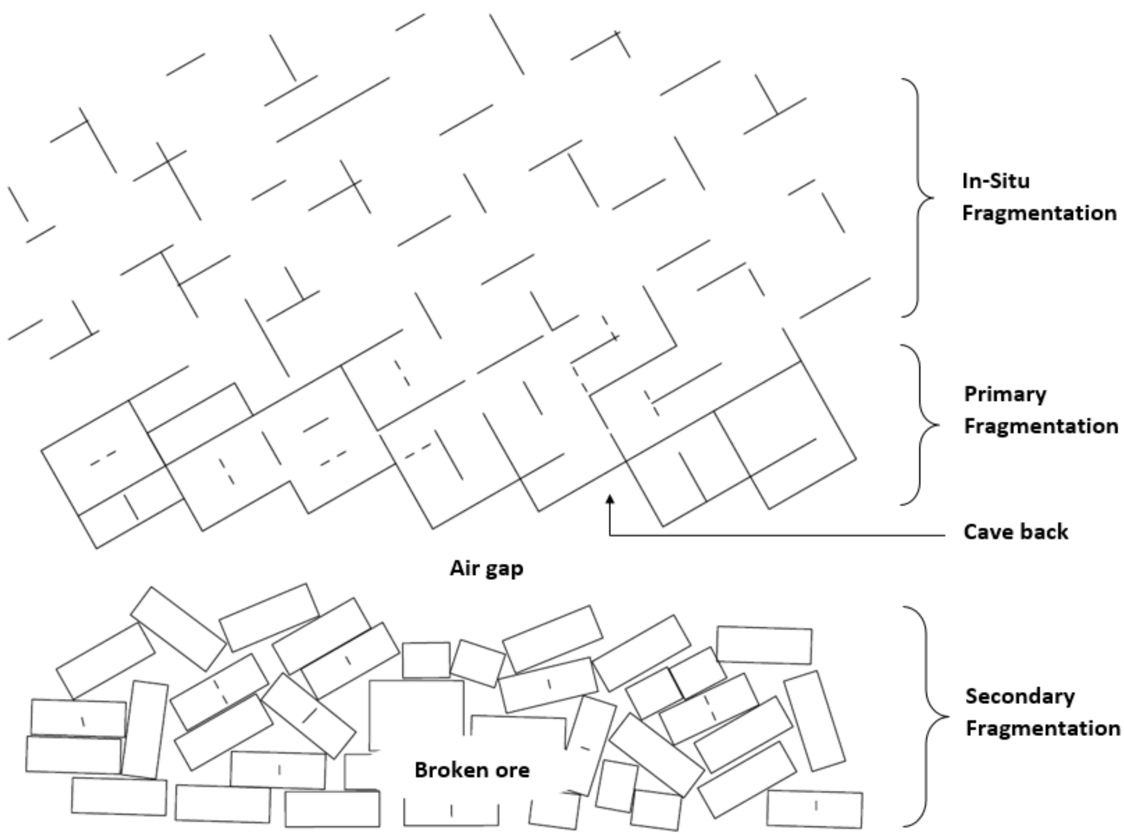

Fig. 1.1: Diagram depicting the fragmentation stages in block caving.

Thus, the fragmentation phenomenon represents a critical component of the caving process, as it shapes the block size distribution (BSD) at the drawpoints. If the fragmentation is oversized, large blocks will severely impact operations by impeding material handling and causing costly delays to clear hang-ups at the draw points. If fragmentation is too fine, narrower draw columns might develop, limiting an interactive broken ore flow between columns (Laubscher 2003).

Regarding production losses due to hang-ups, Dessureault et al. (2000) show a notable difference between the design draw rate and the historical operational draw rate (0.60 and 0.42 t/m2/day, respectively) at El Teniente mine (Chile), due to significant hang-ups and blockage from oversize fragmentation. In addition, van Hout et al. (2004) noted that in any given shift, 34 percent of the available drawpoints were hung up and these were cleared within one day on average. The most exemplary case study of production losses is Palabora mine (South Africa) as no cave operation has undertaken the amount of secondary breaking that has been required at this mine, where some 50% of the initial tonnage has had to be blasted to clear drawpoint hang-ups and blockages (Glazer & Townsend 2008). Note that secondary breaking to clear hang-ups could increase the operational-related cost up to 20%, without considering capital-related costs (Isabel 2016).

As a result, the projected BSD plays an important role in cave mining layout design, planning, production scheduling, and mineral processing (i.e., further comminution). However, secondary fragmentation is poorly understood (Brown 2007), due in part to the numerous variables and complex mechanisms involved. The first complexity associated with the secondary fragmentation process is that broken ore (caved rock) within a draw column inherits and is influenced by key *rock mechanics characteristics* such as the network of natural discontinuities and veins present in the rock. At the same time, however, it behaves as a granular material, resulting in the broken ore material displaying unique geotechnical properties that must be considered in secondary fragmentation analysis. The second (and most relevant) complexity issues is that most of the variables and factors influencing secondary fragmentation are not independent. Rather, they co-vary making it hard to isolate and quantify their particular role in the secondary fragmentation process.

There is therefore a pressing need for comprehensive studies investigating secondary fragmentation to help mining companies properly assess the feasibility of a potential project, as well as to help designers develop a detailed understanding of block caving fragmentation and to assist managers in assessing and managing the risk of poor fragmentation.

1.2 Terminology

A typical block caving layout involves a series of terms and definitions that will be used frequently throughout this thesis. Fig. 1.1 to Fig. 1.3 are included to complement this terminology. In the block caving method, the production and undercut layout are main areas developed through underground excavation, typically using drill and blast techniques. The *production layout* includes all tunnels, adits and raises required for material handling and ore transport from the drawpoints where the ore is mined to its exit out of the mine. The *undercut layout* is positioned above the production level and serves to undermine the orebody to initiate and facilitate the rock fragmentation (Fig. 1.3). After the initiation of the fragmentation process, the *broken ore* (also referred to as *caved rock* or *muck*) moves downward due to gravity action through a *draw column* (ore column) until it reaches a *drawbell*. The drawbell then feeds to the *drawpoints* on the extraction level where it mined. Regarding drawpoints arrays (Fig. 1.2), two of these commonly share a drawbell. Drawpoint are separated by pillars to maintain stability. The broken ore is mined and handled by means of LHDs (Load-Haul-Dump) and then transported to primary crushers located inside the production layout. After this, the ore is conveyed out of the mine to be processed.

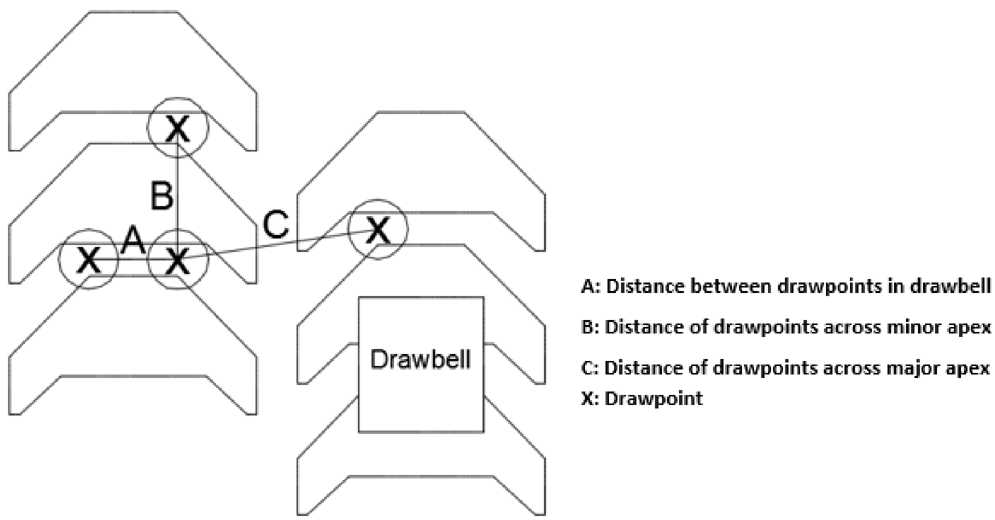

Fig. 1.2: Typical production layout (*herringbone layout)*. Plan view. Adapted from Laubscher (2003)

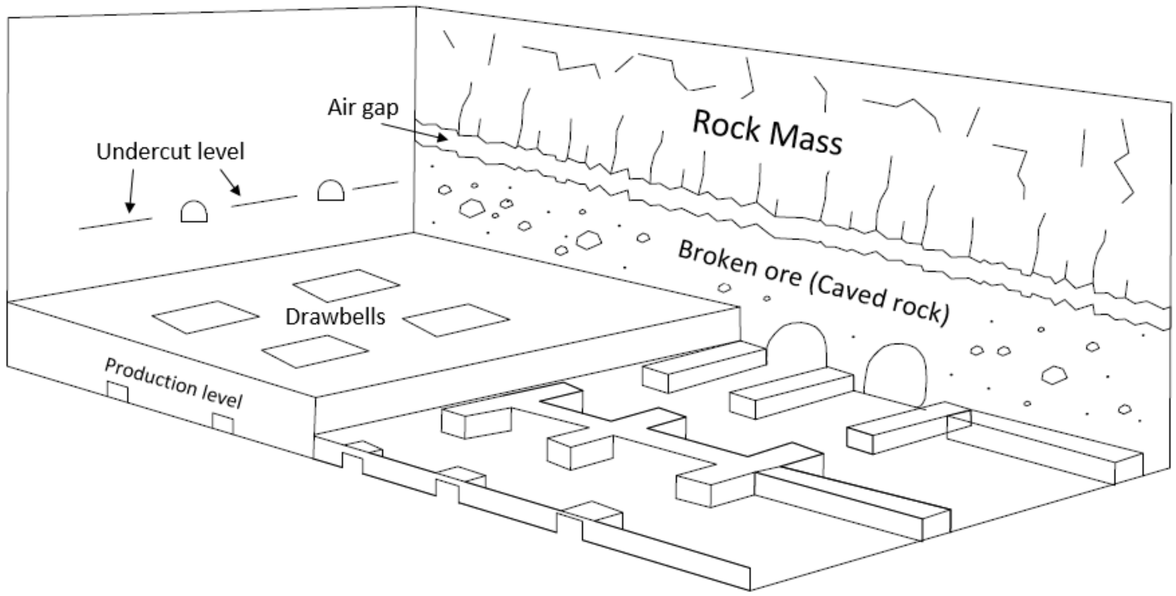

Fig. 1.3: Block cave mining layout. Modified from Hamrin (2001)

1.3 Broken Ore Size Distribution as a Key Factor in Mine Planning Design

In practice, the Broken Size Distribution (BSD) of the ore at the drawpoints is a critical input in block caving design, especially in terms of production efficiency and mine safety (Laubscher 1994, Brown 2007). In practice, *field measurement procedures* at the drawpoints are carried out to corroborate fragmentation predictions from previous design stages. *Hangs-ups*, *drawpoint spacing*, *secondary blasting* and *height of the interaction zone* (HIZ) are key issues in caving design that are dependent on the BSD. Several different methodologies have been employed to measure BSD at the drawpoints (Moss et al. 2004).

Hang-ups in a drawbell correspond to large blocks which impede the flow of ore at the drawpoints. The expected frequency of hang-ups is assessed in practice using empirical methods such as the BCF approach (section 1.4), together with field studies. However, several operating mines have encountered hang-up frequencies at a higher rate than expected, which has affected productivity and profitability (e.g., Palabora, DOZ/ESZ). Hang-ups are commonly solved by secondary blasting or use of high pressure water jets at the drawpoints, with additional costs and loss of production. Furthermore, as a drawpoint must remain closed until the hang-up is freed, the resulting deviation from the mine plan and the associated need to draw more heavily from other drawpoints, can lead to asymmetric draw, asymmetric caving, sterilization of ore, and/or increased dilution, which not only affects draw control but also secondary fragmentation (Chapter 5).

The *drawpoint dimensions and spacing design* depends directly on the final BSD at the production level and thus, the accurate assessment of secondary fragmentation is a key component of drawpoint design. On the one hand, drawpoint size is usually defined as three to six times that of the largest fragment size (Otuonye 2000). Conversely, several authors have proposed alternative approaches to define the drawpoint spacing, including Kvapil (1965), Laubscher (1994), Julin (1992), Hustrulid (2000), Verdugo & Ubilla (2004), Kvapil (2004), Susaeta et al. (2008), Van As & Van Hout (2008), and Castro et al. (2009). The question of optimal values for spacing are still contentious, with a need to balance fragmentation control and material handling with pillar widths required for long-term stability and safety of the drawpoints. The previous authors generally recommend that interactive flow will be achieved under a factor of 1.5 to 1.2 the width of the drawzone. The economic importance of defining an optimal factor (between 1.2 and 1.5) reflects the fact that a common block caving production level usually consists of hundreds of drawpoints, severely impacting the profitability of these projects.

The Height of Interaction Zone (HIZ) is defined as the elevation at which isolated movement zones (IMZs) merge together (Laubscher 1994). Accordingly, the higher the degree of secondary fragmentation, the more the HIZ is reduced. A predictive chart provided by Laubscher (1994) is commonly used to obtain an approximate estimation of the HIZ. The input is the Rock Mass Rating (RMR) and the minimum drawzone spacing across the major apex. The HIZ is directly related to the stress conditions present in the broken ore. In the case of interactive flow, the broken ore will experience anisotropic compression, which in turn will affect the secondary fragmentation (Fig. 1.4). Hence, the concept of far and near field zones (relative to the drawpoints) will be discussed and employed frequently throughout this thesis.

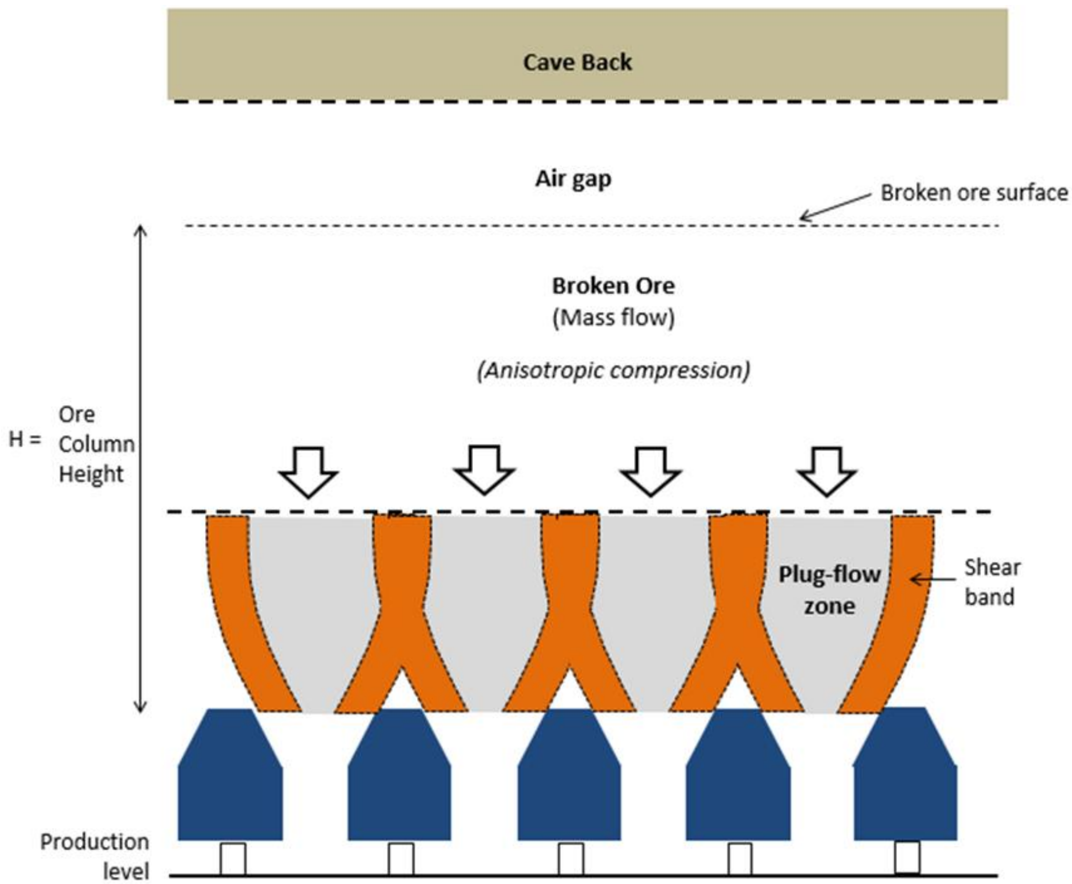

Fig. 1.4: Secondary fragmentation processes in terms of far and near field from drawpoints.

1.4 Fragmentation in Block Caving

For decades, the phenomenon of fragmentation in cave mining has been observed at the drawpoints as varying from large blocks with no fines in the short term (short draw column height), to well graded size distributions of blocks in the long term (taller draw column height). Laubscher (1994) and Eadie (2003) have defined the *fragmentation process* as involving three sequential components: *in situ*, primary, and secondary fragmentation.

In situ fragmentation corresponds to the natural blocks formed by the spacing, persistence and interconnectivity of the natural discontinuities present in the rock mass. After undercutting and during the caving process, the rock mass above the draw column and cave experiences changes in the orientation and magnitude of stresses, which result in the generation of new stress-induced fractures and further fragmentation of the *in situ blocks*. This fragmentation is referred to as *primary fragmentation*. Finally, these blocks are released from the cave back, falling onto and then moving down through the draw column as the broken rock (ore) is extracted from the drawpoints below. This vertical downward movement of the broken ore (or muckpile) results in further fragmentation through point load splitting, corner rounding, comminution and crushing of the blocks. This constitutes the *secondary fragmentation*. These processes result in a non-uniform block size distribution. In addition, another breakage mechanism occurs between the *primary and secondary fragmentation process*, which is linked to block fall impact when there is a sizeable air gap present between the cave back and the top of the draw column (see Fig. 1.1). This impact together with block segregation processes that occur across the draw column surface (Chapter 5) can notably modify the block size distribution after primary fragmentation, which likely leads to the establishment of a *transition stage* between primary and secondary fragmentation (Fig. 1.5).

With respect to the *in situ and primary fragmentation*, important advances and numerical codes have been published including *Joints* (Villaescusa 1991), *JkFrag* (Eadie 2003), *BCF* (Esterhuizen *2005*), and *FracMan* (Dershowitz et al. 1998) among others, most of which are used in practice by industry. In comparison, *secondary fragmentation* has received less intention, despite its critical importance.

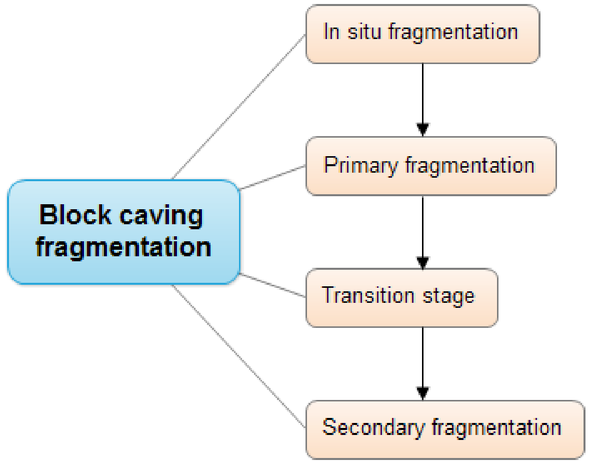

Fig. 1.5: Block caving fragmentation stages

A frequently used empirical approach is the Block Caving Fragmentation (BCF) method, which was developed by Esterhuizen (1994) and updated in 2005 to predict primary and secondary fragmentation (including hang-up frequency). Although this approach is able to quantify secondary fragmentation, it is not always seen as being dependable (Srikant *et al.* 2004, Butcher & Thin 2007). This has more recently let to new methodologies being proposed based on advanced numerical modeling approaches. Pierce (2009) proposed an attractive methodology to evaluate secondary fragmentation built on the discrete-element Particle Flow Code, termed Rebop (Cundall et al. 2000). Two alternative methodologies of note are those proposed by Kojovic (2010) and Rogers et al. (2010). While the former relies mostly on comminution rules, the latter is a DFN (Discrete Fracture Network) based approach. These methods each require further development and numerous variables to quantify secondary fragmentation and BSD at the drawpoints, and are described in detail in Chapter 6.

It is noted here that the effort required to carry out a detailed analysis using more advanced techniques (i.e., based on numerical methods) is such that they are most appropriate for caving projects that have been approved for detailed design and construction. However, the significant investments required and technical challenges involved, require projects to first be scrutinized to see if they are technically feasible and economically viable (feasibility and viability are interdependent). Optimally, the level of effort expended in conducting an assessment should be on par with the stage of approval a project has received, which will also dictate the quality and quantity of the site investigation data collected up to that point that would be available for conducting a secondary fragmentation and BSD analysis. This is a key consideration used for developing and defining the objectives derived for this thesis. As noted above, recent progress has seen the development of several rigorous BSD assessment techniques. Given the level of detailed data (and therefore costly investigation programs) required to properly carry out these analyses, it is suggested here that these are more appropriate for projects that have progressed to detailed engineering design. What is still lacking, however, are simpler techniques more fitting for pre-feasibility and feasibility level studies. Therefore, it is apparent that there is a need for new simpler and less data intensive methods to predict BSD at drawpoints to allow early level feasibility assessments of secondary fragmentation and BSD for decisions on the advancement of block cave projects.

1.5 Relevant Parameters affecting Secondary Fragmentation

Secondary fragmentation in block caving is affected both by broken ore properties as well as factors associated with caving operations. Table 1.1 summarizes the parameters and factors promoting secondary fragmentation as covered by this thesis. However, secondary fragmentation is a complex phenomenon which includes numerous parameters that directly and indirectly influence this fragmentation process as well as zones with distinguished stress states such as the *compression plug-flow zone* and the *outer shear band periphery* (Pierce's gravitational flow model, 2009). A conceptual diagram is presented in Fig. 1.6 which groups the most important parameters affecting the size distribution of broken ore following the primary fragmentation phase through to it reaching the drawpoints.

Table 1.1: Factors affecting secondary fragmentation

Individual blocks	**Draw column**	**Caving operation**	**Other elements**
Block strength (Chapter 4, 5 and 6)	Initial Size distribution of blocks. Primary fragmentation (Chapter 6)	Water within draw columns (Chapter 5)	Rock fall impact fragmentation (Chapter 5)
Size (Chapter 4 and 6)	Bulk density distribution within the ore column (swell or bulking factor) (Chapter 2)	Column height (Chapter 4 and 6)	Fine migration (Chapter 6)
Aspect ratio and Angularity (Chapter 4)	Block strength heterogeneity (Chapter 4 and 5)	Draw rate and sequence (Chapter 5)	Cushioning (Chapter 4 and 5)
Roughness (Chapter 3)	Frictional properties of fragments (Chapter 3)	Air gap thickness (Chapter 2 and 5)	
Veins and small discontinuities (Chapter 4)	Initial block arrangement on the muckpile surface (Chapter 2 and 5)		
	Segregation by large blocks due to surface cone (Chapter 5)		

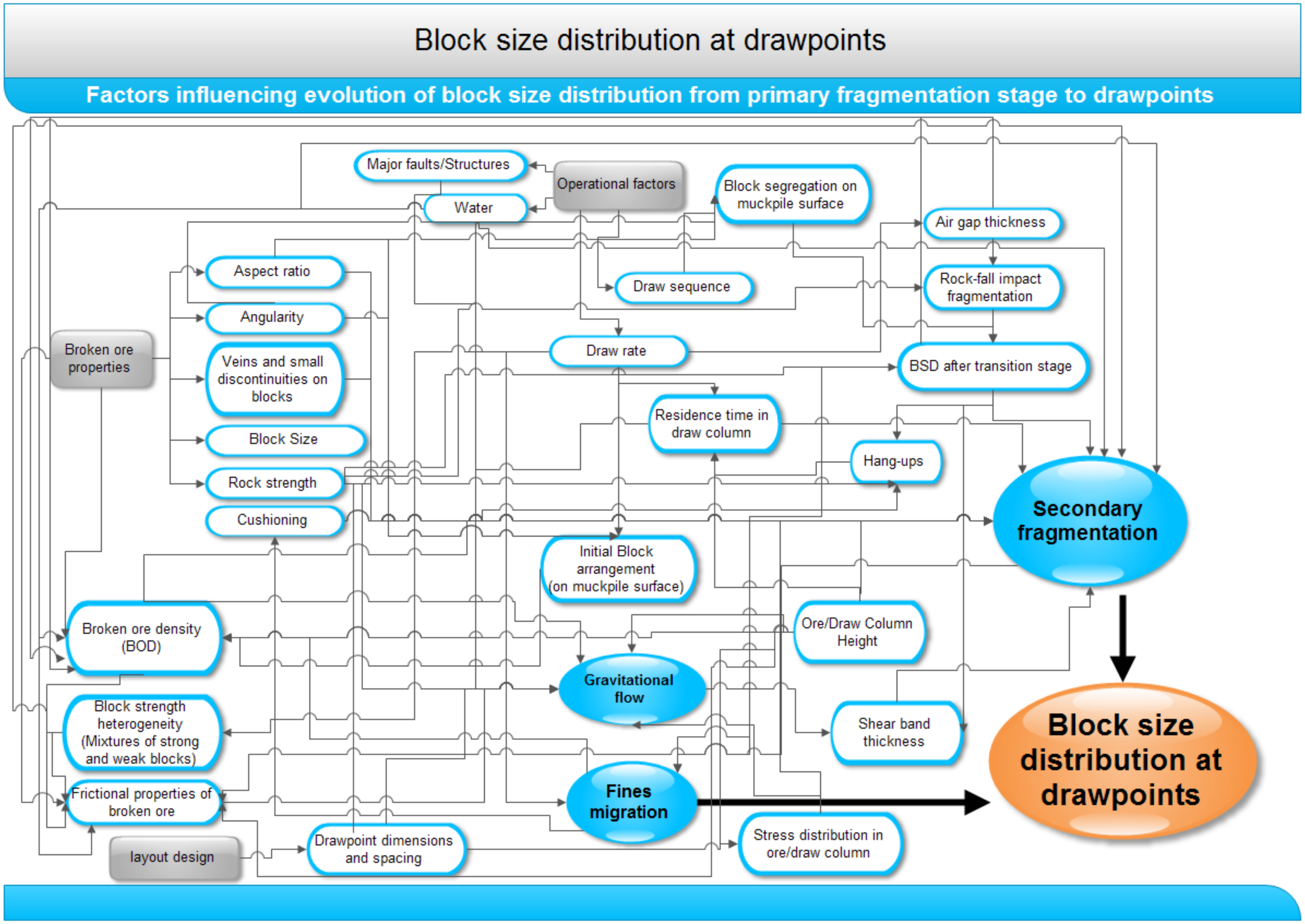

Fig. 1.6: Conceptual map: Factors affecting the evolution of block size distribution from primary fragmentation stage to drawpoint.

It is apparent that two key broken ore parameters need to be studied comprehensively: ***bulk density (swell factor)*** and the ***inter-block friction angle*** within a draw column during block caving. In addition, in depth study is required to investigate ***secondary fragmentation occurring within the compression plug flow zone*** in a draw column. Furthermore, several factors such as: ***air gap thickness, block strength heterogeneity***, and ***cushioning*** among others can contribute further to secondary fragmentation, although consideration of these might not be necessary until more advanced stages of engineering design. These topics are described separately below, with focus on their importance to prefeasibility and feasibility level studies. Accordingly, several important variables specific to more detailed design-level assessments are not fully relevant and therefore fall out of the scope of this thesis. One of these is *the Discrete Fracture Network (DFN)*, or rock mass fabric, which defines the orientations and other geometric characteristics of the key faults and discontinuity sets that will influence caving. DFN's are a powerful means to determine the block shape and size distributions, which in turn directly influences the *in situ* fragmentation, and indirectly the secondary fragmentation. In addition, caving operations can impact secondary fragmentation in terms of *drawpoint spacing* and *undercut design.* The first is relevant in generating interactive or IMZ cave flow (Chapter 6), while the latter could be important during early production.

1.5.1 Broken ore density (BOD) within draw column during block caving

Although the BOD is assumed to be a constant in block caving projects, the broken ore in a draw column can be expected to undergo changes that lead to a heterogeneous density distribution. It is acknowledged that draw column density decreases within the shear bands that develop, resulting in zones of loosening in response to ore extraction. The broken ore in the draw column thus experiences stress and density heterogeneities throughout, depending on the block properties (e.g., shape, aspect ratio and size distribution). Other important factors include air gap thickness, draw rate and draw sequence. In addition, the blocks undergo grinding and breakage (e.g., secondary fragmentation), which increases with draw column height. As such, a conceptual framework of BOD distribution during block caving which can account for isolated and interactive flow modes and whether drawpoints are closed would be extremely valuable for practical usage. Thus, this BOD framework could be effectively used in improving assessments of secondary fragmentation and broken ore characterization.

1.5.2 Inter-block friction angle of broken ore applied to gravitational flow in block caving

The inter-block friction angle (ϕ') is a significant parameter affecting broken ore gravitation flow during the draw process, and that also indirectly affects secondary fragmentation. Despite its importance, there is a lack of standard methodologies to quantify ϕ'. Although this parameter is influenced by a series of block properties, including joint roughness and the intrinsic strength of the broken ore, it also combines with operational factors to influence the maximum ϕ' via the normal stresses that increase with draw column height. Hence, a procedure to evaluate ϕ' on broken ore materials, under both isolated and multiple movement zones is highly required.

1.5.3 Secondary fragmentation and hang-up potential in the compression zone of a draw column during block cave mining

Although it is believed that broken ore does not experience as much fragmentation in the compression plug flow zone as within the shear bands (Pierce 2009), there is a pressing need to understand whether the presence of small discontinuities and defects provides an exception and can facilitate increased fragmentation. However, there are not sufficient empirical and/or numerical studies to adequately evaluate fragmentation within the plug-flow zone under an IMZ scenario. The most relevant study is that by Hardin (1985), which is cited and discussed thoroughly by Pierce (2009). The main concern regarding the utility of this Hardin model is that it quantifies the amount of fragmentation using a single parameter and as such, it is not possible to make straightforward predictions of drawpoint BSD. The model is also based on different granular soils that can not correctly represent *in-situ* broken ore conditions in terms of bulk broken ore density, aspect ratio and block size distributions

It is apparent that a series of controlled laboratory experiments designed to simulate broken ore moving down through a draw column of increasing height will greatly contribute to generating relationships to evaluate the secondary fragmentation within the compression plug flow zone. The main challenge to carry out a comprehensive empirical testing programs or empirically-calibrated numerical models is to carefully control the reduced particles samples used in the experimental tests in terms of their intrinsic properties (size, aspect ratio and strengths), allowing them to represent large broken ore fragments.

1.5.4 Factors affecting secondary fragmentation during block caving

Although several factors affecting secondary fragmentation are common to most early-stage drawpoint layout designs (e.g. column height, rock strength, friction angle, near and far field zones, and shear band thickness), several additional factors may significantly affect secondary fragmentation depending on the characteristics of the specific block cave project. These include: air gap thickness, broken ore density (BOD), segregation and concentration of large blocks due to topology of the muck pile, broken ore strength heterogeneity, block strength reduction mechanisms, presence of water within the draw columns, and cushioning of large blocks by a finer block size matrix. The study of each of these poorly understood factors will likely contribute greatly towards more accurate drawpoint BSD assessments.

1.5.5 Evolution of broken ore size distribution in a draw column during block cave mining

Understanding the evolution of the Block Size Distribution (BSD) in a draw column is essential to properly predicting BSD at the drawpoints. The BSD within a draw column controls, in part, gravitational flow, secondary fragmentation, and fines migration of the broken ore. These represent several key factors required to make reliable feasibility-level assessments for a potential caving operation. However, as previously outlined in Section 1.4, there is a scarcity of procedures or methodologies available to reliably quantify drawpoint BSD. Based on this, the development of an alternative methodology to predict drawpoint BSD for feasibility and early stage design should include *fragmentation by shear* (as is the case for Pierce's REBOP methodology), *fragmentation by confined compression* (e.g. crushing, splitting and chipping), both in the far field and plug-flow compression zones, and also *fines migration*.

1.6 Thesis Objectives

The central objective of this thesis aims to provide an improved understanding of the factors and processes influencing secondary fragmentation during block caving, and to use this knowledge to develop improved assessments of secondary fragmentation and hang-up potential during feasibility-level studies of large block caving projects. This will be achieved through the analysis of empirical data derived from related fields integrated with data from specialized experiments developed and reported in this thesis. These are used to develop a more mechanistically-based empirical understanding of secondary fragmentation and block size distributions encountered at the drawpoints. This research will include a comprehensive study of secondary fragmentation processes, from the first point of blocks breaking away from the cave back (i.e., subsequent to primary fragmentation), to the movement of blocks down through the draw column, through to their extraction at the drawpoints.

The primary objectives of this thesis to achieve the central objective are as follows:

1) Establish a conceptual framework for assessing broken ore density (BOD), including heterogeneity, within draw columns during block caving. Correlations resolved from experiences in other fields of granular mechanics, including unique field data from rockfill and waste rock studies, will be utilized to guidelines for estimating BOD as a function of different ore column heights;

2) Develop a standard methodology to evaluate the inter-block friction angle of broken ore materials (i.e., caved rock) specific for draw columns and caving operations.

3) Generate an empirical methodology and corresponding relationships for evaluating secondary fragmentation and hang-up potential for block caving feasibility studies. This will involve developing procedures for conducting laboratory-scale experiments as a proxy for the different kinds of loading expected in a draw column;

4) Develop a detailed accounting of the diverse factors affecting secondary fragmentation during block caving related to feasibility and advanced engineering stage designs; and

5) Develop a methodology to predict drawpoint broken ore size distributions focused on early stage block caving feasibility assessments and design, and validate using field data. This methodology will be supported based on four main pillars: i) far and near field loading conditions, ii) laboratory testing (one-dimensional and ring shear tests) as a proxy for mine-scale draw column processes, iii) Pierce' gravitational flow model of a central compression plug zone, surrounded by shear bands, and iv) fines migration.

1.7 Thesis Structure

This thesis is structured as follows.

Chapter 1 includes an introduction to secondary fragmentation during block caving, with emphasis on the role of the broken ore size distribution on mine planning design. The motivation, scope and objectives are presented.

Chapter 2 introduces a conceptual framework on assessing the broken ore density (BOD) distribution under both isolated movement zone and interactive flow. This is then used to propose a methodology to evaluate the BOD within draw columns.

Chapter 3 presents the results of a study concerning the frictional strength of broken ore materials, which are used to develop a procedure to evaluate this parameter under different rock properties and draw column conditions.

Chapter 4 describes the methods, results and conclusions of a comprehensive experimental laboratory testing program focused on secondary fragmentation, simulating the loading conditions in the compression plug-flow zone. More than 5,000 concrete cuboids were fabricated, based on a methodology developed to fabricate artificial cuboids, and tested as a proxy for broken ore fragments, carefully controlling their size, aspect ratio and intrinsic strengths. A subset of the cuboids were embedded with a small, non-persistent discontinuity, controlling their length, orientation and thickness to examine the role of small joints and veining on secondary fragmentation processes.

Chapter 5 examines several key factors affecting secondary fragmentation in block caving: *air gap thickness, BOD, segregation of large blocks, broken ore strength heterogeneity, block strength damage and crushing, water within draw columns, and cushioning*. The in-depth understanding gained for these factors is synthesized to contribute to a more precise secondary fragmentation assessments during feasibility and advanced stage engineering.

Chapter 6 presents a new methodology to evaluate BSD at drawpoints for early stage design. This methodology is supported by new laboratory testing data (one-dimensional compression tests), far and near field approaches, Pierce's gravitational flow model, and a simple fines migration approach.

Chapter 7 includes conclusions and recommendations for further investigations. This is followed by Appendix A, which includes the results of the laboratory testing program reported in Chapters 4 and 5.

Chapter 2: Broken Ore Density Distribution within a Draw Column during Block Caving [1]

2.1 Introduction

The swell of a caved rock mass plays a significant role in the planning and design of block cave mines, especially in terms of cave propagation, surface subsidence and ore recovery, although its determination is a very difficult and contentious task as it is virtually impossible to measure in the cave (Van As & Van Hout 2008). In fact, key mine planning parameters such as the draw height are influenced by the swell of the rock. For instance, this parameter is used to evaluate the stresses on the extraction level pillars, to estimate quantities of caved rock remaining in a draw column, and as input in the secondary fragmentation assessments as discussed in Chapters 4 and 6.

In addition, several parameters have been proposed in the literature to define the swell of broken rock, which depends on the caved rock (V_{caved}) and in situ volume ($V_{in\text{-}situ}$). For instance, the bulking factor is defined as $B = (V_{caved} / V_{in\ situ}) - 1$ and the swell factor (S_f) is $(1+B) \times 100\%$. The broken ore density (to be referred to by its acronym BOD in the remaining chapter) is the ratio between the bulk weight and caved volume. Also, the void ratio (e) which is commonly used in geotechnical engineering (ratio of *volume of voids* and *volume of solids*;

[1] Dorador L, Eberhardt E, Elmo D. Broken Ore Density Distribution within a Draw Column during Block Caving. (In review)

i.e., e = B), will be used together with the porosity index η which is equivalent to $\eta = e / (1 + e)$.

The swell of broken rock (S_f) is a major factor in mine planning designs, but poorly understood. As an example, S_f values of 108-116% have been suggested by Laubscher (1994) but values as high as 169% have been reported at the El Teniente mine (Millan & Brzovic 2013). Additional data is provided in Table 2.1, highlighting the large variation of S_f for different block/panel caving operations. In addition, Pierce (2009) has proposed that the gravitational flow of broken ore in a draw column is controlled by two main zones (*shear bands* and a *plug-flow zone),* which in turn would generate different ranges of BOD.

Differentiating the BOD in both shear band and plug-flow zones would allow more accurate assessments of secondary fragmentation, percolation (fines migration) and stress fields as well as improved broken ore characterization regarding inter-block friction angle (ϕ') and deformation modulus. In addition, determining the BOD in both zones would also improve the gravitational flow analysis by means of REBOP (Rapid Emulator Based on PFC, Cundall et al. 2000), frequently employed in block caving projects. Hence, this huge difference of swell factor in cave mines as well as the need to evaluate the BOD in different zones within a draw column firmly motivates the *conceptual framework* developed here for assessing the broken ore density within a draw column during block caving.

Certainly, the swell of a caved rock mass depends largely on the rock mass characteristics and properties (e.g. strength). Important factors include the number of joints, as well as their orientation, spacing and persistence, which control the *in-situ* fragmentation.

Other key factors include the *in-situ* stress conditions and whether an air-gap is present. These influence the primary fragmentation and fall height of the blocks from the cave back, respectively, and therefore the initial block size and shape distributions. The resulting initial configuration of blocks then undergoes changes (secondary fragmentation) as the material moves down through the draw column, with further fragmentation and swell depending on the changing column height (Ross & Van As 2012). Hence, the initial bulk density of a granular assembly is a difficult parameter to predict (Hancock 2013).

Table 2.1: Swell factors reported by different authors.

Mine	Swell factor S_f	References
Andina Mine. Chile	115% - 120%	Alcalde et al. (2008)
Teniente Mine. Chile	119% - 128%	Behn & Brzovic (1997)
Teniente Mine. Chile	130 - 140%	Gonzalez-Carbonell & Duplancic (2012)
Teniente Mine. Chile	142% - 208%	Millan J. & Brzovic A. (2013)
Ridgeway Deeps- Australia	110% (Average)	Sharrock et al. (2012)
Shabanie mine, Zimbabwe	107%-120%	Laubscher (2003)
King mine, Zimbabwe	113%	Laubscher (2003)
San Manuel (South), USA	108.9%	Gilbride et al. (2005)
Lakeshore, USA	109.5%	Gilbride et al. (2005)
Henderson, USA	109.5%	Gilbride et al. (2005)
-	108% - 116% (*)	Laubscher (1994)
-	125% - 166% (**)	Lorig & Pierce (2000)
-	200% (**)	Hancock et al. (2012)
-	121% - 126% (**)	Esterhuizen et al. (2004)

(*) Suggested values; (**) Numerical modelling

Several studies have highlighted that the broken ore undergoes a change in the BOD/swell factor along the ore column (Ross & Van As 2012, Sharrock et al. 2012, Dorador et al. 2014). This matter has also been identified in sublevel caving by Rustan (2000) who noted that properties like swelling, packing, porosity vary so much in space and time during the gravity flow of coarse rock that simulations using constant properties will always fail. Constant values only apply for a very fine, mono grained material. Nevertheless, BOD and S_f are commonly assigned constant values for block caving design software such as PCBC (Personal Computer Block Cave; Diering 2000), REBOP and BCF (Block Caving Fragmentation; Esterhuizen 2005).

Furthermore, a key factor of the BOD not previously addressed is the initial arrangement of blocks released from the cave back, which in turn falls down onto the muckpile surface. As depicted in Fig. 2.1 depending on the air gap thickness, the broken ore could arrange into either a tidy (dense) packing or an untidy (loose) packing. These conditions are summarized in Fig. 2.2 which represent two packing stages of the broken ore. The former considers the broken ore affected by initial packing (*broken ore initial arrangement*) while the latter reflects the BOD influenced by column height (H), gravitational flow, secondary fragmentation, and fines migration.

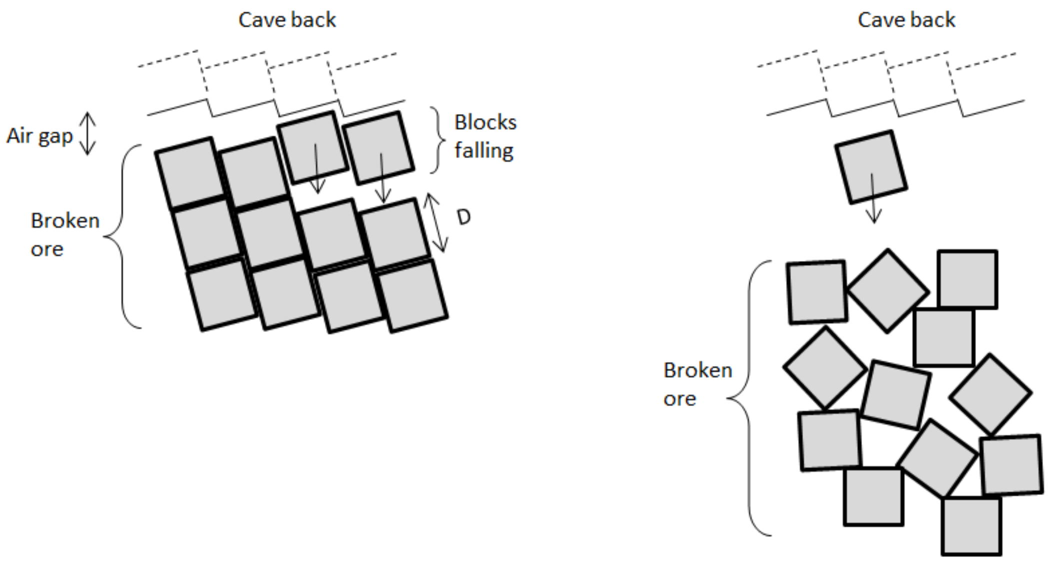

Fig. 2.1: Tidy (dense) and untidy (loose) packing

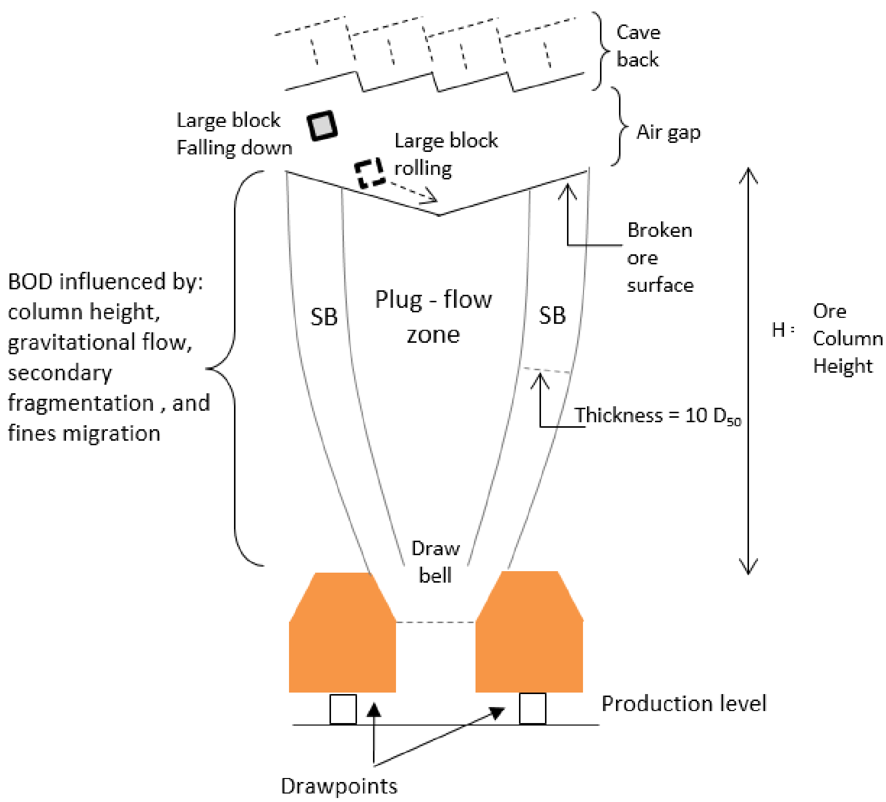

Fig. 2.2: Broken ore under different stresses conditions along single draw column

This chapter investigates these factors depicted in Fig. 1.6 (initial arrangement of blocks, air gap thickness, ore/draw column height, broken ore properties) and uses them to develop a conceptual framework for feasibility-level studies that describes the distribution and zonation of the BOD within a block caving draw column. The broken ore initial arrangement is examined based on near-uniform particle packing, taking into account that the size ranges of blocks will be within the same order of magnitude after primary fragmentation (e.g., uniform gradation). Then, the BOD within a draw column is studied based on existing knowledge from rock fill dams, mine waste rock piles and coarse granular soils, where particles size ranges span several orders of magnitude. Thus, these materials are thought to reflect wide particle size distributions commonly observed at drawpoints. Secondary fragmentation, fines migration and gravitational flow patterns within a draw column (e.g. plug-flow zone and shear bands) are also discussed. Thus, estimations of S_f and BOD (relative to a rock density of 2.7 t/m^3 and rock strength higher that σ_c = 100 MPa) along a draw column are proposed here based on both isolated and interactive flow, including the case of an inactive draw column. Finally, the settlement process of broken ore over time is addressed due to its importance in the broken ore densification and air gap thickness enlargement.

2.2 Broken Ore Density (BOD) Within a Draw Column

2.2.1 Broken ore initial arrangement

Single blocks released from the cave back can align to form numerous block arrangements. As seen in Fig. 2.1 the air gap height is a relevant parameter in this regard. In the case of a negligible air gap, blocks released from the cave back will have less chance to rotate and thus will retain their contact with adjacent blocks. This would lead to a tighter packing and smaller initial swell factor. Intuitively, a tidy (dense) packing would result when the fall height is lower than the block's width. In fact, evidence of negligible air gap has been observed at the El Teniente Mine, Chile (Brzovic & Gonzalez 2015).

In contrast, the presence of a sizeable air gap would facilitate a more disordered block arrangement, increasing the initial swell factor. Of interest is that Esterhuizen & Karacan (2008) have identified from longwall mining observations that when the fall height is larger than the lateral dimension of the rock fragments, they are more likely to rotate and come to rest in a disordered pile. A large air gap would also promote rock-fall impact fragmentation (referred as *impact breakage* by Laubscher 2003), which would induce smaller block sizes and fines (untidy packing). This topic is further developed in Chapter 5. Thus, the air gap thickness could explain in part the large variations of swell factors found at different mines around the world (Table 2.1), although block shape and aspect ratio are also critical parameters in the initial block arrangement. For instance, the air gap thickness at cave initiation would be influenced by the blast rock draw in the undercut level. However, in later stages the air gap thickness could increase due to settlement in time of the broken ore (section 2.7), with variations depending on the draw and cave rate. Thus, both narrow and large air gaps could be developed during the caving process as suggested in Fig. 2.1 and therefore, broken ore with comparable block sizes (e.g., 1 m) could arrange into an untidy (loose) and tidy (dense) packing.

The tidy (dense) packing is of specific interest with respect to the BOD and worthy of further discussion. For instance, this dense packing causes face to face contacts between blocks and so forms larger kinematically interlocked "*effective blocks*" of different sizes (Fig. 2.3), a phenomenon identified as *entrainment* by Hancock (2013). Interestingly, Börzsöny & Stannarius (2013) have noted that sets of very long rods exhibit a solid-like shape stability, which would be comparable with these groupings of interlocked effective blocks. Effective blocks of different sizes within the broken ore would also mean a wider distribution of acting block sizes and therefore higher BOD (as noted in Section 3.1). This phenomenon has also been discussed by Esterhuizen & Karacan (2008) in long wall mining. They recommend, based on a study by Munson & Benzley (1980), that the maximum bulking of the caved rock will occur when the fall height exceeds about twice the block width (without considering rock-fall impact fragmentation), which means that under this height a tidy packing could be generated Finally, this initial tidy (dense) packing is in agreement with a particular mixed disturbance mode of gravity flow, where large interlocking groups of particles act to disturb the flow as noted by Sharrock & Hashim (2009) and later by Hancock et al. (2012).

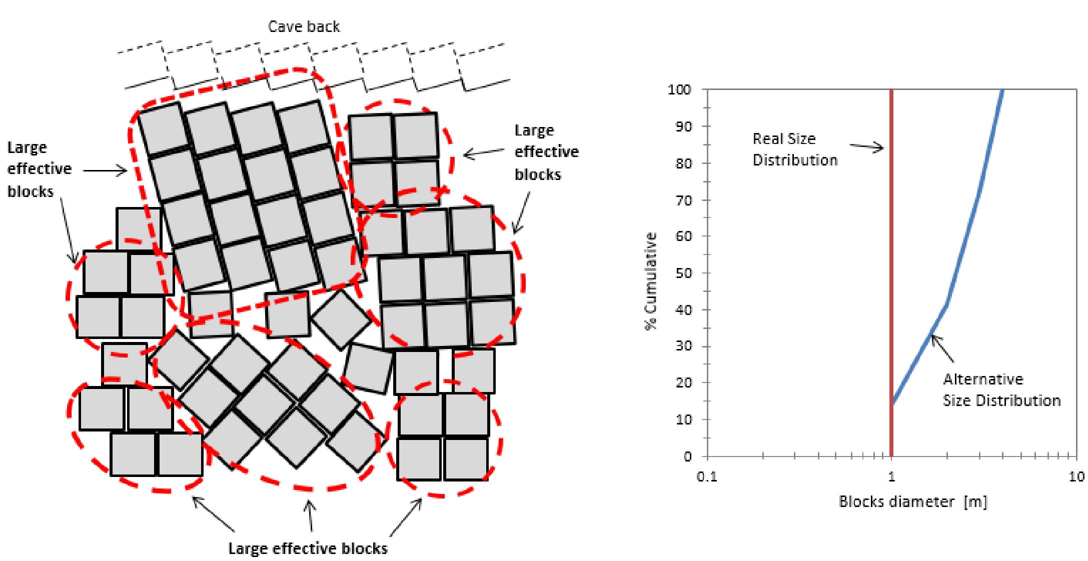

Fig. 2.3: Initial block arrangement during block caving

Thus, based on the previous recommendations by Esterhuizen & Karacan (2008) a simple conceptual description of the expected initial block arrangement of broken ore is introduced. Under a uniform block size distribution and block diameter D: i) fall heights lower than D will promote a tidy packing, ii) fall heights greater than D but less than 2D will promote a mix of both untidy (loose) and tidy (dense) packing, iii) fall heights greater than 2D will generate a untidy (loose) packing mostly.

Others factors influencing the initial block arrangement (e.g. block shape) are briefly addressed as follow.

2.2.1.1 Influence of block shape

Different block shapes would be present on the muckpile surface depending on the in situ and primary fragmentation. From a granular material point of view, Santamarina & Cho (2004) noted that free falling platy particles tend to settle in a horizontal position, which would be comparable to platy-like blocks falling from the cave back as depicted in Fig. 2.4 which will promote a high tidy (dense) packing.

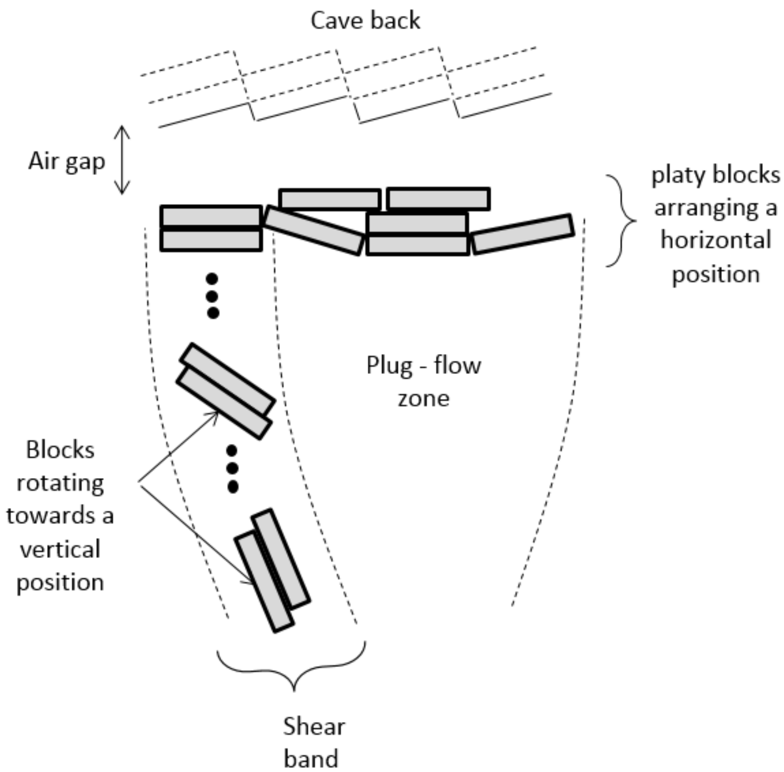

Fig. 2.4: Example of platy blocks arrangement during initial packing and moving downward through a draw column.

2.2.1.2 Other factors

Block roughness is a parameter that must be considered. As blocks slide/roll down across the top of the muckpile surface, block roughness would promote higher friction between contacts, enhancing an untidy (loose) packing. Also, *block rotation* during fall would emerge depending on the geometry of the rock mass discontinuities. Thus, blocks could rotate while falling, which would induce an untidy packing onto the muckpile surface (Fig. 2.5). *Block rebound is* also a factor of significance; blocks with high rebound properties (e.g., coefficient of restitution) would promote disorder and therefore a more untidy packing.

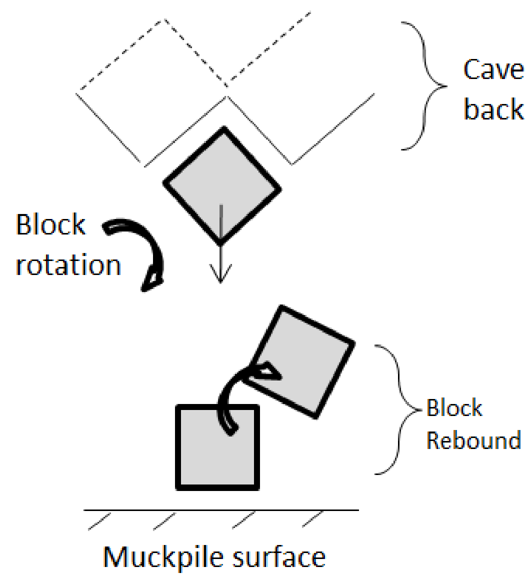

Fig. 2.5: Stages of single block on the initial arrangement

2.2.2 Broken ore along a draw column and close to drawpoints

As a draw column can be characterized by a central plug-flow zone (compression zone) and outer perimeter shear bands during gravitational flow (Pierce 2009), the *block shape* and *size distribution* would likely play a more significant role in the shear bands (due to the continuous rotation, dilation and re-compaction), rather than within the compression zone. However, there is an absence of studies examining the influence of block shape and broken ore size distribution on BOD. Several studies do exist though pertaining to particle shape and sizes on packing.

2.2.2.1 Influence of block shape

With regard to shear bands, noteworthy works by Börzsönyi et al. (2012) and Wegner et al. (2014) indicate that for elongated grains the preferred orientation form is close to the streamlines under shearing. This interesting result would suggests that elongated blocks (and possibly platy-shaped blocks) within the outer periphery could align with the flow direction, due to the permanent shear deformation taking place within this zone, although this could be somewhat offset by secondary fragmentation and dilation taking place at the same time.

Based on studies on hopper flow by Baxter & Behringer (1990), Cleary & Sawley (2002), and Sielamowicz et al. (2005) among others, Börzsönyi & Stannarius (2013) concluded that elongated particles concentrate into a narrow funnel above the hopper opening. This fact is very important in a draw column with broken ore reaching the drawbell because it would allow more elongated blocks to be recovered than other kind of block shapes at drawpoints (e.g., platy or cubes). This agrees with experiences at the Suapi sector in El Teniente mine (Chile) where elongated oversize blocks (longest edge > 2 m) have been observed regularly at drawpoints (Brzovic 2015).

Regarding the plug-flow zone (compression zone), it is hypothesized that the broken ore moves downward within a draw column undergoing internal compression but without a marked relative movement among blocks. Block rotation is restricted. Thus, broken ore moving down through the compression zone would act as an interlocked mass towards the drawpoint (Hancock 2013). However, this compressibility stage would be counteracted by broken ore dilation as the ore approaches the drawbell, which would help to rotate elongated blocks towards a vertical alignment.

Also, as indicated by Biarez & Hicher (1994), particle shape would play a significant role in the bulk density for granular samples with uniform particle sizes. However, the influence of block shape on the BOD would be inhibited by the block size distribution (BSD), especially when the BSD is wide.

Hence, based on these previous findings from granular material studies, the block shape could play a significant role on the BOD within the shear bands more so than within the compression zone. More detailed investigations on this specific topic are recommended.

2.2.2.2 Influence of block size distribution

Broken ore particles could range from oversize blocks (larger than 2 m^3) through to smaller blocks and gravel to sand sized particles, thus spanning at least three orders of magnitude in block diameters. The influence of particle size distribution on maximum density has been reported by Biarez & Hicher (1994) and Dorador & Besio (2013) for granular materials, which correlates well with the densest packing (or minimum void index, e_{min}). The span of particle size distribution is characterized using the uniformity index C_U, defined as the ratio between D_{60}/D_{10}. The standard laboratory procedure to measure the densest packing of a granular material is carried out using a cylindrical mould and vibratory table (ASTM standard D 4253 – 00). The latter promotes rearrangement among particles while minimizing secondary fragmentation. Maximum density is directly related to the uniformity index (C_U). The standard to assess minimum density is determined by simply pouring the material in the same mould

(ASTM standard D 4254-00). Riquelme & Dorador (2014) proposed a correlation from angular gravels using the minimum void index e_{min}. Minimum densities in gravels and rockfill have been reported in the literature by De la Hoz (2007) and Dorador & Besio (2013), which demonstrated that minimum density depends directly on the BSD and block shape (assuming a constant specific gravity, SG). Riquelme & Dorador (2014) also suggest a correlation to assess the minimum density (or maximum void index e_{max}), which can then be used to evaluate the maximum density. These equations are as follows:

$$e_{\min} = 0.7849 \cdot \mathrm{C_u}^{-0.302} \tag{2.1}$$

$$e_{\max} = 1.311 \cdot e_{\min} + 0.062 \tag{2.2}$$

$$BOD = \frac{SG}{1+e} \tag{2.3}$$

As an example, uniform samples (C_U = 1 to 2.5) of sands or gravels with a SG of 2.7 could reach densities from 1.3 to 1.7 g/cm^3 (equivalent to porosity η ranges of 0.37 to 0.52), which agrees very well with results provided by Baker & Kudrolli (2010) who reported ranges of porosities of 0.33 to 0.50 under maximum and minimum stable random packing of different classes of polyhedral particles. Conversely, densities over well-graded samples with C_U of 50 could range between 2.0 and 2.2 t/m^3. Fig. 2.6 depicts examples of both uniform and well graded samples of angular gravels. It is important to note that both correlations do not depend directly on block size (e.g., maximum block size D_{100} or average block size D_{50}).

Hence, it is proposed here that these relationships can be likewise used to estimate the densities of broken ore in a draw column.

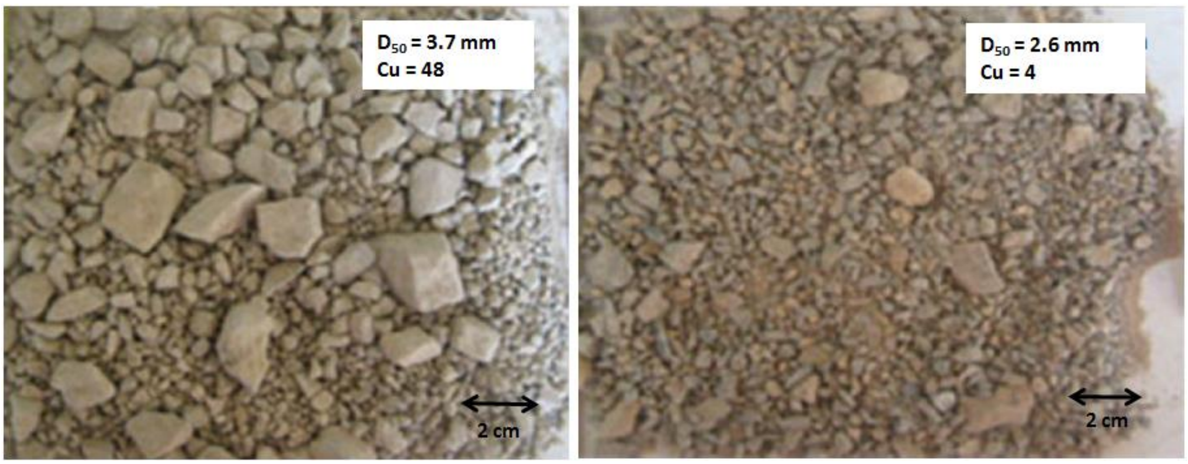

Fig. 2.6: Example of well graded (left) and uniform (right) samples. Dorador (2010)

2.3 BOD during Gravitational Flow

Broken ore within a draw column could experience marked gravitational flow patterns which directly impact BOD. First, *segregation of large blocks* due to irregular draw (cone-shaped free surface) can occur (Chapter 5). In addition, based on image processing on flowing sand by Baxter et al. (1989) and Melo et al. (2008), broken ore during extraction could experience two main flow patterns: *shear bands* and a *plug-flow zone*. Pierce (2009) not only agreed with these two main flow patterns, but also recognized a particular flow behaviour, conical in form, which is generated when the IMZ (isolated movement zone) width is less than 20 particle diameters. Pierce also stated that a reasonable shear band thickness could be 10 times the average size of the broken ore (Chapter 6). Furthermore, the broken ore undergoes *dilation* close to the drawpoint which induces a loose BOD. These considerations should be included in any study of BOD within a block cave draw column.

2.3.1 Segregation of large blocks due to non-uniform draw

An accepted feature during ore draw is the generation of a cone-shaped free surface due to continuing ore extraction (Pierce 2009); its surface inclination could be associated to the angle of repose as indicated by Waters & Drescher (2000). As noted by Dodds (2003), very little force is required to start round particles rolling and to keep them rolling. Although blocks on the muckpile surface are non-rounded, they would still roll down to the centre of a steep cone surface as shown in Fig. 2.2 and therefore, a greater percentage of large blocks could be concentrated within the plug-flow zone facilitating the formation of hang-ups.

This segregation affects the BOD because more large blocks would concentrate within the plug-flow zone rather than within the shear bands along the outer periphery of the draw column. This means wider size distributions in the plug-flow zone and more uniform gradations in the shear bands. Hence, this segregation process would change the block size distributions and therefore the BOD in both shear bands and plug-flow zone. This topic is further developed in Chapter 5.

2.3.2 Plug-flow zone

During broken ore flow, a compression zone (plug-flow zone) is developed (Fig. 2.2) if the diameter of the isolated draw (IMZ) is at least 20 particle diameters; otherwise the plug-flow region disappears, and the velocity profile takes the form of an inverted cone (Pierce 2009). In addition, this plug-flow could be associated with an anisotropic compression of the broken ore, similar to that observed in one-dimensional (1-D) tests as shown in Fig. 2.2. This represents a key hypothesis promoted in this study as σ_1 (vertical stress) and σ_3 (horizontal stress) are indeed variables during the draw process due to the continuous stress re-distribution within the draw column, which means that the ratio σ_1 / σ_3 is not constant. Valuable data on large 1-D compression tests is available in the literature thanks to the works by Marsal et al. (1965), Valenzuela et al. (2008) and Palma et al. (2009), which is depicted in Fig. 2.7.

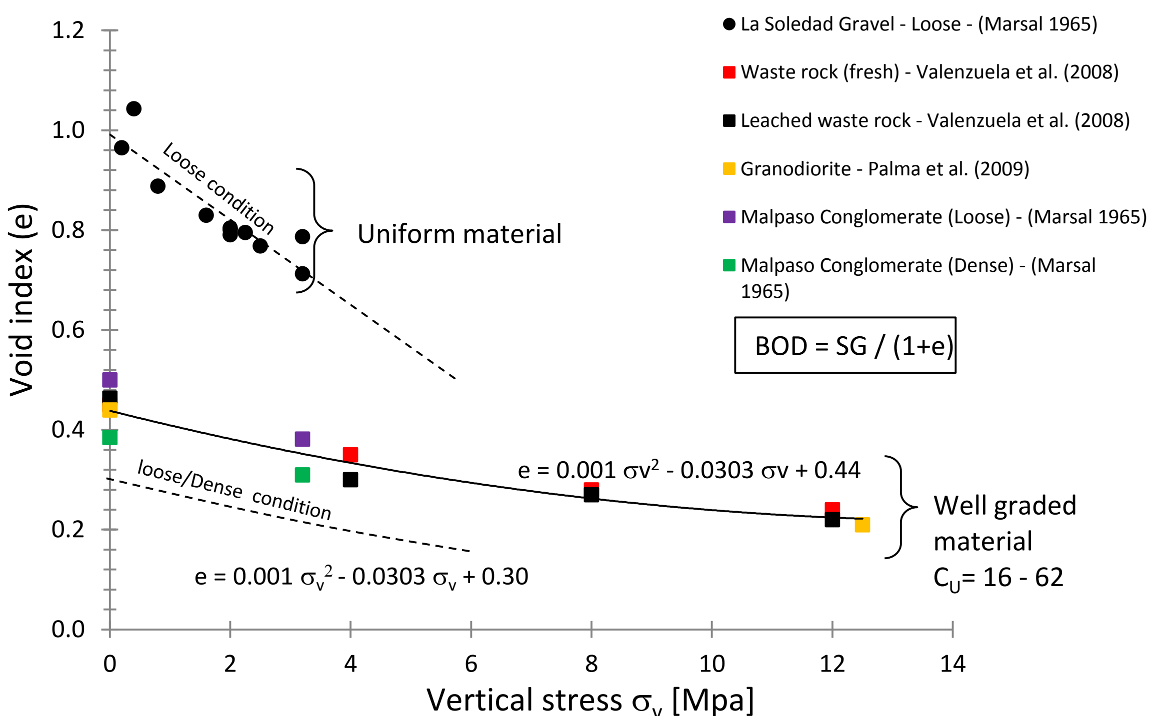

Fig. 2.7: Influence of σ_v on broken ore void index. Data from different authors

In general terms, the compressibility depends mainly on the confining pressure, initial BOD, and block size distribution. This data will be employed in further evaluations of BOD along this work.

2.3.3 Shear bands

According to Pierce's (2009) model, shear bands are generated around the outer periphery within the draw column. Pierce also states that shear band profiles exhibit elevated porosity relative to the plug-flow region. In addition, significant particle rotation occurs within a shear band (Bardet 1994, Matsushima et. al 2003) including large deformations and dilation, which tend to reduce BOD. Also, the broken ore experiences not only secondary fragmentation but also fines migration concentrated along the shear bands which induces changes in the BOD (section 2.4). As suggested by Pierce, a shear band thickness of 10 x D_{50} could be considered. Finally, broken ore within the shear bands would be more uniform in size due to segregation on the *cone-shaped free muckpile surface* (as noted in section 2.3.1).

2.3.4 Loose density above drawpoints

As stated by Melo et al. (2008), broken ore close to the drawpoint tends to dilate likely as arching develops over the drawpoint and ore below passes into the drawbell. Also, during continued ore draw, the broken ore undergoes significant dilation, which could be associated to a minimum density of the broken ore as explained in section 2.2.2.2. However, it is important to note that in cases of low draw rate or no draw, broken ore dilation above a drawpoint will be offset by compressibility due to the column weight, increasing the BOD.

2.4 Secondary Fragmentation and Fines Migration

2.4.1 Secondary fragmentation

The process known as secondary fragmentation is commonly associated with comminution in terms of point load splitting, corner rounding and crushing of blocks due to shear and compressive stresses imposed during vertical movement of the broken ore. This fragmentation process affects the BOD because the average size distribution decreases and the block size heterogeneity increases. As noted previously (Fig. 2.2), a broken ore zone moving downward through an ore column can experience a combination of two modes of loading.

The first can be associated with 1-D compression within the central axis of the column, where the broken ore would predominantly experience fragmentation in terms of splitting and crushing (Dorador et al. 2015). The crushing mechanism would allow a disintegration of blocks, generating smaller fragments and more fines, although these fines and smaller fragments are likely to keep the original shape of the *disintegrated block* due to confinement as its moves downwards through the plug-flow zone, thus inhibiting fines migration. Once it reaches the drawpoint, these fines and smaller fragments would dilate and move more freely, filling voids between merging larger blocks from the plug-flow zone and shear bands.

The second mode of loading involves shear deformations outside the central axis of the draw column, where the broken ore would generate more fines due to shearing and rounding along the block edges, enabling these fines to freely migrate towards the drawpoints (Chapter 6). Hence, the secondary fragmentation of broken ore will result in a dual-mode weighted gradation curve from splitting, crushing and fines generation derived from the two modes of induced stresses.

2.4.2 Fines migration impacting ranges of BOD

Fines migration is another process influencing BOD distribution within a draw column. Fines travel down through the column and fill the voids in between larger blocks, increasing in concentration towards the bottom of the column. In cases where there is a significant amount of fines close to the drawpoint, large blocks may be found floating in a fine matrix of sand and gravel. Although the fines migration process has been investigated in several empirical (Castro 2006, Cheng et al. 2009, Hashim & Sharrock 2012) and numerical modelling (Leonardi et al. 2008, Pierce 2009) studies, there is no standard methodology or procedure to evaluate fines migration through a draw column.

Fines migration is expected to occur mostly in the shear bands due to the continuous internal movement of blocks, enabling smaller particles to travel down faster, therefore generating more uniform size distributions along the shear bands (decreasing the BOD). Also, an appreciable amount of fines generated within the plug flow zone from block crushing would emerge during the broken ore dilation close to the drawpoints. Hence, wider block size distributions near the drawpoints are expected due to the accumulation of fines from both the shear and plug-flow zones.

Fines migration together with secondary fragmentation are evaluated in section 2.5 with respect to BOD within a draw column.

2.4.3 Broken ore size distribution impacting the BOD

In order to analyze the evolution of the broken ore size distribution, equations 2.1 and 2.2 can be applied to estimate BOD as a function of C_U. Fig. 2.8 presents primary fragmentation data from several studies, which ranges from Cu = 2 to 2.5. These represent very uniform gradations and BOD between 1.4 - 1.7 t/m^3. This data compilation is in agreement with a benchmarking study carried out by Castro (2006) who reported an average block size range from 0.5 to 0.9 m and a uniformity index (Cu) of 2.86. Data was also compiled for broken ore size distributions at drawpoints corresponding to different operations and ore columns between 100 to 200 m height, as plotted in Fig. 2.9. This takes into account both secondary fragmentation and fines migration processes. The block size distribution data in terms of C_u ranges from 8 to 18, which represent well-graded curves (in contrast with the primary fragmentation curves) and BOD values of 1.7 to 2.0 t/m^3. Hence, broken ore at the top of a draw column would appear blockier, while at the drawpoints it would entail a *rock/soil matrix.*

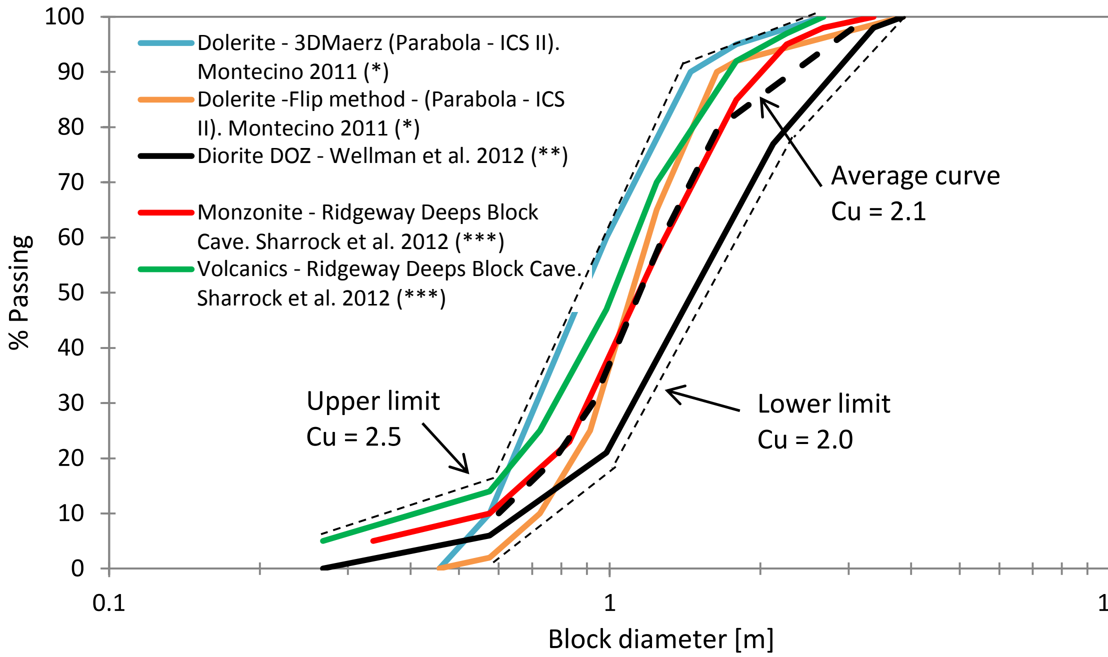

Fig. 2.8: Primary fragmentation curves from different authors. (*) Field estimation (**) Estimation using Core2Frag approach.

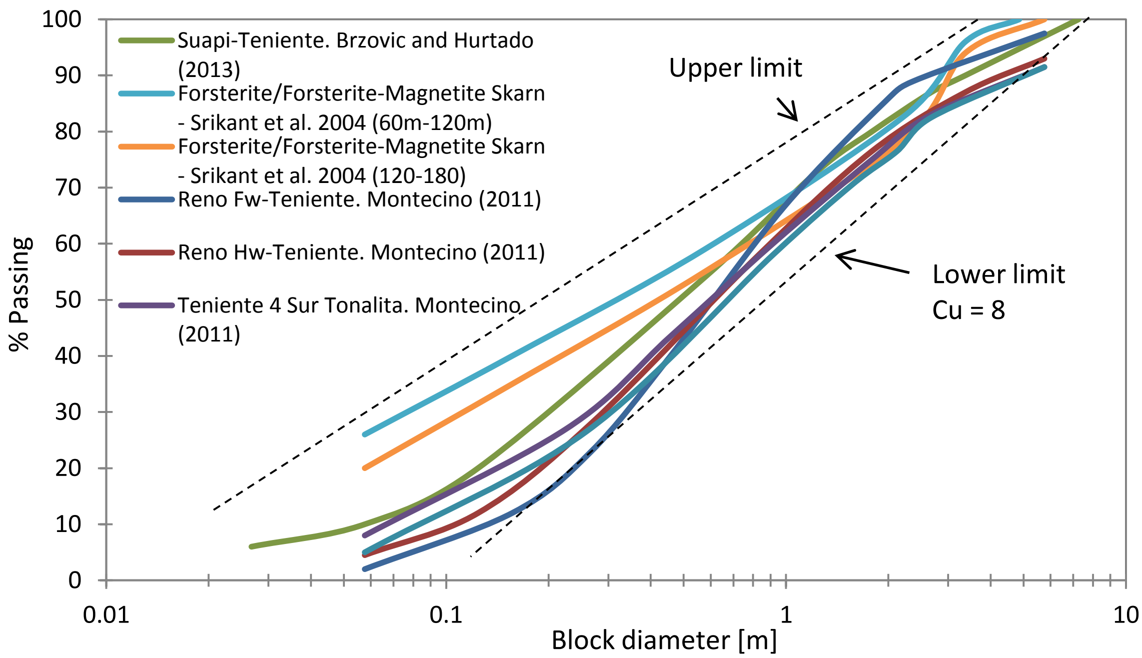

Fig. 2.9: Secondary fragmentation curves by some authors. Column heights from 60 to 180m

2.4.4 Influence of broken ore mixtures and block's strength within a draw column on BOD

Block caving operations could cave through a combination of different lithologies. In such cases, the different mixes of caved rock properties could control most of the secondary fragmentation and gravitation flow within the draw columns. Weaker blocks will be subjected to more fragmentation, which means smaller block sizes. This in turn facilitates a wider block size distribution of broken ore and therefore, higher densities (equations 2.1 and 2.2). Also, fines migration within a draw column would be more accentuated, increasing the BOD closer to the drawpoints (e.g. drawbell) acting counter to the loosening resulting from ore extraction at the drawpoint. The amount of additional secondary fragmentation and fines migration due to mixes of blocks from different lithologies will depend on the strength contrasts and the percentage of mixes between the lithologies (Chapter 5). The wider block size distributions arising from mixes weighted more heavily with weaker rock types will mean higher densities (equations 2.1 and 2.2). In the case of stronger rocks (e.g. El Teniente), no significant secondary fragmentation is expected and so, the BOD won't be affected by the broken ore gradation.

2.5 Empirical Estimation of BOD Distribution into an Isolated Movement Zone

Three scenarios of initial block arrangement are proposed in this work to analyse the BOD distribution in an isolated movement zone (IMZ) which are in agreement with a simple conceptual description of the initial block arrangement proposed in section 2.2.1. The first refers to a loose initial packing of broken ore material involving blocks being released from a cave back with an air gap present, that freely rotate as they fall onto the muckpile surface. This introduces an initial loose state and minimum BOD, to which equations 2.2 and 2.3 would be applied. The second case is referred to as a dense but untidy (chaotic) packing of the broken ore occurring within the plug-flow zone. The third case is where an air gap is not present and the broken ore released from the cave back remains in a dense (tidy) packing. Here the blocks retain their contacts with adjacent blocks in a tight assemblage, and as such, the comparison between broken ore and rockfill or gravels is not applicable and the correlations developed do not apply. These three cases will be developed in the following sections using Fig. 2.10 with the corresponding empirically-derived BOD and swell factor results being presented in Table 2.2.

Table 2.2: Suggested BOD and S_f values under three different packing condition (IMZ)

Loose condition (Untidy)		**Loose/dense (Untidy/tidy)**		**Dense (tidy)**	
BOD [t/m^3]	S_f	BOD [t/m^3]	S_f	BOD [t/m^3]	S_f
D_1 = 1.4 - 1.6	193% - 169%	D_1 = 2.05 – 2.15	132% - 126%	D_1 = 2.7	100%
D_2 = 1.4 - 1.6	193% - 169%	D_2 = 2.05 – 2.15	132% - 126%	D_2 = 2.7	100%
D_3 = 1.5 - 1.7	180% - 159%	D_3 = 1.5 - 1.7	180% - 159%	D_3 = 1.5 - 1.7	180% - 159%
D_4 = 1.5 - 1.7	180% - 159%	D_4 = 2.10 – 2.20	129% - 123%	D_4= 2.7	100%
D_5= 1.6 - 1.8	169% - 150%	D_5= 1.6 - 1.8	169% - 150%	D_5= 1.6 - 1.8	169% - 150%
D_6 = 1.6 -1.8	169% - 150%	D_6= 2.15 – 2.25	126% - 120%	D_6= 2.7	100%

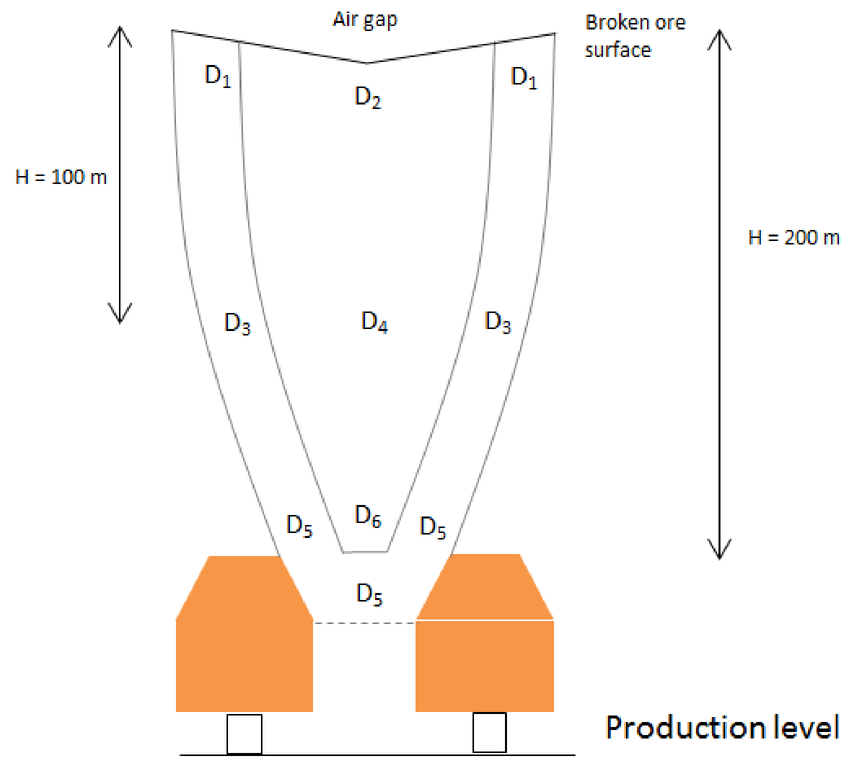

Fig. 2.10: Broken ore density variation within a draw column

2.5.1 Loose packing of broken ore

For this case, the initial BOD close to muckpile surface can be estimated based on Cu = 2 to 2.5 (Fig. 2.8) and equations 2.1, 2.2 and 2.3, which give ranges from 1.4 to 1.6 t/m^3 (for both D1 and D2; see Fig. 2.10). Regarding the BOD close to the drawpoints, it is feasible to consider size distribution ranges from Fig. 2.9 (which represent the broken ore at drawpoints) and so, using equations 2.1, 2.2 and 2.3, ranges of density of 1.6 - 1.8 t/m^3 are obtained for a column height of 200 m (D5 and D6). For an intermediate column height of 100 m a mean density range of 1.5 - 1.7 t/m^3 would be assumed (D3 and D4).

Ranges of BOD within the shear bands and plug-flow zone can vary depending on the column height, especially on ore columns higher than 200 m due to the influence of the mass flow (far field). This topic is further discussed in section 2.6.

2.5.2 Dense (tidy) packing of broken ore

This case would be expected where a negligible air gap is present as explained in section 2.2.1. No mine data or previous studies are available to estimate density values under this packing condition. Taking into account that the broken ore density is limited by a hypothetical maximum dense (tidy) packing of 2.7 t/m^3, which is the rock density used as reference in this work, this limit can then be used to assess BOD under conditions of dense (tidy) packing. This assumption would only apply at the top of the draw column and within the plug flow zone (D1, D2, D4 and D6 from Fig. 2.10), due to the fact that the shear bands will be always undergoing a loose (untidy) packing on broken ore. Thus, values of D3 = 1.5 - 1.7 t/m^3 and D5 = 1.6 - 1.8 t/m^3 could be considered in the outer periphery.

2.5.3 Loose/dense packing of broken ore (irregular draw)

Loose/dense packing reflects the situation when the broken ore experiences an irregular draw rate and sequencing, which would promote both loose (untidy) packing and dense (tidy) packing, or when the air gap thickness would range between D and 2D, with D being the average block diameter (section 2.2.1). Under this scenario, the BOD within the shear bands would keep a loose condition due to continuous block rotation and dilatancy during draw. However, this loose/dense packing would affect the top of the draw column and the entire plug-flow zone before reaching the drawbell.

The BOD at the top of the draw column (D_1 and D_2 in Fig. 2.10) may vary between the loose untidy packing case (BOD = 1.4 to 1.6 t/m^3) and maximum density (2.7 t/m^3), resulting in an average range of 2.05 t/m^3 to 2.15 t/m^3. Then, D_4 could be estimated as the average between 1.5-1.7 t/m^3 and 2.7 t/m^3 (D_4 = 2.10 – 2.20 t/m^3), and D_6 would reach a range of 2.15 to 2.25 t/m^3 based on the average between 1.6-1.8 t/m^3 and 2.7 t/m^3. Finally, D_3 = 1.5 - 1.7 t/m^3 and D_5 = 1.6 - 1.8 t/m^3 could be considered within the shear bands.

2.6 Estimation of BOD Distribution under Interactive Flow

Interactive flow occurs when portions of neighboring draw columns overlap with each other, causing the upper portions of caved rock to descend uniformly (Susaeta 2004). Thus both *near field* and *far field* effects must be accounted for. This is illustrated in Fig. 2.11 where h_c is the critical height of interaction and h_f is the far field height. In order to evaluate BOD within the near field, it is reasonable to consider the hypothesis for an isolated draw column (section 2.5). However, within the far field, the broken ore would be influenced by uniform stress distributions, which could be equated to loading in 1-D compression tests; thus for this scenario, large 1-D compression data from Fig. 2.7 can be used to obtain feasibility-level BOD estimates. It is also important to note that within the far field of the interactive scenario, *secondary fragmentation* processes would induce a better graded block size distribution before the broken ore enters the near zone. These are considered in the following subsections for the three packing conditions representing the BOD under an interactive flow.

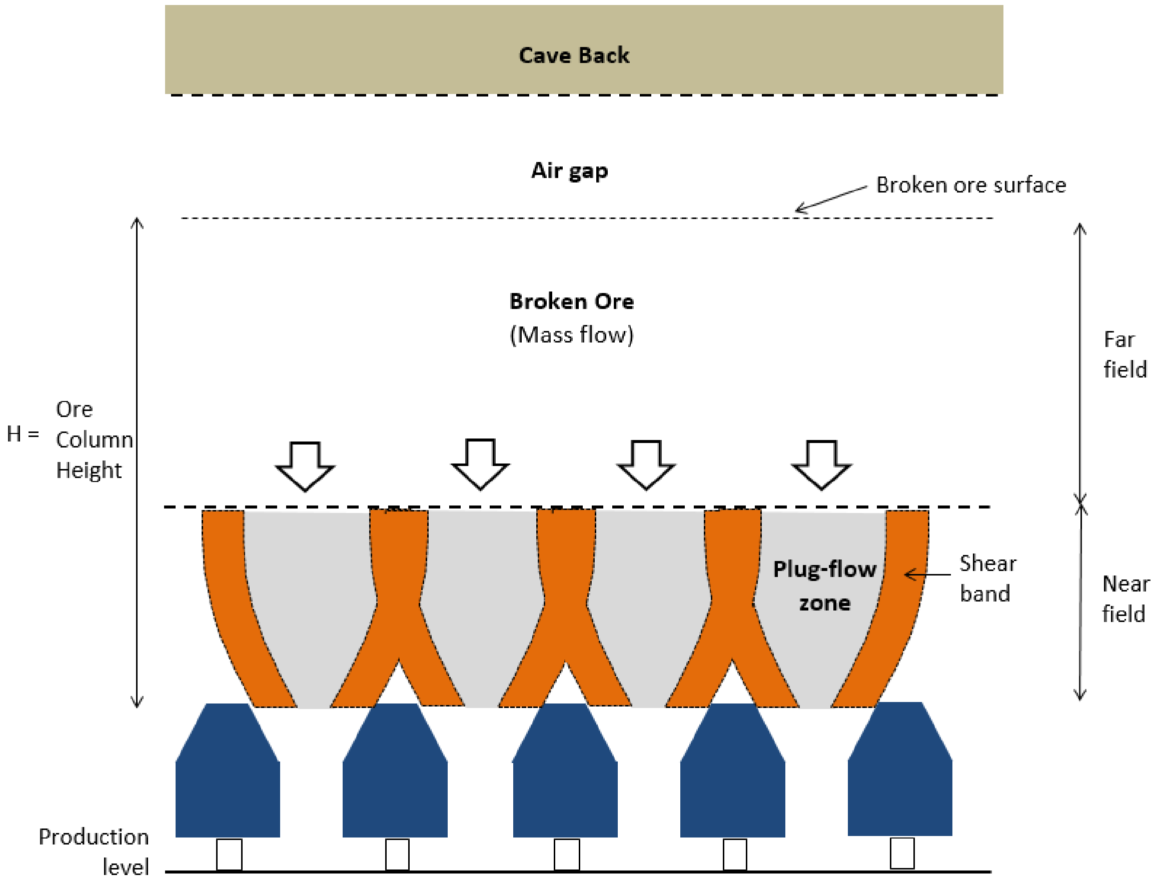

Fig. 2.11: Multiple draw operation scheme

2.6.1 Loose packing

For the analysis carried out here, the critical height of interaction h_c will be assumed to be 50 m for practical purposes (the h_c varies for each block caving operation) and two far field heights are considered: h_f = 150 m and h_f = 300 m. A key consideration accounted for in the analysis is that under appreciable ore column heights, stresses are reduced on the broken ore due to stress arching at the base of the cave.

Regarding the far field, the *loose condition* trend from Fig. 2.7 would apply. Hence, a void index (e) of 0.72 is obtained under a h_f = 150 m which equates to a BOD of 1.6 t/m^3 and S_f = 169% (assuming SG = 2.7). Conversely, the mass flow will influence the density values in the near field. So, D_1 and D_2 would be assumed to be the same as the 1.6 t/m^3 of the far field. Also, this case considers a total height of 200 m which is comparable to the height of the IMZ case from section 2.5. Hence, size distribution at the drawpoints (Fig. 2.9) and equations 2.1, 2.2 and 2.3 can be used, which gives values of D_5 and D_6 = 1.6 - 1.8 t/m^3 (S_f = 169% - 150%). Finally, D_3 and D_4 can be assumed to be a mean value of D_1 and D_2 with D_5 and D_6 obtaining a range of 1.6 – 1.7 t/m^3 (S_f = 169% - 159%).

For the case of a far field height h_f of 300 m, the *loose condition* trend from Fig. 2.7 still also applies. This results in a void index (e) of 0.50, resulting in a BOD of 1.8 t/m^3 and S_f = 150% (assuming SG = 2.7). Regarding the near field, D_1 and D_2 would be assumed to be the same as 1.8 t/m^3 of the far field. Also both D_4, D_6 (densities within the plug-flow zone) are assumed to keep constant (1.8 t/m^3) due to the stress reduction within the plug-flow zone, which impedes an additional density increment of the broken ore. In addition D_3, D_5 (densities within the shear bands) are defined as 1.6 to 1.8 t/m^3 (S_f = 169% - 150%).

2.6.2 Dense packing

In this extreme (and low probability) case, the broken ore would experience a density close to 2.7 t/m^3 along the entire far field for h_f = 150 m and 300 m. In the near field, D_1, D_2 D_4 and D_6 would keep a density value close to 2.7 t/m^3 but along the shear bands (D_3, D_5) the density would decrease strongly to 1.6 - 1.8 t/m^3 (S_f = 169% - 150%) due to the high secondary fragmentation, rotation and block dilation, which would result in a loose density. This sharp drop is heavily dependent on the block strength. For instance, weak blocks (e.g. σ_c lower than 50 MPa) would facilitate more fragmentation within the shear bands inhibiting block dilation and increasing the BOD to higher values of 1.6 - 1.8 t/m^3. Conversely, strong blocks wouldn't be affected significantly by secondary fragmentation, so dilation would take place.

2.6.3 Loose/dense packing

As explained in Section 2.5.3, the broken ore density could be approximated as an average from the loose and dense state of the broken ore, which gives an average value of 2.05 – 2.15 t/m^3 (S_f = 132% - 126%) In the far field, it is expected that the compressibility of the broken ore will result in a higher h_f. Also, the broken ore as shown in Fig. 2.3 could be formed by single blocks and large interlocked effective blocks, which could be envisaged as a well graded block size distribution. Under this scenario, it is feasible to consider the *loose/dense condition* curve from Fig. 2.7. This curve is a projection of the well graded material correlation under an intercept 0.3. From this, void ratios of 0.22 and 0.15, which correspond to density values of 2.2 t/m^3 (S_f = 123%) and 2.3 t/m^3 (S_f = 117%), can be obtained for h_f conditions of 150 m and 300 m, respectively.

Regarding the near field and h_f = 150 m, D_1 and D_2 would be assumed to reach the same density as the far field (i.e., 2.2 t/m^3 and S_f = 123%). Also both D_4, D_6 (densities within the plug-flow zone) are assumed to be constant (2.2 t/m^3). In addition D_3 and D_5 (densities within shear bands) are defined as 1.6 - 1.8 t/m^3 (S_f = 169% - 150%) as considered for the loose packing case (section 2.6.1).

For the case of h_f = 300 m, similar near-field conditions to those for h_f = 150 m are assumed to apply. Thus, D_1 and D_2 would be 2.3 t/m^3 (S_f = 117%), D_4, D_6 would be defined as 2.3 t/m^3 (S_f = 117%), and D_3, D_5 = 1.7 t/m^3 (S_f = 159%).

2.6.4 Estimation of BOD distribution under closed drawpoints

Drawpoints can be closed due to a number of factors, including ground control problems (i.e., tunnel or pillar failures) and operational issues (workers strike, environmental permitting, etc.). If so, broken ore could experience a densification over time when no extraction is carried out, a process described by Susaeta (2004) as uniformity density equalization. Susaeta associated this process to a slow propagation movement within the cave, whereby the broken ore settles uniformly due in part to a lateral movement generated towards the draw columns. Assuming the zonation depicted in Fig. 2.10, it is reasonable to consider that a 1-D compression occurs across the entire broken ore pile, which means that D1 changes to D2, D3 to D4 and D5 to D6, and estimations under loose, dense and loose/dense can be applied from sections 2.6.1, 2.6.2 and 2.6.3, respectively.

2.7 Broken Ore Settlement

As previously identified, the broken ore experiences compressibility during caving and when drawpoints are closed, settlement at the muckpile surface would result. This surface settlement is significant as it might induce an enlargement in the air gap, and therefore influence the subsequent initial block arrangement process as previously discussed in section 2.2.1 and further examined in Chapter 5. Interestingly, the settlement phenomenon of rock-piles has been recognized in other geotechnical fields such as rockfill dams and waste rock dumps, structures that could be comparable to broken ore piles in terms of footprint area and height. Furthermore, waste rock and rockfill materials could share similar characteristics with broken ore in terms of average particle size and particle shape. The key difference between rockfill and waste rock materials is that the latter are dumped on a site without a compaction procedure, in contrast with compacted rockfill used in dams.

2.7.1 Background on rockfill dams settlement

Several reviews of settlement in rockfill dams have been reported in the literature. Sowers et al. (1965) compiled the crest settlement of 14 rockfill dams up to 100 m height, reporting a maximum settlement of 1.5% of dam height. Parkin (1977) also reported a maximum crest settlement of 1.6% from 9 dams. Oldecop & Alonso (2007) conducted a review of settlement in 13 concrete-faced rockfill dams (CFRD) up to 160 m height, reporting crest settlement up to 1.6%. Kim & Kim (2008) compiled data from a larger set of 35 CFRD of up to 187 m height and void ratios ranging from 0.18 to 0.4, obtaining a maximum internal settlement after construction of 1.9% of dam height.

Hence, based on this background review, it is possible to infer that a compacted broken ore (emulating the conditions in a rockfill dam) would undergo internal settlement ranging from 1.5 to 1.9%. In other words, if a draw column (under closed drawpoints) is 200 m high, the internal settlement under a dense broken ore condition can be estimated to result in up to 3.0 to 3.8 m of vertical internal deformation. In this case, based on values from rock fill dams (noting again these involve compaction), settlement would not significantly enlarge the air gap.

2.7.2 Experience from waste rock dumps

Waste rock encompasses coarse materials classified by size as cobbles, boulders, gravels, sands and fines. Waste rock dumps could be compared to large broken ore piles in block caving due to its wide ranges of particle sizes and dump heights which can reach more than 500 m (Valenzuela et al. 2008). Waste rock dump densities typically range between 1.6 and 2.2 t/m^3 depending on whether it is loose or compacted (Williams 2000). In addition, Linero et al. (2007) reported in-situ waste rock density tests (over dump platform) ranging from 1.8 to 1.9 t/m^3 (with a mean SG of 2.7). Thus, waste rock dumps under a loose condition could be associated to densities ranging from 1.6 to 1.9 t/m^3.

However, waste dump compressibility is a continuous process which could persist for even more than 10 years after construction (Naderian & Williams 1996, Naderian 1997). William & Currey (2004) reported settlements of 1.5% of dump height (which is equivalent to a settlement of 3.0 m under a waste dump height of 200 m) but no additional data are available.

2.7.3 Experience from waste rock 1-D compression tests

Due to the lack of information regarding waste dump settlements; it is feasible to use the large 1-D compression tests data from Fig. 2.7 in order to assess the compressibility of waste rock material in a loose condition. Considering a column height (H) of 300 m (closed drawpoints) and a representative density of 1.75 t/m^3, the vertical stress σ_v at the half of the column is 1.75 MPa. Next, using the *well graded material* trend on Fig. 2.7a final void ratio $e_f = 0.39$ is obtained. Using equation 2.4, and assuming an initial void ratio $e_o = 0.44$ associated with a density of 1.75 t/m^3 and specific gravity of 2.7 (thus, Δe = 0.05), a final settlement of 3.5% of the dump height, or ΔH = 10 m, would be calculated.

$$\frac{\Delta H}{H} = \frac{\Delta e}{1 + e_o} \qquad [2.4]$$

Hence, waste rock dump settlements could potentially experience large ranges of 3 to 10 m under a waste rock dump height of 300 m. Therefore, this range of settlement suggests that a large air gap could develop aided by settlement, which in turn would facilitate untidy block packing.

2.8 Summary and Key Findings

The secondary fragmentation of broken ore as it moves down through a draw column must be well characterized during early and advanced design stages as well as during production in order to ensure a successful mine plan and optimized production. A critical but not well studied geotechnical parameter in this context is the broken ore density (BOD), commonly related to the swell or bulking factor. It is hypothesized that BOD decreases (and swell factor increases) along the shear bands within a draw column and close to the drawpoint due to loosening generated by ore extraction. The broken ore in the draw column also potentially experiences stress and density heterogeneities throughout, depending on the block properties (e.g., shape, aspect ratio and size distribution). Important factors identified as influencing the initial BOD include air gap height, draw rate and draw sequence. As secondary fragmentation continues, increasing with increasing draw column height, the ongoing grinding and breakage will generate rounder block shapes and more fines. This in turn will enable different block shape configurations and finer broken ore size distributions. These fines will migrate downwards into the draw column increasing the BOD in the lower half of the draw column.

Of interest here is the compilation of data and observations regarding the calculation of minimum and maximum densities on coarse granular soils, rockfill and waste rock materials. These were used to develop a conceptual framework on BOD and procedure to estimate the ranges and distribution of draw column BOD using a primary block size distribution as an input. Conditioning the primary fragmentation is the orientation, spacing and persistence of the natural discontinuities within the rock mass (i.e., *in-situ* fragmentation), as well as the air gap thickness, presence of veining, and rock mass strength. Here the need to accurately characterize the size and shapes of the blocks falling from the cave back onto the top of the muckpile (i.e., draw column surface) is emphasized, because it controls in part the broken ore packing and the gravitational flow characteristics within the draw column.

The findings presented here indicate that the air gap is a significant factor in the BOD; a negligible air gap will result in a tighter initial arrangement of blocks, while the blocks released from the cave back, as the air gap increases, will have more space to rotate generating a more disordered packing and higher swell factor (i.e. smaller BOD). The latter will intensify due to segregation of large blocks across an irregular draw column surface; an irregular muckpile surface may result from uneven draw rates. In addition, other rock parameters such as block roughness and rebound potential are thought to be of importance. A key extension of findings from the rock fill dam and mine waste rock dump data compiled, which is supported by the large-scale 1-D compression test data, is that broken ore is susceptible to experiencing internal settlement with time, which would enlarge the air gap size.

Three broken ore packing states were proposed: dense (tidy), loose (untidy) and an intermediate loose/dense packing, which covers the large variation in swell factors reported in the literature. The role of the initial block arrangement for each of these packing conditions was defined through a 'D' factor (i.e., average block diameter): i) Dense (tidy) packing for air gap heights less than D; ii) Loose/dense packing for air gap heights between D and 2D; and iii) Loose (untidy) packing for heights greater than 2D. Next, the influence of secondary fragmentation and fines migration on reducing the average block size distribution (BSD) is considered. Using empirical relationships derived from the rock fill dam and mine waste rock data compiled, the broken ore density was shown to be affected by the secondary fragmentation and fines migration but not as significantly as the initial block arrangement. Finally, BOD values under three different flow modes (isolated, interactive, and closed drawpoints) were proposed based on correlations derived from the compiled data.

The conceptual framework presented in this chapter will contribute to a better assessment of BOD and swell factor, contributing to more accurate feasibility assessments and early stage mine planning design. The findings and framework presented in this chapter will also be further considered in Chapters 4, 5 and 6 in order to study the influence of the BOD on secondary fragmentation.

Chapter 3: Inter-Block Friction Angle of Broken Ore Applied to Gravitational Flow in Block Caving [2]

3.1 Introduction

Several key geotechnical properties of broken ore, referred to as caved rock in relation to a block cave operation, influence the caving process. Some of these include: i) block size distribution (which in turn depends on the natural fracture network, secondary fragmentation processes, fines migration, etc.); ii) broken ore density (BOD); iii) deformation modulus (E); and iv) the effective inter-block friction angle of the ore material (ϕ'). When considered in terms of the Mohr–Coulomb shear failure criterion (based on equation 3.1), the inter-block friction angle controls the downward flow of broken ore during the draw process (Verdugo & Ubilla 2004; Rahal 2008; Pierce 2009).

$$\phi' = \sin^{-1}\left(\frac{\sigma_1' - \sigma_3'}{\sigma_1' + \sigma_3'}\right) \qquad [3.1]$$

For instance, ϕ' conditions the growth of the Isolated Movement Zone (IMZ) and the corresponding internal movements associated with each drawpoint (Pierce 2009). This process can be modelled using REBOP (Cundall et al. 2000), Rapid Emulator Based On Particle flow code, for which the inter-block friction angle is a key input. Specific to a draw column, two related parameters can also be defined: *angle of repose* and *slide angle*.

---

[2] Dorador L, Eberhardt E, Elmo D. Inter-Block Friction Angle of Broken Ore Applied to Gravitational Flow in Block Caving. (In review)

Melo et al. (2007), Pierce (2009) and Vivanco et al. (2011) describe the angle of slide as defining the IMZ, while the angle of repose determines the maximum slope on the upper draw column surface (Pierce 2009). Furthermore, ϕ' can be used in practice to estimate the lateral earth pressure coefficient on broken ore materials at rest, which under a geostatic stress field or far field zone (Fig. 3.1), can be calculated using the Jaky (1948) formula, as $K_o = 1 - \sin \phi'$.

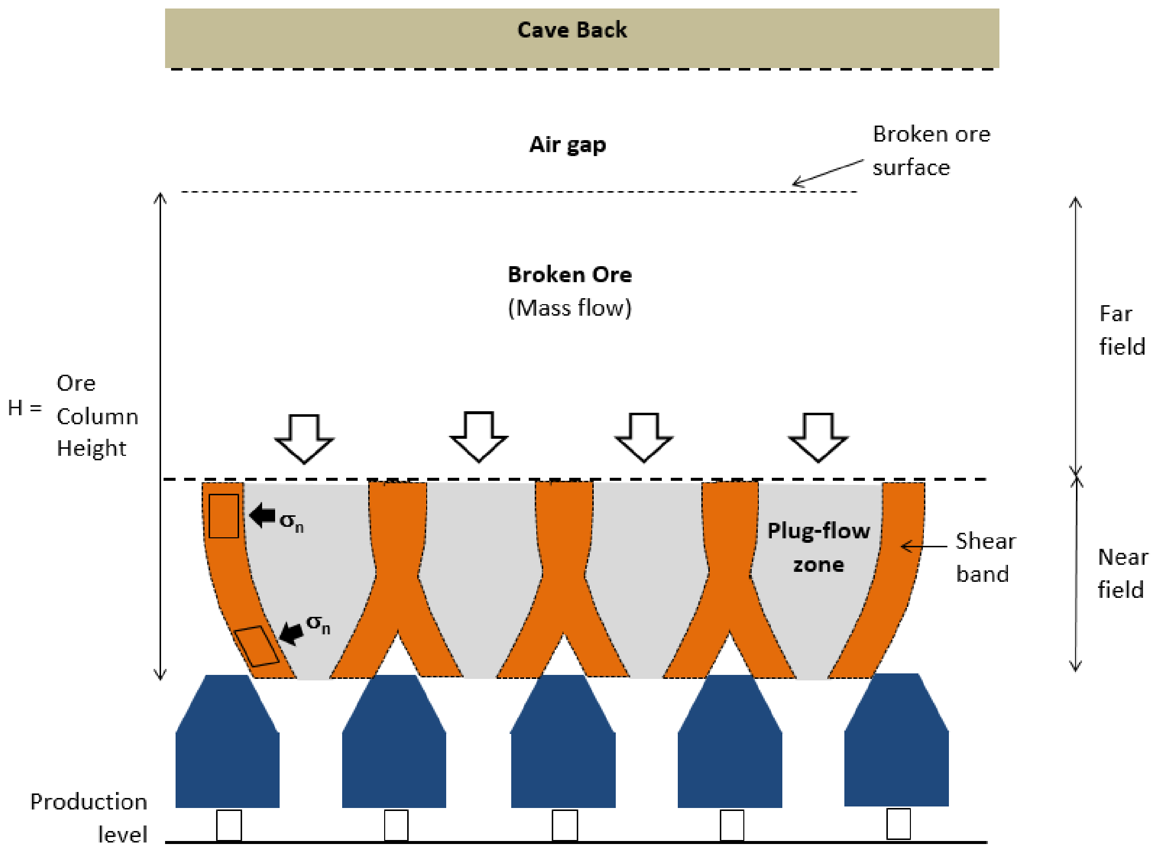

Fig. 3.1: Multiple draw operation scheme (interactive flow)

Despite its importance, assessing the inter-block friction angle of broken ore in the field is complicated by the broad range of block dimensions present, where diameters can reach up to several meters, together with a lack of standard assessment methodologies or absence of data. Existing databases detailing the results of large triaxial shear tests on rockfill and waste rock provide a means to balance the otherwise lack of data for ϕ'. Several attempts to assess the interparticle friction angle from the field of soil mechanics have been made based on experimental models (Barton & Kjaernsli 1981, Uhle 1986, Douglas 2002). Rockfill and waste rock materials share similar block sizes with broken ore, as well as characteristics like block shape and frictional properties. This presents the opportunity to use rockfill and waste rock interparticle friction angle data to characterize the inter-block friction angle of broken ore materials.

Column heights in current block caving projects are on average 160 m (Woo et al. 2013), although several block cave mines are being developed with planned caving heights in excess of 500 m (Hancock 2013, Eberhardt et. al. 2015). Depending on the draw sequencing, two general types of stress conditions are generated within the broken ore during block caving: *isolated movement zone* (IMZ) and *interactive flow*. An IMZ is characterized by a plug-flow zone and an outer annulus where the centre moves more rapidly toward the drawpoint than material at the IMZ limits (Pierce 2009). Plug-flow is defined by a zone of broken ore moving downward through drawpoints while the outer annulus (also referred as shear bands) is where the broken ore experiences large shear deformations. Conversely, interactive flow represents broken ore *moving* uniformly downward towards the drawpoints, which in turn can be divided into *far field* and *near field zones* (Fig. 3.1). While the far field represents a 1-D compression stress condition acting on the broken ore, the near field is characterized by compression plug and shear bands. Both types of broken ore flows *(IMZ* and *interactive draw*) will be considered in the following sections in order to evaluate the inter-block friction angle with a simple empirical methodology. Finally, additional considerations regarding the evaluation of ϕ' are recommended, with some emphasis placed on the influence of fines and water within a draw column in reducing the broken ore strength close to the drawpoints.

3.2 Background on Shear Strength in Granular Soils Applied to Broken Ore Materials

Broken ore materials, treated as an assemblage of particles, can be associated with granular materials, particularly with rockfill. As summarized by Melo (1977), Barton & Kjaernsli (1981), Indraratna et al. (1993) and Douglas (2002), the shear strength as a function of the normal stress (σ_n) for rockfill is non-linear, markedly at low σ_n. This would imply that the inter-block friction angle of broken ore materials, represented by Fig. 3.2a,b, varies with increasing σ_n as can be observed in Fig. 3.2c. A series of broken ore parameters as well as operational factors are explored and discussed in this section, most of these are considered in the assessment of ϕ' under both IMZ and interactive flow (section 3.5 and 3.6).

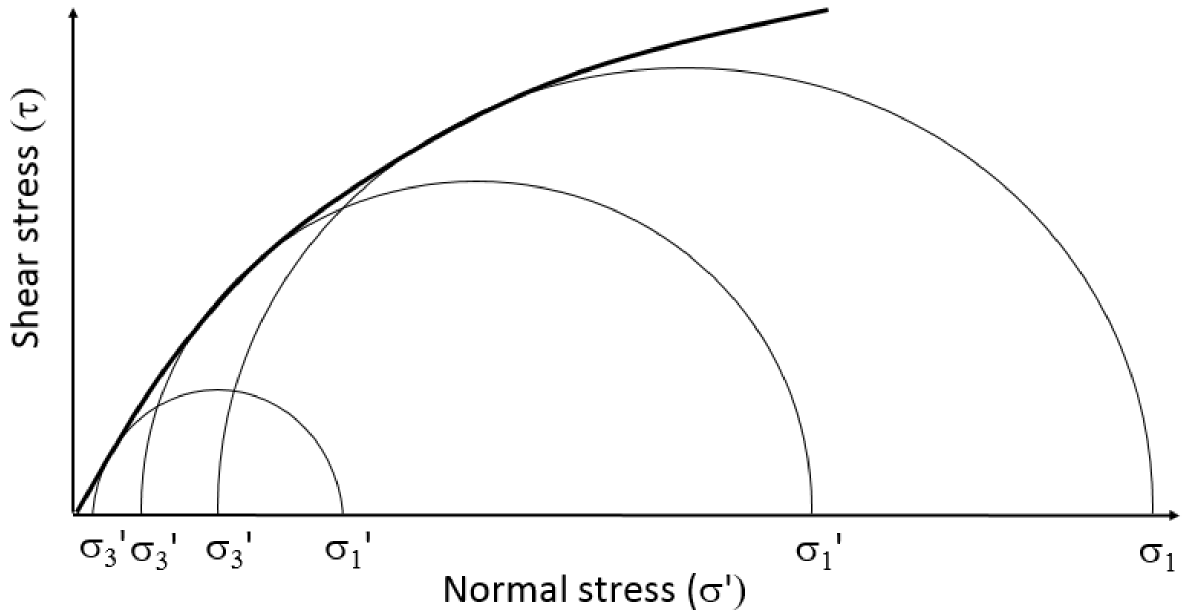

(a)

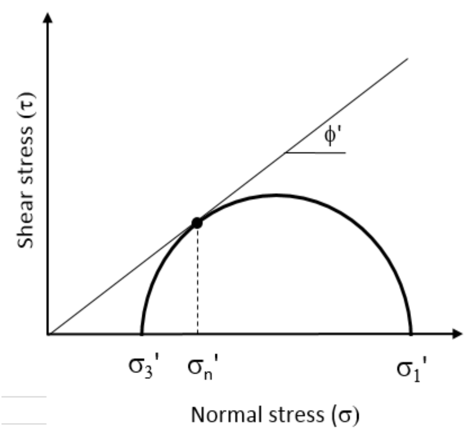

(b)

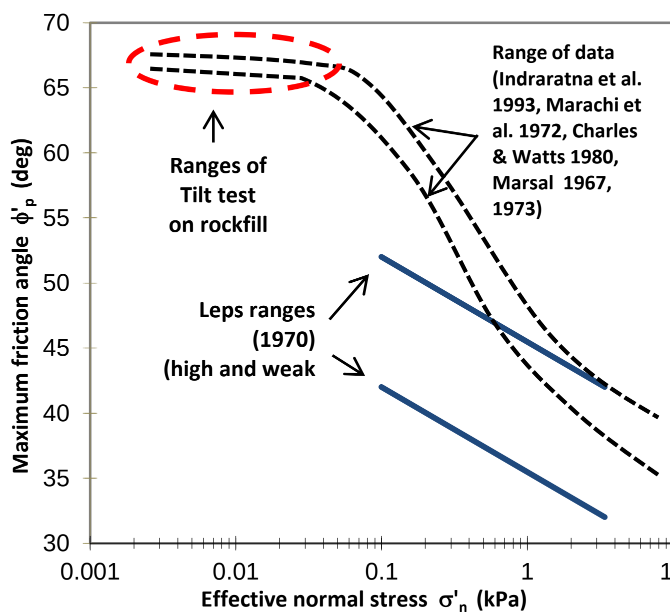

(c)

Fig. 3.2: (a) Non-linear shear strength envelope (b) Representation of ϕ'. (c) Triaxial compression data on ballast and rockfill materials under different ranges of normal stress σ_n. Adapted from Indraratna et al. (1998)

3.2.1 Broken ore properties affecting shear strength

Five block properties have been identified as playing significant roles in the broken ore shear strength: i) Intact *block strength; ii) Block strength heterogeneity; iii) Block size distribution (BSD)*; iv) *Block shape; and v) Block roughness.* In addition, due to the large size of some individual broken ore blocks, the *size scale effect* is another important aspect to consider. Finally, the *broken ore density* (BOD), presence of *water within a draw column* and *column* compressibility over time can also produce major changes in ϕ'. Each of these are discussed below and through sections 3.4 to 3.7 and most of these are depicted in Fig. 1.6.

3.2.1.1 Intact rock strength

The Intact rock strength is a critical parameter for the shear strength of broken ore materials as stronger particles under confinement may undergo either dilatancy as shear bands form within the broken ore, or fragment if the confining stresses suppress shear strength relative to the intact block strength. Hence, shear strength criteria that include the uniaxial compressive strength (σ_c or UCS) have been proposed (e.g., Indraratna et al. 1993). Thus, the UCS is considered as an input parameter in the methodology to evaluate ϕ' (sections 3.5 and 3.6).

3.2.1.2 Blocks strength heterogeneity

The broken ore within a draw column during caving might involve a mixture of variable block strengths owing to a mix of different lithologies. Mixtures of particles with different strengths in granular materials have not been extensively studied in terms of shear strength and compressibility heterogeneity. Intuitively, the shear strength of heterogeneous block mixtures will be controlled by the percentage of strong versus weak particles.

An interesting study was reported by Valdes & Leleu (2008), who conducted simple shear tests on combinations of two types of homogeneous sands: strong grains (rounded quartz) and weak sand (subangular calcareous). The authors found that the presence of weak grains affects the simple shear response of predominantly strong-grained sands. At low normal stresses, the stress-strain response is controlled by particle shape due to its control on dilation; at higher normal stresses the response and particle fragmentation are controlled by weak particle breakage.

D'Espessailles et al. (2014) also executed a simple shear testing program examining two angular sands sourced from mine blasting. The first type of sand was composed of strong particles (quartz and plagioclase feldspar), while the second was formed by weak particles (mostly orthoclase feldspar). Three types of samples were generated under a percentage of strong/weak particles of 100/0, 75/25 and 0/100. As expected, they found that the shear strength decreases under higher percentages of weak particles.

Furthermore, Wang et al. (2016) carried out triaxial compression tests on samples composed of both stronger (sandstone) and weaker (mudstone) particles finding similar results to those obtained by D'Espessailles et al. (2014). As depicted in Fig. 3.3, ϕ' experiences a gentle transition from the samples lacking weak particles through to samples with 100% weak particles. Hence, for practical purposes, these studies suggest that the ϕ' of a broken ore consisting of both strong and weak blocks with inter-block friction angles of ϕ'_{st} and ϕ'_{w}, respectively, could be approximated as a weighted average of the particle content (C) of both strong and weak particles as:

$$\phi' = \frac{\phi'_{w} \cdot C_{w}\% + \phi'_{st} \cdot C_{st}\%}{100} \qquad [3.2]$$

Finally, based on these studies, it can be interpreted that under low normal stresses where the behaviour of the broken ore under shear would be more dilative, intrinsic block properties such as size distribution and aspect ratio would have a greater influence on shear strength. At higher normal stresses (e.g. higher ore columns), where dilation is suppressed, block strength could play a more significant role in fragmentation of the broken ore. This interpretation should be considered as a first approximation because both studies were carried out on sands and the size scale effect (towards broken ore sizes) is not considered.

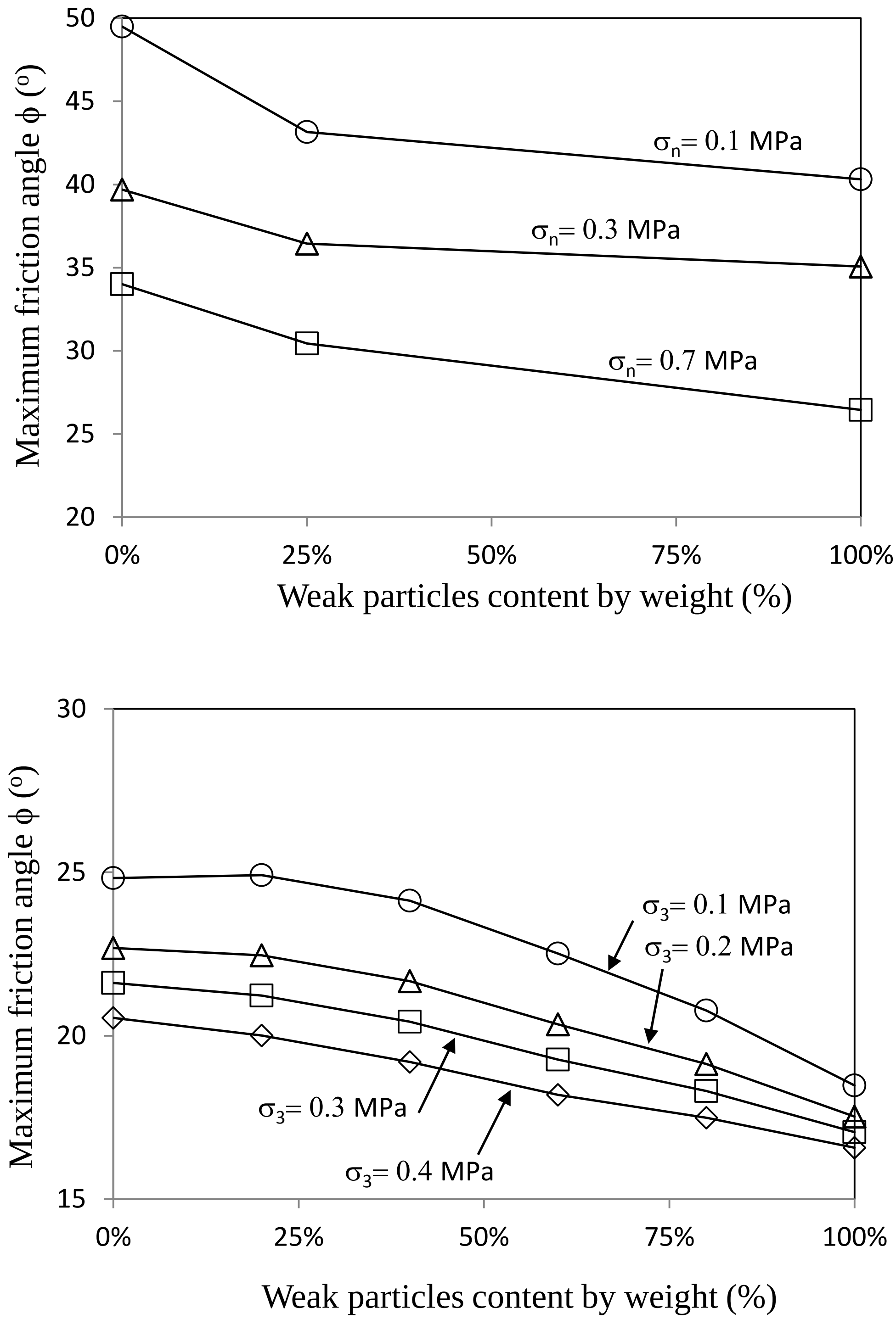

Fig. 3.3: Maximum interparticle friction angle affected by mixture of both strong and weak particles. Top: Data from D'Espessailles et al. (2014); Bottom: Data from Wang et al. (2016)

3.2.1.3 Block size distribution (BSD)

The BSD influences the shear strength depending on whether the broken ore is *uniform* in size (e.g. BSD at the upper draw column surface) or if the broken ore is w*ell graded (e.g. affected by secondary fragmentation)*. For instance, rockfill data from Marsal (1973) revealed that the interparticle friction angle increases under wider size distributions, but this change is also dependent on other properties such as bulk density and particle shape. In terms of broken ore materials, the BSD can be considered mostly uniform when blocks initially fall from the cave back (Chapter 2), but later, due to secondary fragmentation and fines migration process, the BSD evolves into a well graded distribution. Of interest is the role of rock-fall impact fragmentation in influencing a finer BSD, as well as block segregation occurring along the muckpile surface (rilling), which may contribute to a coarser size distribution in the plug-flow zone and a more uniform and finer gradation in the shear bands (Chapter 5).

3.2.1.4 Block shape

Block shape can also be relevant for the shear strength of broken ore materials. Block shape is characterized based upon *angularity* and *aspect ratio*. Broken ore materials tend to be very angular with a limited number of block faces. Conversely, the aspect ratio of broken ore materials can vary significantly, largely depending on the natural fracture network in the rock (i.e., in situ fragmentation). Also, higher aspect ratios (e.g. elongated and platy blocks) induce higher shear strengths, as they generate higher interlocking in between blocks. Furthermore, block shape would have relevance in increasing the shear strength of broken ore when the ore column is low (section 3.2.1.2). However, under moderate and high columns, blocks undergo secondary fragmentation within shear bands, which generates rounder and more spherical block shapes. This results in the interlocking properties of the block shape being strongly affected.

3.2.1.5 Block roughness

Block roughness has been considered as a primary parameter in the shear strength of rockfill by Barton & Kjaernsli (1981), which would also apply to broken ore materials. However, a detailed analysis of the influence of block roughness on shear strength is difficult due to the fact that this parameter varies with other block properties such as aspect ratio and angularity. Also, this parameter would only be relevant in the upper sections of a draw column because the block's roughness would gradually reduce due to the constant movement, rotation (attrition process) and abrasion of the blocks within the shear bands in a draw column.

3.2.1.6 Size scale effect

The experimental knowledge of coarse granular materials has been developed mostly with particle sizes ranging from gravel to rockfill, which are typically up to 20 to 30 cm in diameter. However, the size of broken ore materials can reach up to 1 m of average block diameter (Chapter 2). Thus, a scaling relationship is required to upscale gravel and rockfill properties to values that can be applied to broken ore materials. The most popular techniques to scale geotechnical properties from smaller to larger granular samples is based on the *parallel gradation method* or *parallel size distribution method* first proposed by Lowe (1964). This technique involves shifting the size distribution curve (on a semi-log plot) by a factor "S" to scale the small sample to that of the *in-situ* rock-pile material (Fig. 3.4). De la Hoz (2007) demonstrated that this technique is sufficient to scale gravels towards sands, but when scaling to samples with larger dimensions (e.g. rockfill) the strength and stiffness tend to decrease towards large sized particles due mainly to reduced particle strengths for larger sizes (Frossard et al. 2012). Also, other intrinsic block properties such as block shape and block roughness could also change due to scale effects. If so, the use of the parallel gradation method on broken ore materials must take into account this size scale effect. Particularly, the block strength reduction due to the size scale effect is considered in the methodology proposed to evaluate ϕ' in section 3.5 and 3.6.

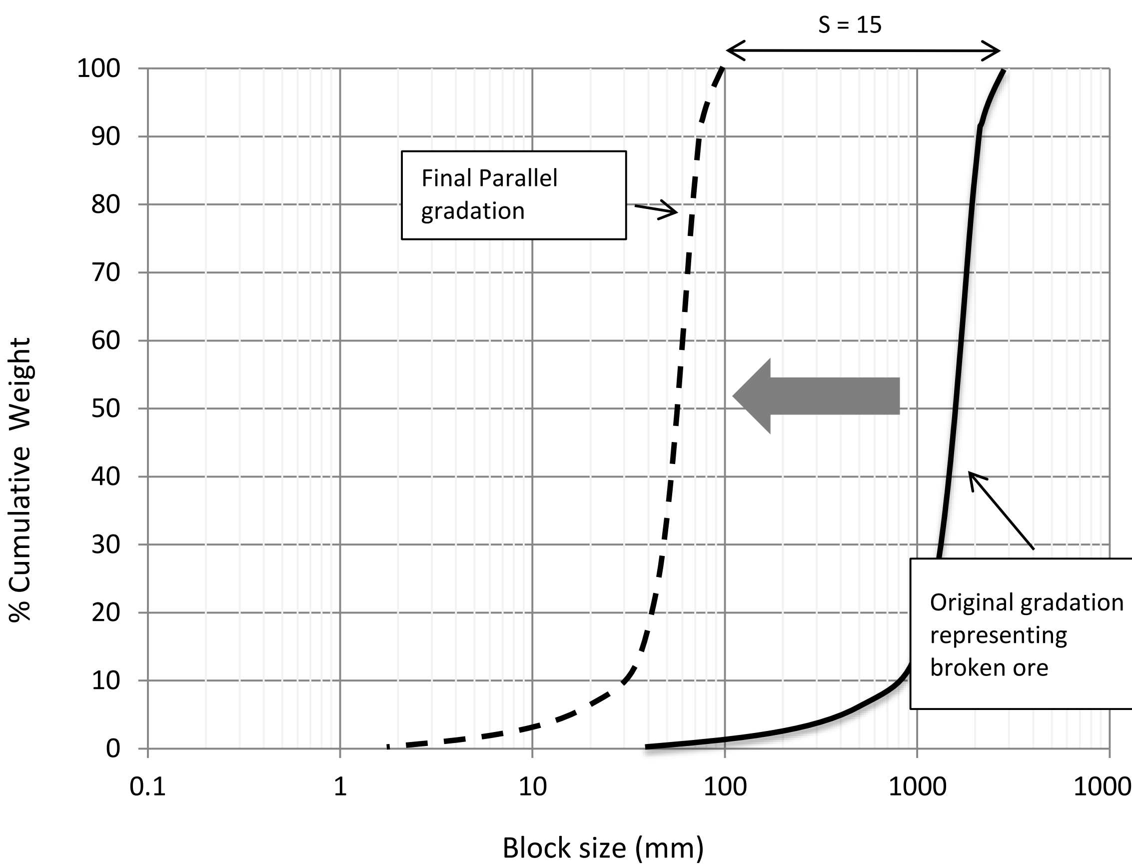

Fig. 3.4: Parallel gradation method applied on broken ore materials

3.2.1.7 Broken ore density (BOD)

Broken Ore Density *(BOD)* influences the shear strength of broken ore materials. As suggested in Chapter 2, loose packing broken ore (low density) would be found mostly within shear bands, and this will not likely have a critical effect on ϕ'. An exception is when a dense packing of broken ore comes from a far field and enters into the shear band, which would generate high dilatancy at the top of the near field, thus increasing ϕ'. However, as previously noted, this effect would rapidly diminish downward due to the constant movement and block rotation experienced by the broken ore within the shear bands.

3.2.1.8 Influence of water within draw columns

The influence of water is a significant variable to consider in the shear strength of broken ore. Although groundwater in block caving projects is generally drained during operation, ore columns could still be affected by water due to rainfall or snowmelt entering fractures, scarps and collapse structures when the cave daylights at surface. If so, the water and mud would reduce the effective stresses at the contacts between blocks within a draw column, enhancing sliding and reducing the overall broken ore shear strength. In addition, water could flow downwards and saturate the broken ore closer to the drawpoints. This situation could enhance mudrush risks in case of significant fines within the broken ore. This topic will be discussed in section 3.4.

3.2.1.9 Column compressibility over time

A draw column compression phenomenon could occur due to low draw rates or closed drawpoints (i.e., long broken ore residence times). This compressibility increases the BOD along the column, enhancing the shear strength of the broken ore. This phenomenon would be significant in cases of irregular draw sequencing under an interactive flow (Chapter 5), because the strength parameters of a draw column under operation will increase with adjacent columns affected by this compressibility process. Thus, this factor should be considered in advanced engineering design stages, as opposed to early stage feasibility and design.

3.2.2 Operational factors

Operational factors can indirectly affect the shear strength of broken ore materials. For instance, the *draw column height* is associated with the normal stresses acting on the broken ore, which in turn influences ϕ' assuming a nonlinear shear strength envelope. Higher *draw rates (*to maximize net profit*)* could promote a sizeable *air gap,* which in turn promotes rock-fall impact fragmentation, enhancing secondary fragmentation and modifying the BSD of the broken ore (section 3.2.1.3). *Draw sequencing* (e.g. non-uniform draw) may cause an irregular muck pile surface that in turn may result in rilling of large blocks downward into the centre of cone depressions that form over the drawpoints (Chapter 5). This will lead to concentrations of large size blocks, changing once more the BSD of the broken ore (e.g. coarser gradation in the plug-flow zone and finer gradation within the shear bands). The influence of these factors on the inter-block friction angle of broken ore material is discussed below and in sections 3.5 and 3.6.

3.2.2.1 Ore/draw column height

The draw column height directly influences the normal stress (σ_n) acting on the broken ore. The draw column height typically correlates with the height of the orebody. This parameter is considered in the methodology to evaluate ϕ' under both isolated movement zone (IMZ) and interactive flow cases in sections 3.5 and 3.6.

3.2.2.2 Air gap height

The air gap height not only controls the way the broken ore is initially packed in the draw column, via the ability of the blocks to detach and rotate from the cave back (Chapter 2), but also the impact energy and fragmentation experienced by the blocks based on rock-fall height (Chapter 5). In this case, a sizeable air gap helps in promoting impact fragmentation of blocks released from the caved back on the muckpile surface, which in turn could modify the BSD of the broken ore into a wider and finer size distribution, enhancing the inter-block friction angle (3.2.1.3).

3.2.2.3 Broken ore segregation

Under certain conditions, such as irregular draw (producing a cone-shaped free surface), large blocks can undergo segregation on the muckpile surface by rolling down to the centre of the cone (referred to as rilling). Within an IMZ, this process induces changes in the BSD in terms of promoting coarser size distributions in the plug-flow zone, and gradations without oversize blocks in the shear bands. This topic is discussed in Chapter 5 and a procedure to correct the BSD at the top of a draw column is provided.

3.2.2.4 Fines migration

The occurrence of fines migration during block caving is expected, especially under irregular extraction at drawpoints. The *fines percolation* is mainly vertical as noted by Pierce

(2009), while Hancock (2013) proposes that the majority of fines migration would occur within the shear bands. As introduced further in Chapter 6, two percolation mechanisms can be defined: *spontaneous* and *shear-induced* (Khola 2015). The former refers to when percolating particles are so small that they move down due to the action of gravity only, while the latter is associated with percolation due to continuous shearing. It is believed that fines migration contributes to the inter-block friction angle of broken ore materials in two ways: *fines acting to lubricating large blocks* and by promoting a *well-graded block size distribution*.

First, from the soil mechanics perspective, finer fractions in a sample of granular materials may reduce sliding resistance and subsequently lower the shear strength of broken ore. This is because fines lubricate larger particles, facilitating the sliding process (Lee 1986). Marsal & Fuentes de la Rosa (1976) found that the type of “fines” (sands or silts) within rockfill materials can result in marked shear strength variations. For instance, they concluded that in a mix of 70% rockfill and 30% silt, the overall shear strength was comparable to the shear strength of the silt. Of interest is that this result is in agreement with a shear strength model of coarse and fine grains mixed together first proposed by Siddiqi (1984) and complemented by Fragaszy et al. (1990). This model considers that if the granular material contains less than 40% of fines (in weight), large particles will control the strength due to their contacts among them. However, under a higher amount of fines, large particles will have the chance to *float* in this fine matrix and the strength will depend on both fine and coarse particles. Therefore, these results could be extrapolated to broken ore columns, especially closer to the drawpoints, because the strength of the broken ore within the shear bands could strongly decrease in the presence of sufficient amounts of fines (due to *percolation*) within the voids left by large blocks.

Second, a typical uniform broken ore size distribution within the shear bands at the top of a draw column will evolve into a well graded BSD along a shear band in the case of significant fines migration combined with the secondary fragmentation process (Chapter 6). A well graded BSD will increase the inter-block friction angle as noted in section 3.2.1.3. This topic is further discussed in sections 3.5 and 3.6.

3.2.2.5 Shear band thickness reduction due to secondary fragmentation and fines migration

As discussed in Chapter 6, the average size of the broken ore (d_{50}) within shear bands decreases under higher ore columns and so, the shear band thickness is also reduced (considering for example the relationship of 10 times D_{50} by Pierce 2009). Thus, it is expected that the shear band thickness reduction would induce a finer and more uniform size distribution of the broken ore, reducing the final value of ϕ'.

3.3 Laboratory Tests to Evaluate the Inter-Block Friction Angle of Broken Ore Materials

A literature review of shear strength tests derived from a soil mechanics perspective is carried out below, and applied to the shear strength of broken ore. Based on this literature review, *large triaxial tests* are expected to represent the broken ore shear strength and so, data from these laboratory tests is used to develop a procedure to evaluate ϕ' in section 3.5 and 3.6.

3.3.1 Background on shear strength tests applied to broken ore materials

Several laboratory testing devices are available to assess the interparticle friction angle of granular materials, most of which are undertaken as part of standardised testing: Direct shear (ASTM D3080 / D3080M – 11); Triaxial compression CID (ASTM D7181 – 11); Simple shear (ASTM D6528 – 07); Annular ring shear (D7608 – 10); Torsional hollow cylinder (Ampadu & Tatsuoka 1993), and plane strain (Marachi et al. 1969, Marsal 1973). Due to the large shear displacement experienced by the broken ore in the outer periphery of a draw column, *ring shear* would seem to be the ideal test to evaluate the shear strength of broken ore materials within the shear bands. However, the ring shear device was designed to test sand and gravels which greatly differ from broken ore materials when employing the parallel gradation method (3.2.1.6).

Of interest is that the maximum interparticle friction angle derived from ring shear tests for sands, which have been reached shear strains close to 30% (Coop et al. 2004, Luzzani & Coop 2002). Thus, taking into account this reduced shear deformation (in comparison with the large shear deformations being experienced by broken ore within shear bands), other shear devices limited to smaller shear strains (e.g. 20%) but able to test larger size materials, for example using *large triaxial compression* or *large plane strain* (capable to test particles up to 17 cm diameter), could be more representative to evaluate the inter-block friction angle of broken ore materials. Thus, large scale tests appear to be a valuable means to assess ϕ' of broken ore materials, although any large scale laboratory testing is inherently difficult, time consuming, and expensive.

3.3.2 Large triaxial compression and plane strain tests

Various large scale shear tests have been reported in the literature, including *large triaxial compression tests* by Marsal (1967), Marachi et al. (1969), Marsal (1973), and Valenzuela (2008) among many others, and to a much lesser extent *large plane strain tests* by Marachi et al. (1969), Becker et al. (1972) and Marsal (1973). These tests have provided invaluable data related to the shear strength of rockfill and coarse granular soils such as that represented by the Leps' chart (1970) and the Barton & Kjaernsli shear strength criteria (1981). Due to the preferential sliding of mass flow through shear bands (outer periphery) towards the drawpoints, the internal deformations experienced by broken ore might be better represented by a plane strain test rather than by a large triaxial compression test. However, the large amount of data on large triaxial tests generated to date allows the development of acceptable relationships to estimate the inter-block friction angle of broken ore materials. Then, these tests will be complemented with large tilt rockfill test data (Fig. 3.5), which allows evaluation of the shear strength of broken ore materials at very low stresses.

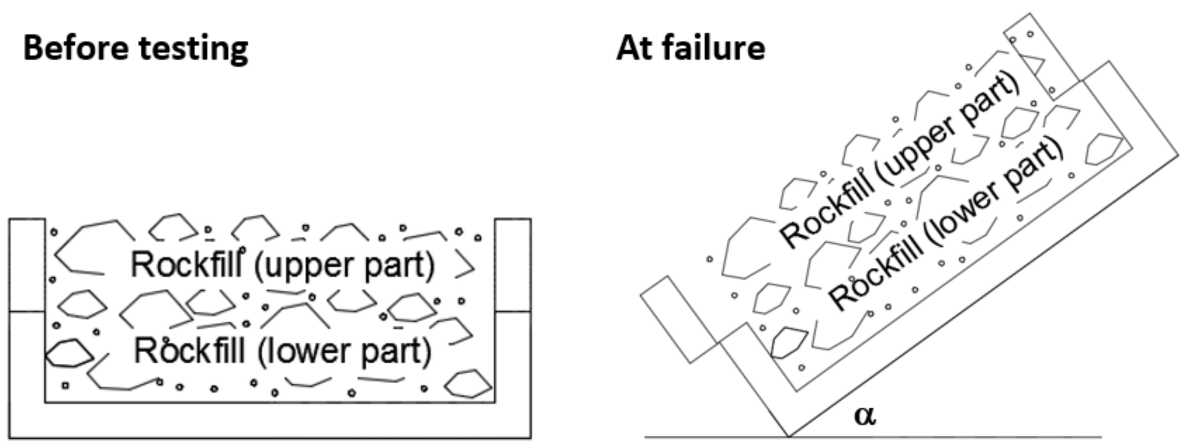

Fig. 3.5: Tilt test on rockfill. Adapted from Barton (2013)

3.4 Methodology to Evaluate ϕ' For Broken Ore Material – Key Considerations

A methodology to evaluate ϕ' for both IMZ and interactive flow under early stage design is presented in section 3.5 and 3.6, including its application to an ideal case study in section 3.7. Several considerations need to be outlined.

- A value of UCS is required for the broken ore material and this value needs to account for scale effects, as recommended via equation 3.5. An exception is the use of the Barton & Kjaernsli (1981) relationship (equation 3.4), which includes its own chart to scale the block strength.
- In the case of mixed broken ore with different block strengths, equation 3.2 can be considered.
- The block size distribution (BSD) is not explicitly accounted for in this methodology. However, the BSD is an important parameter in more advanced engineering design stages.
- Block shape is not an independent variable in this methodology. The relationships and charts presented are based on angular and subangular particle shapes in order to represent broken ore materials.
- Block roughness is only considered based on ϕ_b in equation 3.4 for broken ore materials under low σ_n.

- The parallel gradation method is not used in this methodology (due to the fact that the BSD is also neglected by this methodology). Note that it should be considered in more advanced engineering stages.

- The BOD is required to evaluate the far field overburden and then the σ_n on the boundary between the far and near field zones (equation 3.6). Also, the BOD is used to evaluate σ_v close to the drawpoints.

- The influence of water within a draw column is not considered explicitly in this methodology. However, a rock strength reduction due to moisture and its effect on strength degradation can be considered (e.g. UCS test data involving saturated specimens).

- Regarding operational factors, the ore column height is the only independent parameter used in both IMZ and interactive flow. Other variables such as broken ore segregation at the top of a draw column, fines migration, and shear band thickness reduction are required for higher level design studies.

3.4.1 Variables to evaluate ϕ' not considered by the methodology

Several factors influencing ϕ' not included in this methodology, which should be considered in advanced design engineering stages, are:

- The influence of *water* on the inter-block friction angle of broken ore is disregarded in this methodology due to its complexity (as briefly discussed in section 3.2.1.8). For strong and moderate broken ore materials, water promotes block sliding, which can reduce its overall bulk shear strength. It is important to note that water combined with a sufficient amount of fines can generate mudrush risk. In such cases where this hazard may be present, the influence of water should be considered in advanced design stages.

- *Influence of fines on broken ore strength close to drawpoints*: as noted in 3.2.2.4, fines between a set of large blocks may contribute to a notably reduced inter-block friction angle because they can act to lubricate the large blocks, facilitating the sliding process. This methodology does not consider a broken ore shear strength reduction, due to the lack of studies related to this theme. This factor should be considered in higher level engineering designs, when broken ore size distributions would be available and the amount of fines present can be evaluated.

- Finally, the *block size distribution (BSD)* of broken ore materials is a fundamental parameter in the assessment of ϕ'. Typically, a BSD evolves from a uniform gradation in the upper part of the draw column to a well graded gradation along the shear bands due to secondary fragmentation and enhanced by fines migration. Although a methodology to evaluate the BSD for broken ore materials during block caving is proposed in Chapter 6, insufficient data is available in the literature to include the BSD as an independent parameter in the methodology to evaluate ϕ' proposed in section 3.5 and 3.6. However, it is highly recommended to consider this parameter for higher level design stages (e.g. detailed design) together with the key factors that influence the BSD such as rilling, dilution, and rock fall fragmentation. Thus, the BSD can be corrected within a draw column and supported by laboratory testing to provide a more accurate assessment of the shear strength properties of broken ore.

3.5 Methodology to Evaluate ϕ' For Broken Ore Material - Isolated Movement Zone (IMZ)

This section presents a procedure to evaluate ϕ' under an IMZ, as represented in Fig. 3.6. Important considerations such as the reduction of vertical stress close to the drawpoints are also included in this section, which allows estimation of ϕ' under a wide range of normal stresses (σ_n). A flow chart for this purpose is included in Fig. 3.7.

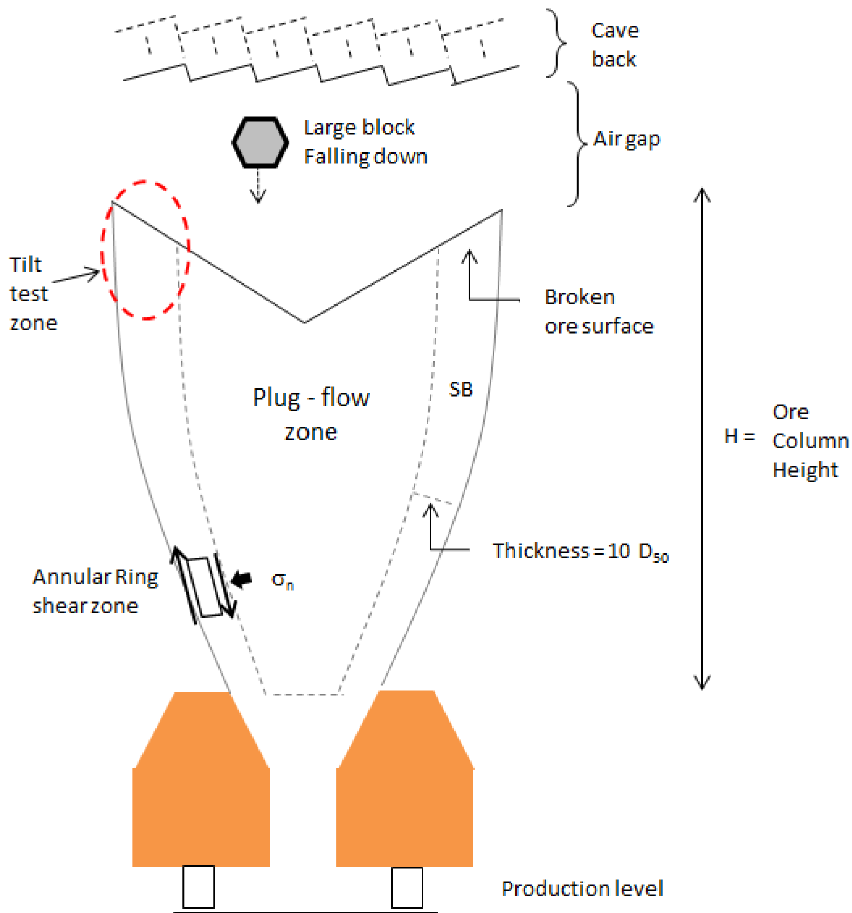

Fig. 3.6: Draw column scheme. Tilt test and annular ring shear test representing the shear strength on broken ore within an IMZ.

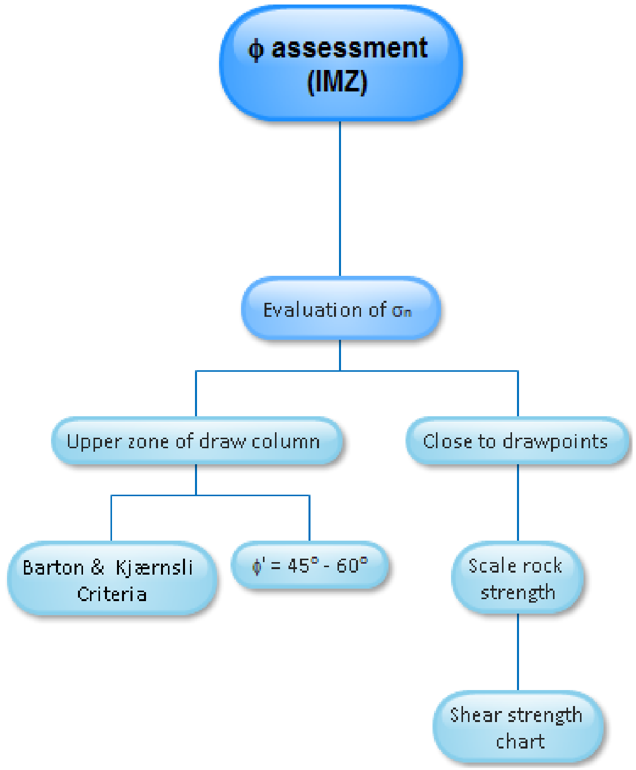

Fig. 3.7: Flow chart. Isolated movement zone (IMZ)

3.5.1 Relation between σ_v and column height (H)

As discussed previously, ϕ' is strongly dependent on the normal stress (σ_n) acting on the broken ore within the shear bands as shown previously in Fig. 3.7, assuming a non-linear shear strength envelope is appropriate. For an IMZ condition, a stress assessment using the Janssen formula (1985, 2004) could be performed as recommended by Castro et al. (2014). This equation relates σ_v to ϕ', Ko (lateral earth pressure coefficient) and R_h (hydraulic ratio):

$$\sigma_v = \frac{R_h \cdot \gamma}{K_o \cdot \tan\phi'}\left(1 - e^{\frac{-K_o \cdot (\tan\phi') \cdot H}{R_h}}\right) \qquad [3.3]$$

Of interest is that Pierce (2009) found that stress rotation occurs near the drawpoint, within 16 times the average block size at the drawpoint, which means that broken ore close to drawpoints can undergo an isotropic stress condition. Hence, this finding can be interpreted as the vertical stress σ_v approximately corresponding with the normal stress σ_n acting on the broken ore within the shear bands close to the drawpoints; assuming a non-linear shear strength envelope, σ_n can then be used to assess ϕ' in section 3.5.3. Since σ_v depends on ϕ' (equation 3.3), it is recommended to first define an estimate ϕ' (e.g. 40°) and then evaluate σ_v. Hence, after the evaluation of ϕ', σ_v could be calculated again and an iterative process could continue if necessary.

3.5.2 Assessment of ϕ' under low σ_n (upper zone of draw column)

The inter-block friction angle ϕ' of the broken ore in the upper sections of the draw column s (i.e., under low normal stresses) can be approximated by means of a large tilt test (Fig. 3.5), such as that used in rockfill characterization. However, as introduced in section 3.3, any large test program is expensive, time consuming and sometimes unfeasible. Thus, literature regarding large tilt and triaxial tests has been compiled and presented below to develop relationships to estimate ϕ' for early stage designs on block cave projects.

A well-known shear strength criterion was proposed by Barton & Kjaernsli in 1981. This criterion was intended to be used for rockfill and it is represented by Equation 3.4:

$$\phi' = R \cdot \log(\frac{S}{\sigma'_n}) + \phi_b \qquad [3.4]$$

where ϕ' is the friction angle of the rockfill, σ_n is the effective normal stress, S is the equivalent particle strength obtained from (Fig. 3.8 a) and the parameter R is the equivalent roughness (Fig. 3.8.b). About the parameter R, an important consideration regarding the use of *rockfill porosity* values is the fact that the broken ore size distribution in the upper part of a draw column can be highly uniform with a uniformity coefficient (C_u) ranging from 1 to 3 (Chapter 2). Finally, ϕ_b is the basic friction angle; although ϕ_b is a key parameter in estimating the friction angle of rockfill there is a lack of sources and related literature to reliably estimate this parameter. Barton & Kjaernsli (1981) suggested values from 25^o to 35^o. Also, Alejano et al. (2012) conducted a useful literature review of basic friction angle of several types of rock and suggested that for intrusive rocks, ϕ_b ranges between 29^o and 38^o. In addition, Grasselli & Egger (2003) estimated ϕ_b of 34^o for fresh granite.

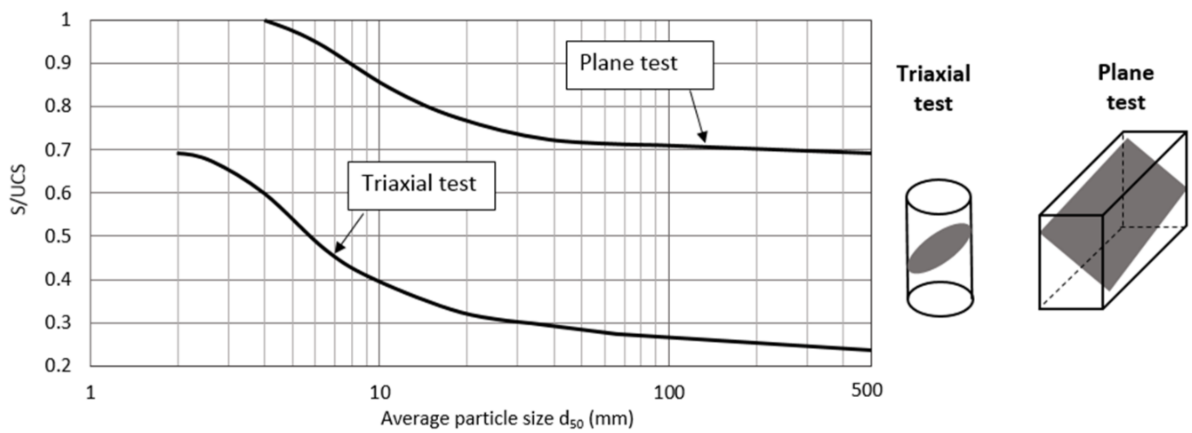

a)

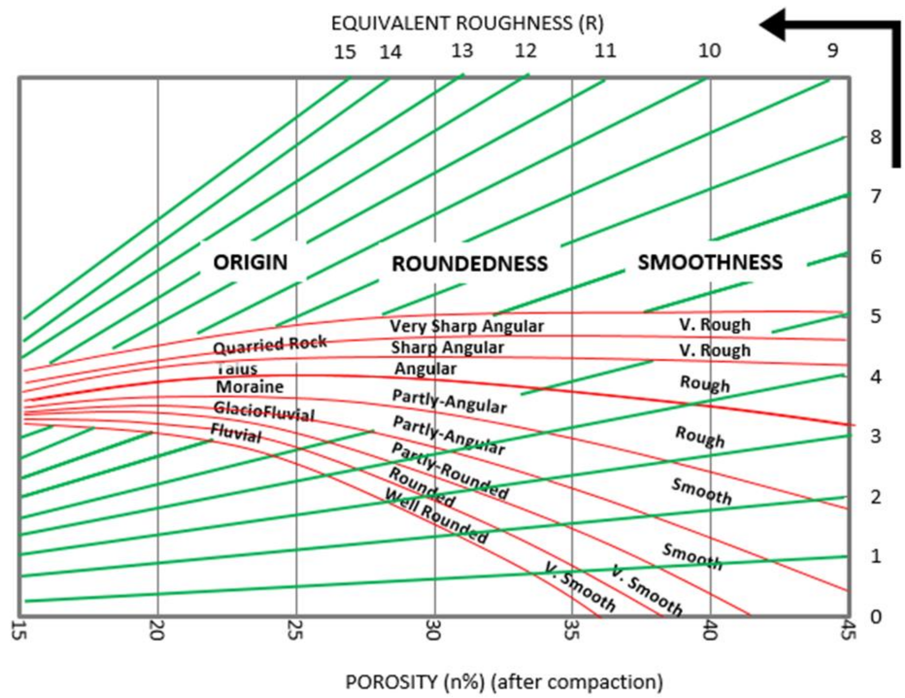

b)

Fig. 3.8: (a) Equivalent particle strength S. (b) Equivalent roughness R. Adapted from Barton and Kjærnsli (1981)

Although limited data on rockfill tilt tests is available in the literature, a large amount of data can be found on triaxial compression tests conducted mainly on ballast materials. Valuable large tilt tests on marble from a waste rock material were conducted by Iabichino et al. (2014) resulting in values ranging from $\phi' = 46.7^o$ up to 57.5^o under normal stress (σ_n) lower than 0.1 MPa. A key characteristic of the tilt tests is the very low σ_n generated on the sample (just the overweight of the upper part of the sample) which strongly influences ϕ'. Also, interparticle friction angles higher than 60^o have been reported on ballast materials (Ionescu 2004) and interparticle friction angles on large triaxial tests between 45.6^o to 53.3^o under low confining stresses of $\sigma_3 = 0.02$ to 0.04 MPa (Marsal 1973). Hence, it is practical to consider an interparticle friction angle under low σ_n ranging from 45^o to 60^o.

Therefore, a rough estimation of the inter-block friction angle assessment under low normal stresses could be carried out by the Barton & Kjærnsli methodology or considering an approximate range between 45^o to 60^o.

3.5.3 Assessment of ϕ' under higher σ_n (along shear band of an IMZ)

The broken ore shear strength, assuming a nonlinear strength envelope, can decrease significantly depending on the normal stress σ_n. Leps (1970), Duncan & Chang (1970) and Barton & Kjaernsli (1981) have proposed that the maximum interparticle friction angle decreases in a logarithmic scale with σ_n (see Fig. 3.2c). Thus, in order to apply this relationship to broken ore materials, a compilation of various studies involving large triaxial tests under angular/subangular rockfill and waste rock materials published by different authors from 1967 to date is presented in Table 3.1. In Fig. 3.9 this data for strong and medium strong rocks is presented and subdivided based on their uniaxial compressive strength under a threshold of 125 MPa. Weak broken ore materials can also occur within a draw column. However, no significant data is available to generate acceptable correlations to evaluate ϕ'. Several triaxial compression tests on rockfill and gravels are depicted in Fig. 3.10 as a reference to evaluate roughly the inter-block friction angle under weak broken ore materials. These charts allow evaluation of the inter-block friction angle of broken ore under moderate and high σ_n (0.1 to 1 MPa and 1 to 5 MPa respectively).

Table 3.1: Materials associated with interparticle friction angles in Fig. 3.9. Overall (arithmetic) average D_{50} is 36 mm.

Author	**Materials**	**D_{50} (mm)**
Marachi et al. (1969)	Crushed material (Basalt)	38
Becker et al. (1972)	Venato (Sandstone)	40
Marsal (1973)	El infiernillo (Silicified Conglomerate)	50
	El infiernillo (Diorite)	60
	Malpaso (Conglomerate)	25
	San Francisco (Basalt)	10
Contreras (2011)	Fresh waste rock (Porphyry and Granodiorite)	36
	Leached waste rock (Granodiorite)	36
	Crushed waste rock (Granodiorite)	72
Palma et al. (2009)	Porphyry	32
	Granodiorite	22
Dorador (2010)	E.R (Weathered Andesite)	38
	R.L (Granodiorite)	15

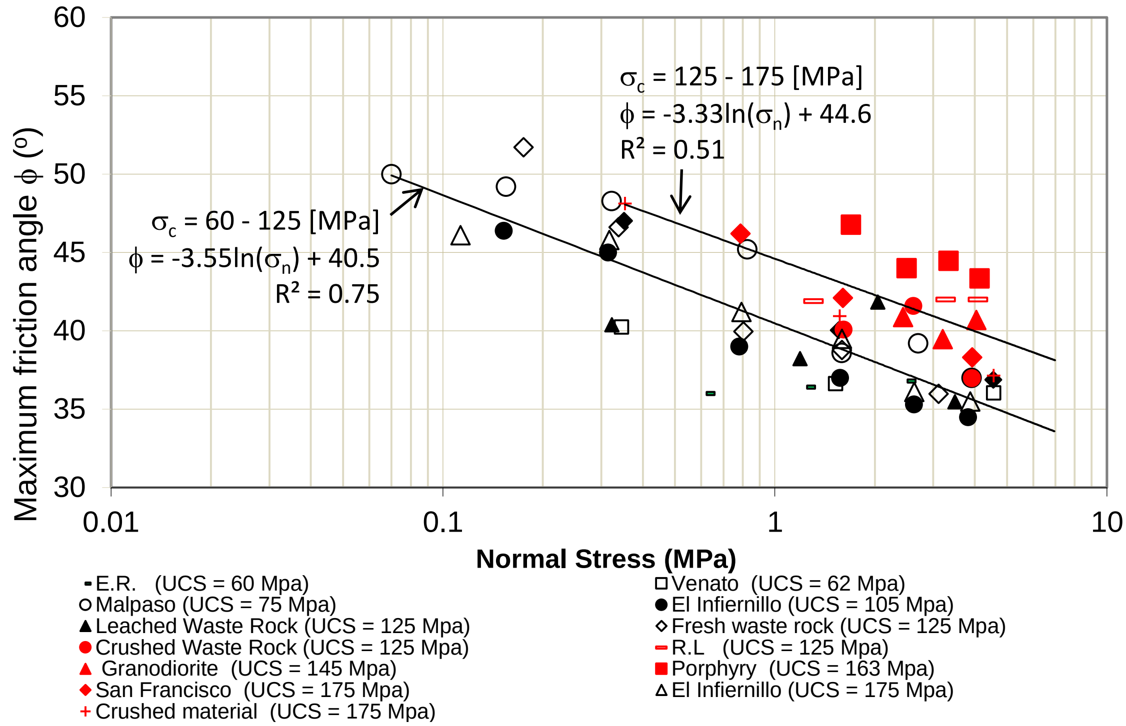

Fig. 3.9: Inter-block friction angle under different intrusive rock types (see Table 3.1).

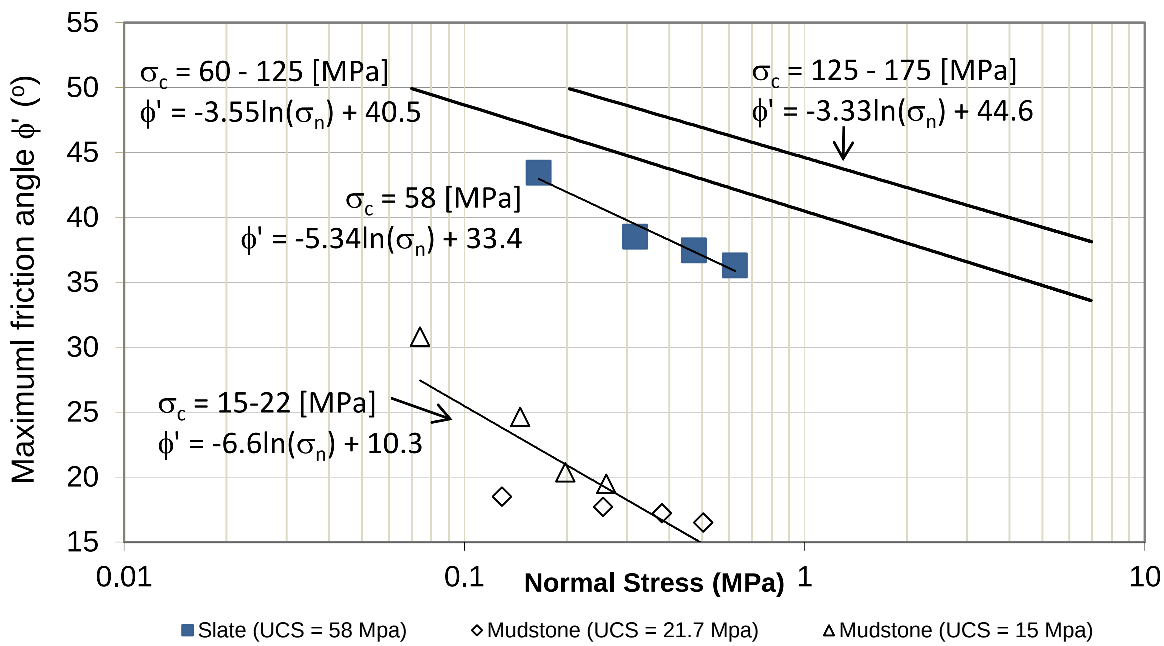

Fig. 3.10: Inter-block friction angle for strong and weak broken ore materials. Different authors (see Table 3.2)

Table 3.2: Materials associated with inter-block friction angles in Fig. 3.10

Author	**Materials**	**D_{50} (mm)**
Wang et al. (2016)	Mudstone	2.5
Chen et al (2014)	Mudstone	22
Charles & Watts (1980)	Slate	5

Finally, based on the proposed correlations, ϕ' could reach values higher than 60° and lower than 35° for medium to strong rock types, depending on σ_n. ϕ' can also notably vary depending on rock strength with values between 50° and 15° under moderate σ_n (σ_n between 0.1 to 1 MPa, respectively). Thus, these results suggest that σ_n and UCS are the two key parameters to consider in evaluating ϕ' under early-stage engineering design.

3.5.4 Rock strength scaled by size

An additional factor to consider is related to the reduction in intact strength of rock due to size effects, especially when the broken ore material is subjected to moderate and high normal stresses. For instance, correlations of data involving moderate to strong broken ore materials presented in Fig. 3.9 are made with respect to uniaxial compressive strength (ASTM D7012 – 14) and overall particle size (D_{50}) of 36 mm (see Table 3.1). For this, σ_c needs to be scaled to block sizes appropriate for broken ore materials (e.g. D_{50} of 0.5 m or 1 m diameter). Similar associations should be carried out for weak broken ore materials (Fig. 3.10 and Table 3.2). Hence, in order to scale the strength for larger sizes, the formulation by Yoshinaka et al. (2008) can be used:

$$\frac{\sigma_c}{\sigma_{c.0}} = \left(\frac{d_e}{d_{e.o}}\right)^{-k} \quad [3.5]$$

where σ_c is the uniaxial compressive strength associated with an equivalent length $d_e = V^{1/3}$, V is the block volume, $\sigma_{c.o}$ is the uniaxial compressive strength associated with an arbitrary length $d_{e.o}$, and k is an empirical rock parameter.

3.6 Methodology to Evaluate φ' For Broken Ore Material - Interactive Flow

Under an interactive flow, both *near field* and *far field* conditions are generated during block caving (which is depicted in Fig. 3.1). Near field conditions are assumed here to correspond to broken ore within 50 to 100 m of the drawpoints. In this case, the gravitational flow is governed by Pierce's model (2009) which includes a plug-flow compression zone and an outer peripheral shear band. On the other hand, far field conditions are associated with a geostatic stress state. A flow chart to estimate φ' is provided in Fig. 3.11.

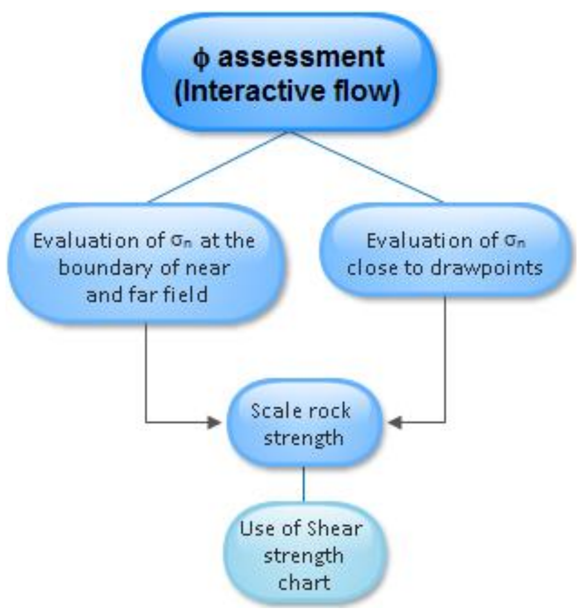

Fig. 3.11: Flow chart to evaluate φ'. Interactive flow

3.6.1 Inter-block friction angle assessment

In order to evaluate the inter-block friction angle in the shear bands within the *near field*, the same procedure carried out in section 3.5 can be employed. This first requires the evaluation of σ_n of the broken ore along the shear bands. In the upper part of the shear bands, σ_n can be estimated assuming a geostatic condition (assuming that a broken ore element will retain its stress condition from the far field). Hence, σ_n can be assumed as:

$$\sigma_n = \gamma \cdot H \cdot K_o \qquad [3.6]$$

where, γ' is the bulk density of the broken ore in the far field; *H* is the far field height and Ko is the lateral earth pressure coefficient of the broken ore (Ko = 1- sin ϕ').

Conversely, the normal stresses acting on the broken ore in the lower part of the shear band can be estimated assuming isotropic conditions in the draw column as would be expected close to the drawpoints (section 3.5.1). Hence, the vertical stress can be estimated and equated to σ_n as previously applied in Section 3.5. The strength reduction of individual rock blocks due to size effects can also be carried out if required. Therefore, the inter-block friction angle of broken ore can be evaluated considering both ranges of σ_n from the upper and lower zone of the shear band, rock strength scaled by size (section 3.5.4), and using the relationships shown in Fig. 3.9 and Fig. 3.10.

3.7 Application of Methodology to Evaluate ϕ' For Broken Ore Material

3.7.1 Assessment of ϕ' under IMZ

A sample calculation is included in this section to demonstrate the procedure developed to estimate ϕ' under an IMZ. Consider the following input values, which represent typical block caving design parameters: Ore column height (H) = 300 m and R_h = 11.5. Assumed are the following broken ore properties: BOD = 1.7 t/m^3 (porosity of 0.37), average block diameter (D_{50}) = 736 mm, and UCS = 133 MPa (associated with a test sample 70 mm in diameter and 140 mm in height). Using equation 3.5, together with d_e = 58.1 mm and k = 0.25 (diorite) the UCS is scaled to 70.5 MPa. In the upper zone of a draw column, the Barton & Kjaernsli criteria can be used. Thus, based on Fig. 3.8, R = 6, S/σ_c = 0.2 and then, S = 26.6. Considering a low normal stress of 0.1 MPa and ϕ_b = 30^o, a final ϕ' **= 44.5^o** is obtained using equation 3.4. Regarding the assessment of ϕ' close to the drawpoints, σ_n can be evaluated using equation 3.3. Considering the next parameters: H = 300 m (total height), ϕ' = 44.5^o (obtained for the upper zone of the draw column); Ko = 0.30; BOD = 1.7 t/m^3 and R_h = 11.5, σ_n = 0.78 MPa. Thus, using Fig. 3.9 a value of ϕ' **= 41.4^o** is obtained.

3.7.2 ϕ' assessment under interactive flow

A second sample calculation is provided in this section in order to evaluate ϕ' based on the flow chart from Fig. 3.11 for an interactive flow case. The inputs are as follows: Ore column height (H) = 300 m; near field height = 75m; far field height = 225 m and R_h = 11.5. The broken ore properties are: BOD = 1.7 t/m^3, average block diameter (D_{50}) = 736 mm, UCS

= 133 MPa, d_e = 58.1 mm and k = 0.25 (diorite). Again, the UCS is scaled to 70.5 MPa. Considering the boundary between the near and far field, it is assumed ϕ' = 45^o; then Ko = 0.29 and using equation 3.6, σ_n = 1.12 MPa. Therefore, using a scaled UCS of 70.5 MPa, σ_n = 1.12 MPa and Fig. 3.9 ϕ' = 40.1 is obtained. This value of ϕ' = 40.1 can be used again as an input of Ko and using equation 3.6, σ_n = 1.36 MPa is obtained. Finally, using Fig. 3.9, ϕ' is 39.4^o and after one more iteration it converges to a value of **39.3^o.** Regarding ϕ' close to the drawpoints, σ_n can be evaluated using equation 3.3. Using the next inputs: H = 300 m (total height), ϕ' = 39.3^o; Ko = 0.37; BOD = 1.7 t/m^3 and R_h = 11.5, a value of ϕ' **= 42^o** is obtained. The increase of ϕ' is explained due to the σ_n reduction close to the drawpoints.

3.8 Discussion of Methodology to Evaluate ϕ' For Broken Ore Material

A simple guideline has been presented to evaluate the inter-block friction angle (ϕ') of broken ore materials during block caving. Particularly, two factors influencing ϕ' need to be further discussed:

- *Block roughness and block shape:* as discussed in 3.2.1.5, *block roughness* would only affect the inter-block friction angle in the upper part of a draw column; this guideline suggests estimating ϕ' based on the Barton & Kjaernsli criteria (Section 3.5.2, which implicitly considers the roughness based on parameter R). Nevertheless, in the case of estimating ϕ' for advanced engineering design, the roughness should be a parameter to take into account. Regarding *block shape*, the data used in this work is based on angular to subangular rockfill and waste rock particles, which fairly represent the block shape of broken ore materials. This is because rockfill can contain a larger amount of block faces than broken ore, which affects the packing properties (as noted in Chapter 2).

- *Broken ore strength heterogeneity*: as discussed in section 3.2.1.2, equation 3.2 has been recommended to evaluate ϕ' for early stage design under a broken ore comprised of two different lithologies. However, the influence of broken ore strength heterogeneity on ϕ' is a more complex phenomenon which covaries with other broken ore properties, mainly with the block size distribution, block shape and presence of water. This factor should be considered in advanced design stages based on results from a tailored laboratory testing program.

3.9 Summary and Key Findings

The assessment of geotechnical properties of broken ore materials are critical to the success of a block caving operation. Amongst these, the *inter-block friction angle* (ϕ'), is of key importance given its decisive influence on the gravitation flow of the broken ore during draw. Despite its importance, there is a lack of standard methodologies to quantify this parameter. Although a number of block properties and operational factors influence this parameter, two key variables have been identified in this chapter as being especially important: i) the *normal stress*, due to the nonlinear strength envelope that characterizes broken ore, and ii) the *strength properties* of the broken ore.

This chapter presents an empirical methodology, together with guidelines on its use, for evaluating ϕ' for broken ore materials based on data compiled from shear tests on rockfill and waste rock materials. The methodology accounts for both isolated movement zones (IMZ) and interactive flow behaviour in the draw columns. It is concluded that ϕ' varies along a draw column, reaching values higher than 60° for stronger blocks under low confining stresses, but lower than 30° for weaker blocks and/or under higher confining stresses. These values are based on the mechanistic postulation that the shear strength of broken ore is non-linear, with ϕ' being strongly dependent on whether the normal stresses (σ_n) acting on the broken ore (equated to draw column height) are high enough to suppress dilation relative to the intact block strengths. Hence, emphasis is placed on reliably estimating σ_n, taking into account the vertical stress reduction occurring in the draw column closer to the drawpoints.

Hence, this work provides a new approach for assessing the inter-block friction angle of broken ore. Its empirical nature makes it appropriate for early level feasibility studies of large block caving projects. Others parameters such as block size distribution, presence of water, column compressibility over time, fines lubricating large blocks, broken ore density, block shape, and block roughness are also of importance to, but they do not have as strong an influence on ϕ' as does σ_n or block strength.

Chapter 4: Experimental Investigation of Secondary Fragmentation and Hang-Up Potential in the Compression Zone of a Draw Column during Block Cave Mining [3]

4.1 Introduction

Rock mass *fragmentation* related to block caving is critical to ensure an optimal broken ore size distribution at the drawpoints during extraction. If too fine, narrower draw columns might develop, limiting interaction between columns and promoting preferred flow paths that might leave valuable ore behind or rapidly introduce dilution (a phenomenon described as rat holes by Laubscher 2003). Laubscher also indicates that a uniformly fine fragmentation increases the potential for mud flow hazards. Conversely, if the fragmentation is too coarse, large blocks will severely impact operations by impeding material handling and causing costly production delays to clear hang-ups at the draw points. This in turn may be accompanied by potential damage at the drawpoints along the brow due to secondary blasting if required to clear the hang up.

The fragmentation process in caving operations has been identified by Laubscher (1994) and later by Eadie (2003) who proposed three components: *in-situ*, *primary* and *secondary* fragmentation.

[3] Dorador L, Eberhardt E, Elmo D. Experimental Investigation of Secondary Fragmentation and Hang-Up Potential in the Compression Zone of a Draw Column during Block Cave Mining. (In review).

In-situ fragmentation refers to the blocks formed by the spacing, persistence and interconnectivity of the natural discontinuities present in the rock mass prior to mining. *Primary fragmentation* occurs after undercutting and the initiation of the caving process, where changes to the in situ stresses result in the generation of new stress-induced fractures and further fragmentation of the in-situ blocks. The release of these blocks from the cave back then contributes to further *secondary fragmentation* due to rock-fall impact and the subsequent breakage of these fragments as they move down through the draw column in response to ore extraction from the drawpoints below. This vertical movement of the broken ore is accompanied by shear and compression stresses developing within the broken ore, which results in additional secondary fragmentation in terms of corner rounding, crushing and splitting of irregular shaped blocks.

Although a number of studies related to secondary fragmentation are available in the literature (e.g., Laubscher 1994, Esterhuizen 2005, Pierce 2009, Pierce et al. 2010), an understanding of the change of the block size distribution is not well understood (Brown 2007). This is due in part to the complex mechanisms and interactions involved and the numerous factors that influence them. For example, the broken ore size distribution at the surface of the draw column is a function of the in-situ and primary fragmentation. The former is controlled by the spatial characteristics of the discontinuity network (e.g., orientation, spacing, persistence, interconnectivity, etc.), together with the presence of lithological contacts, faults, tectonic damage zones, and hydrothermal alteration. The latter is controlled by the rock mass characteristics, including the intact rock strength and presence of non-persistent discontinuities, veining and rock bridges, together with the in-situ stress state and stress redistribution during undercutting (e.g. abutment stresses) and operations (i.e., caving). These factors subsequently influence the secondary fragmentation, first via their control on the initial block size, shape and density distributions at the top of the draw column, and then through the influence of embedded small, non-persistence discontinuities, veins and stress-induced damage within the blocks that promote easier fragmentation as the material flows downwards during draw. Superimposed on these are several operational factors that can further have a significant effect on the secondary fragmentation including: column height (i.e., vertical loading), draw rate, draw sequence, air gap thickness, undercut design, and the presence of water and/or water management. Given this complexity, Chitombo (2010) and Eberhardt et al. (2015) identified secondary fragmentation as a key topic requiring further research if the next generation of larger and deeper caving operations will meet with success.

Pierce (2009) defined the volume of mobilized broken ore associated with each individual drawpoint as the Isolated Movement Zone (IMZ). This is in contrast to the surrounding stationary material referred to as the stagnant zone. The same author also proposes that the IMZ can be characterized by a central compression zone, also referred to as the plug-flow zone, surrounded by an outer shear band zone (Fig. 4.1). These conditions arise when the IMZ diameter is greater than 20 mean particle diameters (an inverted cone develops when the IMZ diameter is less than 20 mean particle diameters; Pierce, 2009). The central plug-flow zone takes relevance because oversize blocks (>2m^3) tend to concentrate there. This is due in part to the rilling of oversize blocks along the top surface after they fall from the cave back and roll down into the central inverted cone (as depicted in Fig. 4.1). It is also due to the types of loading experienced by the block fragments in the compression zone. Although an IMZ can occur during block caving, the practice indicates that large draw columns (e.g. 200 m) can be working simultaneously (*interactive flow*), which in turn can be divided into a *far field* and *near field* (Fig. 3.1).

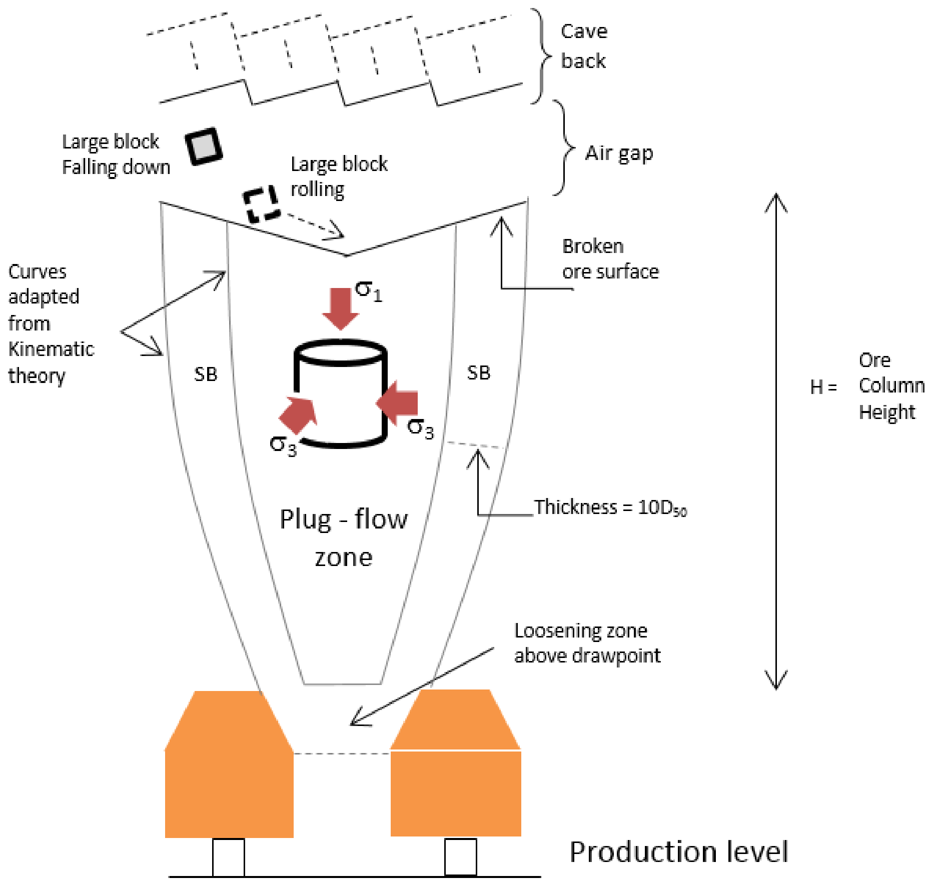

Fig. 4.1: Draw column scheme. SB = Shear band

This chapter investigates the influence of loading and compression in the central plug zone, and their influence on block size distribution with focus on oversize blocks. As previously noted, the presence of oversized blocks can have a significant impact on operations due to difficulties and inefficiencies in material handling by LHD loaders, or temporary closer of drawpoints and disruptions to production to dislodge hang-ups. Here, we explore secondary fragmentation generated within the compression zone through a series of controlled laboratory experiments designed to simulate broken ore moving down through a draw column of increasing height.

4.2 Review of Factors Influencing Secondary Fragmentation of Broken Ore

This section explores the factors and variables affecting the secondary fragmentation within a plug-flow zone in a draw column. These are divided into: intrinsic properties, state variables, and operational factors. Mops of these factors are depicted in Fig. 1.6.

4.2.1 Intrinsic properties of broken ore

4.2.1.1 Block shape and size distributions

Initial block shape and size distributions define the starting point for the block size distribution later encountered at the draw point. Block shape distribution is important as blocks that are more elongated than cubical have a significantly increased likelihood of experiencing further fragmentation. This is because of the bending loads they attract. Block shape can be characterized by its aspect ratio, as described by Esterhuizen (2005) and Kalenchuk et al. (2006). Block size distribution, in addition to defining the initial block sizes, is important because it also influences the susceptibility of the blocks to further fragment. Numerous authors such as Hoek & Brown (1980), Santamarina & Cho (2004) and Yoshinaka et al. (2008) have observed that rock strength decreases as the size of the block being tested increases. This scale effect is explained by the fact that larger blocks have a greater likelihood of containing more defects, veins, and smaller discontinuities, which contribute to weakening the block, thus contributing to increased fragmentation. Although it is well accepted that veins and small discontinuities act to reduce strength, exceptions may occur. At the El Teniente mine in central Chile, blocks were found to contain intermediate to high strength veins, which served to resist further fragmentation of larger sized blocks (Brzovic & Villaescusa 2007). Separate from influencing block strength, larger blocks embedded in a matrix of smaller blocks may experience less fragmentation given its higher coordination number in comparison with smaller blocks. The coordination number refers to the average number of contact points with neighbouring blocks. In effect, larger blocks are cushioned when embedded in a matrix of smaller blocks. This factor is discussed in more detail later in the chapter.

4.2.1.2 Strength heterogeneity

The broken ore within a draw column might involve a mixture of blocks with different lithological origins. Hence, individual blocks with different strengths will interact and contribute differently to the overall secondary fragmentation observed at the draw point; i.e., weaker blocks will undergo more fragmentation than stronger blocks. Also contributing to strength heterogeneity is the presence of small-scale discontinuities and veins (defects), as previously noted. Their influence in promoting secondary fragmentation in broken ore has yet to be studied extensively. Two key vein characteristics affecting secondary fragmentation are examined in this study. These include *vein/defect orientation* – it is hypothesized that any block discontinuities aligned with the stresses or point loads would promote easy splitting along the discontinuity, resulting in a small number of moderately smaller blocks. Conversely, block discontinuities aligned perpendicular to the applied stress would promote compressive failure requiring higher stress magnitudes, resulting in increased fragmentation as reported by Dorador et al. (2015). *Vein thickness* is another key parameter influencing rock fragmentation.

As noted by Brzovic & Villaescusa (2007), rock veins are clearly comprised of an altered halo surrounding the vein infill. These authors found that vein thicknesses greater than 2 mm tend to significantly increase the fragmentation of caved rock blocks.

4.2.2 State variables of broken ore

Some state variables of broken ore can have a moderate influence on the secondary fragmentation process, for example moisture content and temperature, while others like the broken ore density (BOD) could play a more important role. The latter will be examined in detail here, and is also used in association with the *swell factor* (V_{caved} / $V_{in\ situ}$) x 100. Table 4.1 presents a wide range of swell factors reported for different mine projects.

Table 4.1 : Swell factors by different authors

Mine	**Swell factor S_f**	**References**
Andina Mine. Chile	115% - 120%	Alcalde et al. (2008)
Teniente Mine. Chile	119% - 128%	Behn & Brzovic (1997)
Teniente Mine. Chile	130 - 140%	Gonzalez & Duplancic (2012)
Teniente Mine. Chile	142% - 208%	Millan J. & Brzovic A. (2013)
Ridgeway Deeps- Australia	110% (Average)	Sharrock et al. (2012)
Shabanie mine, Zimbabwe	107%-120%	Laubscher (2003)
King mine, Zimbabwe	113%	Laubscher (2003)
San Manuel (South), USA	108.9%	Gilbride et al. (2005)
Lakeshore, USA	109.5%	Gilbride et al. (2005)
Henderson, USA	109.5%	Gilbride et al. (2005)

From a granular mechanics perspective, *broken ore density* is a critical variable due to its dependence on the coordination number (number of contact points between blocks/fragments of broken ore). As a consequence, blocks with more contact points are generally subjected to a lower probability of further fragmentation under shear and compression, due to the fact that the contact loads will be widely distributed (McDowell et al. 1996, Wood & Maeda 2008). Thus, any large blocks adjacent to a number of smaller blocks (or floating in a matrix of smaller blocks) will be less susceptible to fragmentation due to its higher coordination number. This implies that the large block portion of a well-graded block size distribution would undergo less fragmentation than those from a more uniform size distribution (mono-size particles). This topic is discussed later in section 4.4.2.

The broken ore also experiences ranges of varying bulk density constrained by maximum and minimum densities (ASTM D 4253 – 00 and ASTM D 4254 – 00). This range of densities is strongly dependent on the distribution of block size and block shape. Furthermore, it is inferred that the blocks at the top of a draw column may vary between a dense, ordered initial arrangement to a loose, disordered arrangement. This initial density depends on the size of the air gap developed between the cave back and the muckpile surface; a large air gap would promote a loose face-to-end packing (Fig. 4.2a) while a negligible air gap would facilitate a dense face-to-face packing (Fig. 4.2b). These two kinds of packing have been also identified by Hancock (2013) in studies related to numerical modelling on gravitational flow. These two conditions represent lower and upper bounds, with a range of intermediate packing conditions existing in between in response to irregular draw rates and sequencing (Fig. 4.2c). It is important to note that although a sizeable air gap would promote a loose initial density, it also promotes additional block fragmentation due to the increased impact experienced by the falling blocks onto the muckpile surface.

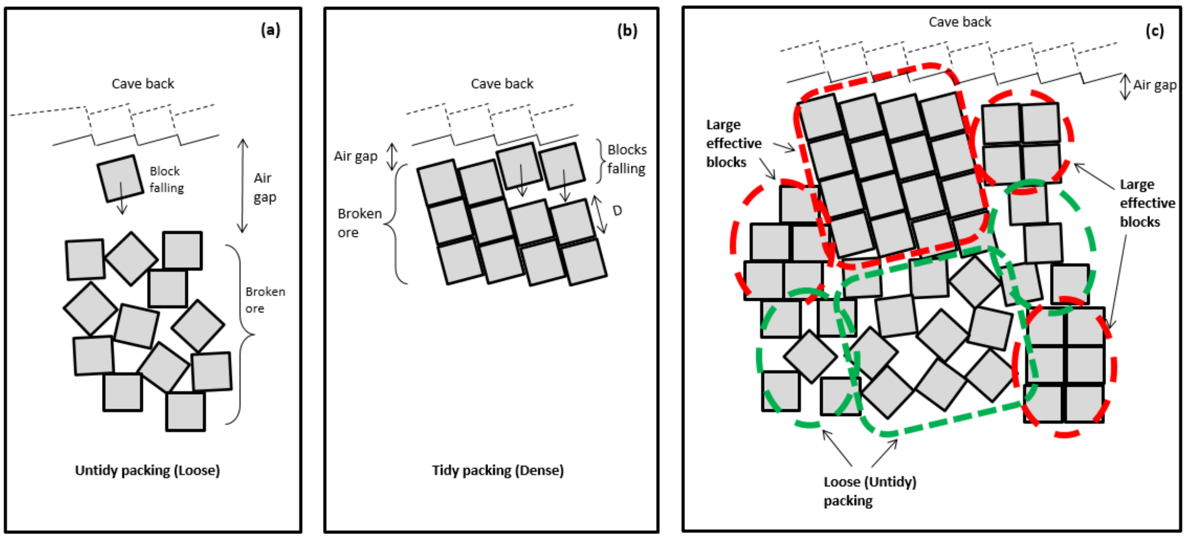

Fig. 4.2: a) Sizeable air gap and loose untidy packing. b) Negligible air gap and tidy dense packing. c) Tidy-untidy packing (variable air gap thickness)

4.2.3 Operational factors

Operational variables such as draw rate and residence time within a draw column are also key factors influencing secondary fragmentation. Slower draw rates or closure of a draw point due to a hang up will result in longer residence times for the ore in the draw column and therefore increased compaction and stress corrosion cracking. Compaction of broken ore arises due to stress re-distribution in response to active caving and increasing of the column height (caving rate > draw rate), together with ongoing fragmentation and collapse of voids. Additional fragmentation due to increased *residence time* would also be expected when blocks contain a higher intensity of veins and small discontinuities, as increased time permits greater propagation of cracks. A key consequence to draw interruption or draw point closure is that the increased residence time and consolidation will allow settlements at the top of the draw column (i.e., the muckpile surface), which in turn will serve to increase the air gap. As previously noted, this will impact the initial block arrangement and broken ore density and therefore secondary fragmentation.

4.3 Bench-Scale Experiments

4.3.1 Setup and apparatus

A series of bench-scale 1-D compression tests were carried out to simulate the secondary fragmentation of broken ore in the central compressive plug zone of a draw column (Fig. 4.1). These tests were performed using a standard Proctor compression mould, which was loaded using a Wykeham Farrance WF-5562s deformation-controlled machine. Proctor moulds are typically used for assessing the relationship between moisture content and density in fine soils (ASTM-D558 - 03), but in this case was used as a 1-D compression cell (Fig. 4.3). The ratio of mould height to diameter was maintained between 0.6 and 0.7 to decrease arching due to side friction acting on the specimens. The testing configuration allowed the vertical stress, representing the major principal stress (σ_1), to be controlled; the minor principal stress (σ_3) aligns with the horizontal plane. It is important to note that stress rotation occurs near the drawpoint. Pierce (2009) found that this distance can be estimated as being 16 times the average block size at the drawpoint; i.e., for an average block size less than 1 m, stress rotation would only be a factor within 16 m from the drawpoint. Thus, the 1-D test setup was considered as a practical and efficient means to empirically study secondary fragmentation within the compression/plug-flow zone. Details of each test (stress-strain response, size distribution after testing and photos) are presented in the appendix A.

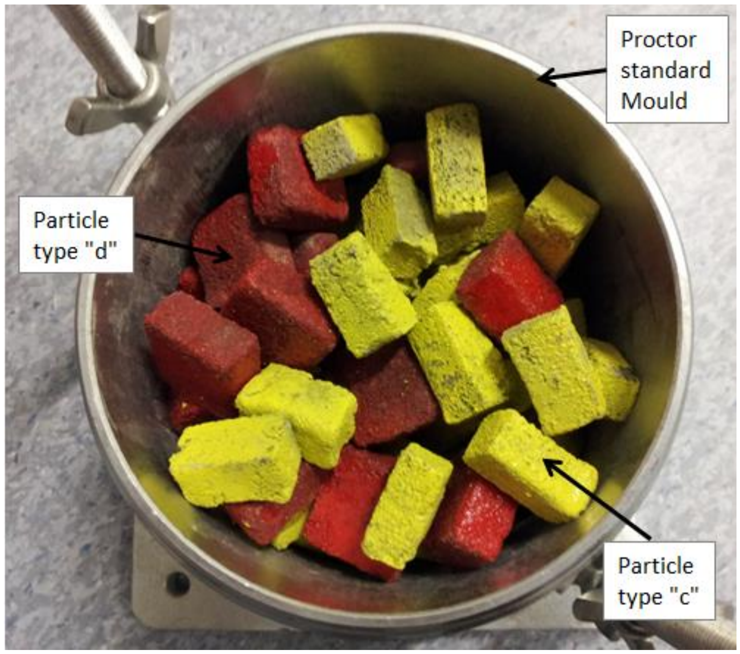

Fig. 4.3: Sample T-37 before testing. Random packing

To simulate broken ore, more than 5,000 concrete cuboids were fabricated and tested, carefully controlling their size, aspect ratio and intrinsic strengths. A subset of these was embedded with a small, non-persistent discontinuity, controlling its length, orientation and thickness to examine the role of small joints and veining on secondary fragmentation. Details are provided in the next section. Broken ore packing density was also studied and controlled during testing. Tests on loose samples were conducted with a mean sample porosity of 0.54, while tidy (dense) samples were tested with a total porosity of 0.36. The deformation rate applied in the tests was 0.5 mm/min and the final vertical deformation was variable, from 4.6% through 43% for each test.

4.3.2 Sample preparation – Concrete cuboids as a proxy for broken ore

Considering the inherent heterogeneity of the blocks making up the broken ore material in a draw column, any applicable parametric study would benefit from minimizing the degree of material variability and enabling such key parameters as sample strength, shape, size and/or packing to be controlled during testing. This favours using a fabricated material which offers more uniformity and control in material properties and characteristics, compared to using actual rock sampled from a caving operation. Alternatives successfully used as a rock substitute include acrylic resins (Horii & Nemat-Nasser 1986, Hakami & Larsson 1996, Hong et al. 2015) and Plaster of Paris/gypsum (Sagong & Bobet 2002, Gehle & Kutter 2003, Ghazvinian et al. 2012, and Singh et al. 2015). The use of concrete (Seidel & Haberfield 2002; Cheon et al. 2011, among others) likewise provides a favorable option due to its curing and hardening characteristics, providing strengths similar to rock, as well as the flexibility it provides in producing batches with specific strengths using different mix ratios of cement, sand and water. This alternative requires somewhat more preparation time due to the longer curing times required to reach full strength.

Plaster of Paris and early high strength cement (both mixed with sand and water) were used for preliminary trial tests during the planning stages of this investigation. Results suggested that the early high strength cement (EHSC) was more suitable for meeting the testing requirements because it was able to reach its maximum strength in only 2 to 3 days, enabling different batches of cuboids to be prepared with different strengths (thus providing a control in testing the influence of strength heterogeneity). Hence, an EHSC produced by Lafarge (2014) was used together with standard Fraser River sand and water to prepare concrete mixtures for subsequent preparation of cuboids for testing. Table 4.2 lists the properties of the EHSC used in this study. The geotechnical characteristics of the Fraser River sand is presented in Table 4.3.

Table 4.2: Early high strength cement properties (*)

	C1	**C2**
Air Content of mortar (%) (c 185)	6	7
Blaine Fineness (m2/kg)	518	399
Autoclave expansion (%)	0.00	-0.03
Compressive Strength (MPa) – 28days	49.2	44.7

(*) More information about mechanical and chemical properties of this special cement can be found in www.Lafarge.com

Table 4.3: Fraser River sand properties

Diameter (mm)	**Sand Nº1**	**Sand Nº2**	**Sand Nº3**
D90	0.52	0.50	0.56
D60	0.25	0.24	0.40
D30	0.19	0.18	0.24
D10	0.13	0.14	0.16
Specific gravity ASTM-D 854 (*)	2.71	2.71	2.71

(*) Values assumed from Wijewickreme et al. (2005)

To manufacture the cuboids, a variety of steel tubing with different sizes and profiles were cut to serve as moulds with different lengths, widths and heights. An example is provided in Fig. 4.4. Mixes of cement (C), sand (S) and water (W) were used in proportions of 1.75 : 2.2 : 1 (C:S:W). Two kinds of Lafarge cement were used (C1 and C2 in Table 4.2). The procedure to prepare the concrete cuboids included several steps. First, the cement, sand and water mixture were placed in an open tray. The interior wall of the mould was greased using cooking oil and pressed into the mixture. The excess mix was then removed and the mould was left in place for approximately 2 hours to allow the concrete to partially set before being removed. Finally, the cuboids were removed from the steel mould and cured, under controlled temperatures (19^o - 21^o) and humidity (50% to 70%), between 2 to 3 days. Quality control was carried out through point load testing (ASTM D5731-08) of cuboids randomly sampled from each batch. The outer faces of the cubes were then colour tinted to ease visual identification in tests with mixes of different cuboid shapes and strengths. A set of cuboids ready for testing is shown in Fig. 4.5. The geometry and size of these cuboids utilized in the laboratory testing program are presented in Table 4.4. These cuboid sizes are intended to represent block sizes of 0.5 to 1.0 m, which are realistic sizes for blocks within a compression zone.

Fig. 4.4: Steel moulds placed on the mix. Cube mould of 17 mm edge length

Fig. 4.5: Prepared cubes after curing and ready for testing (1.7 cm edge length cubes).

Table 4.4: Shape and size classes of test cuboids. Note that all classes involve early strength concrete cubes except Class B which involved sugar cubes

Shape and Size Class	Aspect Ratio (*): $AR = \frac{Area \cdot L}{6 \cdot Vol}$	Size [mm]	Shape
A (Cube)	1	L=17;W=17;H=17	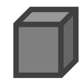
B (Cube - Sugar)	1	L=15.5;W=15.5;H=15.5	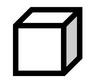
C (Elongated)	1.67	L=20;W=10;H=10	
D (Platy)	1.33	L=20;W=20;H=10	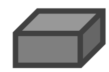
E (Cube)	1	L=20;W=20;H=20	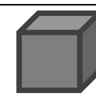
F (Cube)	1	L=13;W=13;H=13	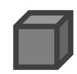
G (Cube)	1	L=10;W=10;H=10	

L: Length, W: Width, H: Height; Area: Total surface area, Vol: Volume. (*) Aspect ratio formula from Esterhuizen (2005)

4.3.3 Intrinsic cuboid strengths

Several different intrinsic cuboid strengths were obtained using different mixes of the early strength concrete. Point Load Testing (PLT) of cubes (1.7 cm edge length) prepared using standard mix proportions (C:S:W = 1.75:2.2:1) with the C1 and C2 cements (see Table 4.2) returned mean strength values of 3.10 MPa (std. dev. = 0.49 MPa) and 2.28 MPa (std. dev. = 0.33 MPa), respectively. For contrast, a set of significantly weaker cubes were prepared using a reduced amount of cement (PLT strength = 0.81 MPa), and a set of significantly stronger cubes were prepared using an alternative slow curing process (PLT strength = 5.44 MPa). A summary of the mechanical properties of the concrete cuboids is presented in Table 4.5. In addition to the point load tests, four uniaxial compressive tests (ASTM D7012 – 14) were carried out on the C2 concrete mix, for which a mean UCS value of 31 MPa was obtained.

Table 4.5 : Strength classes of Early Strength Concrete (ESC) cubes based on point load testing (PLT)

Strength Classes	# of PLT conducted	Mix characteristics (cement:sand:water)	Type of cement	Mean PLT [MPa]	Standard Deviation [MPa]
Standard	690	C:S:W 1.75:2.2:1	C1	3.10	0.14
			C2	2.28	0.10
Weak	40	C:S:W 3.76:1:1	C1	0.81	0.08
			C2	-	-
Strong	30	C:S:W 1.75:2.2:1	C1	5.44	0.92
			C2	-	-

4.3.4 Sample packing

When a sizeable air gap exists, the broken ore at the top of the draw column will be in a more random arrangement, and therefore a looser, less dense, initial state, due to the kinematic freedom falling blocks from the cave back have to rotate (Fig. 4.2.a). In the experiments conducted in this study, this loose state is simulated by filling a cylindrical mould with cuboids dropped from a height resulting in a minimum bulk density (or maximum porosity). This follows the standard procedure to obtain the minimum density of granular materials (ASTM D 4254 – 00). A practical example of loose packing of broken ore is at the

El Teniente mine in Chile, where Millan & Brzovic (2013) measured an average broken ore density of 1.6 t/m^3, which is equivalent to a swell factor (S_f) of 169% (based on an in situ rock density of 2.7 t/m^3).

When a negligible air gap is present, falling blocks from the cave back are confined and unable to rotate, resulting in a denser arrangement of blocks (Fig. 4.2b). In the experiment setup, cubes were hand placed in the cylindrical mould to ensure face to face contacts and a maximum bulk density (or minimum porosity). This type of packing can be associated with low swell factors (S_f) of 108% to 116% recommended by Laubscher (1994). Examples of low S_f include values between 115%-120% reported from the Codelco-Andina mine (Alcalde et al. 2008) and values between 104-112% reported at the Ridgeway Deeps mine (Sharrock et al. 2012). This particular packing condition has been suggested as being significant in the gravitational flow behaviour of broken ore, although to-date, this has not been fully studied (Hancock 2013).

Where the air gap height varies due to irregular draw or caving into the draw column, the broken ore density will likely reach its maximum heterogeneity, with intervals of blocks fitting a dense packing adjacent to intervals of blocks with a loose packing (Fig. 4.2c). In this scenario, the BOD within the shear bands would keep a loose condition due to continuous block rotation and dilatancy during draw; in the plug zone, the varying dense/loose packing will likely significantly affect the flow and final BOD observed at the drawpoints, and thus would influence the frequency of oversize and hang ups encountered.

4.3.5 Testing procedure and quantification of fragmentation

The 1-D compression testing program included sample mixes involving regular cubes, cuboids with different aspect ratios and size distributions, and cubes with embedded veins. Details are provided in Table 4.6, Table 4.7, and Table 4.8**.**. The design of the testing procedure included reviewing several common parameters used to quantify particle fragmentation associated with 1-D compression testing. These included particle breakage "b_g" (Marsal et al. 1965), surface area "Sa" (Miura & Yamanouchi 1975, Hyodo et. al 2002), and relative breakage "B_r" (Hardin 1985). For this study, Hardin's relative breakage index Br was adopted.

The Hardin (1985) procedure works as follows. First, the initial and final size distributions from a compression test (i.e., 1-D, triaxial, etc.) are plotted as a cumulative passing percentage. The area between these two size distribution curves represents the total fragmentation (B_t) of the sample after testing (Fig. 4.6). Next, the potential fragmentation (B_p) is assessed, which corresponds to the area between a vertical line drawn at d = 0.075mm and the initial size distribution curve (Fig. 4.7). The ratio of these two terms is defined as the relative breakage B_r:

$$Br = \frac{Bt}{Bp} \tag{4.1}$$

A higher Br ratio indicates a higher degree of fragmentation, with a value of zero indicating no fragmentation and a value of 1 representing the maximum theoretical fragmentation.

Table 4.6 : List of tests on regular cube samples

Sample Nº	**Packing**	**Shape Type**	**Point Load Strength [MPa]**	**Packing Porosity**
T-1 to 8	Loose (Random)	A	3.10	0.54
T-9 to 24	Dense (tidy)	A	3.10	0.36
T-25 to 31	Dense (tidy)	B	0.42	0.36
T-71 to 74	Loose (Random)	B	0.42	0.54

Table 4.7 : Tests on cuboids with different aspect ratio and size.

Sample Nº	Packing (*)	Equivalent PLT Strength (MPa)	Mix of Shape and Size Classes
T-32	Loose (Random)	3.10	C = 100%
T-33	Loose (Random)	3.10	
T-34	Loose (Random)	3.10	
T-35	Loose (Random)	3.10	D = 100%
T-36	Loose (Random)	3.10	E = 100%
T-37	Loose (Random)	3.10	C = 50%; D = 50%
T-38	Loose (Random)	3.10	E = 50% ; A = 50%
T-39	Loose (Random)	3.10	
T-40	Loose (Random)	3.10	E = 3.5%; A = 11%; F = 25.5%; G = 60%
T-41	Loose (Random)	3.10	E = 40%; A = 35%; F = 15%; G = 10%
T-42	Loose (Random)	5.54	G = 100%
T-43	Loose (Random)	5.54	E = 100%
T-44	Loose (Random)	5.54	D = 100%
T-45	Loose (Random)	5.54	A = 100%
T-46	Loose (Random)	5.54	A = 100%
T-47	Loose (Random)	5.54	C = 50% ; D = 50%
T-66	Loose (Random)	(**)	E = 3.5% ; A = 11% ; F = 25.5% ; G = 60%
T-67	Loose (Random)	(**)	E = 40%; A = 35%; F = 15%; G = 10%
T-68	Loose (Random)	(**)	E = 20%; A = 25%; F = 25%; G = 20%
T-69	Loose (Random)	(**)	E = 20%; A = 25%; F = 25%; G = 20%
T-70	Loose (Random)	(**)	C = 50%; D = 50%

(*)Initial sample porosity = 0.54. (**) Variable Point load strengths of cuboids MPa.

Table 4.8 : Tests on cubes (Type A) with embedded veins (*)

Sample Nº	Packing	PLT Strength (MPa) (**)	Vein width [mm]	Vein Thickness [mm]	Vein Orientation
T-48 to 50	Dense (tidy)	3.10	8.0	0.3	Vertical
T-51 to 53	Dense (tidy)	3.10	16.0	0.3	Vertical
T-54 to 55	Dense (tidy)	3.10	8.0	0.3	Horizontal
T-56 to 57	Dense (tidy)	3.10	16.0	0.3	Horizontal
T-58	Dense (tidy)	3.10	Regular cubes (no veins; control sample)		
T-59 to 60	Dense (tidy)	2.28	Regular cubes (no veins; control sample)		
T-61	Dense (tidy)	2.28	16.0	0.02	Vertical
T-62	Dense (tidy)	2.28	16.0	0.1	Vertical
T-63	Dense (tidy)	2.28	16.0	0.3	Vertical
T-64	Dense (tidy)	2.28	16.0	0.02	Horizontal
T-65	Dense (tidy)	2.28	16.0	0.3	Horizontal

(*)*For samples 58 to 65, the cement used is C2.* Initial sample porosity of 0.36.

(**) Cube strength without embedded veins.

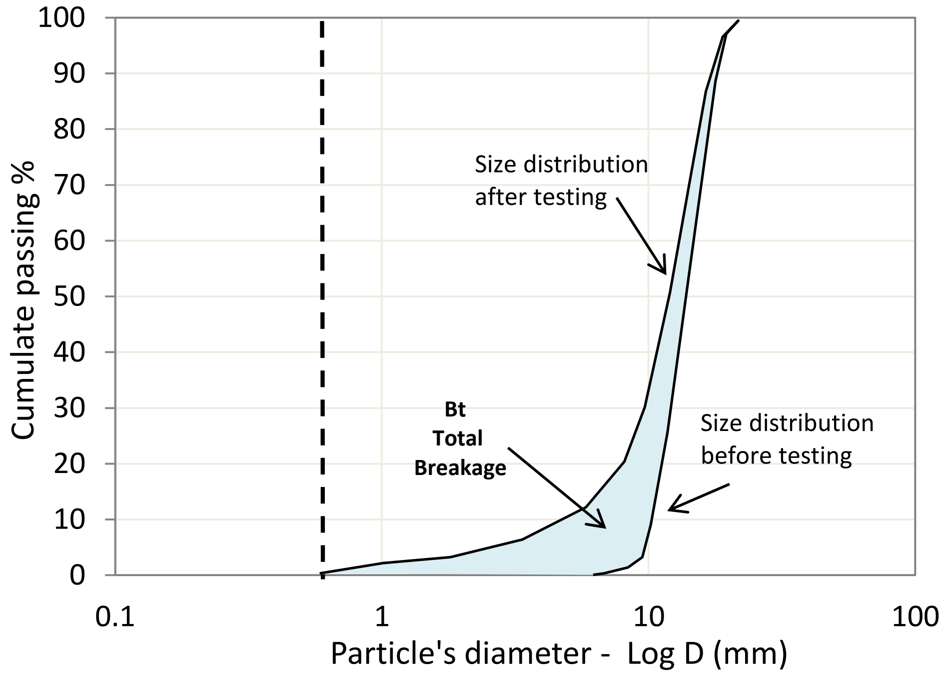

Fig. 4.6: Total breakage parameter (B_t) by Hardin (1985)

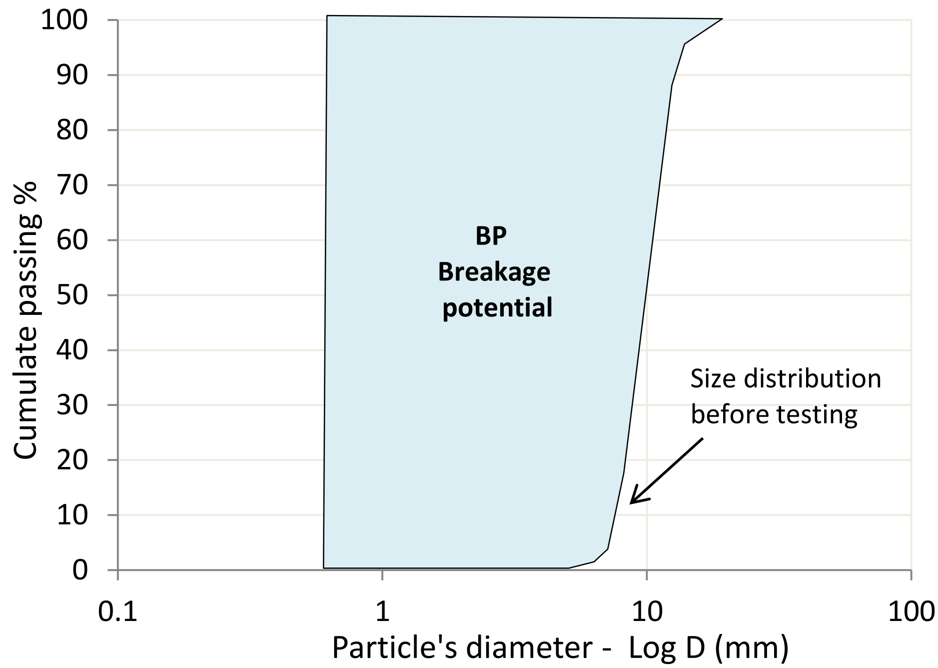

Fig. 4.7: Breakage potential parameter B_p by Hardin (1985)

The laboratory testing program consisted of 1-D compression tests on cubes and cuboids with respective minimum and maximum sizes of 10 x 10 x 10 mm and 20 x 20 x 20 mm. The size distribution after testing was estimated by weighing each fragment rather than sieving them (in order to avoid further damage and breakage), an approach permitted due to the fact that both size and weight are directly proportional given the use of a controlled material (i.e., concrete). Thus, after weighing each fragment, the particle volume is obtained based on material density (approximately 2 g/cm^3), and the equivalent particle ratio is obtained assuming the volume of a sphere. Regarding the post-gradation analysis, the minimum equivalent diameter measured is 0.66 cm which implies that the ratio of maximum/minimum particle size used to evaluate the Br ranges from 3.2 to 4.1. Fig. 4.8 provides two examples of particle size distributions obtained after testing (specifically, T-55 and T-60) and the equivalent Br for each test.

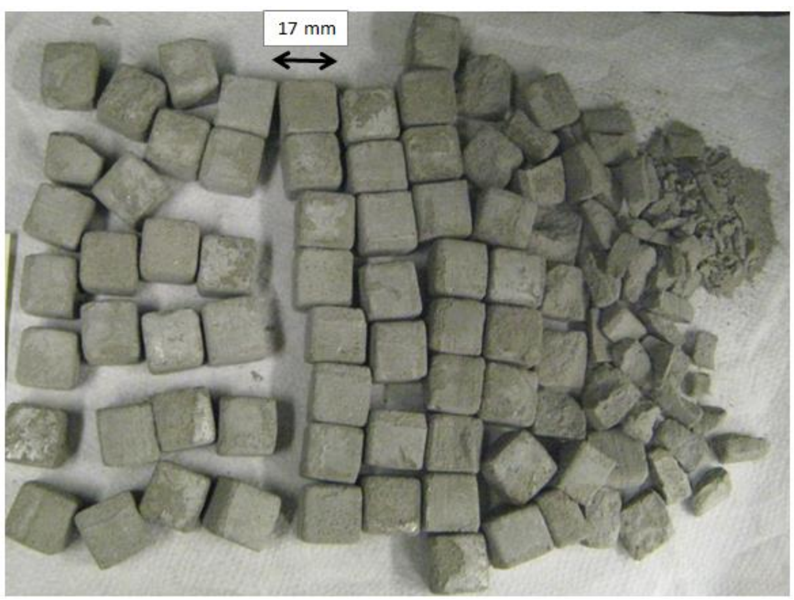

Fig. 4.8: (top) Size distribution after testing. T-55 and **Br = 0.80.** (Bottom) Size distribution after testing. T-60 and **Br = 0.08.**

4.4 1-D Compression Test Results

4.4.1 Influence of size distribution and aspect ratio on blocks

Fig. 4.9 and Fig. 4.10 show the results from several series of tests in terms of the energy (E) input applied to the sample (i.e., work) and the corresponding fragmentation parameter Br. A marked proportional trend can be observed between E and Br, for a variety of bulk samples with different particle shape and size distributions. As would be expected, stronger cubes exhibit less relative breakage than those with lower strengths. This highlights the importance of block strength with respect to other parameters such as shape and size distribution. Comparing cubes and cuboids with similar strengths (PLT = 3.10 MPa), cuboids with irregular shapes (elongated and platy) tend to undergo comparable fragmentation than regular cubes. However, when differentiating bulk samples with a mixed size/shape distribution (see filled circles in Fig. 4.10), they show less breakage, compared to mixes that are more uniform in size and shape (solid black curve in Fig. 4.10).

Therefore, based on the experimental results presented in Fig. 4.9 and Fig. 4.10, for a given energy input, the influence with respect to increasing fragmentation progresses from high strength to low strength cubes, and mix of sizes that are cube shaped to those that are elongated and platy (labelled ‘C’ in Fig. 4.10). In all cases, fragmentation was seen to increase with increasing energy applied to the sample, which equates to a draw column increasing in height over time. This is seen to significantly influence the degree of secondary fragmentation.

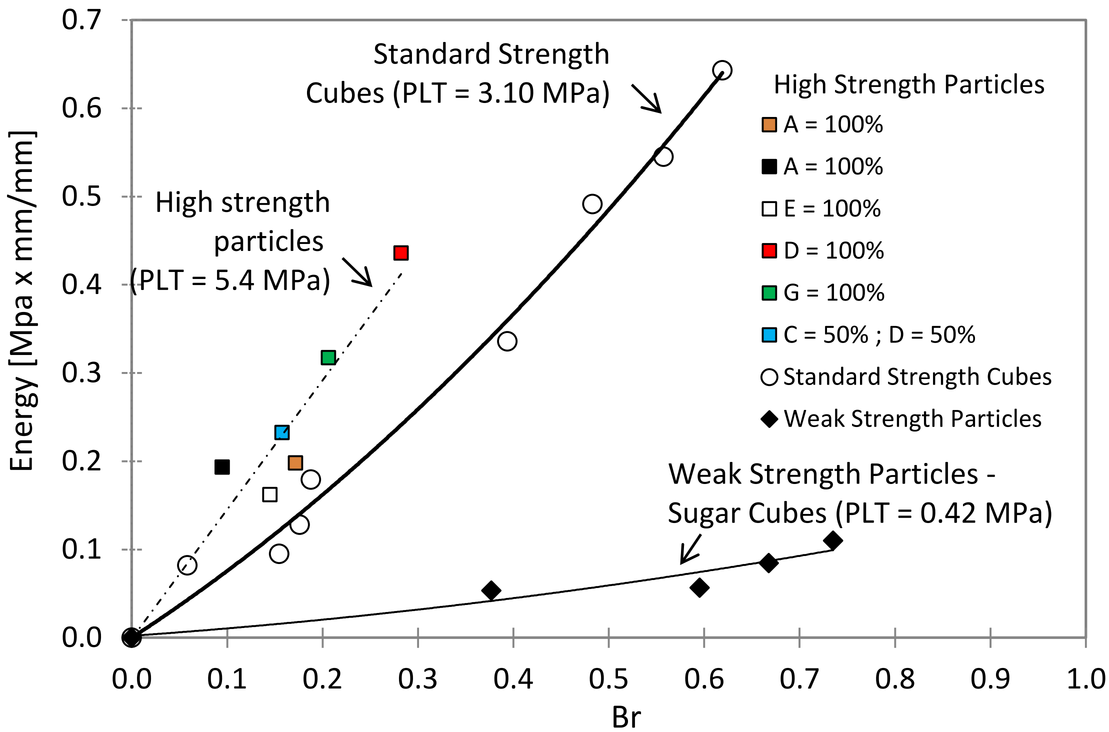

Fig. 4.9: Fragmentation results for different particle's strength

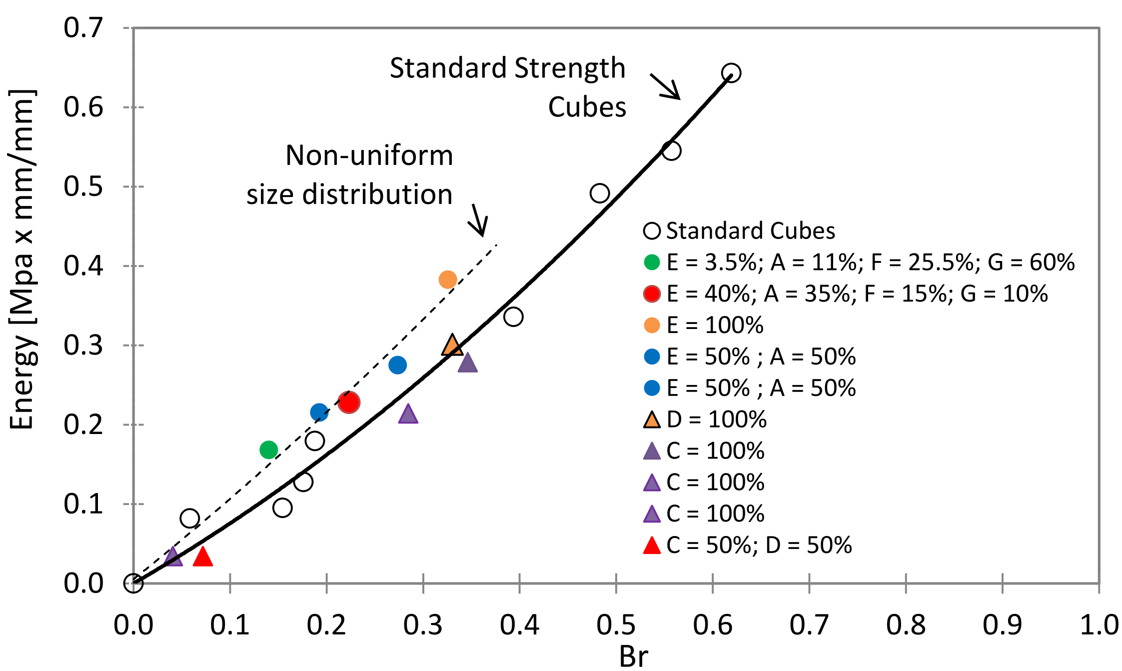

Fig. 4.10: Fragmentation results for different particle's shape and strength

4.4.2 Influence of broken ore density (BOD)

As previously discussed, the broken ore at the top of a draw column can either amass in a loose, dense or intermediate packing state depending largely on the air gap size. In order to study the influence of the BOD on secondary fragmentation, several tests were conducted on either a loose packing of cubes (tests T-1 to T-8) or a dense packing (T-9 to T-17). The latter were carried out under a tidy arrangement as shown in Fig. 4.11. Although this cube arrangement optimizes the maximum density, voids were left between the cubes and the cylindrical wall in order to mimic the loose broken ore flowing through the shear bands adjacent to the central compressive plug zone. This helps to better simulate the actual conditions experienced within a draw column.

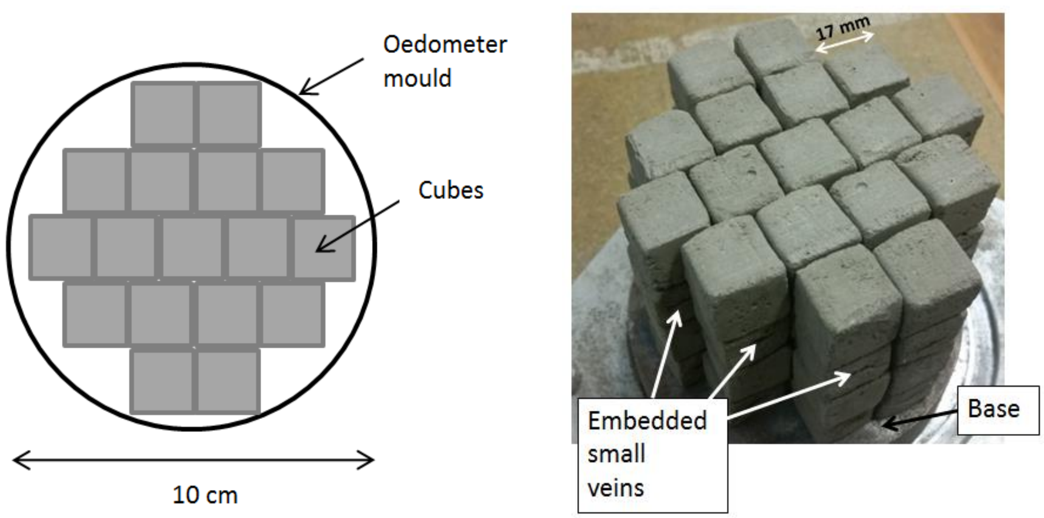

(a) (b)

Fig. 4.11: (a) Plan view of 1-D compression tests (tidy packing). (b) Tidy (dense) cube arrangement for Test T-55.

The results presented in Fig. 4.12 show a noticeable difference in behaviour between the two BOD states. Under conditions of loose packing, fragmentation is proportional to the degree of external energy applied to the sample. In contrast, the dense packing state initially exhibits a higher fragmentation for the same Energy input compared to the loose packing, but then sharply reaches a maximum level for additional energy inputs.

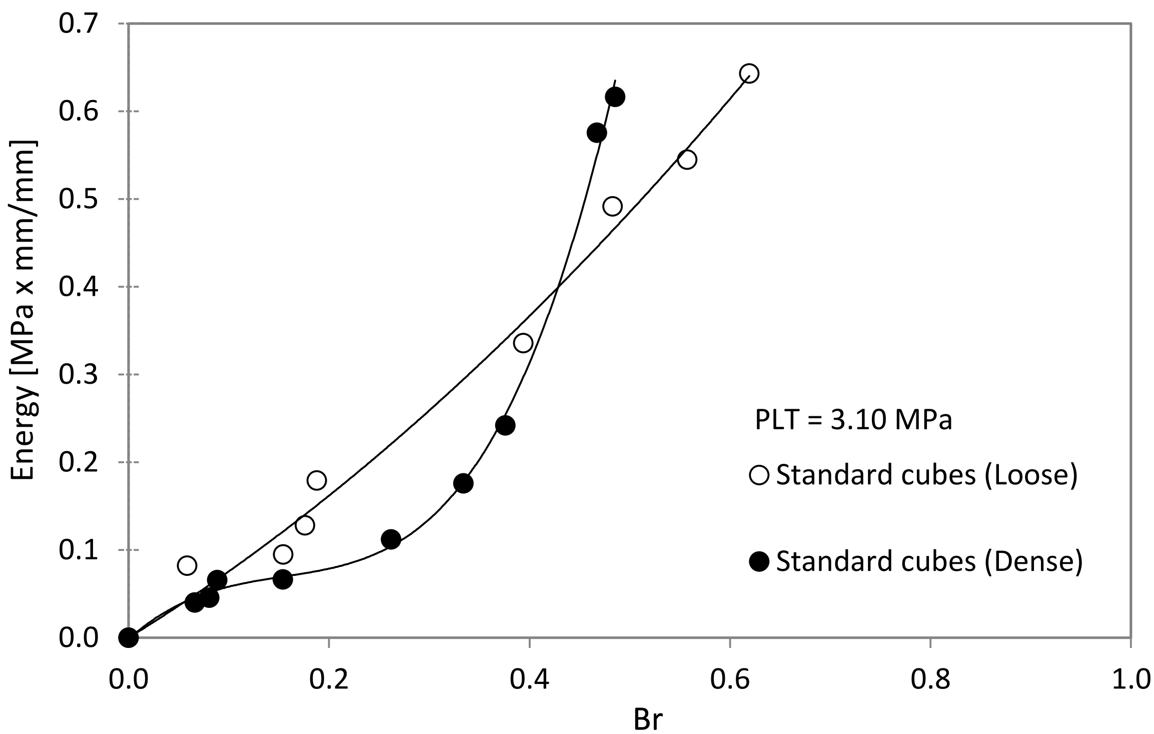

Fig. 4.12: Fragmentation results under different packing conditions.

To further investigate this dense packing behaviour, testing of samples with contrasting cube strengths was conducted (Fig. 4.13). Sugar cubes were added as a test material (tests T-25 to T-31) to provide an alternative low strength material (PLT = 0.42 MPa), together with the low strength concrete cubes (T-21 to T-24) and standard strength cubes (T-9 to T-17). The results in Fig. 4.13 show similar trends for the low strength cubes and sugar cubes under a dense packing arrangement (i.e., high BOD); i.e., high fragmentation levels (especially with decreasing cube strength) as the Energy input is initially increased, followed by diminishing increases in fragmentation with similar increments of Energy input.

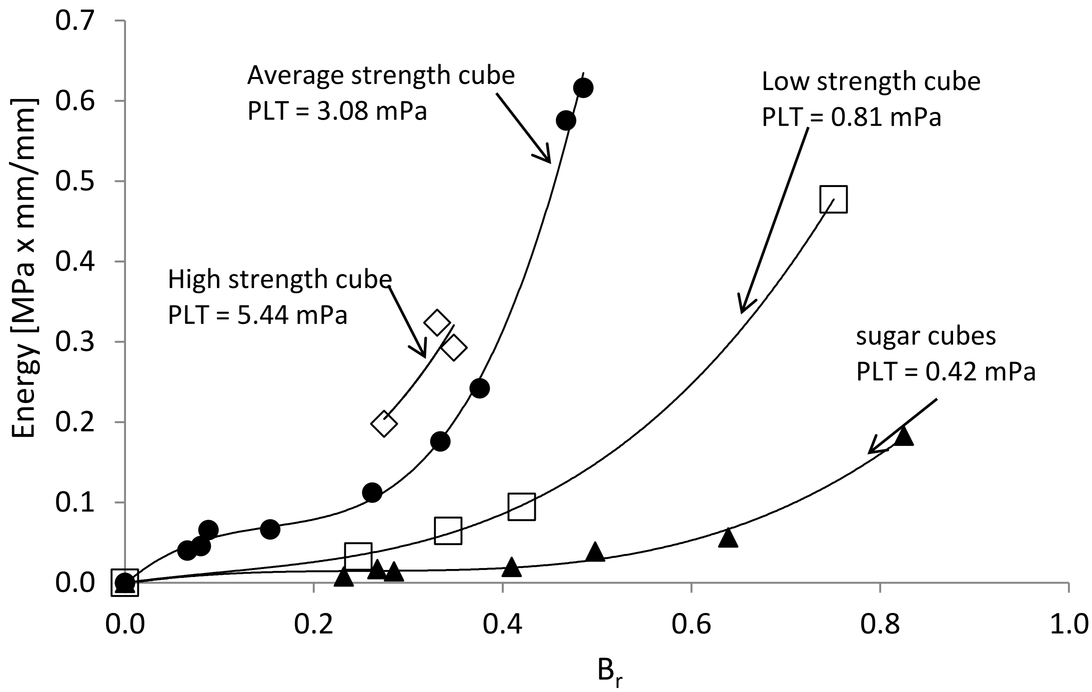

Fig. 4.13: Fragmentation results for different sample strengths.

Regarding the mechanics of secondary fragmentation, further examination of these results indicate that a dense packing response exhibits three key stages representing changing behaviour as identified by Dorador et al. (2015): i) *splitting initiation,* ii) *matrix collapse and fragment reorganization,* and iii) *matrix support strengthening* (Fig. 4.14). It is important to note that this kind of behaviour (collapse and reorganization) has also been recognized in part by Tsoungui et al. (1999) and Muller & Tomas (2013) using uniaxial compression tests on synthetic spheres.

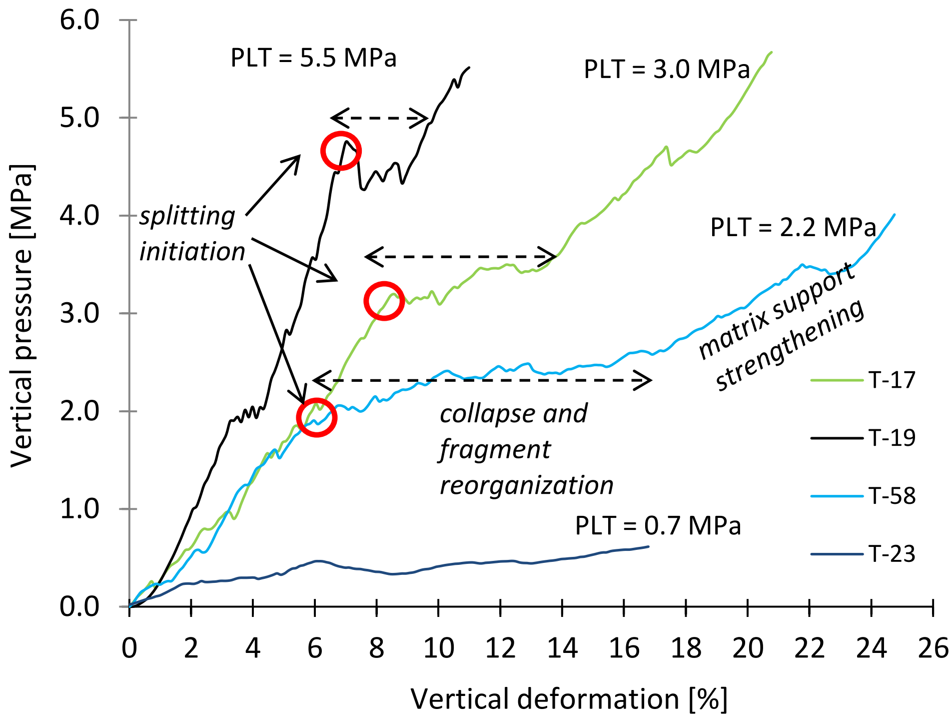

Fig. 4.14: Vertical pressure v/s vertical deformation for tests using concrete cubes with different PLT strengths and tidy packing.

The mechanistic behaviour observed here helps to explain why the dense packing arrangement experiences more fragmentation than the loose packing state. Fig. 4.15 compares the loose and dense packing results in terms of stress-strain curves. For a loose packing state, the different cubes are randomly oriented and those most adversely positioned will experience stress concentrations and point load splitting first, followed by localized collapse and reorganization in their immediate vicinity to fill any voids. As the energy input increases, the stress heterogeneity will shift and the cubes will progressively fragment and reorganize until a denser matrix state is achieved. Conversely, when starting with a dense packing state, a greater percentage of the cubes are in face-to-face contact with adjacent cubes. This would result in a more even stress distribution throughout the sample, promoting the simultaneous fragmentation of larger groupings of cubes via crushing and splitting. These results suggest that a denser packing would be more efficient in generating a higher degree of fragmentation.

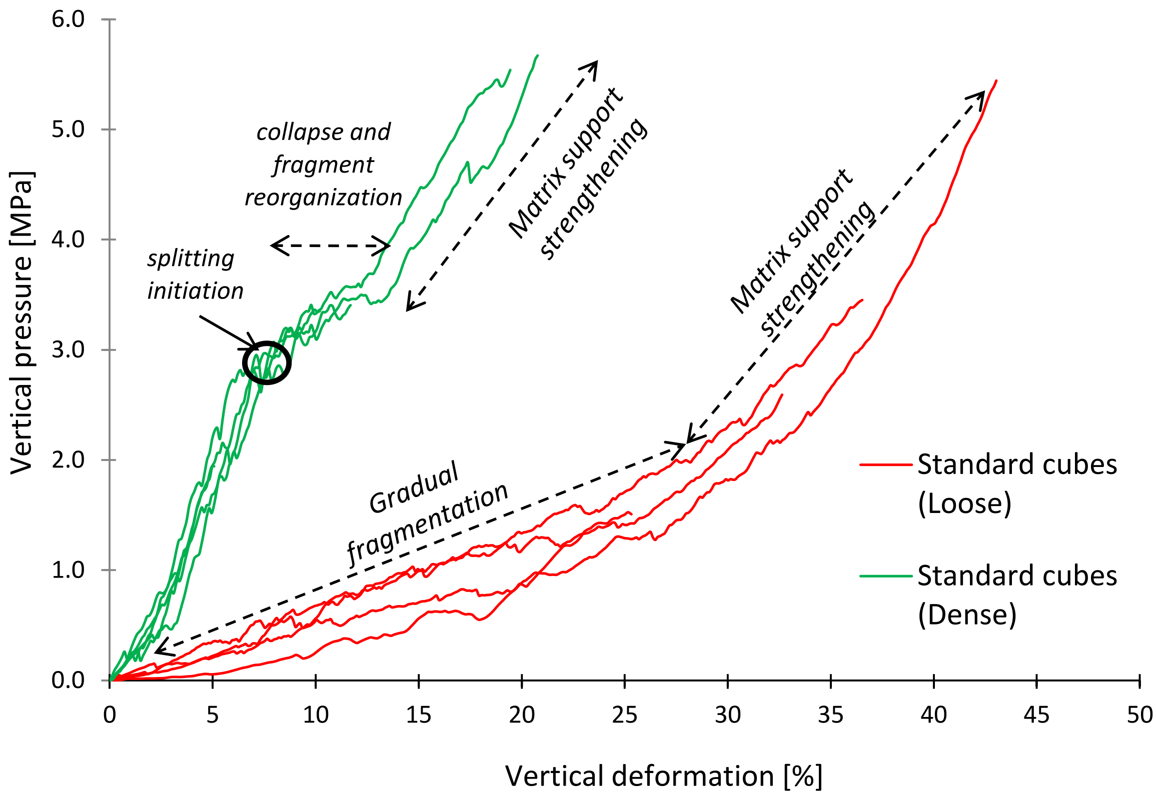

Fig. 4.15: Vertical stress vs vertical deformation for tests under different initial packing states.

4.4.3 Influence of embedded veins on blocks

Veins embedded within blocks can significantly affect secondary fragmentation, especially in stronger rocks. In order to study the influence of embedded veins, several tests were conducted (T-48 to T-57) using the A-size cubes (17 mm edge length) and small joints were included within the concrete cubes by pressing a thin piece of cardboard into the setting concrete. After curing, the cardboard pieces were removed from the concretes cubes, leaving an open gap. The parameters varied include: i) vein trace lengths, 8 and 16mm (as measured on the face of the cube); and vein orientation relative to loading, horizontal and vertical (Fig. 4.16). The depth of the veins for each sample was kept constant at 17 mm (i.e., penetrating completely through the cube). Results are presented in Fig. 4.17 and reveal that embedded veins promote higher fragmentation (the black line represents results for cubes without a vein). However, comparison of the results for the 8 and 16 mm vein lengths indicate that there is little noticeable difference in fragmentation, thus suggesting that vein length relative to the block size is a less sensitive parameter for these 1-D compression tests results. In contrast, a noticeable difference in fragmentation was observed in terms of vein orientation. Vertical veins, aligned parallel with the 1-D loading direction, resulted in less fragmentation than veins aligned horizontal (i.e., perpendicular to the loading direction). This corroborates findings by Dorador et al. (2015) that *vein orientation* serves to promote different secondary fragmentation mechanisms, where loading parallel to the vein results in block splitting, which limits further fragmentation, whereas loading perpendicular to the vein results in compressive failure of the block resulting in more (and therefore smaller) fragments. Note that this testing results applies to tidy broken ore packing under anisotropic compression.

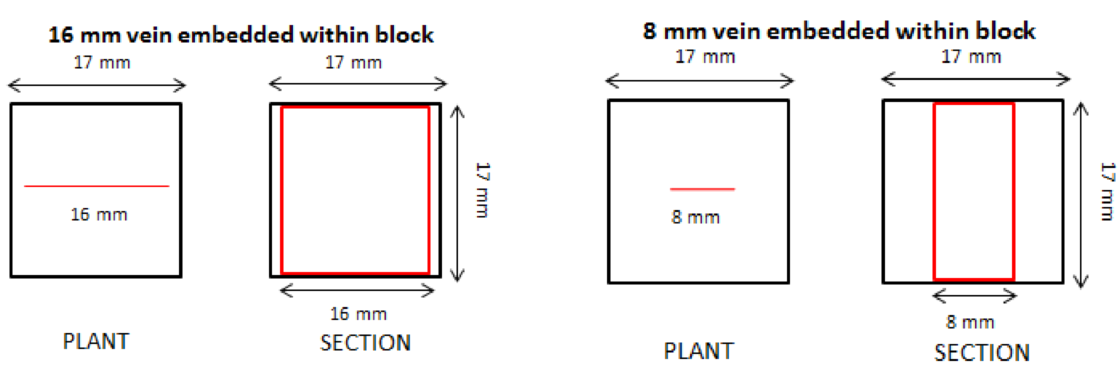

Fig. 4.16: Plan and section view of cubes with embedded discontinuities

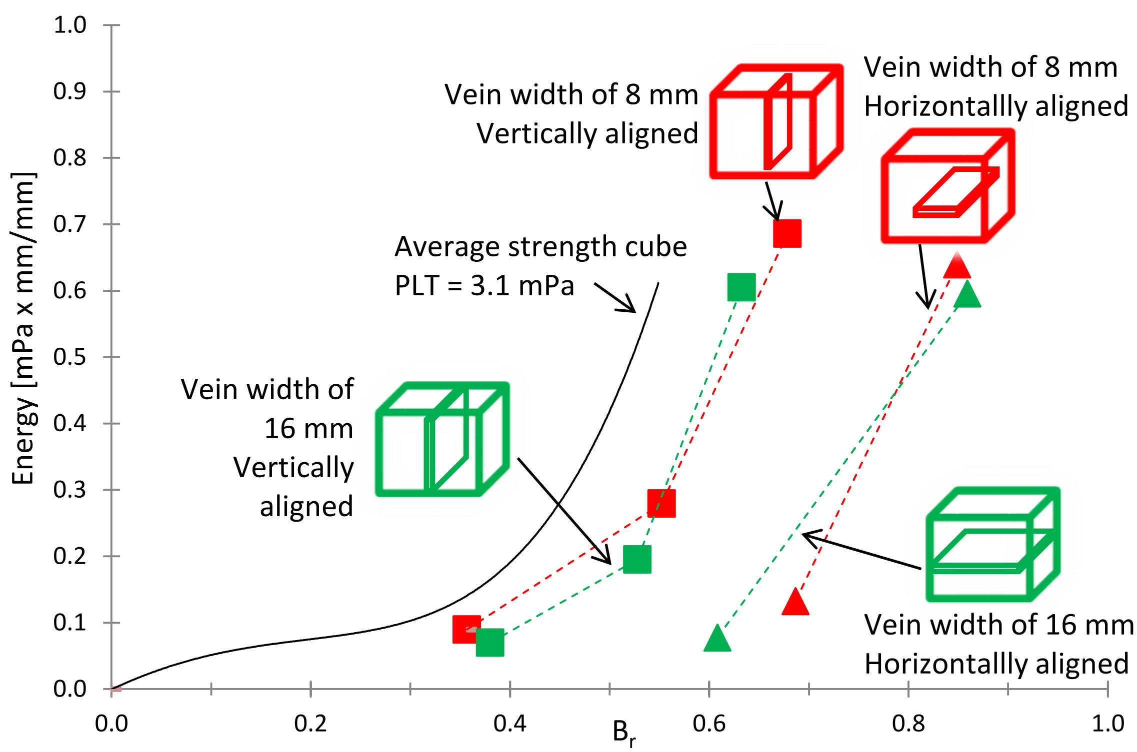

Fig. 4.17: Fragmentation test results investigating the influence of embedded veins and their orientation. Note the black line represents the trend for cubes without an embedded vein for comparison.

To corroborate these results, four graphs are included in Fig. 4.18. These compare two cases of small and large veins, aligned either vertically (Fig. 4.18 a, b) or horizontally (Fig. 4.18 c, d). In each case, the standard cubes samples (dashed curves) show much lower fragmentation than cubes samples with embedded veins under comparable vertical confining pressures (σ_v). Of interest are the shapes of the post-test size distribution curves. For samples without an embedded vein, the fragmentation curves (dashed black lines in each plot) show a uniform post-test size distribution. This is commonly observed in 1-D compression testing.

However, this trend was not observed in the samples with embedded veins. Instead, these showed gaps in the larger particle sizes.

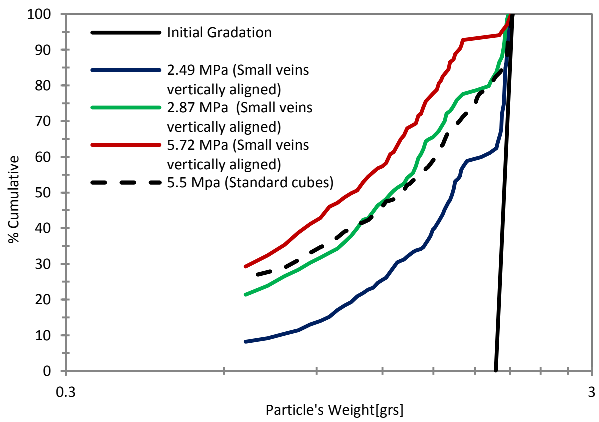

(a)

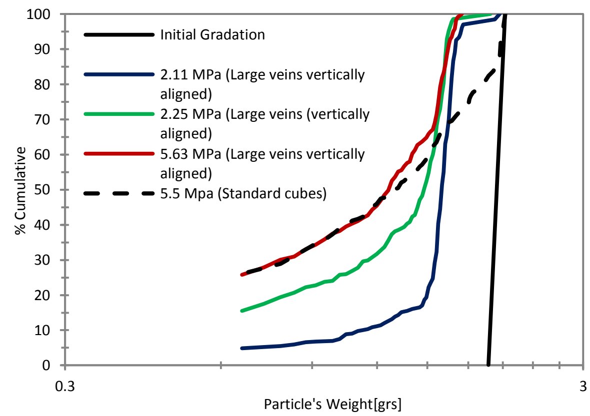

(b)

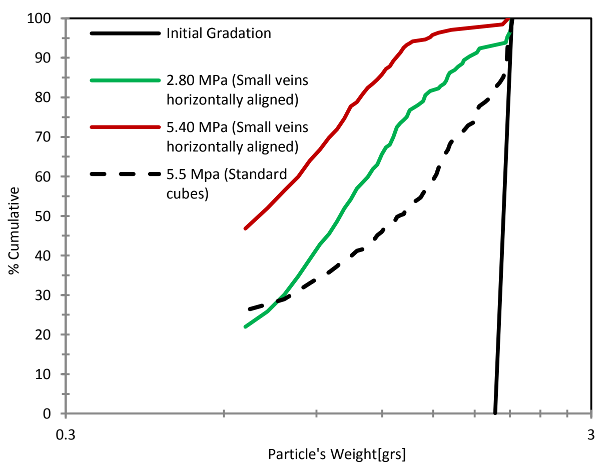

(c)

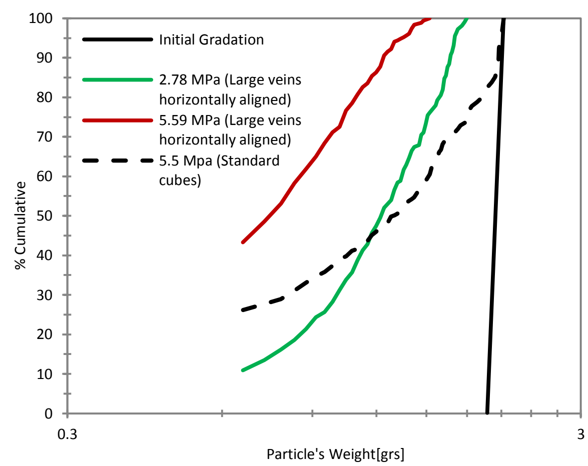

(d)

Fig. 4.18: Fragmentation comparison with block size distributions before and after testing. (a) Small vein vertically aligned. (b) Large vein vertically aligned. (c) Small vein horizontally aligned. (d) Large vein horizontally aligned

It should be noted that the vein thickness in these tests was 0.3 mm, which is large relative to the cube's edge length (17mm). Based on this, two additional vein thicknesses (0.1 mm and 0.03 mm) were analyzed, with data shown in Fig. 4.19. Here, the ratio between the tightest vein thickness (0.03 mm) and cube length more closely approximates those found in actual blocks; e.g., a 2 mm vein thickness found in block sizes of 1 m edge length (see Brzovic & Villaescusa 2007). The results indicate that higher fragmentation develops for larger vein thicknesses, regardless of whether the veins are loaded vertically or horizontally. Nevertheless, vein thickness was seen to be less important than the orientation of the veins themselves.

Comparing the different experimental results, it was found that tests with horizontally embedded veins and those with lower cube strengths generated the greatest fragmentation. An upper bound on fragmentation (i.e., maximum) was obtained in tests performed on sugar cubes, which are several times weaker than the concrete cubes without veins. As can be observed in Fig. 4.20, similar values are obtained under low loading conditions (i.e., around 0.1 MPa·mm/mm) but then diverge at higher values, with the embedded vein results following trends between the weaker sugar cubes and stronger concrete cubes without veins. Thus the increased fragmentation seen for the horizontally embedded veins is not simply due to compressive failure as would also be experienced by the concrete cubes without veins, but is influenced by the presence of the vein.

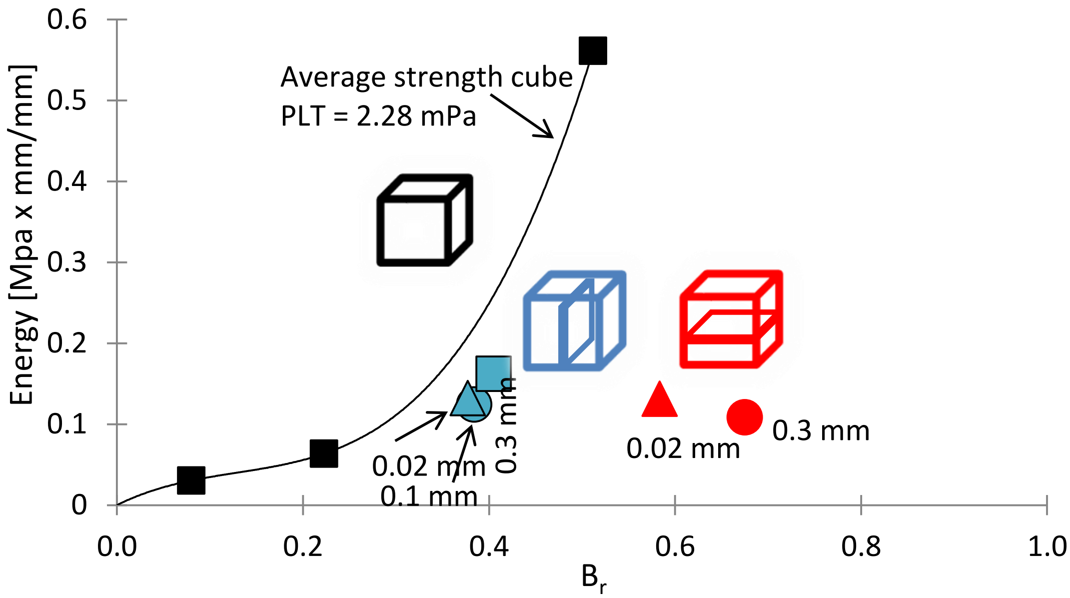

Fig. 4.19: Fragmentation test results investigating the influence of embedded vein thickness.

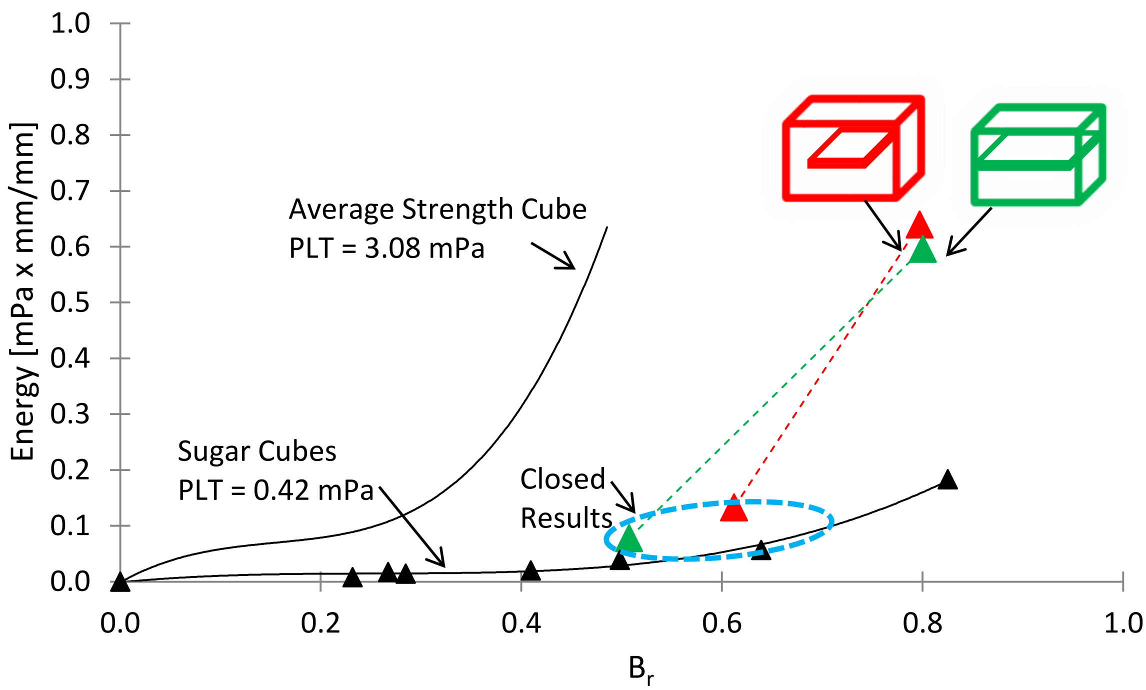

Fig. 4.20: Fragmentation test results showing results for cubes with and without an embedded vein.

4.5 Upscaling: Fragmentation Assessment of Broken Ore within the Compression Zone

In order to study the progressive secondary fragmentation of broken ore within the compression zone, data from Fig. 4.12 was plotted in terms of size distribution before and after testing under loose and dense packing states (Fig. 4.21 and Fig. 4.22), together with different applied vertical stresses. As can be observed, the fragmentation curves increase under increased compression energy and rise sharply as it approaches its largest equivalent fragment diameter. This agrees with the findings of Pierce (2009) for block cave draw columns, as well as findings from 1-D compression tests on sands by Fukumoto (1992) and Leleu & Valdes (2007), gravels by Vallejo et al. (2011), and rockfill by Marsal et al. (1965). Note that Fig. 4.21 and Fig. 4.22 can be related to broken ore materials under draw column heights between 88 to 318 m (see Table 4.9).

Table 4.9 : Maximum vertical stress on samples

	Loose packing (BOD =1.7 t/m^3)					Dense packing (BOD =2.6 t/m^3)					
Sample	T-1	T-2	T-3	T-4	T-5	T-10	T-12	T-14	T-15	T-16	T-17
σ_v [MPa]	5.4	4.3	3.5	2.6	1.5	2.3	2.8	3.4	3.4	5.5	5.7
Overload height (*)	318	253	206	153	88	88	108	131	131	212	219

(*) These overload heights do not consider stress reduction due to arching effects.

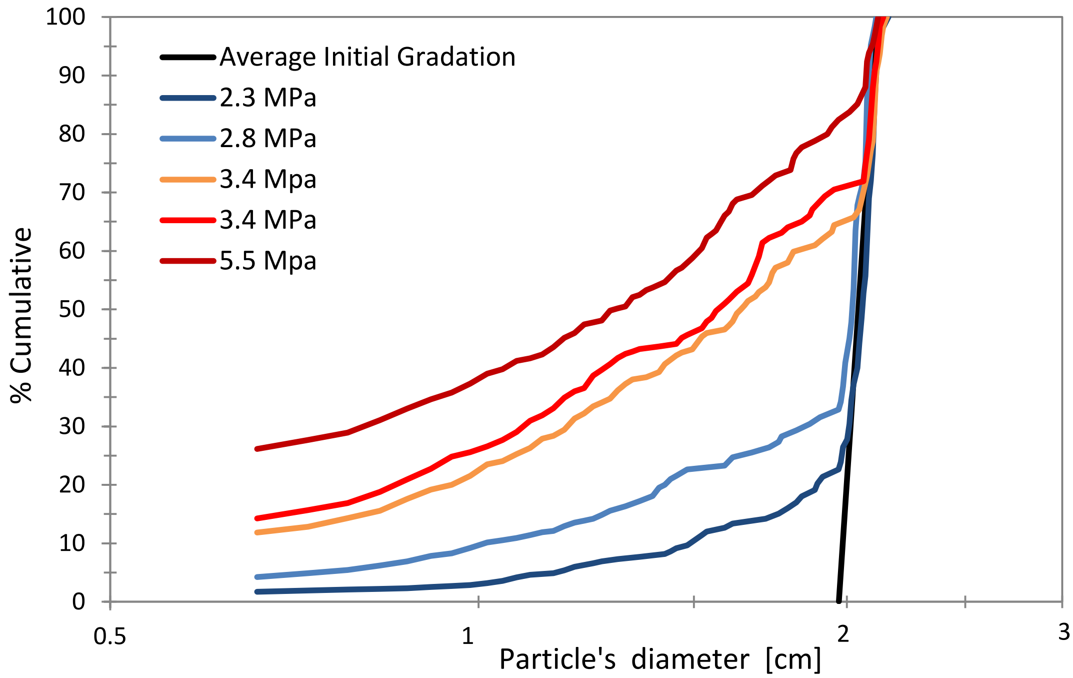

Fig. 4.21: Evolution of secondary fragmentation on compression zone (Dense packing)

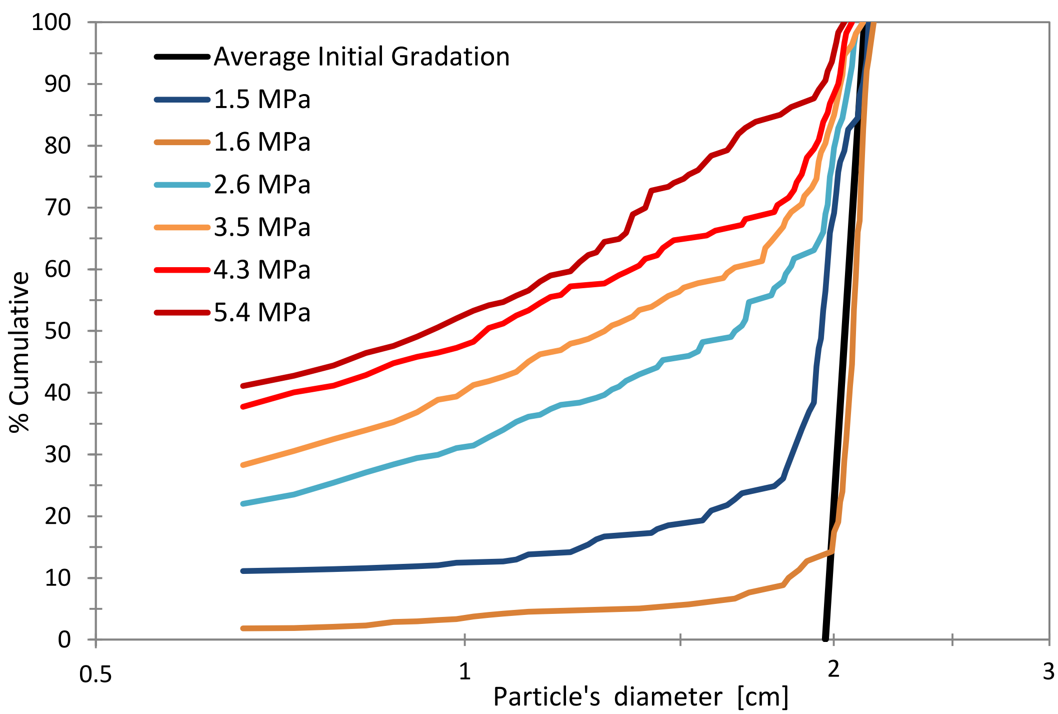

Fig. 4.22: Evolution of secondary fragmentation on compression zone (loose packing).

In extending the laboratory results to the secondary fragmentation present in a draw column, it is also necessary to consider scale effects (section 4.2.1.1). Although scale effects related to rock strength has been the subject of numerous studies (e.g., Hoek & Brown 1980), scale effects in concrete has not been studied as extensively. Elfahal et al. (2005) conducted uniaxial compressive strength tests on concrete cylinders of diameter 75, 150 and 300 mm (maintaining a height to diameter ratio of 2). However, their results did not reflect a clear drop in strength with increasing sample size as seen in rock. This lack of clear drop in strength with increasing sample size was also seen by Darlington et al. (2011) based on tests by Blanks & McNamara (1935) and Symons (1970). Hence, based on these studies, it can be assumed that concrete does not contain the same natural defects that rock does that contributes to lower strengths. An additional consideration is that reduced strengths with increasing scale in soft rocks has been found to be less significant, as the matrix in these cases is of similar weakness as any defects that are also present (Yoshinaka et al. 2008). This would apply to blocks in the draw column that have significant veining or are highly damaged due to stress-induced fracturing during primary fragmentation or due to impact with the muck pile after caving.

Therefore, assuming that scale effects related to the concrete cubes are marginal, σ_c was scaled for larger draw column block sizes to be 31 MPa (section 4.3.3). This was used to generate three feasibility-level empirical design charts that can be used to approximate the fragmentation within the compression (plug-flow) zone in an isolated movement zone or under interactive flow (Fig. 4.23 to Fig. 4.25).

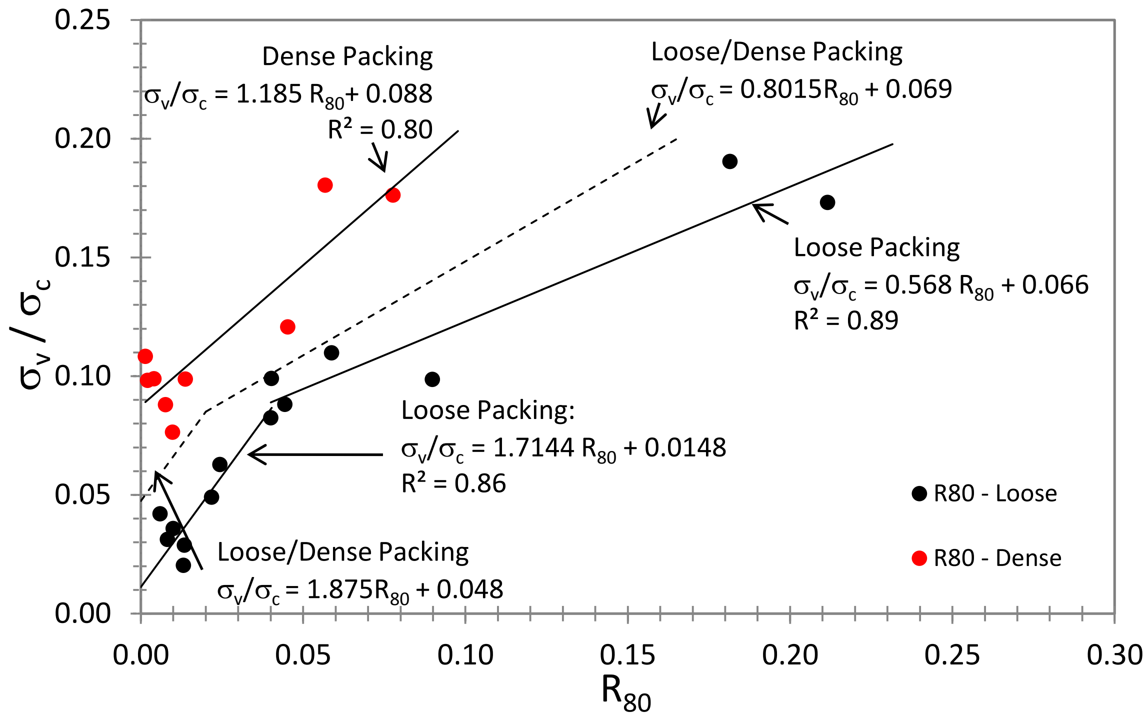

Fig. 4.23: Chart to estimate R_{80}

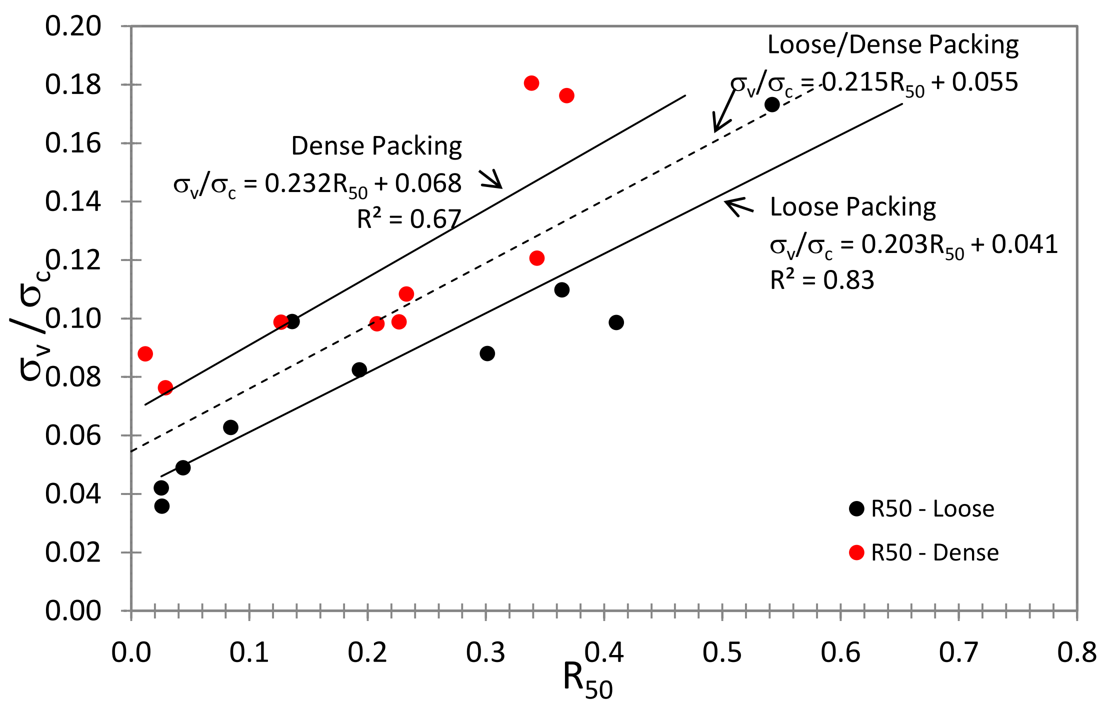

Fig. 4.24: Chart to estimate R_{50}

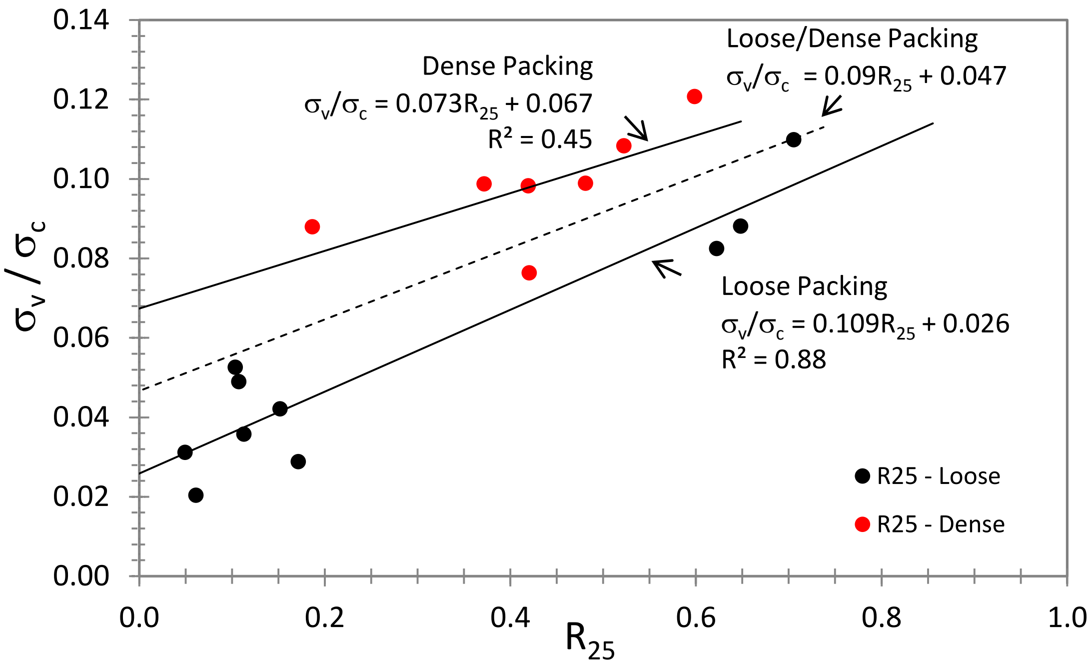

Fig. 4.25: Chart to estimate R_{25}

These relate the vertical pressure σ_v (equivalent to the draw column height) and the uniaxial compressive strength of the rock (σ_c) together with the parameter R defined as follows:

$$R = 1 - \frac{Df}{Di} \qquad [4.2]$$

where D_i and D_f are the initial and final diameters, respectively, for cumulative percentages of 80, 50 and 25% as specified in Fig. 4.23to Fig. 4.25. The initial diameter D_i can be estimated from the primary fragmentation, while D_f requires the followings steps before being evaluated:

1) Estimation of the vertical stress acting on the broken ore σ_v under an IMZ, obtained using either the Janssen equation (Janssen 1985, Janssen 2004, see equation 3.1), or emulators such as Rebop (Cundall et al. 2000). In case of multiples draw columns working simultaneously (interactive flow), vertical stresses can be related to the draw column height above the broken ore (Chapter 6).
2) Estimation of the uniaxial compressive strength, σ_c, of the broken ore. After evaluating this parameter, it is necessary to consider accounting for scale effects, which can be carried out using a power function constrained by laboratory tests for specimens of 30 to 200 mm diameter as recommended by Yoshinaka et al. (2008).
3) Define the packing density. Fig. 4.23 to Fig. 4.25 provide correlations which depend on the packing condition. *Dense packing* should be used for very low swell factors S_f (close to 100%). *Loose packing* is recommended for S_f of 170%, while an intermediate packing density (*loose/dense*) is defined for a S_f of 135%.
4) Determine diameters Di_{85}, Di_{50}, and Di_{25} from the primary fragmentation curves.
5) Obtain the R_{8o}, R_{50} and R_{25} from Fig. 4.23 to Fig. 4.25. The diameters Df_{8o}, Df_{50}, and Df_{25} can then be evaluated using equation 4.2.

4.6 Upscaling: Assessment of Oversized Blocks (Hang-Up Potential)

Studies by Laubscher (1994) and Brown (2007) have identified hang-up potential in drawpoints as one of the key factors determining the success of a block caving operation. Laubscher also suggests that large rocks forming hang-ups correspond to oversize coarse fragmentation at the drawpoints resulting in material handling difficulties. A practical hang-ups representation is given in Fig. 4.26 by Laubscher (2000). These findings are corroborated by observations of hang-up occurrences at several block caving mines such as Palaboa (Penswick 1997, Ngidi & Pretorious 2011), DOZ (Botha et al. 2008), and El Salvador (Barrera et al. 2014). Another phenomenon of interest is that if the air gap is large enough, oversize blocks would tend to roll towards the centre of the ore column down across the cone-shaped free surface (Chapter 5). This is commonly observed in waste rock dumps where coarser blocks roll to the bottom of the rock pile after dumping (Lighthall et al. 1985, McCarter 1985, Nichols 1986). Hence, the susceptibility of fragmentation by oversize blocks within the compression plug-flow zone of a draw column is of considerable interest. A procedure to evaluate the percentage of oversize blocks (Df_{80}) within a plug-flow zone can be carried out following the recommended steps outlined in the previous section (Fig. 4.23). This should be done recognizing the underlying assumptions of uniform broken ore size distribution, low aspect ratios, and uniform block strengths.

It is hypothesized that where a variable size distribution is present, the oversize blocks will experience reduced fragmentation in comparison with smaller blocks due to cushioning in the finer rock matrix (i.e., higher coordination number). However, strength heterogeneity is also present and weaker oversize blocks could be in contact with stronger smaller blocks. This topic is further developed in Chapter 5.

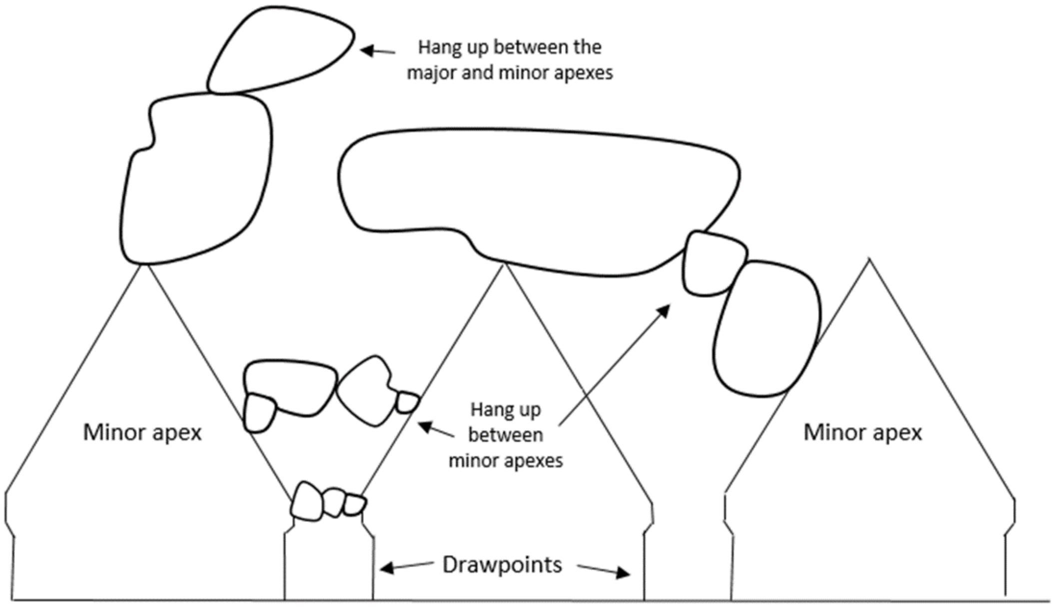

Fig. 4.26: Types of hang-ups occurring at drawpoints (adapted from Laubscher 2000)

4.6.1 Influence of block strength and block size distribution on oversize

In order to study heterogeneity in block strength under variable block size distributions, six additional 1-D compression tests were carried out. Fig. 4.27 presents results from test T-41, which involves a mix of different cube sizes (E = 40%; A = 35%; F = 15%; G = 10%) but with a uniform cube strength (PLT=3.10 MPa). Compared are the results for test T- 66, which involves the same mix of cube sizes but with mixed cube strengths. Specifically, the smaller cubes (Type A, F and G) are stronger (PLT=5.54 MPa) than the largest cubes (Type E, PLT = 3.10 MPa). The results indicate that the largest cubes experience less fragmentation relative to the smaller cubes, with 30-40% cumulative passing remaining at the same Type E size compared to the starting distribution of 40% (see T-41 in Fig. 4.27). When stronger cubes are substituted for particle types A, F and G (see T-66), it can be seen that all Type E cubes fragment somewhat more, causing the coarse branch of the fragment size distribution to shift to the left. This result indicates that there is a threshold of vertical pressure related to the fragmentation of oversized blocks. In this case, the σ_v is 1.3 MPa which can be equated directly to a broken ore in the *far field* (section 4.1) under an *overburden height of 76 m.*

Similar results can be seen in Fig. 4.28 where a larger percentage of smaller cubes are tested (E = 3.5%; A = 11%; F = 25.5%; G = 60%). Again, the largest cubes experience little to no fragmentation, whereas the smaller cubes do, for testing involving a uniform equivalent strength of 3.10 MPa. Interestingly, this cushioning effect protecting the cubes from fragmentation extends to the next smaller cube sizes, with only the smallest cube size experiencing significant secondary fragmentation. When stronger Type A, F and G cubes are introduced (see T-67), the largest cubes do undergo fragmentation, while decreased fragmentation is seen in these cubes. In this case, the oversize blocks fragmented under a σ_v = 2.6 MPa, which can be equated to a*n overburden height of 153 m* (using same inputs as previous stated).

To complement the previous results, two additional tests on samples under different cube sizes are depicted in Fig. 4.29. These tests consist of particles class E = 20%; A = 25%; F = 25%; G = 20%. The first test (T-68) is comprised of cuboids with equivalent particle strength of 5.54 MPa, while the second test (T-69) consists of weaker type E and A particles

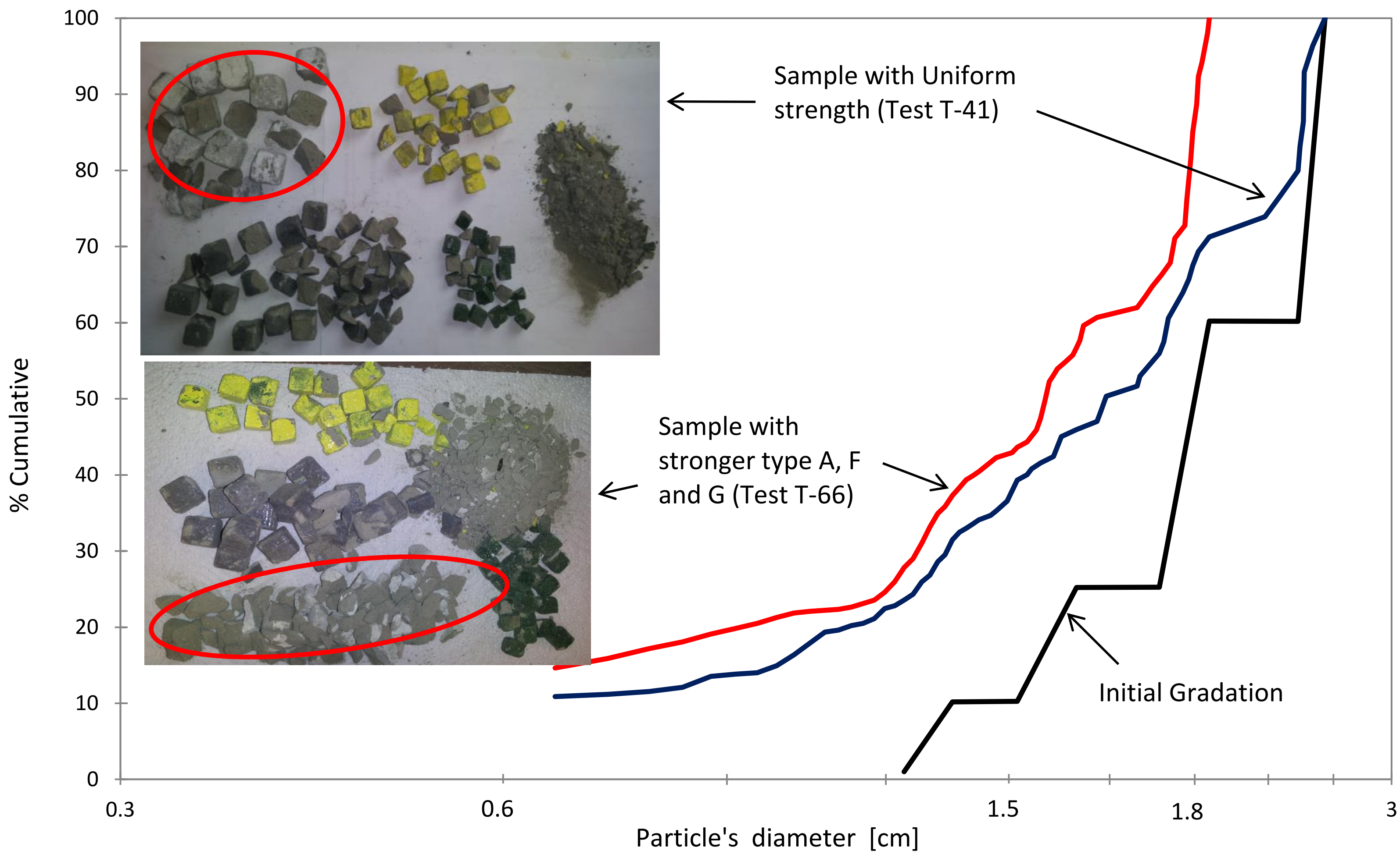

Fig. 4.27: Test comparison with a mixed size and shape distribution (E = 40%; A = 35%; F = 15%; G = 10%), but with one maintaining uniform strength (T-41) and other (T-66) with a weaker Type E component (3.1 MPa instead of 5.4 MPa).

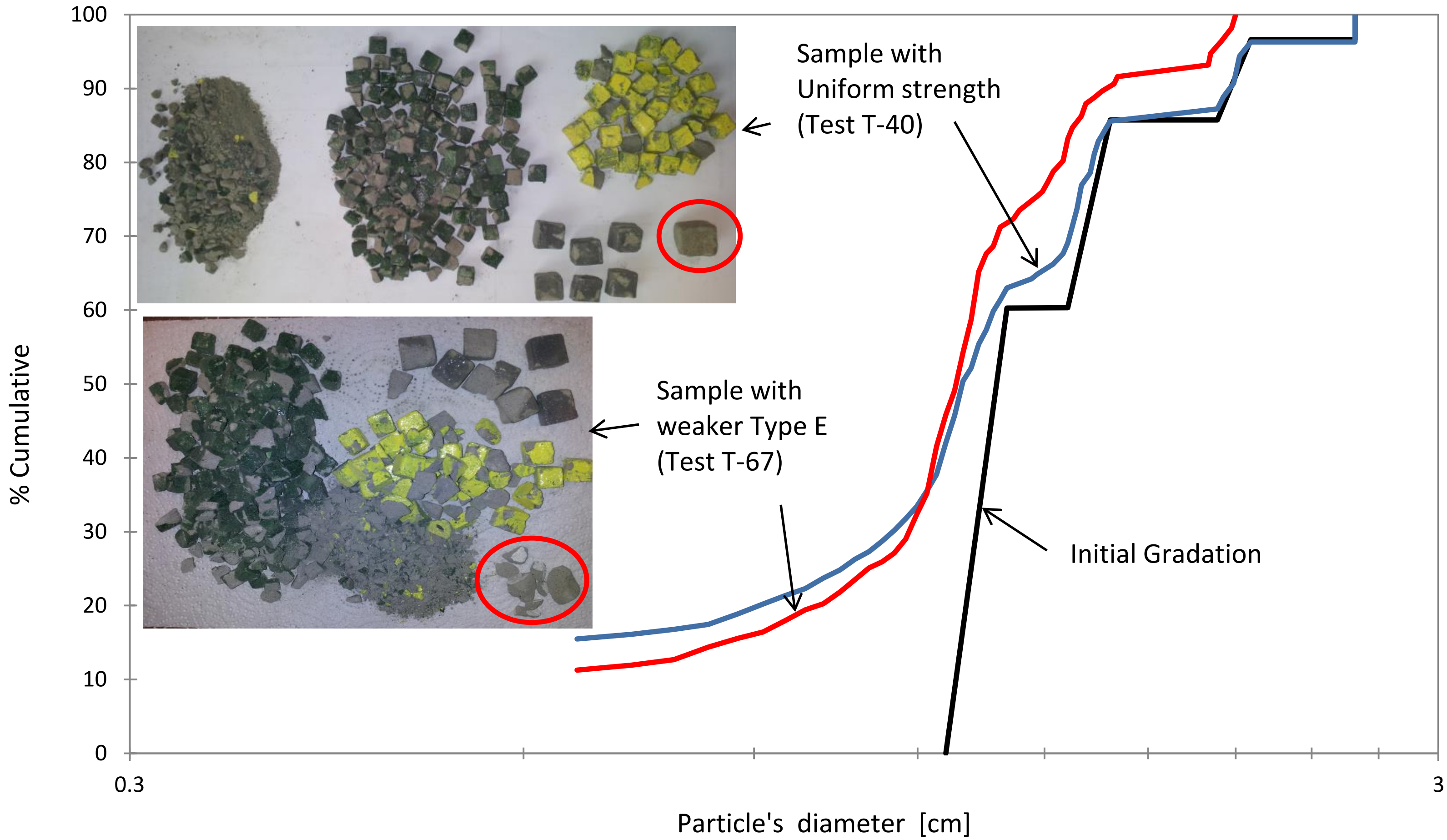

Fig. 4.28: Test comparison with a mixed size and shape distribution (E = 3.5%; A = 11%; F = 25.5%; G = 60%) but with one maintaining uniform strength (T-40) and other (T-67) with a weaker Type E component (3.1 MPa instead of 5.4 MPa).

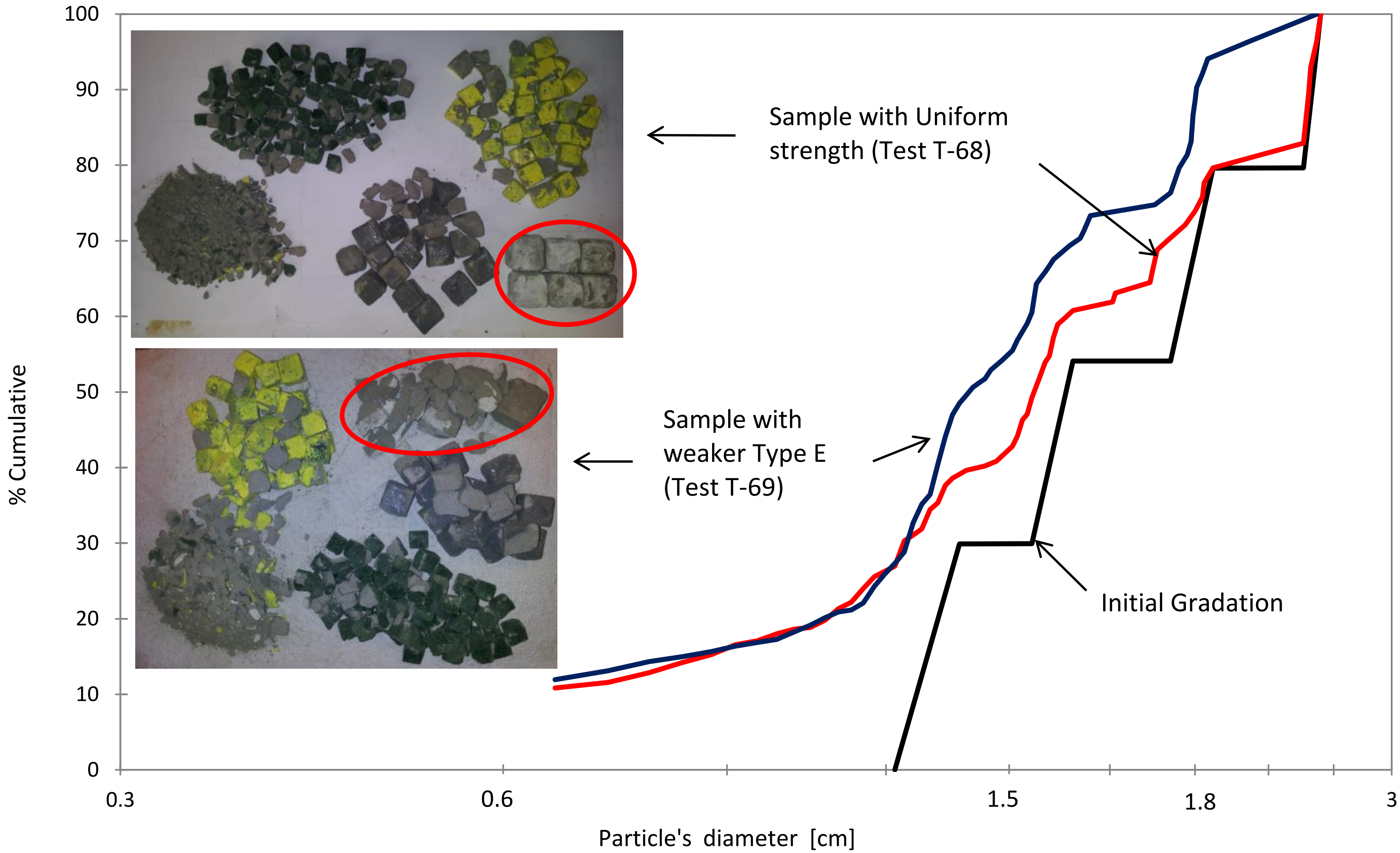

Fig. 4.29: Test comparison with a mixed size and shape distribution (E = 20%; A = 25%; F = 25%; G = 30%) but with one maintaining uniform strength (T-68) and other (T-69) with a weaker Type E and A component (3.1 MPa instead of 5.4 MPa).

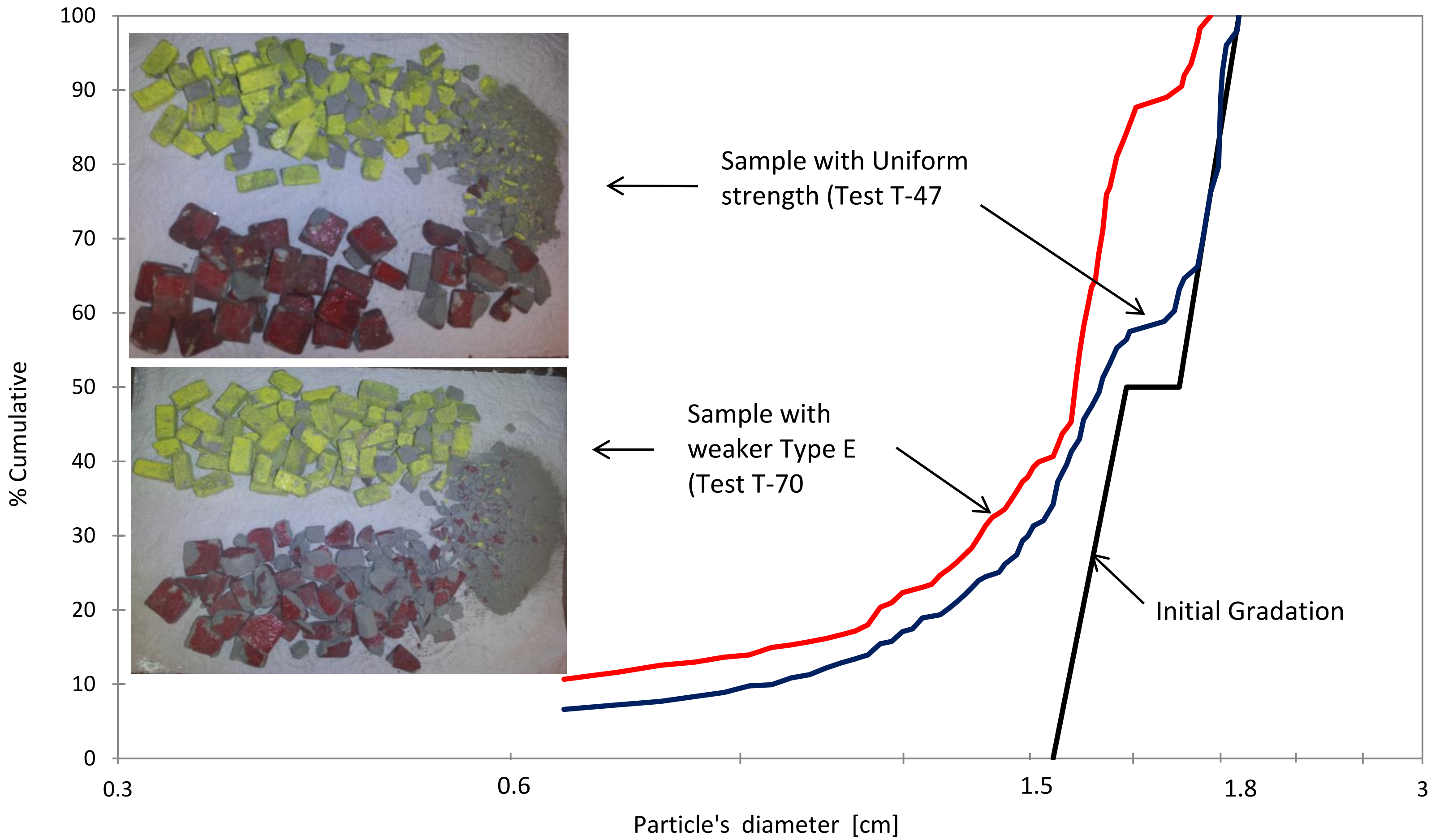

Fig. 4.30: Test comparison with a mixed size and shape distribution (C = 50% and D = 50%) but with one maintaining uniform strength (T-47) and other (T-70) with a weaker Type D component (3.1 MPa instead of 5.4 MPa).

(equivalent strength of 3.10 MPa). Samples with uniform cuboid strengths (T-68) didn't experience fragmentation of the larger particles under σ_v = 1.7 MPa, while test T-69 experienced fragmentation of its larger particles with reduced strengths at σ_v = 2.4 MPa (*overburden height of 141 m*).

Hence, taking the findings from Fig. 4.27 to Fig. 4.29 oversized blocks can undergo fragmentation but only under certain conditions: under high vertical confining stresses and for weaker oversized blocks (e.g., those with high vein intensities). Hence, based on these results, it is expected that the presence of fines is a significant factor dictating the fragmentation of oversize blocks.

4.6.2 Influence of block strength and block shape distribution

As previously shown in Fig. 4.10 block shape does not have as strong an influence on fragmentation that block strength (for the range of block shapes and strengths tested). To further study the heterogeneity of block shape and block strength on hang-up potential, two additional tests are presented in Fig. 4.30. In this case, samples with particle class C = 50% and D = 50% are employed. The former tests considered the same equivalent particle strength for both particles class (5.4 MPa) and a maximum vertical stress of 2.1 MPa. Fragmentation occurred primarily for the type C particles (elongated). Conversely, the latter test considered the same proportion of particle class C and D and a σ_v = 2.0 MPa (*overburden height of 118 m*), but an equivalent strength of 5.4 MPa and 3.1 MPa for particle types C and D, respectively. The results clearly show a higher fragmentation for the weak particles (platy), which demonstrate the significance of particle strength in comparison to block shape. It should be noted that block shape could be a more significant factor for blocks located within the shear bands adjacent to the compression zone, due to preferential block shapes migrating downwards and arriving at the drawpoints quicker.

4.6.3 Summary comparison of results

Based on the results presented in Fig. 4.27 through Fig. 4.30, block strength was seen to be a more significant parameter with respect to hang-up potential in comparison with the block shape and size distributions. As such, a key finding of these experiments is that the final block size distribution encountered at the draw points will include a higher percentage of large blocks (i.e., hang ups) if the primary fragmentation at the top of the draw column likewise includes: i) a larger percentage of large blocks; ii) blocks with a low intensity of veining and/or small discontinuities. This would suggest that preconditioning the rock in the cave back to decrease the initial block size would be more effective at reducing hang up potential than relying on secondary fragmentation with the expectation that high draw column heights will impose high enough loads to break blocks down. Mitigating the need for preconditioning would be whether the large blocks are inherently weak or are weakened by the presence of veins. Moreover, the role of draw control is crucial since it can help to limit large blocks segregating on the muckpile surface as would occur in case of irregular draw (as further discussed in Chapter 5). This in turn would reduce the amount of large blocks within the plug flow zone and thus reduce the hang-up potential.

Another key result is that during the 1-D compression tests, all samples experienced a certain amount of fragmentation accompanied by a high densification, independent of the block properties. This is important given that broken ore densification can facilitate hang-ups forming at the drawpoints.

Finally, the testing carried out in this chapter was developed with a focus on the broken ore material within a plug-flow zone within an isolated movement zone (IMZ). Hence, the case of an interactive flow is not treated in this chapter despite its importance. An interactive flow generates a *far field zone* where the broken ore material can be modeled within a geostatic stress condition, which in turn is associated with further fragmentation. This topic is discussed in more detail in Chapter 6.

4.7 Summary and Key Findings

The secondary fragmentation of broken ore within the central plug flow compression zone in a draw column is a topic not well studied. Empirical and/or numerical methods provide a means to address knowledge gaps and improve existing approaches to evaluating secondary fragmentation during block caving. This chapter reports and analyses a detailed experimental study examining secondary fragmentation and hang-up potential during block caving, for the case of an isolated movement zone. The laboratory program consisted of 74 small-scale one-dimensional compression tests designed to simulate broken ore (caved rock) moving down through the plug-flow compression zone of a draw column. More than 5,000 concrete cuboids were fabricated and tested as a proxy for broken ore, carefully controlling their size, aspect ratio and intrinsic strengths. A subset of these were embedded with a small, non-persistent discontinuity, controlling its length, orientation and aperture in order to examine the role of small joints and veining on secondary fragmentation processes. The packing density of the broken ore was also studied and controlled during testing.

Several key observations and findings were derived from these experiments, which can be summarized as follows:

- Broken ore density (BOD) is an essential parameter influencing both compressibility and the secondary fragmentation process. It was shown that dense packing conveys three marked *fragmentation stages: i) splitting initiation, ii) collapse and fragment reorganization,* and *iii) matrix support strengthening.* Loose packing was observed to undergo a *gradual fragmentation* followed by *matrix support strengthening*. Given that the packing conditions largely depend on the height of the air gap, this variable is revealed as a fundamental element to be controlled during mining when if possible.
- The influence of veins and small discontinuities on the fragmentation of broken ore was examined in detail. Vein thickness was shown to be a key parameter due to the fact that thicker veins trigger a different fragmentation mechanism compared to thin veins. In terms of vein orientation, block discontinuities aligned with the loading direction contribute to fragmentation through splitting of the blocks. Conversely, block discontinuities aligned perpendicular to the loading direction promote increased fragmentation through compressive failure. Vein orientation relative to loading in the draw column is of course random, although possibly less so if there is a pervasive veining direction and a dense initial packing. The effect of embedded veins is such that blocks with enhanced (7x) strength including embedded veins showed comparable

levels of fragmentation as weaker blocks without embedded veins. The characterization of veining intensity using discrete fracture network (DFN) modelling techniques may be an attractive means to provide input using the charts developed to assess secondary fragmentation occurring within the compression zone (plug-flow zone) in an IMZ.

- The fragmentation potential of oversize blocks surrounded by smaller particles was also studied using one-dimensional compression tests. It was demonstrated that large blocks can undergo fragmentation under moderate to high loads, as can weaker oversize blocks (i.e., large blocks with high vein intensities) within a matrix of smaller strong blocks. This outcome could be a topic for further study combining additional laboratory tests with advanced numerical modeling in order to improve the empirical methodologies presented here to predict block size distributions at drawpoints.
- We empirically demonstrated using samples with comparable block strength that the block size distribution (BSD) curve hinges around the largest block sizes. However, as previously noted, this does not apply to large blocks with strengths half that of the smaller matrix blocks or with embedded veins. For these, the BSD curve after testing experience both reduction of the large particles sizes and rotation of the BSD curve around the new largest block size on the sample.
- Based on the interpretation of the laboratory test results, three predictive charts have been produced to help guide pre-feasibility assessments of secondary fragmentation with emphasis on the compression zone in an IMZ providing the block diameters Df_{8o}, Df_{50} and Df_{25}.

Chapter 5: Factors Affecting Secondary Fragmentation during Block Caving [4]

5.1 Introduction

Secondary fragmentation in block caving is attributed to a combination of block splitting and rounding, with block movement being controlled through a combination of shear and compressive stresses occurring in draw column zones (Pierce 2009). Secondary fragmentation, as a component of the block caving design (Chapter 1), has been the subject of various studies, as several key characteristics are not well understood (Brown 2007, Chitombo 2010). Factors affecting secondary fragmentation are typically associated with:

- *Intrinsic rock properties*: Block strength, size, aspect ratio, angularity, roughness, and presence of small, incomplete discontinuities and vein fabric.
- *Variable states of broken ore (caved rock or muckpile)*: Block size distribution (BSD), density distribution in the draw column (also referred to as *swell factor*), and groundwater.
- *Operational factors*: Draw rate, draw sequence and drawpoint closures.

[4] Dorador L, Eberhardt E, Elmo D. Factors Affecting Secondary Fragmentation during Block Caving. (In review).

Some of these factors are recognized as being major variables in secondary fragmentation assessments, for example block strength and ore column height. Major variables are defined as those that must be considered in the early-stages of a project (e.g. conceptual, feasibility) as they can impact the viability of the operation. Others variables can also be critical depending on the specific characteristics of the block caving project (e.g. groundwater, major faults). These should be considered in higher level engineering design stages (e.g. detail engineering). This chapter contributes to the study of seven themes associated with the evaluation of secondary fragmentation at the feasibility and advanced engineering stages, all of these represented in Fig. 1.6:

- Air gap thickness
- Broken ore density
- Segregation of large blocks due to development of a surface cone
- Block strength heterogeneity
- Block strength damage and crushing under high confining stresses
- Water within the draw columns
- Cushioning

5.2 Air Gap Thickness

A large air gap not only introduces an air blast hazard but also facilitates *rock-fall fragmentation through impact* with the muckpile from the cave back above (also referred to as *impact breakage* by Laubscher 2003). The air gap height, which depends largely on differences between the draw rate and cave propagation, also controls the initial broken ore densities at the top of the draw column, which in turn influences secondary fragmentation. Fig. 5.1 presents four key different air gap height scenarios, which will be considered in this section.

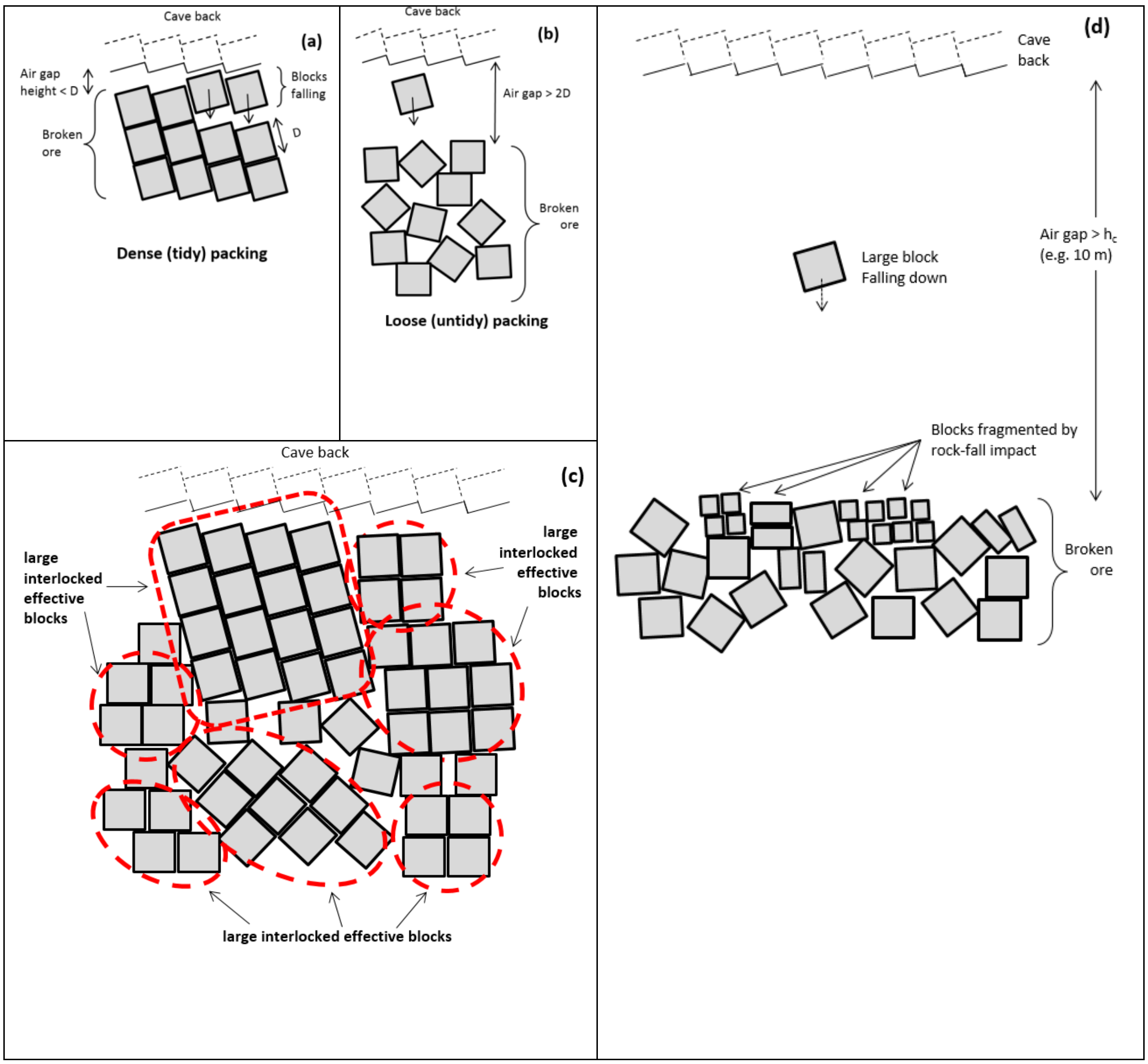

Fig. 5.1: a) Negligible air gap and tidy dense packing. b) Sizeable air gap and loose untidy packing (limited rock fall impact fragmentation). c) Intermediate loose/dense packing within an ore column d) Sizeable air gap with rock fall impact fragmentation.

5.2.1 Air gap variation during operation

It is accepted that the air gap thickness will vary during ore extraction operations. For instance, in the El Teniente mine, Chile, air gap thicknesses of 10 m at low ore column heights have been observed (Encina 2015). However, under a higher ore column, the air gap thickness is strongly controlled by the draw rate and caving rate. In addition, other phenomena such as column compressibility due to broken ore overburden can also take place (Chapter 2), moderately increasing the air gap size. Hence, for draw control purposes, Laubscher (2003) suggests that the height of the air gap must be known at all times.

5.2.2 Initial block arrangement

The air gap height (h) also controls the initial broken ore arrangement at the top of a draw column, influencing the *broken ore density* (BOD), which in turn affects the gravitational flow and secondary fragmentation process. In Chapter 2, a conceptual description of the air gap height as a key factor in broken ore characterization and secondary fragmentation during block caving was proposed (Fig. 5.1): For $h < D$, where D is the diameter of the broken ore (under uniform BSD), a dense (tidy) packing will be generated (Fig. 5.1a). For h higher than 2D, a loose (untidy) packing will occur (Fig. 5.1b), while for $D < h < 2D$, an intermediate loose/dense packing will develop (Fig. 5.1c).

5.2.3 Rock-fall impact fragmentation

As caving progresses, primary blocks detach from the cave back onto the muckpile, undergoing fragmentation due to rock-fall impact (Laubscher 2003, Pierce 2009). However, it is difficult to precisely define the amount of fragmentation generated. Rock-fall impact fragmentation not only depends on the air gap height but also on other factors such as primary block size (as depicted in Fig. 5.2), block shape, presence of discrete fractures within blocks, and elastic parameters (elastic modulus and Poisson's ratio). Wang & Tonon (2009), using a DEM code, showed that both *incidence angle* and *ground condition* are important parameters influencing impact fragmentation, highlighting that stiff and horizontal impact surfaces trigger the highest fragmentation. In order to develop our understanding of how rock-fall impact fragmentation affects secondary fragmentation, a literature review of previous studies is conducted in this section. A consideration of additional fragmentation of blocks lying on the muckpile surface due to rock fall-impact is also of interest, but this topic is not developed in this chapter, though it deserves further investigation.

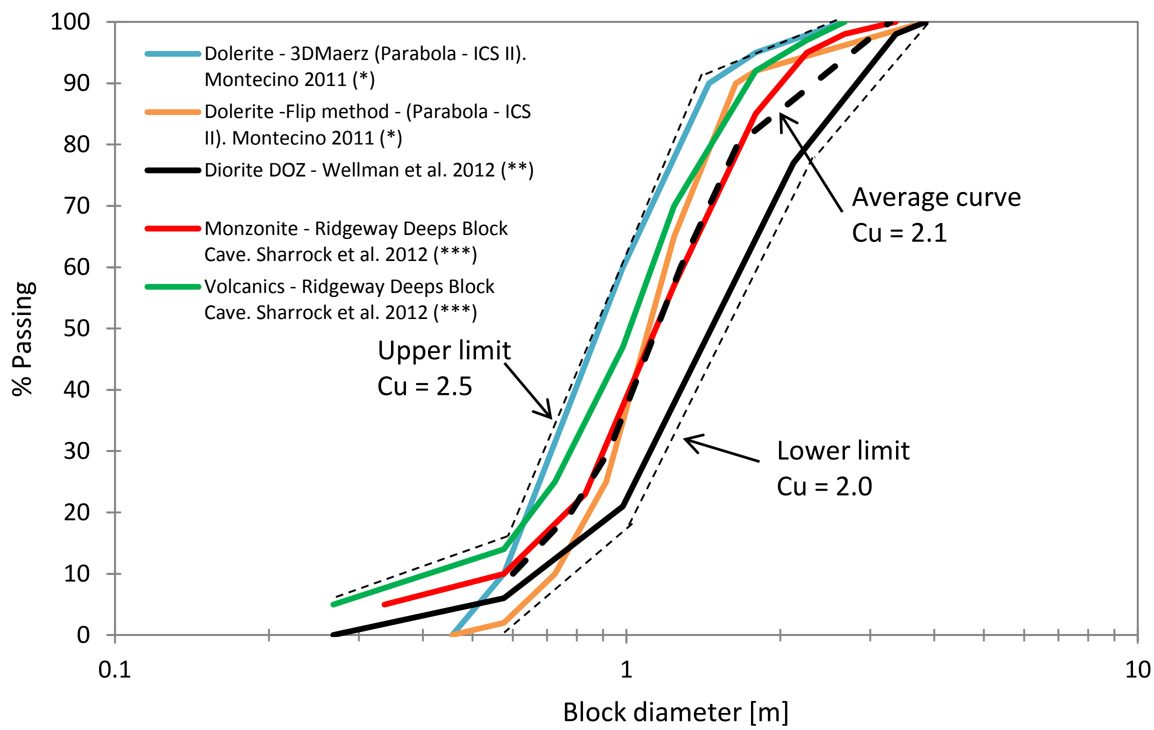

Fig. 5.2: Primary fragmentation curves from different authors. (*) Field estimation (**) Estimation using Core2Frag approach.

5.2.3.1 Rock-fall impact fragmentation in other engineering fields

Although rock-fall impact fragmentation during block caving could occur if there is a sufficient air gap size, measurement of this is extremely difficult based on current technologies (e.g. geophysical measurements). Despite this, experiences can be derived from *rock-fall fragmentation* studies related to rock slope rock fall hazard investigations in Civil Engineering (urban areas and roads). These studies suggest that *rock-fall fragmentation* remains the most complicated and poorly understood aspect of rock-fall analysis (Wang & Tonon 2012). Based on this knowledge gap, a search of related studies was carried out uncovering field investigations by Wang & Tonon (2012) and Giacomini et al. (2009), as well as laboratory tests by Khanal et al. (2008). This data is summarized in Table 5.1.

An extensive body of work related to particle comminution by impact loading has also been developed in the field of mineral processing (Kapur et al. 1997). This shares similarities with the rock-fall impact fragmentation mechanism. Unfortunately, this type of single-particle breakage drop test is commonly conducted on small particles (e.g. gravels), which contrast with the block sizes released from the cave back, which tend to be larger than 1 m diameter as noted in Chapter 2. Also, these single-particle breakage drop tests consider tens of simultaneous drop impacts, which differs from a one-time rock-fall impact. However, this information remains relevant to further studies related to rock-fall impact fragmentation on block caving.

Table 5.1: Summary of previous works

Author	**Type of tests**	**Rock type**	**Critical height**	**Block size (diameter)**	**Amount of fragmentation**	**UCS (MPa)**	**E (GPa)**	**Surface type**
Wang & Tonon (2012)	Field tests	-	9.6 m	0.2 m to 0.3 m	10% fragmentation probability (*)	52-91	66 (estimated)	Hard and soft surface
Khanal et al. (2008)	Impact test (Laboratory)	Concrete composites	Equivalent to 3 m	0.15 m	Splitting into 4 new fragments	35	3.69	Hard surface
Khanal et al. (2008)	Impact test (Laboratory)	-	Equivalent to 23 m	0.15 m	Total fragmentation	35	3.69	Hard surface
Giacomoni et al. (2009)	Field tests	Serizzo	10 – 40 m	1.12 m	Total fragmentation	127 (**)	-	Hard surface
Giacomoni et al. (2009)	Field tests	Beola	10 – 40 m	1.11 m	Total fragmentation	200 (***)	-	Hard surface

(*) Fragmentation observed only on hard surface (**) obtained from Corbella & Zini (1988)

(***) http://www.chooseby.com/mar_dett.php?cod_mar=166

5.2.3.2 Critical height of rock-fall impact fragmentation

The most relevant work conducted to date which likely represents the rock-fall impact fragmentation on block caving is provided by Giacomini et al. (2009). They conducted 20 block fall tests (drop heights from 10 to 40 m) with a representative block diameter of 1.1 m (uniaxial compressive strength, UCS, ranging from 127 to 200 MPa) on a hard impact surface. All tests underwent fragmentation in terms of splitting, ranging from 2 to 22 new fragments from each original block. Based on these results, an *impact fragmentation critical height* h_c of 10 m for a block size of 1 m diameter and intact UCS of 127 to 200 MPa, is suggested.

In addition, Wang & Tonon (2012) also conducted field block drop tests on a hard impact surface under a drop height of 9.6 m. The rocks used were marble, quartzite and skarn with an estimated UCS of 87, 91, and 52 MPa respectively, but under a reduced block size of 0.2 m to 0.3 m. They reported fragmentation in just 10% of the total tests. Hence, it is interpreted that smaller blocks released from the caved back will undergo less fragmentation than larger blocks.

Khanal et al. (2008) carried out horizontal impact tests on concrete composite spheres (0.15 m diameter) with a UCS of 35 MPa, which underwent splitting into four new fragments at a velocity of 7.7 m/s (equivalent to 3 m fall height assuming $h = v^2/2g$). These results could be associated with weaker rock; the *critical height* would be reduced to 3 m under this case.

All tests described above were carried out involving a hard impact surface, which could be representative of a dense tidy packing or an intermediate loose/dense packing at the top of the muckpile (see section 5.3). Also, it is important to mention that the *impact fragmentation* *critical height* will be different for varying rock mass conditions. For instance, in the El Teniente mine where both the rock and embedded veins are characterized as strong, the critical height would be higher. Thus, the impact fragmentation critical height suggested in this section should be considered as a first approximation for design purposes.

5.2.3.3 BSD after rock fall fragmentation

With regard to secondary fragmentation assessments, it is difficult to evaluate the block size distribution arising from rock fall fragmentation. In the field of rock slope rock fall hazards, some authors, such as Ruiz-Carulla et al. (2015), suggest that the size distribution of the new fragments can be characterized by a power law distribution.

$$P(V_{\min} \leq V_o) = C \cdot V_o^{-b} \qquad [5.1]$$

where C is a parameter associated with the minimum significant block volume (V_{min}), and b is the slope of the distribution in a log-log representation. This equation, combined with further empirical and numerical investigations on rock-fall impact fragmentation, could allow a more precise evaluation of the secondary fragmentation assessment.

Therefore, the *impact fragmentation critical height* (Fig. 5.1d), together with the conceptual description of the initial block arrangement (loose versus dense), points to the air gap thickness being a major factor in the broken ore characteristics and secondary fragmentation process during block caving. Future efforts should be expended towards evaluating this variable in the field to better constrain means to assess it.

5.3 Broken Ore Density (BOD)

As developed in Chapter 2, the BOD in a draw column is variable and the initial broken ore arrangement developed when blocks fall freely from the cave back onto the muckpile surface is a significant factor in this regard. Two draw column flow scenarios are analyzed in this section: Interactive flow and Isolated Movement Zone (IMZ). Of interest here is not only the importance of BOD on the geotechnical characteristics of the broken ore but also its relevance with respect to the evaluation of stresses acting within the draw column.

The BOD can experience significant variation under a multiple draw operation (Fig. 5.3a). During the initial block arrangement, blocks can undergo three distinctive packing alternatives, as already described in Section 5.2.2: dense (tidy) packing, loose (untidy) packing, and intermediate loose/dense packing. In the far field (mass flow zone), the broken ore experiences overload compression which increases the BOD, while in the near field and within the shear bands the BOD decreases towards a loose density due to particle rearrangement and dilation, while no major changes of BOD are expected in the plug-flow zone until the broken ore is close to the drawpoints where it undergoes high dilatancy, reducing the BOD. More details regarding the BOD within a draw column can be found in Chapter 2.

Regarding an IMZ scenario (Fig. 5.3b), the BOD will also experience marked changes within the draw column. The BOD in the shear bands will be loose, while it will increase in depth within the plug-flow zone until it undergoes a high BOD reduction due to a decrease in confinement and high dilation response occurring close to the drawpoints.

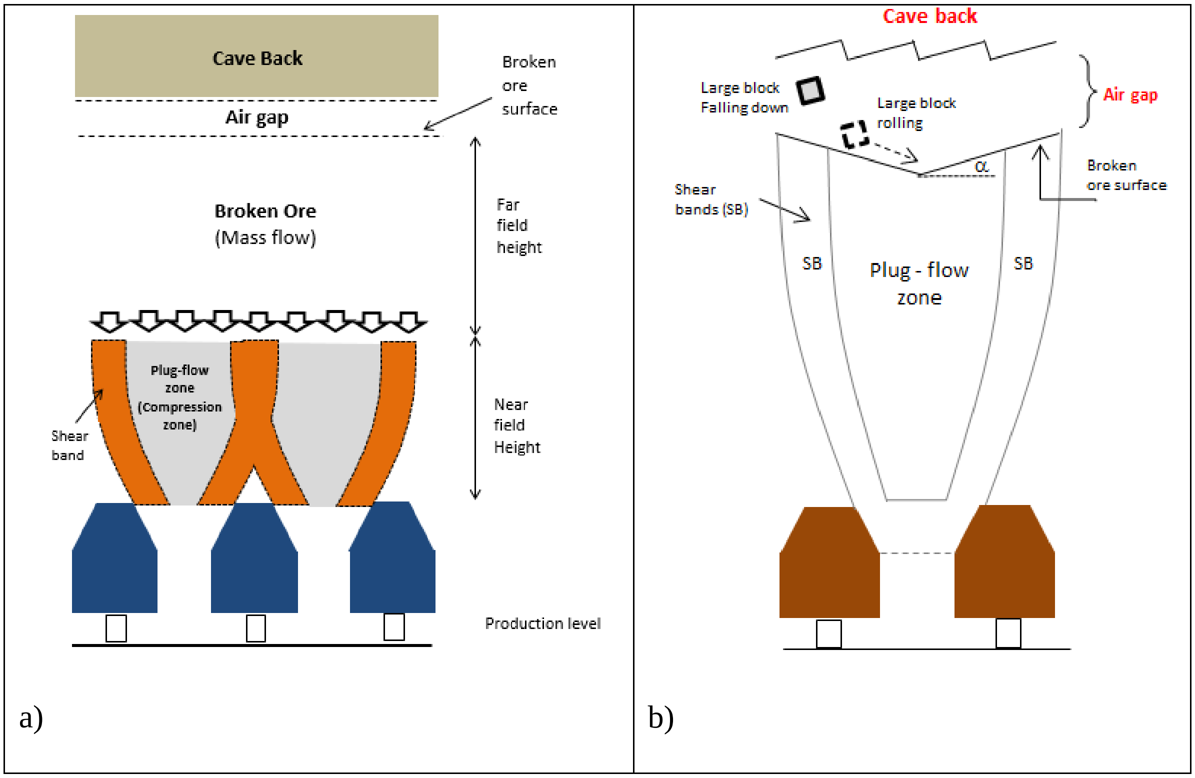

Fig. 5.3: (a) Multiple draw operation. (b) Isolated movement zone (IMZ)

5.3.1 Influence of BOD on secondary fragmentation under interactive flow – Far field

Small scale 1-D compression tests on concrete cubes under dense (tidy) and loose (untidy) arrangements were carried out in Chapter 4 in order to study the secondary fragmentation of a broken ore material within the plug-flow compression zone (Fig. 5.3b), where it was demonstrated the importance of broken ore packing under confined stresses (1-D compression). Results of these tests are plotted in Fig. 5.4 in terms of the compression energy (work) and the fragmentation index Br (Hardin 1985), where a Br equal to zero represents no fragmentation, while a Br value of 1 represents maximum fragmentation. Under loose packing conditions, fragmentation is proportional to the degree of external energy acting on the sample under a gentle quadratic trend. However, the dense (tidy) packing exhibits a higher fragmentation in comparison with the loose packing under energy values from 0.05 to 0.45 MPa x mm/mm.

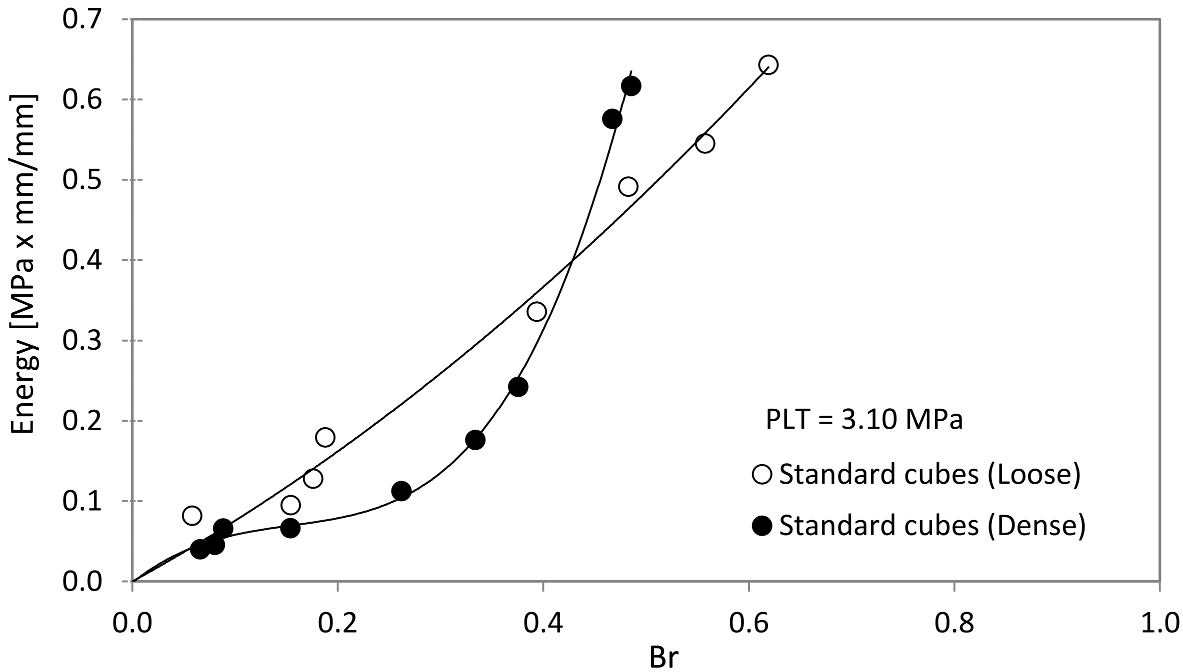

Fig. 5.4: Influence of compression energy (work) and packing on fragmentation under 1-D compression tests

Based on the results from the concrete cube samples, Fig. 5.5 shows the same data, this time plotted maximum vertical pressure (σ_v) reached at the end of testing versus Br, under both dense and loose arrangements. A loose packing yields a quadratic fragmentation curve, while a dense packing undergoes low fragmentation until σ_v = 3 MPa, transitioning then to matrix collapse and significant fragmentation. Based on these results it is hypothesized that a critical vertical pressure associated with particle fragmentation could be reached for dense (tidy) packing of the broken ore materials under a critical fragmentation ratio σ_v / UCS = 0.1, in this based on a representative UCS of 30 MPa for the tested material (Chapter 4). These tests need to consider the strength reduction due to size scale effect in order to be compared with broken ore materials. As indicated in Chapter 4, scale effects are marginal for these concrete samples, so the UCS scaled to large block sizes can be assumed to be approximately 30 MPa and the critical ratio be considered as 0.1. For instance, broken ore with a UCS of 50 MPa (after strength reduction due to scale effects) would have a critical vertical pressure σ_v of 4.85 MPa, which in turn could be equivalent to a column overload height of 194 m for a BOD of 2.5 t/m^3. This column overload height could be defined as H_{cf}. Therefore, these results clearly show a significant influence of the BOD in the secondary fragmentation within the far field zone.

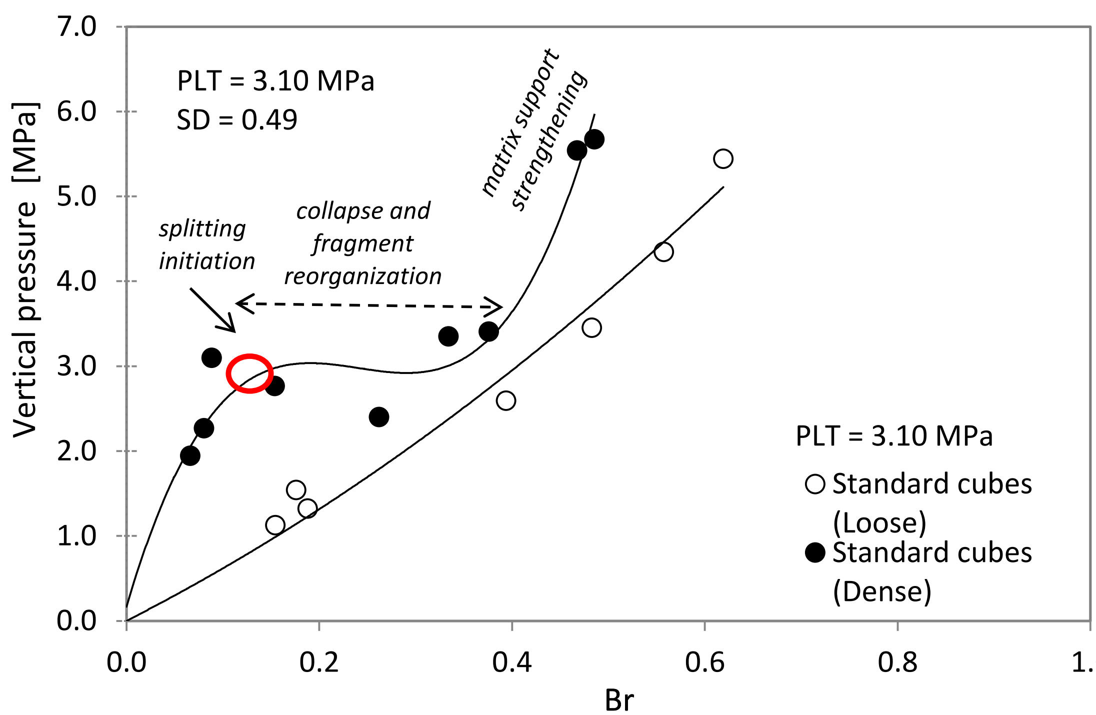

Fig. 5.5: Fragmentation stages on 1-D compression tests under vertical pressure. SD = Standard deviation

5.3.2 Influence of BOD on secondary fragmentation under interactive flow – Near field

Regarding the near field, the plug-flow zone and the shear bands (outer periphery) are affected by mass flow from the far field. A dense (tidy) packing from the far field would experience a strong dilation in the outer periphery, offset by fragmentation due to high normal pressures acting on the shear bands. Loose (untidy) packing would also induce a high level of fragmentation due to significant normal pressures acting on the shear bands caused by greater ore column heights. The intermediate loose/dense packing in the outer periphery would result in an average level of fragmentation between the dense (tidy) and loose (untidy) arrangements. Conversely, no additional fragmentation would be expected in the plug-flow zone, due to the continuously decreasing stresses as the blocks move closer to the drawpoints.

5.3.3 Influence of BOD on the secondary fragmentation under an IMZ

BOD under an IMZ varies for both the plug-flow zone and adjacent shear bands (Chapter 2). On the one hand, it is believed that under low ore column heights (e.g. 50 m), fragmentation within the plug-flow zone will be minor due to the low stresses acting in the centre of the draw column, and so BOD will not significantly influence the secondary fragmentation. Conversely, the BOD under low ore column heights could be relevant within the shear bands under a dense (tidy) packing, due to the fact that the broken ore is affected by a greater degree of dilation at the beginning and along the shear band. At the other extreme (e.g. loose untidy packing), continuous fragmentation would occur. In either case, the amount of fragmentation would not be significant due to the low confining stresses acting on the shear bands, even though significant shear deformation would take place. Unfortunately, there is little data available regarding the influence of bulk density on broken ore fragmentation under large shear deformations.

On the other hand, fragmentation within both plug-flow zone and shear bands will be significant under higher columns, due to the higher stresses acting in the draw column. In terms of BOD within the plug-flow zone, correlations to evaluate the secondary fragmentation for three density ranges were derived from small-scale 1-D compression tests (Chapter 4). In terms of shear bands, the BOD can vary significantly in the upper part of the draw column. However, it is expected that a loose density will be found mostly along the shear band. If so, then the influence of the BOD on secondary fragmentation within shear bands wouldn't be significant.

5.3.4 Influence of BOD on the overburden stresses on broken ore.

The BOD has been studied in sections 5.3.1 to 5.3.3 in terms of its direct influence on the secondary fragmentation. In addition to this, the BOD is proportional to the weight and overburden stresses acting on the broken ore. For instance, in a hypothetical far field of 100 m height and BOD of 1.8 t/m^3 and 2.3 t/m^3, vertical stresses of σ_v = 1.8 MPa and 2.3 MPa can be obtained for the boundary between the near and far field, which means a difference of 28%. This simple example shows the importance of carefully evaluating the BOD in order to estimate reliable stresses on the broken ore within a draw column. Chapter 2 provides a simple procedure to evaluate the BOD within a draw column.

5.4 Segregation by Large Blocks Due to Surface Cone

It is accepted that cone-shaped free surfaces develop over the drawpoints due to continuing ore extraction (Pierce 2009). Treating broken ore as a particulate material, the slope of this surface depends largely on the angle of repose of the granular material as indicated by Waters & Drescher (2000). As noted by Dodds (2003), very little force is required to initiate and maintain rolling of round particles, although this is sensitive to block size. For example, Samadani et al. (1999) experimentally showed the segregation of particles in a quasi-two-dimensional silo experiment, where larger particles rolled further down the inclined surface than smaller particles. In addition, their data supports the presence of a secondary segregation mechanism at the silo surface involving void filling, in which smaller particles have an increased probability of filling a void in comparison to larger particles for the same sized void. The first segregation mechanism is strongly supported by evidence in waste rock dumps associated with open pit mining (Piteau Associates Engineering ltd., 1991 and Hungr et al., 2002), where larger blocks regularly reach the toe of the dump after the waste rock is dumped at the top of the slope. Fig. 5.6 shows an example of this segregation phenomenon in a rockfill stockpile.

Fig. 5.6: Block segregation on rockfill borrow stockpile. Photo by A. Breitenbach. Available online at http://www.geoengineer.org/

Thus, under an isolated movement zone (IMZ), it can be assumed that large blocks on the muckpile surface will roll down to the centre of the cone surface, resulting in a higher percentage of larger blocks concentrating within the plug-flow zone (see Fig. 5.3b). This would contribute to an increasing frequency of hang-ups. It is inferred that in the case of interactive flow, a sloped surface would also be generated as depicted in Fig. 5.7. However, as shown in this figure, the direction of rolling, and therefore the drawpoints that would receive a higher percentage of large blocks is dependent on the draw distribution.

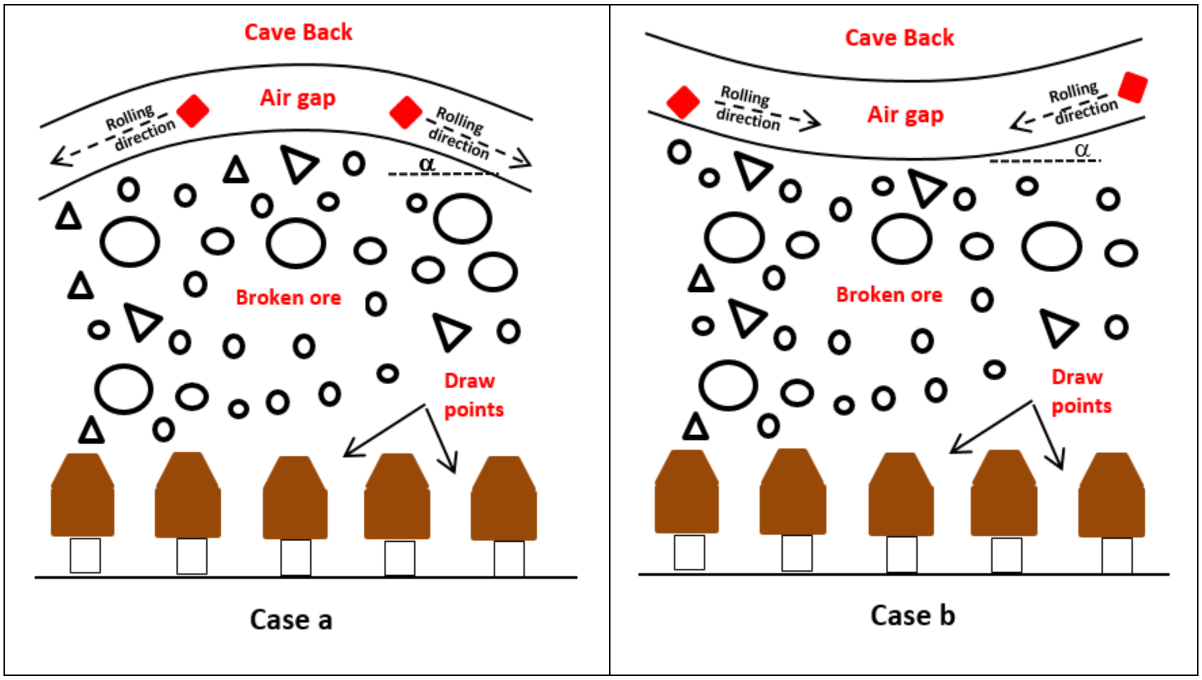

Fig. 5.7: Two representative cases of block's segregation under several draw columns working together.

The segregation that develops affects the BSD and BOD, especially under an IMZ regime, because more oversize blocks concentrate within the plug-flow rather than within the outer shear bands. This in turn results in coarser size distributions in the plug-flow zone and finer gradations in the shear bands. Hence, this segregation process would modify the block size distributions as well as the broken ore densities in both shear bands and plug-flow zone. A procedure to correct the BSD for the upper part of the draw column is proposed in section 5.4.4 to evaluate the block segregation potential and to improve secondary fragmentation assessments.

5.4.1 Influence of block size

As indicated by Fityus et al. (2013), Pfeiffer & Bowen (1989) and Dorren (2003), the size of the block relative to the slope surface roughness also controls the likelihood that its motion will or will not be sustained. Larger rocks have greater physical size and greater momentum, which means they are less likely to lodge amongst irregularities on a slope of given roughness (Ritchie 1963). In terms of block size released from the cave back (Fig. 5.2), oversize blocks would likely have diameters of around 3 m or more, although oversize blocks up to 8 m in diameter have been reported (Brzovic, 2015).

5.4.2 Influence of block shape

Considering the block shapes from Fig. 5.8, acute edges exhibit relatively little tendency to initiate or sustain motion. For instance, pyramid shaped blocks and conical shaped blocks do not generally display the tendency to roll (Fityus et al., 2015). The threshold for either shape to roll is between 8° and 10°, but only when the starting arrangement includes the release from a corner (Fityus et al., 2015; Fig. 5.9). Fityus et al. also corroborated that velocity increases with slope angle and those shapes with rounded surfaces (spheres and cylinders) roll faster than shapes with flat surfaces. Hence, based on the results from Fityus et al. (2015), Fig. 5.9 and Fig. 5.10 can be used as a first approximation of segregation potential of oversize blocks on the muckpile surface. For instance, based on Fig. 5.10 a 50% segregation probability under a ramp slope of 20° could be expected for the different block shapes.

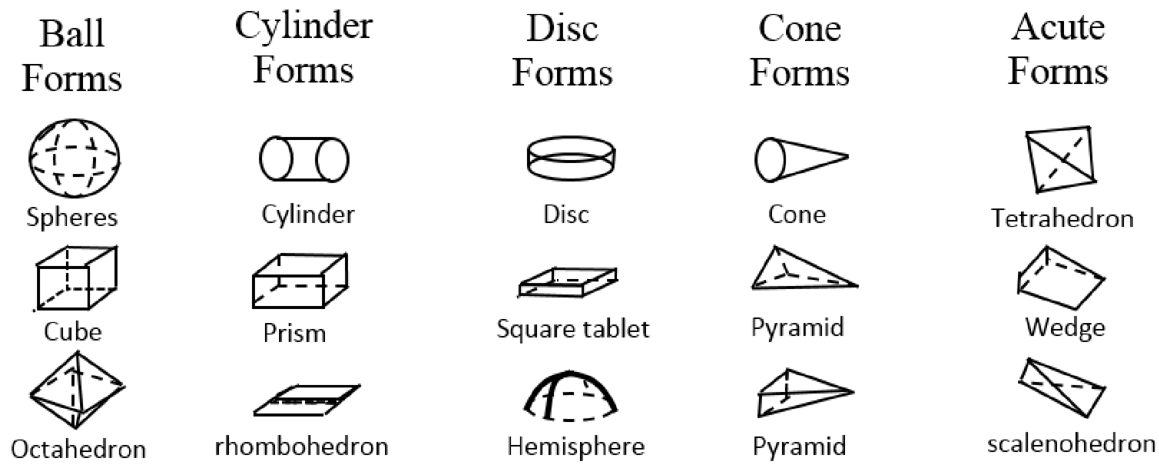

Fig. 5.8: Block shape categories related to rolling motions (adapted from Fityus et al. 2015)

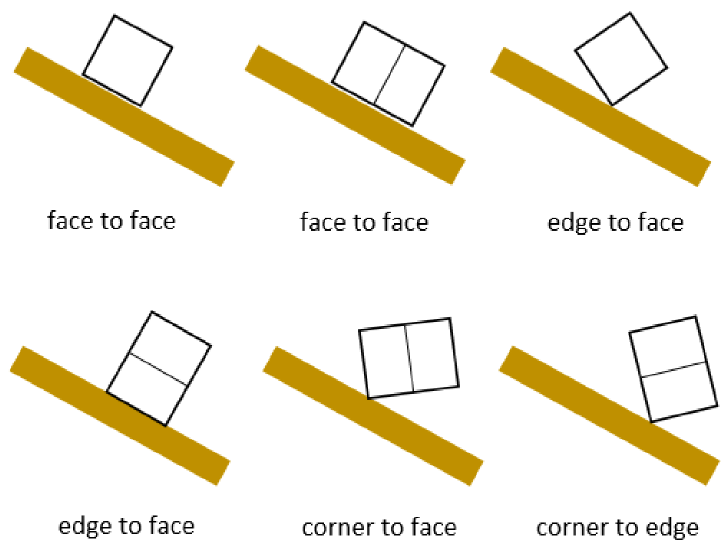

Fig. 5.9: Release positions for cubic specimen (adapted from Fityus et al. 2015)

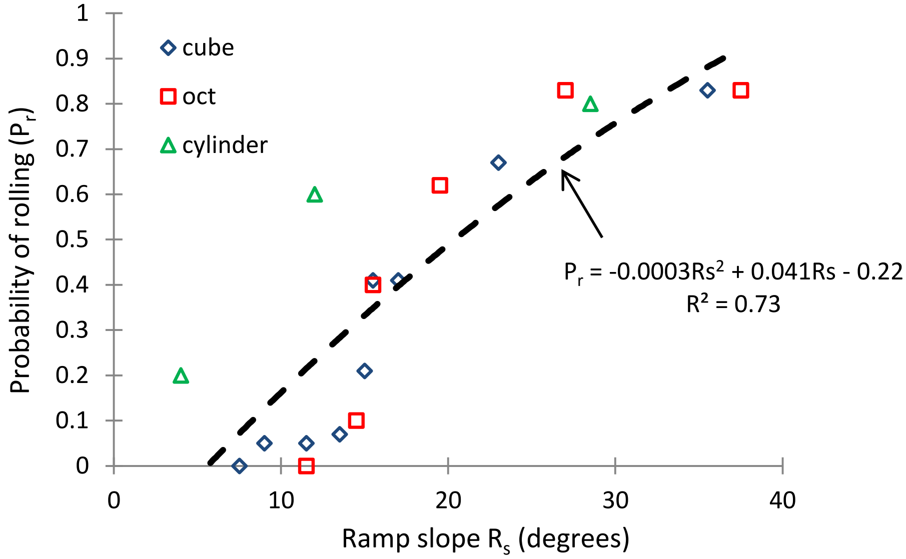

Fig. 5.10: Likelihood of a block rolling and rolling sustainably as a function of the slope steepness (adapted from Fityus et al. 2015)

5.4.3 Influence of angle of repose on broken ore

Another key element influencing the segregation of large blocks is the angle of repose (α) of the broken ore. This parameter can be easily described by a large *in-situ* tilt test (Fig. 5.11), but this is rarely carried out in the field. For instance, tilt tests on marble from a waste rock dump were carried out by Iabichino et al. (2014), obtaining values of α ranging from 47^o to 58^o under normal pressures σ_n lower than 0.1 MPa. A key characteristic of the tilt test is that the normal pressure applied to the sample is very low, which strongly influences higher interparticle friction angle values for the material. For example, interparticle friction angles (ϕ') higher than 60^o under low normal pressures have been reported on ballast material (Indraratna et al. 1998; see Fig. 5.12) In addition, the interparticle friction angles measured during large triaxial tests under σ_n of 0.04 to 0.07 MPa on intrusive and metamorphic rockfill are in the range of 46° to 53° (Marsal 1973).

Considering the above literature review examining the angle of repose α and ϕ' under low σ_n, values of α ranging between 45° and 60° are recommended. This means that if the broken ore at the surface reaches the angle of repose, almost all large blocks falling down from the cave back will roll to the bottom of the surface, according to Fig. 5.10.

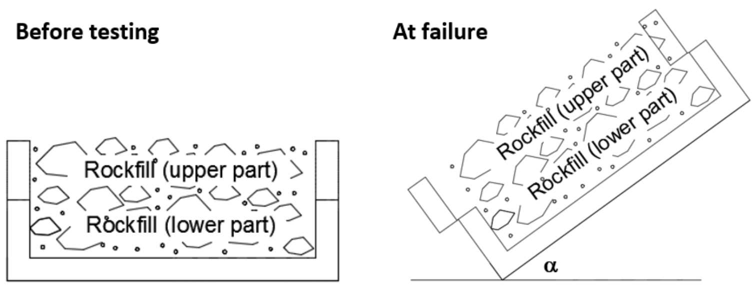

Fig. 5.11: Tilt test on rockfill. Adapted from Barton (2013)

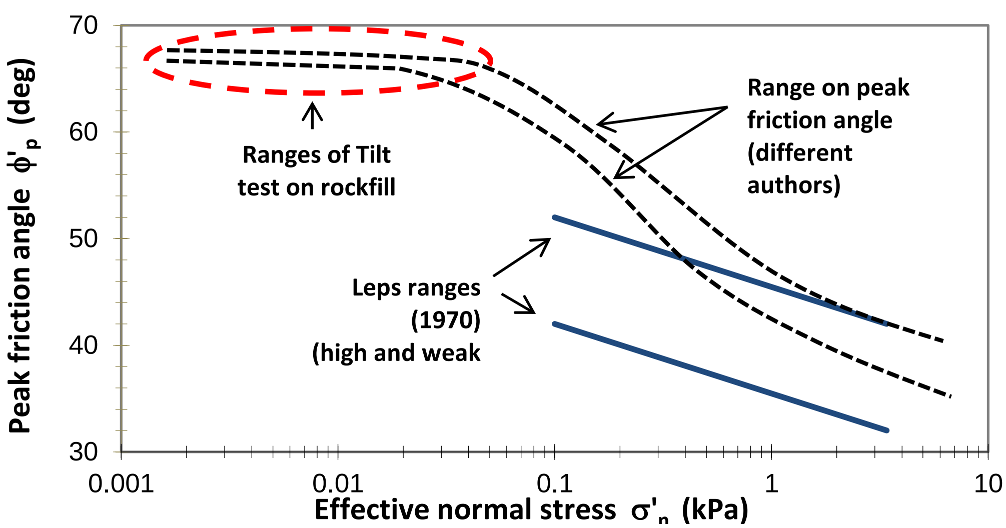

Fig. 5.12: Triaxial compression data on ballast and rockfill materials under different ranges of normal pressures σ_n. Adapted from Indraratna et al. (1998)

5.4.4 Procedure to correct the BSD at the top of a draw column

Assuming an IMZ, the following steps are provided as a suggested means to correct the estimate of BSD at the top of the muckpile due to block segregation. This will facilitate a better assessment of the block size distribution within a draw column and hang-up potential at the drawpoints.

a) Determine the block size distribution after primary fragmentation including rock-fall impact fragmentation (BSD). Guidelines to assess primary fragmentation are included in Chapter 6. Then, define the values of D_{100}, D_{80}, D_{50}, D_{25}

b) Estimate the *angle of the repose* of the broken ore. Although large tilt test is the ideal means to evaluate it, a value between 45° and 60° could also be defined.

c) Evaluate the *probability of rolling* (% Pr*)* using Fig. 5.10. Consider the ramp slope angle to be equal to the *angle of the repose* of the broken ore.

d) Split the BSD into a coarse and fine gradation. Both gradations are defined here as G_c and G_f (see Fig. 5.13a). For practical purposes, the split could be done at the D_{50} of the BSD. Representation of both shear band and inner plug flow zone is provided.

e) Calculate the plan view areas of the inner plug flow zones (A_{PLF}) and outer shear band (A_{SB}) (Fig. 5.13b). Considering a draw column diameter (D) and a shear band thickness (t) as 10 times D_{50} (Pierce 2009), the A_{PLF} is the circular area of diameter D-2t, while the A_{SB} is the difference between the plan view area of the draw column (circular area of diameter D) and the A_{PLF}.

f) Obtain the percent weight for the BSD, G_c and G_f for the size fraction defined. For this example, the size fractions are 4m, 2m, 1m, 0.5m and 0.2m.

g) Correct the plug-flow zone gradation (BSD_{pf}). Consider equation 5.2 to obtain the final weight by size fraction based on the BSD and the Gc.

$$weight(\%) = weight\%(BSD) + weight(G_C) \bullet P_r \bullet \frac{A_{SB}}{A_{PFZ}} \qquad [5.2]$$

h) Correct the shear band gradation (BSD_{SB}). Consider equation 5.3 to obtain the final weight by size fraction based on the Gf and the Gc.

$$weight(\%) = weight\%(G_f) + weight(G_C) \bullet (1 - P_r) \qquad [5.3]$$

A simple example is provided as follow: Let considers a BSD after primary fragmentation with D_{100} = 4 m, D_{80} = 3m, D_{50} = 1 m, D_{25} = 0.5 m (Fig. 5.13a). Regarding step b and c, if the *angle of the repose* is 35°, then the *probability of rolling* is 85%. On step d, the BSD is spitted into a coarse and fine gradation (Fig. 5.13a). Next, assuming a draw column diameter D = 45 m, and t = 10 m (10 times D_{50}) the areas A_{SB} and A_{PLF} are evaluated as 1100 m^2 and 491m^2. Finally, step f is conducted and then, BSD_{pf} and BSD_{SB} are obtained using equations 5.2 and 5.3. Table 5.2 is included to verify the calculus.

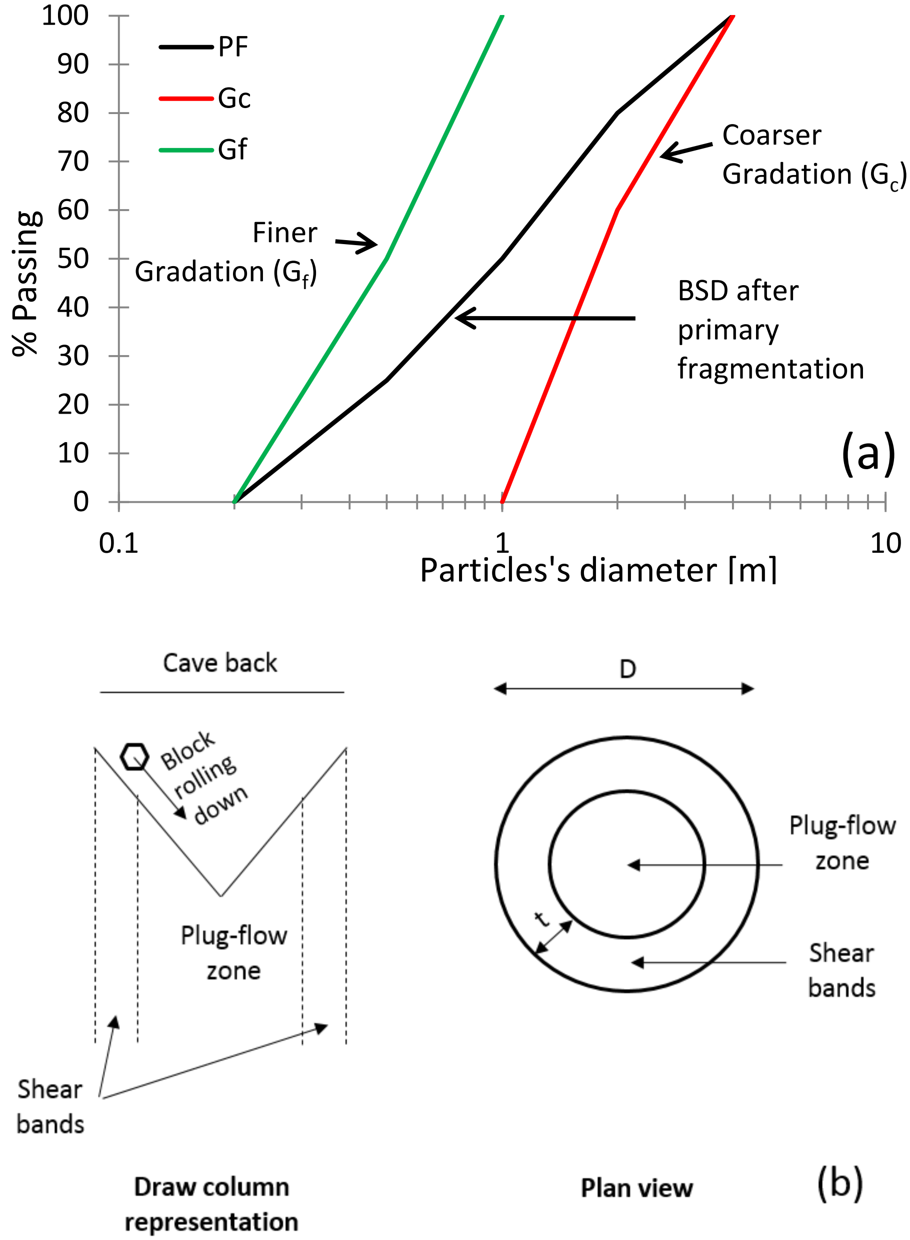

Fig. 5.13: a) Split of BSD into a coarse and fine gradation. b) Plug-flow zone and shear band sections

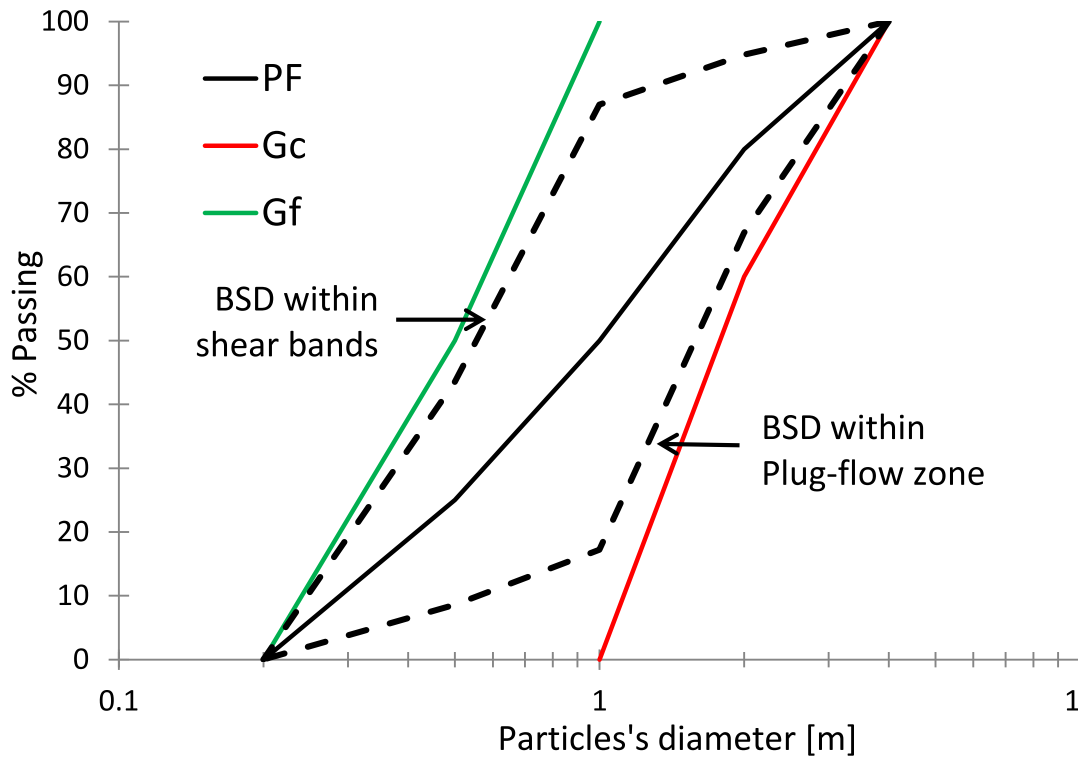

Fig. 5.14: Final BSD of both plug flow zone and shear bands from example.

Table 5.2: Calculus to obtain the BSD_{PFL} and BSD_{SB} for the example provided

Size fraction (m)	**Cum. BSD**	**% weight BSD**	**Cum. Gc**	**% weight Gc**	**Cum. Gf**	**% weight Gf**	**% weight (Plug flow zone)**	**Cum. BSD_{PFL} (*)**	**% weight (Shear band)**	**Cum. BSD_{SB} (*)**
4	100		100					100		100
2	80	20	60	40			96	67	6	95
1	50	30	0	60	100		144	17	9	87
0.5	25	25			50	50	25	9	50	43
0.2	0	25			0	50	25	0	50	0
							$\Sigma = 290$		$\Sigma = 115$	

(*) The cumulative curves for both plug-flow zone (BSD_{PFL}) and shear bands (BSD_{SB}) are obtained from the % weight of each size fraction and normalized by the sum of all % weight by size fraction. ($\Sigma = 290$ and $\Sigma = 115$).

5.5 Block Strength Heterogeneity

According to Howson (2004), the rock volume to be caved is rarely homogenous. Specifically, a rock body will be subject to zones of weakness mixed with those of stronger rock. Strength heterogeneity may be in the form of changing lithologies, varying discontinuity intensities, and varying degrees of veining, which may either be weaker or stronger that the rock they are disseminated with. This heterogeneity in the rock mass translates to heterogeneity that will then be present in the draw column (i.e., muck pile). It is also believed that the amount of broken ore heterogeneity will depend on its location within the draw column (e.g. plug-flow zone or shear bands).

Unfortunately, there is a knowledge gap related to the role of broken ore strength heterogeneity during secondary fragmentation in block caving. In the field of soil mechanics, several works have been reported regarding particle fragmentation under samples with different particle strength (e.g. Leleu & Valdes 2007), which can be applied to better understand the role of block strength heterogeneity on secondary fragmentation during block caving. However, comprehensive studies are still required in order to generate a standard procedure to evaluate the block strength heterogeneity, such as the nomogram used to determine the corrected Intact Rock Strength (IRS) value used in the Mining Rock Mass Rating (MRMR) system (Laubscher & Jakubec, 2001).

5.5.1 Laboratory testing under 1-D compression

1-D compression tests serve as a lab-scale proxy for both the plug-flow zone related to the IMZ flow scenario and the far field zone related to the interactive flow scenario. Two published works are referenced in this section. Leleu & Valdes (2007) conducted an empirical investigation related to the crushing of sands subjected to 1-D compression. Tests were carried out on a mix of quartz (strong) and calcareous (weak) sands under vertical pressures from 4 to 67.5 MPa. Unfortunately, the authors did not provide strength values for the two types of sand. They concluded using the B_r parameter (Hardin 1985, see section 5.3.1) that weak particles can be crushed more easily than strong particles for different proportions of strong-to-weak particles (Fig. 5.15a). However, the effects of particle strength heterogeneity on crushing behaviour diminish with increasing stress. Papas & Vallejos (1997) also carried out an 1-D compression testing program on heterogeneous samples composed of strong limestone particles (UCS = 179 MPa) and weak shale particles (UCS = 27 MPa), see Fig. 5.15b, which would yield a strong-to-weak strength ratio of 6.6. They likewise concluded that the amount of fragmentation increases under higher percentages of weak particles, although they employed an alternative parameter referred to as the *particle breakage factor*, which consists of summing the differences in percentage of rock particles passing each sieve (after and before the test); hence, this factor would increase for higher fragmentation.

Based on the previous findings, it is inferred that under low ore column heights, weak blocks could undergo some degree of fragmentation in contrast to a negligible amount of fragmentation in strong blocks. However, under higher ore columns, both weak and strong blocks could experience fragmentation, albeit *cushioning* effects (section 5.8) must then be considered, which would inhibit the fragmentation of stronger blocks. Finally, acknowledging the lack of studies involving 1-D compression testing and block strength heterogeneity, it is reasonable to consider as a first approximation a linear increase of fragmentation (based on parameter B_r) as a function of increased percentages of weak particle content.

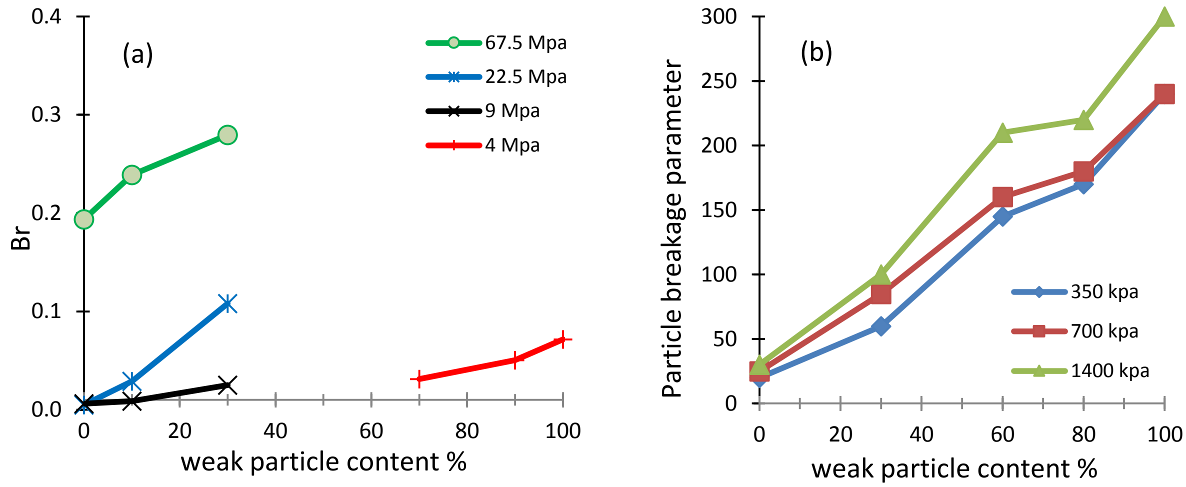

Fig. 5.15: a) 1-D compression testing data from Leleu & Valdes (2007). b) Papas & Vallejos (1997)

5.5.2 Laboratory testing under simple shear

These tests serve to represent the shear bands in both the IMZ and near field zone in the case of interactive flow. Of special interest are annular ring shear tests, which allow the specimen to undergo large shear displacements, which can be equated to a broken ore material undergoing high displacement downwards through the shear bands. Unfortunately, similar to 1-D compression tests, there is a lack of studies examining the influence of block strength heterogeneity on secondary fragmentation under large shear displacement conditions. However, two studies involving simple shear tests under small angular displacements have been reported by Valdes & Leleu (2008) and D'Espessailles et al. (2014), which will be considered in this section.

Valdes & Leleu (2008) conducted simple shear tests on two types of homogeneous sands: rounded quartz grains (strong) and subangular calcareous sand (weak). Three volumetric ratios of strong (quartz) and weak (calcareous) were considered, with mixes of 0%, 10% and 40% calcareous sand. Testing involved normal stresses between 147 kPa and 824 kPa, and shear strain (angular deformations) from 0.2 to 0.3. The authors found that the presence of weak grains affects the simple shear response of predominantly strong-grained sands. At low normal stresses, the stress-strain response and particle fragmentation are controlled by particle shape; at higher normal stresses, the response and particle fragmentation are controlled by weak particle breakage. Some of these results are presented in Fig. 5.16a, where it is clear that fragmentation is increased by the amount of weak particles.

D'Espessailles et al. (2014) executed a simple shear testing program examining two angular sands sourced from mine blasted rock. The first type of sand was composed of strong particles, predominantly quartz and plagioclase, while the second was formed by weak particles (mostly orthoclase particles). Three types of samples were generated under a ratio of strong/weak particles of 100:0, 75:25 and 0:100. In terms of particle strength, strong particles reached an average individual compressive strength of 10.7 MPa, contrasting to that of weak particles (2.8 MPa), which gives a strong/weak ratio of 3.8. Normal stresses of 100 to 700 kPa and angular deformations of up to 0.6 were applied during tests. To quantify particle fragmentation, Marsal's B_g index (1973) was considered; B_g is equivalent to the sum of the positive values of the differences (ΔW) between the percentage retained by weight under each particle size fraction before and after testing. Accordingly, $B_g = 0$ is equivalent to zero fragmentation while $B_g = 100\%$ is equal to the maximum theoretical fragmentation. As shown in Fig. 5.16b, higher fragmentation was obtained under higher normal stresses and higher proportions of weak particles.

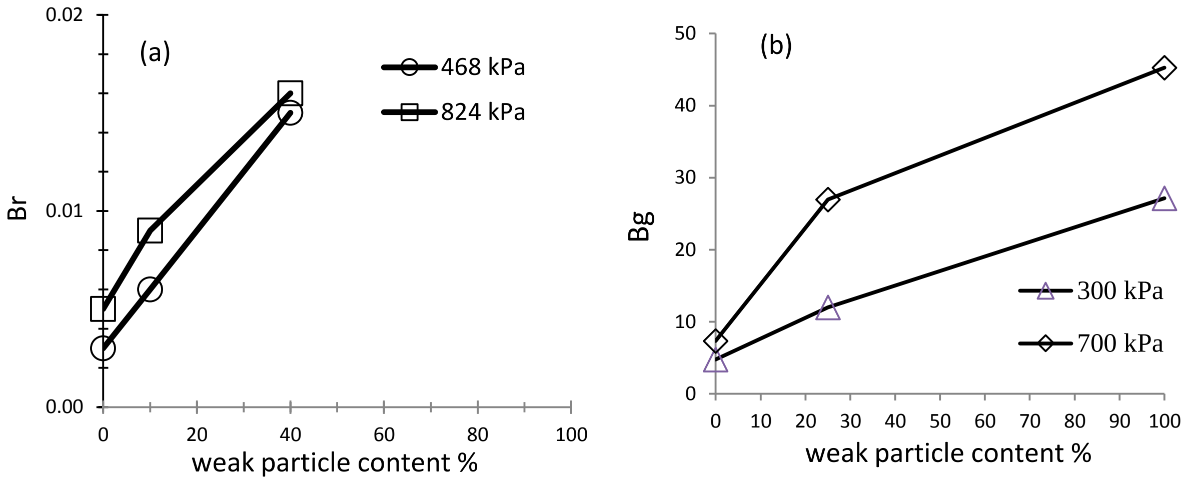

Fig. 5.16: a) Direct simple shear testing data (Valdes & Leleu 2008). b) D'Espessailles et al. (2014)

From these studies, it is expected that broken ore consisting of different block strengths would undergo fragmentation involving mostly weak blocks within the shear bands. In the case of low normal stresses acting on the broken ore, other intrinsic properties such as size distribution and aspect ratio could enhance fragmentation in contrast to block strength. At higher normal stresses (e.g. higher draw columns), weak blocks could take on a significant role in fragmentation. Unfortunately, several questions still remain unanswered, including the significance of the *strength ratio* on strong and weak particles and the role of strength heterogeneity on large blocks including veins, defects and small discontinuities. The fragmentation of broken ore mixtures from two lithology bodies (based on parameter B_r and B_g) could be represented by a linear fragmentation increment under higher weak particle content. This proposition should be considered as a first approximation only, until more comprehensives studies are conducted that can provide a better understanding of this topic.

5.6 Block Strength Damage and Crushing Under High Confining Stresses

All factors discussed in this chapter are focused in terms of a block's secondary fragmentation within a draw column due to shear and compression stresses. However, there is a knowledge gap regarding whether blocks also experience a transition in failure mode resulting in stress-induced damage and strength reduction under increasing confinement as blocks move deeper down through a high draw column (i.e., from far field to near field). Thus, this section examines laboratory test results presented in Chapter 4 to investigate broken ore strength as a function of increasing confining stresses.

5.6.1 1-D compression tests to simulate secondary fragmentation within a far field zone

A laboratory-based testing program by means of 1-D compression tests was presented in Chapter 4 to study secondary fragmentation within the plug-flow zone of an IMZ. Favourably, the far field under interactive flow can be represented as a mass flow of broken ore subjected to uniaxial loading and fixed confinement, thus making 1-D compression tests a suitable representation of secondary fragmentation in the far field zone. This laboratory testing program is further considered in a method to evaluate secondary fragmentation in Chapter 6.

Under 1-D compression tests, a fraction of particles undergo crushing, chipping and splitting (e.g. Dorador et al., 2015), while the remaining particles survive without breaking down. In these tests, the amount of fragmentation is directly dependent on the compression energy (section 5.3, Fig. 5.4). However, although the survivor particles do not experience a noticeable change to their geometry, this does not mean they might not incur damage that could cause degradation of the blocks strength properties, especially under confining stresses. The lack of experimental data is explained in part by the fact that most experiments investigating particle fragmentation under confined stresses are carried out on heterogeneous particles in terms of size, shape and particle strength. Although the size and shape of particles could be controlled in experiments, particle strength has not been investigated as the key parameter to control. Thus, the technique to prepare concrete particles presented in Chapter 4, which allows control of not only the size and shape of particles but also the particle strength, contributes a favorable method to study the influence of strength degradation as a function of increasing confined stresses.

5.6.2 1-D compression test results

Twenty tests were conducted to study particle strength degradation under 1-D compression loading. Details are provided in Chapter 4, with the exception of T-75 (see appendix A for more information). The tests considered here are T-1 to T4, T9 to T-20, T-58 to T-60 and T-75. Test were done on concrete cubes 17 mm edge under dense and loose packing. Tests with dense packing included 68 cubes composed of two samples of 34 cubes (these samples are defined in this section as part 1 and part 2), while tests with loose packing included 59 to 60 concrete cubes composed of two samples of 29 and 30 cubes. Point Load Tests (PLTs) were conducted for quality control following the standard ASTM D5731-08; the PLT results and the corresponding standard deviation (SD) for each portion (part 1 and part 2) are included in Table 5.3. An arithmetic average was calculated for the test sample PLT combining the part 1 and 2 strengths (pre- testing). After testing, survivor blocks were collected and 10 of these were randomly selected for point load testing. Hence, the parameter De% (equation 5.4) is defined as the ratio between the point load compressive strength (PLT before and after testing.

$$De\% = \frac{PLT_{\text{After testing}}}{PLT_{\text{Before testing}}} \tag{5.4}$$

As noted in Fig. 5.17a, the strength of survivor cubes decreases with higher applied compression energy with a marked strength degradation in dense packing tests compared to the loose packing tests. Also, the strength reduction of survivor cubes is highly variable, as can be inferred from the standard deviation (SD) results, which contrast with the low SDs of samples before testing. Also, a more refined analysis can be carried out considering dense packing tests only. Hence, tests T-9, T-11, T-12, T-18, T-19, T-20, T-75 are comprised of two parts of cubes with negligible PLT strength differences (tests type A), while tests T-10, T-13, T-14, T-59 and T-60 hold the same shape characteristics as type A but the part 1 and 2 have contrasting PLT strengths, with test type B being the lowest. From Fig. 5.17b, type A tests correlate very well under a power relationship, while tests under samples with low PLT strength difference reach higher degradation under same amount of compression energy on samples. Interestingly, under a higher amount of energy, blocks undergo more degradation until a point where survivor blocks reach low strength degradation. Therefore, there is an energy threshold which divides *block's cushioning* (section 5.8) from further strength reduction. Finally, the degradation index De% reaches a limit of approximately 60%.

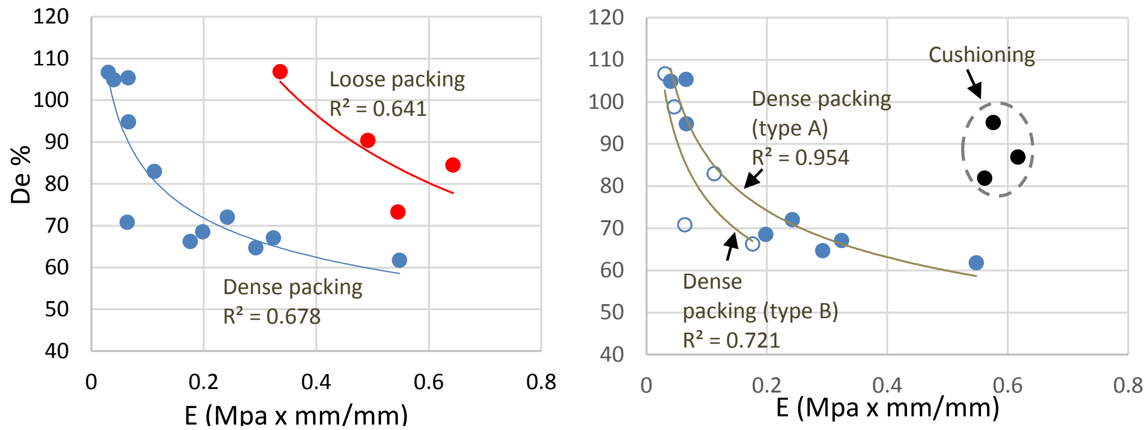

(a) (b)

Fig. 5.17: (a) Strength degradation (De %) being increased by compression energy under loose and dense packing. (b) Influence of slight initial heterogeneity in De % under dense packing

Table 5.3: Summary 1-D compression testing results

Test	E MPa x mCam/mm	σ_1 max	PLT part 1	SD part 1	PLT part 2	SD part 2	PLT Before testing (average)	Δ PLT	PLT after testing (average)	SD after testing	De %	% part. surv.	σ_1* max corr.	σ_1*/ UCS
T-1	0.64	5.4	1.75	0.31	1.89	0.41	1.82	0.08	1.54	0.41	84.5	11.9	5.25	0.169
T-2	0.34	2.6	2.20	0.43	2.25	0.37	2.23	0.02	2.38	0.66	106.8	25.4	4.34	0.077
T-3	0.55	4.3	1.79	0.38	2.48	0.26	2.13	0.32	1.56	0.75	73.3	13.6	3.84	0.140
T-4	0.49	3.5	1.72	0.50	2.50	0.31	2.18	0.37	1.97	0.81	90.4	16.9	2.40	0.124
T-9	0.04	1.9	3.00	0.57	3.02	0.58	3.01	0.01	3.16	0.66	104.6	11.9	2.28	0.074
T-10	0.05	2.3	3.20	0.42	4.34	0.80	3.28	0.30	3.24	0.77	74.6	35.6	2.31	0.075
T-11	0.07	3.1	3.20	0.42	3.46	0.80	3.28	0.08	3.45	0.59	99.7	30.5	2.42	0.078
T-12	0.07	2.8	2.78	0.41	2.80	0.42	2.79	0.01	2.64	1.04	94.6	32.2	2.42	0.078
T-13	0.11	2.4	2.19	0.58	2.96	0.50	2.58	0.30	2.14	0.80	72.2	25.4	2.68	0.086
T-14	0.18	3.4	3.12	0.69	3.67	0.79	3.39	0.16	2.25	1.50	61.3	20.3	3.03	0.098
T-15	0.24	3.4	3.22	0.52	3.48	0.43	3.35	0.08	2.42	1.62	69.5	16.9	3.40	0.110
T-16	0.58	5.5	2.88	0.87	2.94	0.88	2.91	0.02	2.77	0.97	95.1	15.3	5.24	0.169
T-17	0.62	5.7	3.02	0.54	3.05	0.55	3.04	0.01	2.64	0.78	86.9	18.6	5.47	0.176
T-18	0.20	5.5	6.48	1.32	6.60	0.77	6.54	0.02	4.48	1.28	67.9	28.8	3.15	0.102
T-19	0.32	5.5	5.31	1.13	5.66	0.66	5.49	0.06	3.68	1.61	65.0	18.6	3.85	0.124
T-20	0.29	5.6	4.15	0.67	4.43	0.59	4.29	0.07	2.77	1.51	62.6	22.0	3.68	0.119
T-58	0.56	4.0	1.89	0.63	2.53	0.35	2.21	0.29	1.81	0.81	81.9	20.3	5.16	0.167
T-59	0.06	2.4	2.08	0.50	2.33	0.38	2.20	0.11	1.56	0.86	67.0	30.5	2.41	0.078
T-60	0.03	1.7	2.04	0.35	2.77	0.41	2.41	0.30	2.57	1.03	92.6	28.8	2.22	0.072
T-75	0.55	5.6	3.27	0.19	3.31	0.47	3.29	0.01	2.03	0.71	61.4	15.3	5.09	0.164

5.6.3 Broken ore strength degradation within a far field zone

Based on results from Section 5.6.2, it is concluded that concrete cube samples not only undergo fragmentation under loading, but that surviving cubes that do not fragment also experience damage and therefore a significant strength reduction. Applying this result to the far field zone, this means that broken ore would experience compressive strength reduction when it enters and passes through the near-field zone. Accordingly, the block strength needs to be corrected to evaluate the secondary fragmentation within the near field zone, as the damage incurred will result in a finer BSD at the drawpoints.

Fig. 5.18 shows that it is possible to relate the compression energy (E) with the maximum vertical stress (σ_1). Using both correlations from this figure, corrected values of σ_1 can be obtained as shown in Table 5.3 (column σ_1* max. corrected). In addition, UCS of the concrete cubes is 31 MPa, which can be considered constant for larger block sizes (e.g. 1 m block diameter) as explained in Chapter 4. A ratio $R_s = \sigma_1^*/UCS$ can be determined for each test, which in turn can be used to estimate an approximate far field height (H_{ff}) as

$$H_{ff} = \frac{R_s \cdot UCS}{BOD} \qquad [5.5]$$

where BOD is the broken ore density and UCS is associated with the scaled strength accounting for block damage. For practical purposes, the loose packing is associated with a BOD of 1.7 t/m^3, while the dense packing is associated with a BOD of 2.5 t/m^3. Next, the degradation index De% is plotted against different far field heights under four different UCS values of 31, 60, 100 and 150 MPa (Fig. 5.19). These curves are used as a first approximation of the compressive strength reduction of the broken ore blocks at the boundary between the far and near field zones. Fig. 5.19 can also be very useful in calibrating large numerical models of broken ore during block caving using computing intensive approaches such as FEM-DEM (e.g. Vyazmensky 2008) or the synthetic rock mass PFC analysis (Mas Ivars et al. 2011).

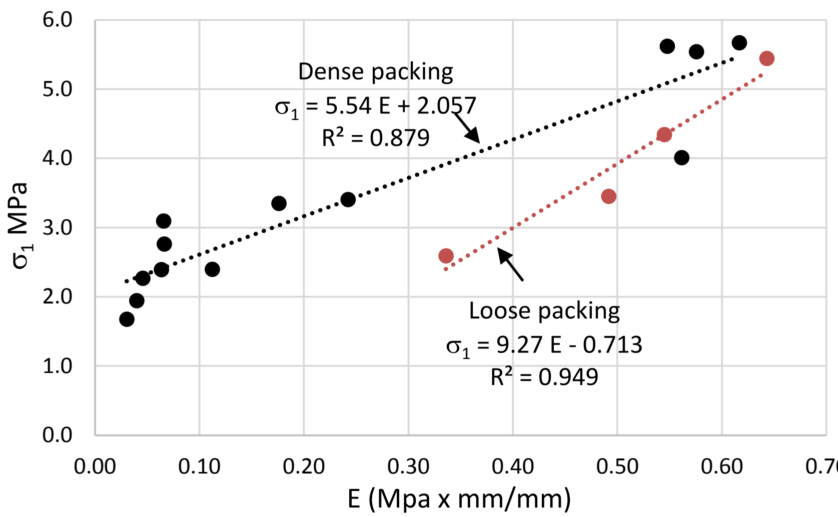

Fig. 5.18: Relationship between compression energy and maximum vertical pressure for loose and dense packing.

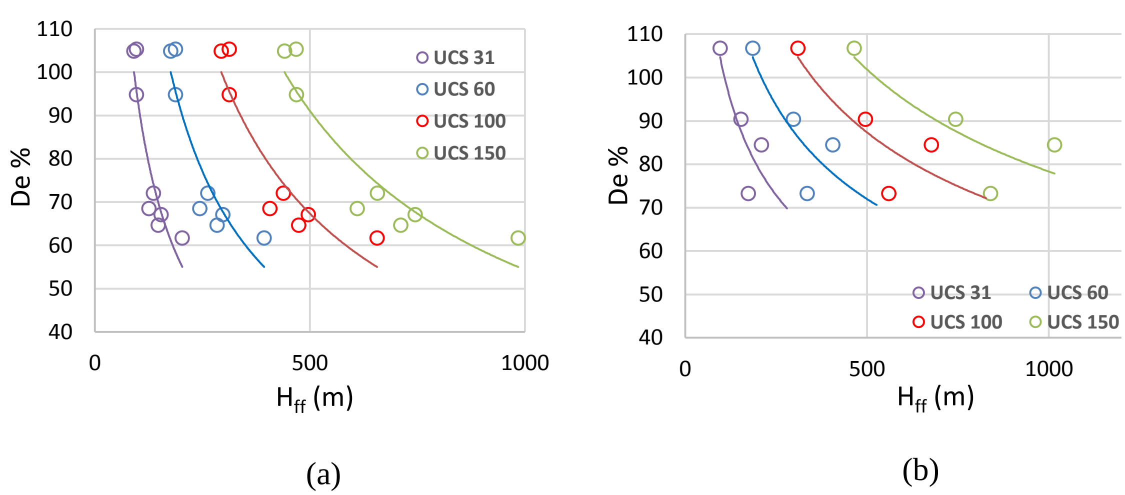

Fig. 5.19: Relationship between De % and far field height (H_{ff}). (a) Dense packing (b) Loose packing.

5.7 Water within Draw Columns

Water is a critical factor in block cave design, especially in rock strength parameters such as the MRMR (Laubscher & Jakubec 2001) and Q (Barton et al. 1974), as well as risk hazards such as mudrush. Water in block cave operations is comprised mostly of groundwater, but after the cave has broken through to surface, can also include water directly from surface runoff during rainy season. In the case of groundwater, dewatering programs are carried out during early stage design to drawdown the water table (Laubscher 2003); thus, groundwater is not assumed to be an issue in this section. Rainwater or snowmelt is a more significant contributor of water inflow into block cave mines once the draw columns reach the surface (break through), after which water can easily penetrate into the broken ore, affecting its *moisture content* (MC %) and strength through processes such as stress corrosion.

Regarding secondary fragmentation, water can degrade the broken ore strength over time. Bauer (2009) explains this from a granular material perspective as a stiffness degradation of the solid material due to its reaction with water, which leads to grain abrasion and grain breakage and consequently to a particle's rearrangement into a denser state. In addition, a phenomenon recognized in rockfill design and referred to as *collapse* can occur, most commonly in soft rockfill and triggered by flooding conditions (Maranha Das Neves & Veiga Pinto, 1989). However, this situation is less frequent within a draw column because water coming from the upper half will flow downward, reducing its residency time in the upper half and probably never submerging the broken ore at the bottom where it drains from the drawpoints. On the other hand, water can *wash fines* from the broken ore, which can affect the amount of fines encountered at the drawpoints. Specific factors such as temperature affecting the moisture content within a block caving operation are not considered.

5.7.1 Water as a factor influencing broken ore fragmentation potential

With regard to an interactive flow scenario (Fig. 5.3), water will not significantly affect the broken ore in the case of hard rock in the far field. Water can reduce the effective stress along the contacts between blocks, promoting more sliding between particles and washing fines. However, in the case of weathered rocks, water can decrease the rock strength through slaking. That being said, comprehensive studies have not been carried out to quantify the effects of different MC% on secondary fragmentation. In order to include the moisture in secondary fragmentation assessments, it would be reasonable to reduce the rock strength parameter (e.g. UCS) as a function of moisture content, and thus apply a corrected rock strength parameter for the secondary fragmentation analysis, for example if using Pierce's (2009) method or one of the alternative methods proposed in Chapter 6.

Valuable studies have been reported in the technical literature regarding the uniaxial compressive strength of soft or weathered igneous rocks under different moisture contents (MC %). Martin (1966) reported a strength decrease ratio $r = UCS_{sat} / UCS_{dry}$ between 64% and 35% on magnetite, hematite, porphyry and quartzite rocks. Gupta & Seshagiri Rao (2000) reported UCS tests on moderate (W2) to complete (W4) weathered quartzite, granite and basalt rocks, finding a ratio between 89% and 19%, averaging 63%. Also, valuable data of more than 200 UCS tests were reported by Gu et al. (2008) on basalt rocks (Fig. 5.20), where the UCS strength is intensely affected by a coupled effect of MC% and weathering. In addition, Prakoso

& Kulhawy (2011) proposed a strength decrease ratio of 79% under a database from different authors, which includes mostly volcanic and sedimentary rocks. Finally, Verma et al. (2014) reported 29 UCS tests with MC % between 0% to 4% finding an average of r =88%, although this ratio is reduced to 71 % for MC% between 3% and 4%. Based on these studies, it is reasonable to propose a strength reduction r = 70% for practical purposes, especially for early stage feasibility studies. For higher-level engineering design stages, UCS tests under both dry and saturated conditions (ASTM D7012 − 14) are recommended to evaluate the strength reduction due to MC %.

Regarding the near field conditions, the corrected rock strength parameter could also be used as proposed for the far field. However, a considerable amount of fines could be expected close to the drawpoints, which can potentially be saturated, triggering mudrush events.

5.7.2 Water washing fines

Under a sufficient amount of water flowing downward through a draw column, water can wash loose fine into the voids within the broken ore matrix, which contributes to a further amount of fines travelling downward to the drawpoints. Of interest is that this topic is comparable to the *internal erosion* process in dams. Numerous studies are available regarding fines segregation in granular materials (internal erosion), notably the works by Kezdi (1979), Sherard (1979) and Kenney & Lau (1985), which make possible the assessment of segregation potential of fines (e.g. < 4.75 mm size) from larger particles (>4.75 mm up to 1000 mm). These methods focus on fines segregation due to seepage through an earth fill dam, which can be somewhat comparable to flow down through a draw column. For instance, applying Kezdi's (1979) method to a draw column, the initial gradation can be divided into a coarse and fine gradation as shown in Fig. 5.21. The key hypothesis of this method is that the segregation of the fine gradation will occur if the ratio D_{15} /d_{85} is higher than 4, where D_{15} is the particle diameter for the 15% of mass passing of the coarse gradation and d_{85} is the particle diameter for the 85% of mass passing of the fine gradation. Thus, the internal erosion approach could be considered as a quantitative alternative to correct the BSD at the drawpoints.

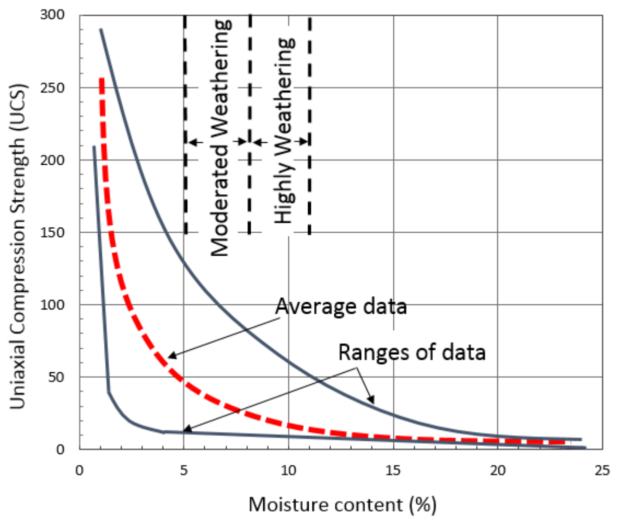

Fig. 5.20: UCS v/s moisture content %. Adapted from Gu et al. (2008)

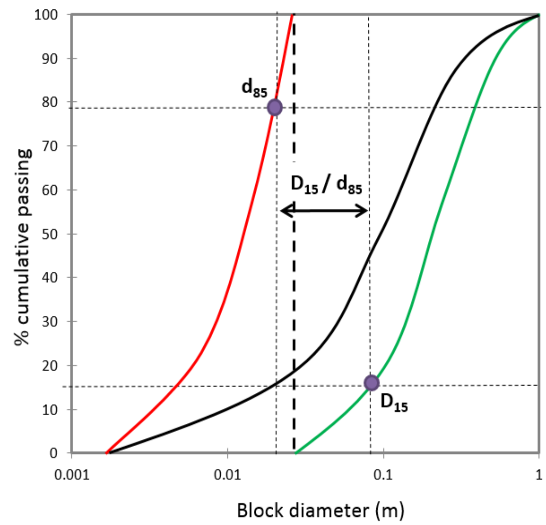

Fig. 5.21: Kezdi method (1979)

5.8 Cushioning

Cushioning has been discussed by several practitioners such as Laubscher (1994, 2003), Dolipas (2000), Pierce (2009) amongst others. Cushioning consists of fines surrounding and cushioning large blocks during drawdown, which has been corroborated by means of field evidence by Laubscher (2003) in chrysotile asbestos block cave mines. This author also suggests that fines generated during the primary fragmentation stage will act as a cushion to larger blocks. Another contributing factor in cushioning is the cave caving into a major fault and/or shear zones, which generate a significant amount of fines (Laubscher 2003). Cushioning could also be associated with the phenomenon defined as ballast fouling within the transport engineering field. Fouling corresponds to fine particles (clay and silt) which contaminate the particle surfaces, affecting the interaction between particle structure and reducing the frictional resistance of the material (Indraratna et al., 2013), which in the long term could affect the broken ore's compressibility.

Broken ore materials can reach large sizes in comparison with other granular materials (Fig. 5.22a), and so they have more likelihood to undergo cushioning. However, two main factors can strongly reduce the cushioning potential: i) *Block strength reduction due to size scaling,* and ii) the *location of cushioning within the draw column*. This section discusses the fragmentation potential of large blocks surrounded by smaller particles from a granular material perspective.

5.8.1 Block strength reduction due to size scaling

The strength ratio (R_s) between the larger blocks and smaller particles plays a major role in cushioning potential. It is logical to assume that the smaller particles are comprised of weaker materials (e.g., weathered rock) than the larger blocks (e.g. fresh rock) they are cushioning. This cushioning can even apply to smaller and larger particles with the same approximate strengths, which is supported by Tsoungui et al.'s (1999) empirical evidence (Fig. 5.23). This is explained by the fact that large blocks contain a higher coordination number (i.e., number of contact points) relative to the smaller particles surrounding them. This phenomenon has been corroborated by McDowell et al. (1996) and Wood & Maeda (2008) who propose that large particles surrounded by smaller grains tend to survive during compression and shear tests. It should be noted that these last two studies were based in part from empirical tests on standard sands, which greatly differ from broken ore materials whose blocks contain defects, veins, and smaller discontinuities.

In contrast, larger but weaker blocks could experience fragmentation under stronger but smaller particles, which was demonstrated in the 1-D compression tests in Chapter 4 (Fig. 4.27, 4.28 and 4.29). These tests were carried out on artificial cube particles based on particle sizes from 1 cm to 2 cm edge length and a *strength ratio* of 0.5 between large and small particles. Also, evidence of block disintegration has been observed at drawpoints in Chilean cave mines (Encina 2015), which suggests that large blocks undergo high fragmentation within the draw columns. Of interest is that Yoshinaka et al. (2008) reported numerous data from different authors regarding UCS tests of strong rocks under different specimen diameter and k exponent. Extrapolating these data using a relationship applicable for large broken ore sizes (D = 1 m), an average strength reduction of 46 % is obtained. This strength reduction is higher for intrusive rather than sedimentary rocks and can be even greater in the case of water being present as previously noted in section 5.7. Hence, this analysis suggests that broken ore materials are weaker under larger sizes and they could undergo fragmentation surrounded by smaller particles within a draw column.

$$UCS = UCS_{50}\left(\frac{D}{50}\right)^{-k} \qquad [5.6]$$

On the other hand, the block *size ratio* (R_{bs}) between large block diameters D and smaller particles of diameter d is another key parameter to consider. Broken ore can be quite different in comparison to typical granular materials (e.g. gravels, rockfill) because of the sizes involved (Fig. 5.23b). In the case of smaller particles comparable in size to the large block (e.g. R_{bs} = 2), the smaller particles can rapidly reach a stable structure under confining stresses, providing more chances for the large block to undergo fragmentation. As the ratio increases (e.g. R_{bs} = 100), smaller particles will have much less overall stiffness in comparison to the large block; then, smaller particles will undergo high internal deformation under confining stresses, reducing the chances of fragmentation by the large block.

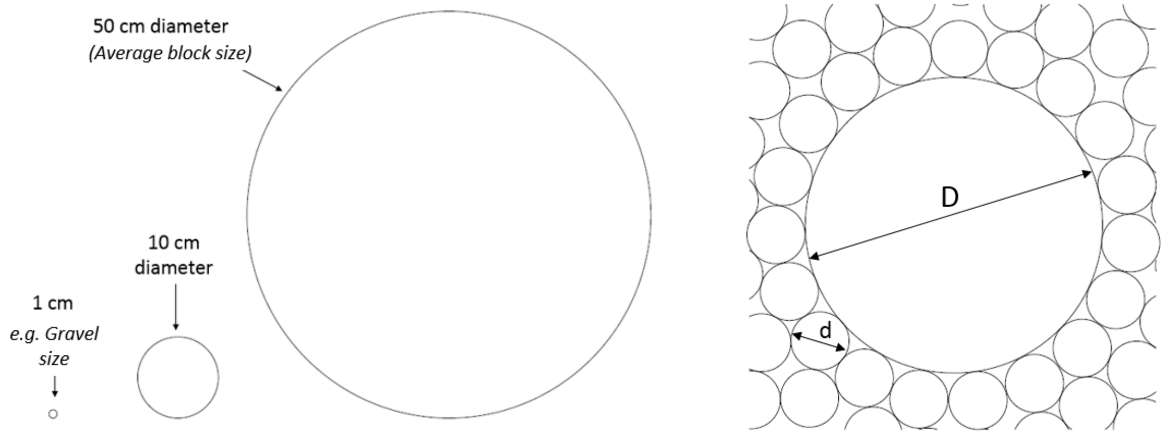

(a) (b)

Fig. 5.22: a) Size representation of broken ore material. b) Largest block surrounded by smaller particles.

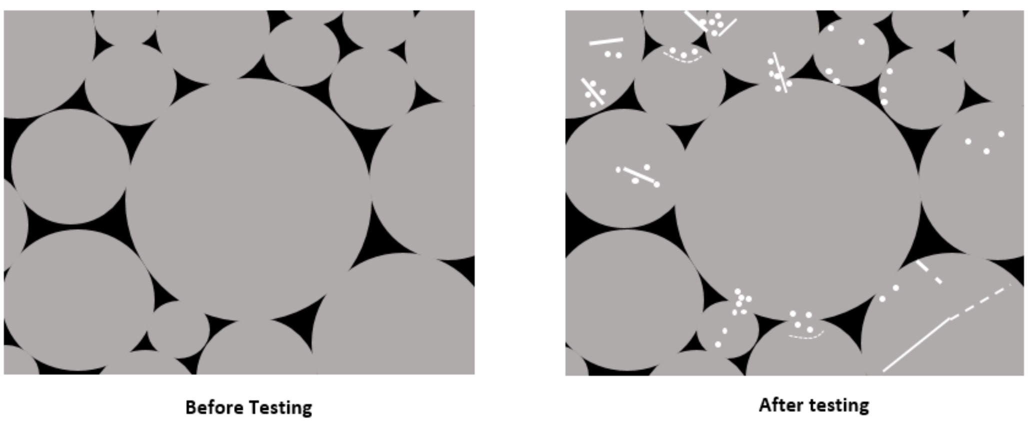

Fig. 5.23: Empirical test showing large block survival under compression, after Tsoungui et al. (1999)

5.8.2 Cushioning potential within a draw column

Cushioning potential will depend on the location of large blocks within the draw column. In the case of an IMZ, the largest blocks will most probably concentrate within the plug-flow zone surrounded by smaller particles of comparable size (section 5.4). In this condition the case of R_{bs} = 2-3 (Fig. 5.2) is highly expected, where large blocks can reach 2 to 3 m and the average size of smaller particles can be defined as 1 m (fines are not expected to participate in the force chains of the broken ore structure). However, as a large block nears a drawpoint, it could undergo cushioning if a sufficient amount of fine material is surrounding it. Regarding an *interactive flow*, in the far field a similar situation of broken ore reaching an R_{bs} = 2-3 is expected, and large blocks dispersed along the far field zone may experience cushioning depending on the far field height and rock properties (section 5.7). In the near field, large blocks can experience a high degree of cushioning within the outer periphery (shear bands) due to significant fines migration occurring within the shear bands. Cushioning could also occur within the plug-flow zone closer to the drawpoints under the same circumstances as IMZ.

In summary, cushioning can occur close to the drawpoints and within the outer periphery of a draw column, but it will depend on the broken ore properties (e.g., large and small block strength, block size ratio R_{bs}, far field height). Table 5.4 provides a summary of different cases where cushioning could occur. Hence, cushioning is a factor that in some cases should be considered in block cave design, to be evaluated in parallel with secondary fragmentation and fines migration assessments.

Table 5.4: Cushioning probability in a draw column (low, moderate and high)

Flow type		Mixture of Weathered and fresh rock	High strength reduction by size
IMZ	Plug- flow	Moderate	Low
	Shear band	Low	Low
	Close to drawpoints	High	Moderate
Interactive flow – far field	Confined compression	Moderate – high (*)	Moderate – high (*)
Interactive flow - near field	Plug- flow	Moderate	Low
	Shear band	High	Moderate
	Close to drawpoints	High	Moderate

(*) it will depend on far field heigh

5.9 Summary and Key Findings

Key variables influencing secondary fragmentation that play an important role in early feasibility and layout design assessments of a block caving project include planned ore column height, rock strength, inter-block friction angle, near and far field zones, and shear band thickness. In addition, a number of additional site/operation specific variables can similarly have a significant influence, including: air gap thickness, BOD, segregation of larger blocks due to muckpile surface topology, broken ore strength heterogeneity, block strength damage and crushing under high confining stresses, presence of water within draw columns, and cushioning. Each of these factors were studied independently in this chapter, examining data from laboratory testing conducted in this thesis, as well as compiling relevant data from the literature. From these several relationships and procedures were developed to account for their influence in secondary fragmentation assessments for both feasibility and advanced engineering design stages.

The main findings derived from the work presented in this chapter are summarized as follows:

i) The *air gap height* is not only a key concern with respect to creating an air blast hazard, but also promotes rock-fall impact fragmentation of blocks released from the cave back. Based on observations and data reported in the literature, a critical fragmentation height h_c of 10 m is suggested as a first approximation for strong rock. The air gap height also influences the initial arrangement of blocks at the top of the draw column, which in turn affects the overall broken ore density within the draw columns.

ii) The *broken ore density (BOD*) also affects the secondary fragmentation assessment. Under interactive flow, the BOD can range from a loose to a very dense packing within the far field, which can cause important differences in secondary fragmentation. For the near field, the BOD is not a critical variable; no further fragmentation is expected within the plug-flow zone (due to stress reduction), while the BOD will be mostly loose in the shear bands without undergoing significant changes, and then without influencing secondary fragmentation. Under an IMZ, the BOD will be relevant under high draw columns only. In the plug-flow zone, the BOD will also vary from a loose to a dense state, in a similar way to what occurs in the far field during interactive flow; in the shear bands a continuous loose BOD is expected, not causing variations in secondary fragmentation. Finally, the BOD will be significant in the overload stress assessment within draw columns, which directly affects the secondary fragmentation.

iii) *Segregation of large blocks due to the development of a surface cone* along the top surface of a draw column can be triggered by irregular draw. Irregular draw can also lead to increased dilution. The segregation of large blocks will result in more oversize blocks being retained within the plug-flow zone, which implies wider size distributions in the plug-flow zone and finer gradations in the shear bands. This needs to be considered in any fragmentation assessment and BSD prediction at drawpoints. Hence, a simple procedure to correct the BSD within a draw column due to block segregation is proposed.

iv) The *broken ore could be highly heterogeneous*, which facilitate mixtures of strong and weak blocks within a draw column. Considering the parameters B_r by Hardin and B_g by Marsal, a linear increase of fragmentation under a higher weak particle content has been proposed as a first approximation, while new empirical/numerical comprehensives studies will be carried out to contribute more precise secondary fragmentation assessments.

v) It was demonstrated experimentally that *block strength degradation* can occur on broken ore materials subjected to large overload stresses. Blocks within a far field zone can undergo an average compressive strength reduction down to 60% for dense samples and 70% for loose samples.

vi) *Water*, especially inflows from rainwater or snowmelt can cause degradation of the broken ore with time, for example through stress corrosion, which will be more accentuated in weathered rocks. This factor needs to be considered in secondary fragmentation assessment by means of reducing the block strength parameter due to moisture content. A rock strength reduction of 70% has been proposed, appropriate for early stage feasibility studies based on observations and data compiled from the literature. Water can also wash fines downwards through the broken ore skeleton within a draw column, which would result in the accumulation of fines closer to the drawpoints. This would affect the BSD at the drawpoints as well as increase the potential for mud rush. Results reported in the literature related to internal erosion have been proposed to evaluate this factor.

vii) *Cushioning*, where large blocks are impeded from undergoing further fragmentation due to smaller particles surrounding them, has been also examined in this chapter. Cushioning could occur during block caving depending on the broken ore properties (i.e. rock strength), especially where large blocks within a draw column are located close to the drawpoints and/or within the outer periphery of a draw column. Block cushioning could also occur within the far field zone subjected to high overload broken ore heights.

It is important to consider that several of these factors depend directly on the *draw rate and sequence of draw*, which place emphasis on the importance of draw control for a successful block cave operation. Therefore, from these seven factors studied in this chapter, it is possible to predict and/or evaluate more carefully the BSDs encountered at drawpoints, which will help in the design of drawpoint size and spacing, hang-up potential, and necessity of using pre-conditioning, amongst other feasibility and design questions, contributing to more efficient extraction level layout designs (see Fig. 5.24).

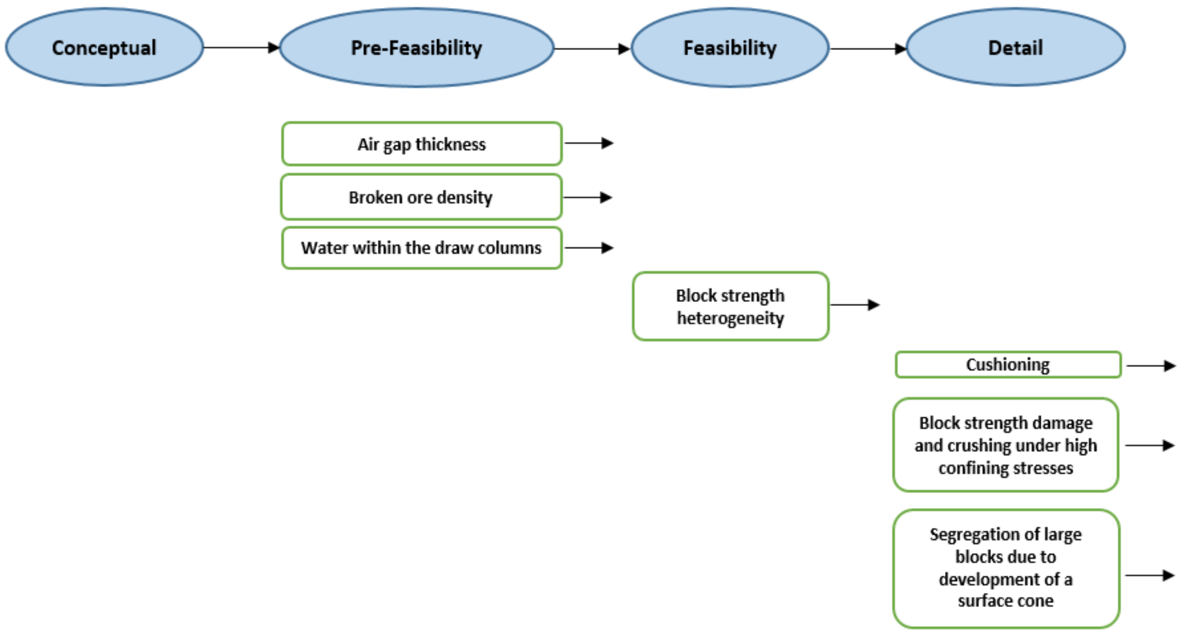

Fig. 5.24: Flow path regarding secondary fragmentation factors analysed in this chapter under different stage level of a block caving project

Chapter 6: Evolution of Broken Ore Size Distribution in a Draw Column during Block Cave Mining [5]

6.1 Introduction

Reliable estimates of rock fragmentation are essential for pre-feasibility and feasibility-level assessments of draw point productivity in the planning of a block caving operation. This is emphasized by Brown (2007) who points to fragmentation as being one of the key factors determining the overall performance, success and profitability of a caving operation. If the fragmentation is too fine, then a narrow draw zone, high dilution and potential for mud rush might be expected; while if the fragmentation is too coarse, oversize blocks and hang-ups will impede material handling, causing need for secondary breakage and costly production delays at the drawpoints. As a project proceeds to detailed design, the degree of fragmentation expected will influence the drawpoint spacing (and therefore equipment selection and performance), together with the frequency of hang-ups, need for secondary breakage in the drawpoints, need for underground crushers, and ability to achieve production targets (Brown 2007).

[5] Dorador L, Eberhardt E, Elmo D. Evolution of Broken Ore Size Distribution in a Draw Column during Block Cave Mining. (In review).

It is well accepted that the broken ore extracted at the drawpoints is dependent on a fragmentation process which incorporates three components: 1) the in situ, representing the natural discrete fracture network distributed throughout the rock mass; 2) the primary, arising from stress-induced fractures propagating in the cave back; and 3) the secondary, which first involves rockfall impact onto the muckpile surface (when an air gap is present) and then splitting and rounding of the blocks as they move downwards through the draw column towards the drawpoint (Laubscher 1994, Eadie 2003). These are depicted in Fig. 6.1.

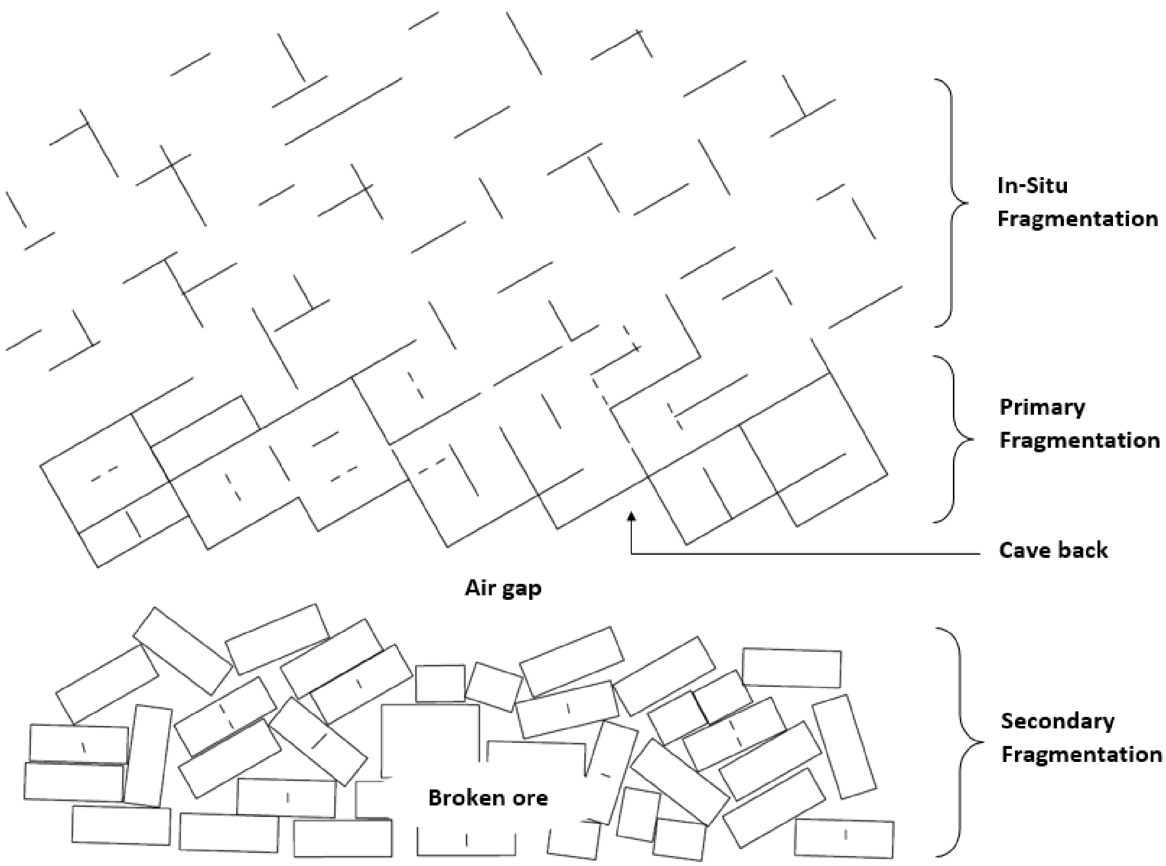

Fig. 6.1: Schematic diagram depicting the fragmentation process in block caving.

The Block Caving Fragmentation (BCF) software developed by SRK Consulting (Esterhuizen 2005) represents one of the few established tools used by operators to assess fragmentation and hang-up potential. The software uses rock mass classification inputs and empirical rules to predict how blocks in a draw column reduce in size, from in situ to secondary. Although this approach is able to quantify secondary fragmentation, its reliability has been questioned due to a lack of calibration and/or unreliable results (Rubio & Scoble 2004, Butcher & Thin 2007, Ngidi & Pretorius 2011). Pierce (2009) proposed a more rigorous and robust methodology to evaluate secondary fragmentation based on the gravity flow simulator REBOP (Cundall et al. 2000) and calibrated using empirical relationships by Bridgwater et al. (2003). The more detailed nature of this method and required use of proprietary software suggest that it more appropriately addresses higher level feasibility and detailed engineering design studies. Pierce (2009) also found that the logic may over predict secondary fragmentation due to the assumption of an initially uniform fragment size in the empirical model.

Given the lack of procedures for assessing secondary fragmentation in early stage feasibility studies, more work is required to provide additional empirical tools that can be used in parallel for comparative analyses. This chapter first investigates secondary fragmentation and the mechanistic controls that affect an evolving block size distribution (BSD) within a draw column, and then uses these together with laboratory and field data compiled from the literature to develop an empirical method to estimate BSD. The method builds on the draw column model of Pierce (2009), where compression deformation develops within a central plug flow zone and shear deformation occurs along outer shear bands and close to the drawpoint (Fig. 6.2). The latter is a more complex phenomenon involving interactions between adjacent draw columns, for which differentiation is made between *near field* and *far field* effects (Fig. 6.3). For the purpose of this work, near field corresponds to broken ore within 50 to 100 m of the drawpoint where the fragmentation process is governed by Pierce's (2009) Isolated Movement Zone (IMZ) model comprised of a central compression plug zone and outer shear bands. Far field considerations account for the influence of 1-D compression stresses on the broken ore at greater distances away from the draw points, acknowledging that many block cave mines are being developed with planned column heights in excess of 500 m (Hancock 2013, Eberhardt et al. 2015). The main reason to distinguish between near and far field is because each of these induce different stress fields within a draw column, which affects significantly the type and amount of fragmentation generated (e.g. splitting, corner rounding, chipping, etc). Finally, the chapter concludes with a comparison of results obtained using the method developed with field data from the El Teniente mine in Chile, which is used to both calibrate the model and determine its limitations.

The methodology proposed in this work is mostly focused on cases where multiple draw columns interact with each other, although the charts and relationships proposed can also be employed to evaluate the BSD at drawpoints under an IMZ.

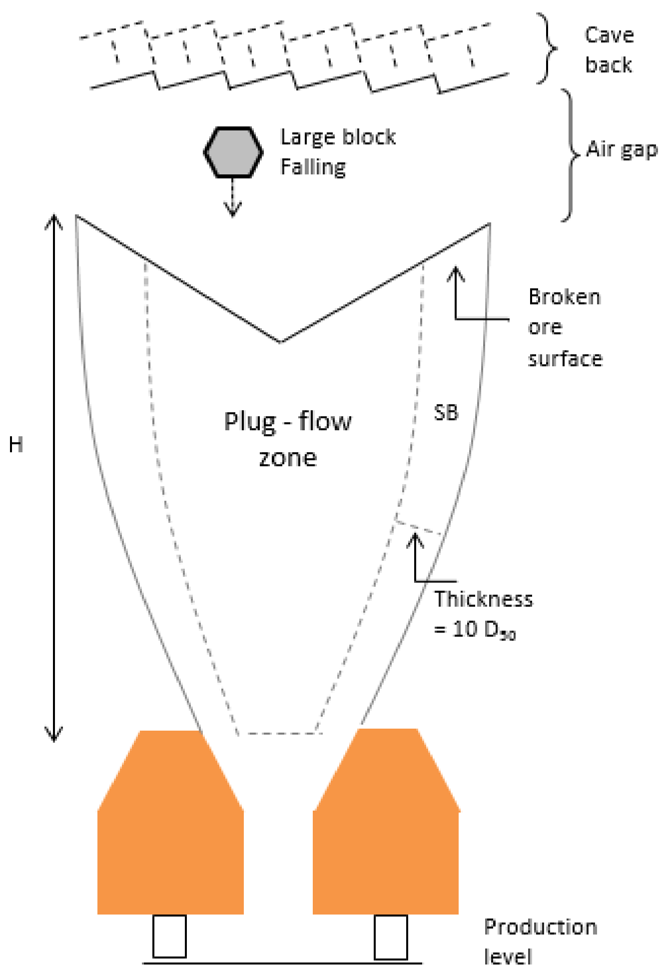

Fig. 6.2: Broken ore under different stress conditions along a draw column (IMZ)

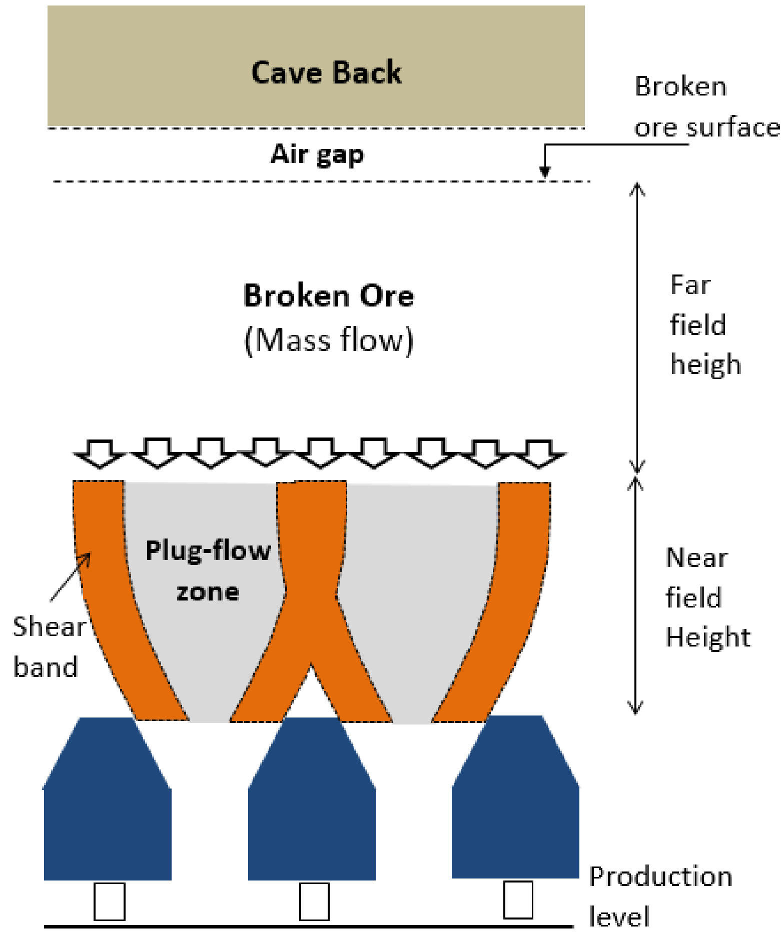

Fig. 6.3: Secondary fragmentation process in terms of far and near field from drawpoints

6.2 Background: Secondary Fragmentation and Block Size Distribution

6.2.1 Broken ore behaviour and secondary fragmentation processes

The difficulty of studying broken ore behaviour in terms of gravitational flow, fines migration and secondary fragmentation is the wide block size distribution (BSD) encountered. This varies by several orders of magnitude from several meters diameter to millimeter-sized grains. The BSD not only impacts the ore recovery at the drawpoints but also the *broken ore density*, the development of *cushioning*, and operational risks such as *mudrush*. For instance, it was shown that a well graded BSD facilitates a higher broken ore density (Chapter 2) and increased cushioning (Chapter 5), which in turn reduces the degree of secondary fragmentation of larger blocks resulting in increased potential of oversize and hang-ups. Conversely, a more uniform BSD within the draw column promotes a lower broken ore density and reduced cushioning.

Secondary fragmentation is itself a multi-variable process (Chapter 1, Fig. 1.6), which depends not only on the intrinsic and state variables of caved rock but also on operational factors and the stress path experienced by the broken ore as it moves downwards towards the drawpoints. It involves a mechanical comminution of splitting, crushing, chipping and corner rounding that varies according to two different drawpoint interaction scenarios: isolated movement zone (IMZ) and multiple draw movement (Pierce 2009). Thus, it is reasonable to suggest two distinct zones of secondary fragmentation behaviour depending on the broken ore proximity to the drawpoints, and the development of shear bands relative to a central plug-flow zone within the draw column.

6.2.2 Secondary fragmentation assessment tools

Laubscher (1994) lists several of the key block caving design parameters dependent on fragmentation and BSD assessments, including: drawpoint size and spacing; equipment selection; draw control procedures; production rates; hang-ups and the need for secondary blasting; staffing levels; and subsequent comminution processes and costs (e.g., underground crusher). It is noted here that not only are these key parameters for detailed engineering design, but they can also have a major impact on the mine economics. Therefore, the need for effective methodologies to evaluate secondary fragmentation and BSD, is one that encompasses tools that extend from early stage project development (e.g., feasibility-level studies) to those that are more rigorous and appropriate for advanced mine design.

6.2.2.1 Pre-feasibility

The BCF methodology (Esterhuizen 2005) is one of the few industry-accepted tools for quantifying secondary fragmentation (Butcher & Thin 2007). It involves an expert system program incorporating analytical and empirical rules describing the factors influencing caving fragmentation, with focus on the evaluation of *primary* and *secondary* fragmentation as well as frequency of *hang-ups*. To assess secondary fragmentation, this software requires the primary fragmentation as an input, which is previously obtained using the same software, as well as some additional information: draw height, maximum caving height, draw width, swell factor, rock density and rate of draw. In addition to assessing the crushing and attrition of blocks, BCF has the advantage of considering draw rate as an input. The method also has its limitation, which Butcher & Thin (2007) list as:

- BCF historically has produced conservative results (coarser size distributions);
- Fragmentation computation at drawpoints can be underestimated. The software requires an input of BSD after primary fragmentation to predict secondary fragmentation. However, it does not account for the impact of small joints on fragmentation, with the consequence that the BSD in the draw column is projected to be coarser than it actually is, and therefore the BSD at the drawpoints is estimated to be coarser than that later encountered.
- The draw rate is assumed to be constant in the software. However, experience suggests that draw rate is far from constant and varies in response to drawpoint closures for repair, seismicity, flooding, or any other factor that may interrupt operations.

Another shortcoming of BCF is its bias against generating well-graded BSD curves, especially towards the distribution of larger block sizes. This is demonstrated by comparing Fig. 6.4(a), which plots BSD data collected at the drawpoints of several different operations and broken ore (caved rock) column heights, to Fig. 6.4(b), which plots the secondary fragmentation curves obtained by different authors when using BCF. Although the comparison includes different cases, the general trends indicate that the BSD data in terms of C_u (D_{60}/D_{10}) ranges from 8 – 18 which represent well-graded curves, which contrast with those predicted by BCF associated with more uniform gradation curves. Given these shortcomings and issues related to obtaining reliable results (see Butcher & Thin 2007), its use is recommended for early stage feasibility level studies.

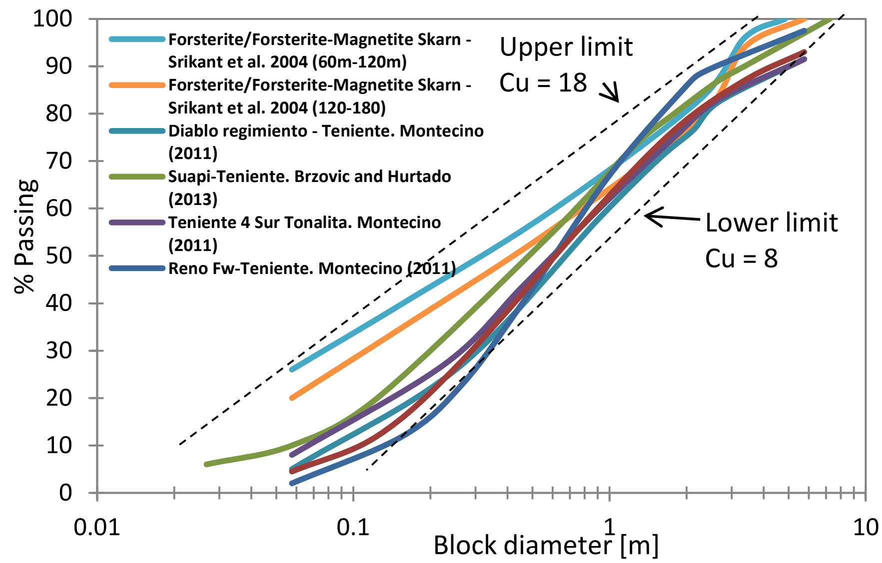

a) BSD at drawpoints measured for several different operations and draw column heights.

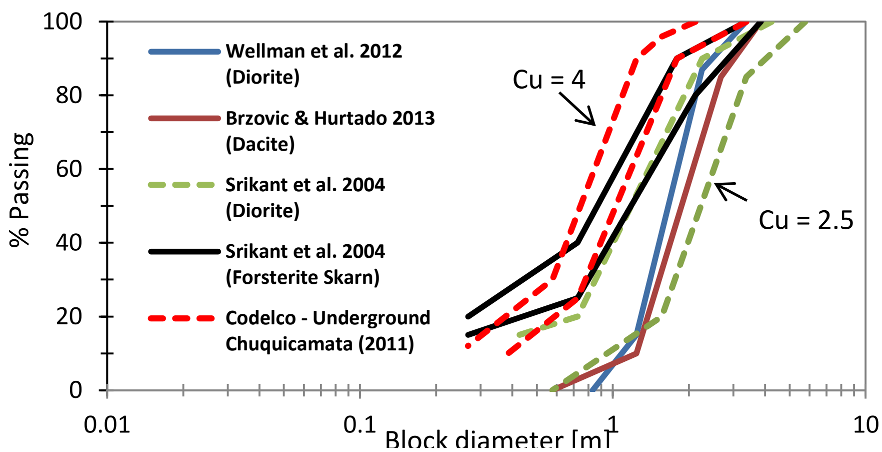

b) BSD at drawpoints predicted using BCF. Data sources as indicated.

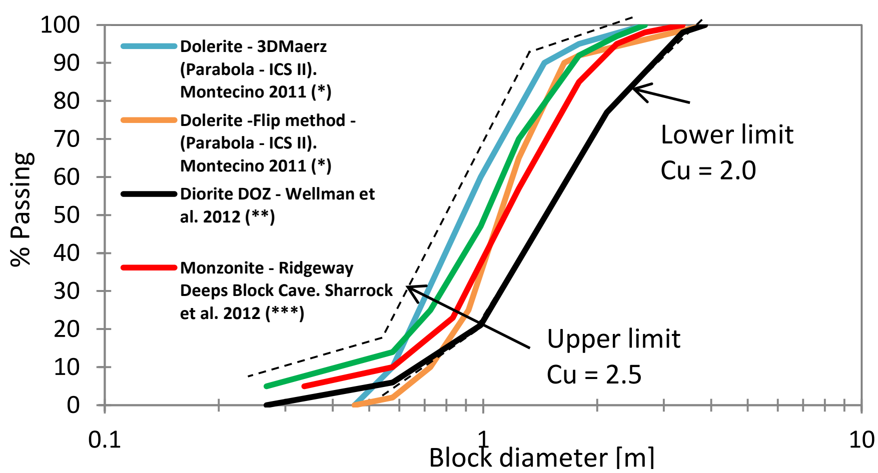

c): Primary fragmentation curves from different authors. (*) Field Estimation (**) Estimation using Core2Frag approach. (***) Estimation using BCF

Fig. 6.4: Broken ore size distributions

6.2.2.2 Advanced feasibility and detailed design

Recent efforts to better quantify secondary fragmentation in block/panel caving have largely focussed on the use of advanced numerical modelling, and therefore are seemingly directed at higher-level feasibility or design stages of a project. Pierce (2009) proposed the first of these using the gravity flow simulator REBOP (Rapid Emulator Based On PFC), which itself was developed based on flow patterns observed in 3-D discrete-element simulations of draw using PFC3D (Cundall et al. 2000). Pierce's hybrid approach uses REBOP to calculate stress and strain histories in the broken ore during gravity flow, which are then used to establish equivalent comminution energies and breakage models. When applied to a primary fragmentation size distribution curve, obtained in part using discrete-element synthetic rock mass principles (Pierce et al. 2007), and calibrated against laboratory testing by Bridgwater *et al.* (2003), a prediction of drawpoint size distribution is obtained. The use of numerical output of the stresses at different locations within the ore column allows for the compression and shear zones developing within the broken ore to be accounted for. In doing so, this method is one of the more effective procedures for evaluating secondary fragmentation, with recent application demonstrated by Fuenzalida et al. (2014).

Kojovic (2010) proposed an alternative approach to evaluating secondary fragmentation based on experiences in mineral processing. This method integrates numerical models and empirical relationships, and assumes that rock mass fragmentation is analogous to comminution relationships used in mineral processing (Weatherley 2010). Kojovic (2010) indicates that four inputs are needed to employ this methodology: i) the primary fragmentation size distribution curve of the broken ore; ii) *the in-situ* rock strength; iii) a rock fragmentation function for different applied comminution energies; and iv) the effective comminution energy applied to the material when its passes through the draw column (i.e., in the mineral processing analogy, the material passing through the milling circuit). The comminution energy input is the most difficult of these parameters to quantify, but can be obtained from REBOP simulations. This technique has been applied and calibrated at the Newcrest Ridgeway Deeps caving operation. However, it has not been extensively used at other operations and questions arise as to: i) the reliability of the rock fragmentation function for different applied comminution energies, ii) the extrapolation of intact rock properties to larger block sizes given the strong influence of discontinuities, defects and veins in the overall strength of the block, and iii) in the effectiveness of using energy outputs from REBOP as input for the comminution model.

A third methodology has been proposed by Rogers et al. (2010) based on discrete fracture network (DFN) modelling of a cubic block that accounts for fabric in the form of veins and discontinuities using the 3-D volumetric fracture intensity parameter P32 [m^2/m^3]. P32 is a measure of the total surface area of the fractures present per unit volume. A probability function of the block degradation is subsequently obtained using the Monte Carlo simulation and optimization software Crystal Ball (2012). To generate this function, numerical simulations of 2-D uniaxial compression tests are conducted using the hybrid finite-/discrete-element brittle fracture software ELFEN (Rockfield 2009). Confining pressures are varied to represent different draw column heights. Multiple scenarios of P32 are analyzed considering different confining pressures and particle arrangements. Subsequently, it is possible to define the breakage efficiency function, which gives as output the amount of blocks undergoing breakage. Rogers *et al.* (2010) indicate that this technique allows for the representation of the first order of the secondary fragmentation process. However, this methodology is not able to quantify the fines generated by the abrasion and corner rounding among particles and requires validation in a real caving operation.

6.2.3 Shear bands and fragmentation

6.2.3.1 Shear band evaluation under laboratory testing

In terms of broken ore within a shear band, any fragmentation analysis ascribed to shear bands should include large-strain deformations in order to mimic the broken ore flowing through the shear bands within the near field of a draw column. Ring shear is a standard soil mechanics test that has recently been used for studying particle breakage under large deformations (Bridgwater et al. 2003; Coop et al. 2004; Luzzani & Coop 2002; Sadrekarimi & Olson 2010), although it generates shear fragmentation in a narrow band within the sample. Thus, a more sophisticated alternative such as the torsional *ring shear test* (ASTM D6467 – 1) could be employed to reproduce large-strain shear displacements under a wide shear band, as would be expected in broken ore material within a draw column.

6.2.3.2 Particle fragmentation in shear bands

Several authors have contributed to the study of particle fragmentation in shear bands. Lieou et al. (2014) used studies by Chambon et al. (2006), Rice (2006) and Sammis et al. (1987) to show that grain splitting contributes significantly to comminution at small shear strains, while grain abrasion becomes dominant at large shear displacements. On the other hand, empirical studies from Ghadiri et al. (2000) and Bridgwater et al. (2003) suggest that corner rounding tends to be the dominant mode of fragment yield at low ratios of normal stress to intact strength, while splitting becomes more dominant at higher ratios. Hasan & Alshibl (2012) also suggest that particles in a shear band undergo significant rotation, which would be related to fragmentation in terms of corner rounding. In addition, Mairs & Abe (2011) found that grain splitting dominates under high normal stress and at small shear strains, while grain abrasion dominates under low normal stress and at large shear strains. Coop et al. (2004) found through ring shear tests on carbonate sand that at very large displacements the soil reaches a stable grading, which in turn depend on the applied normal stress and the initial grading.

Based on these studies, it can be concluded that corner rounding is generated throughout shear deformation, but more accentuated at large deformations (due to particle rotation), while splitting occurs under both small and large shear displacements depending more strongly on the ratio of normal stress to intact particle strength. Of interest is that each of these experimental studies was conducted on sand-sized particles, which differ significantly in size in comparison with broken ore materials. These involve metre-scale diameters resulting in an increased likelihood that the blocks contain defects in terms of veins and small discontinuities, influencing more splitting under low normal stresses and higher fragmentation under larger shear deformations. Hence, the BSD would evolve in a wider and finer size distribution (as the BSD shown in Fig. 6.4a), including a size reduction on its largest block. In addition, from a granular matter perspective, confined particle's fragmentation reaches a point where it follows a fractal size distribution (McDowell et al. 1996, Einav 2007). In addition, Wood & Maeda (2008) agree that particles under continued shearing would encourage crushing in a *self-similar* or *fractal* size distribution. This last finding could apply to the secondary fragmentation process because broken ore within shear bands experience large shear deformation during ore draw. McDowell et al. (1996) proposed that the ultimate grain size distribution (GSD) can be characterized by a power law relationship, with a fractal dimension α = 2.5 to 3.0, which means a linear particle size distribution on the double logarithmic graph, although this ultimate GSD is generally unknown (Tengattini et al. 2014).

Based on the experiences presented above, it is expected that the broken ore within the shear band in a draw column evolves to encompass a wide BSD, which will significantly influence the final BSD encountered at the drawpoints.

6.2.3.3 Shear band thickness

Most of the investigations regarding shear band thickness has been developed based on mono-sized granular materials. According to Tejchman (2000) the observed thickness of shear zones varies from 5 to 20 times the mean particle diameter (D_{50}) based on results from Vardoulakis (1980), Desrues & Hammad (1989) and Yoshida et al. (1994). Schall & Van Hecke (2010) state that a shear band width is typically 5 to 15 grain diameters. Mohamed & Gutierrez (2010) concluded that rolling resistance is a significant parameter influencing the shear band thickness, observing that particles rotate significantly within the shear band. Tejchman also indicated that the shear thickness is not only affected by the layer height and particle diameters but also by the void ratio (or sample porosity). Finally, Pierce (2009) recommends that a shear band thickness of 10 grain diameters should be used to represent the size of the outer annulus (i.e., shear bands) within a draw column.

Conversely, broken ore materials within a shear band in a draw column are not mono-sized particles but rather poorly graded to well-graded as suggested in Fig. 6.4 (a) and Fig. 6.4 (c). Thus, the shear band thickness needs to be related to the particle size distribution. Here it is important to refer to the work carried out by Lieou et al. (2014). They concluded based on geophysical observations that in a sheared fault gouge, particles are significantly smaller than those outside of the shear band. This observation could apply to secondary fragmentation of broken ore within a shear band because significant splitting and corner rounding would be occurring in combination with a fines migration process which would decrease the average block size (D_{50}) and therefore, the shear band thickness. The shear band thickness on broken ore materials is further analyzed in section 6.3.2.2.

6.2.4 Fines migration

Fines migration has been identified as a key element in draw control, cushioning of oversize blocks, and mudrush risk (Laubscher 1994, Jakubec et al. 2012). Thus, fines migration has attracted the attention of several authors through empirical studies (Hashim & Sharrock 2012, Chen et al. 2009, Castro 2006) and numerical modelling (Leonardi et al. 2008, Pierce 2009). It is well accepted that a fraction of these fines are generated after primary fragmentation and rock-fall impact, while the remaining fraction is generated later through secondary fragmentation. Fines migration is mainly vertically downwards as noted by Pierce (2009), while Hancock (2013) proposes that the majority of fines migration would have to occur outside of this region in the shear band which surrounds the central plug flow zone. As a consequence, most of the fines migrated from upper intervals will reach the drawpoints, although a portion will become trapped in the stagnant zones between draw columns. Also, a moderate amount of fines can be generated from rock-fall impact depending mostly on the air gap height (Chapter 5). In the case of a single draw column, these fines would have the ability to travel through the cave in areas of high shear as noted by Hashim et al. (2008). In the case of interactive flow, these fines wouldn't have much chance to migrate freely, but might accumulate between and move with large blocks. In order to evaluate fines migration within a draw column, valuable data and observations involving fines segregation drawn from the literature is provided below.

6.2.4.1 Percolation

Fines migration can also be related to an inter-particle percolation process (Pierce 2009). Percolation has been the subject of many studies, yet it is still one of the most poorly understood mechanisms contributing to size-based segregation (Khola 2015). Two kinds of percolation processes can occur: *spontaneous* and *shear-induced*. *Spontaneous percolation* refers to the ability of small particles to percolate under gravity forces alone, with a critical ratio of d_f/d_c around 0.155, where d_f and d_c are the diameters of the fine and coarse particles. For example, for a uniform broken ore in the upper draw column with d_{50} = 2 m, particles finer than 31 cm would be able to migrate downward more quickly than the surrounding matrix.

Regarding *shear-induced percolation*, Bridgwater et al. (1978) proposed valuable empirical relationships to evaluate the mean percolation distance which depend mostly on the shear strain and particle diameters of the bed and percolation, with current improvements by Hashim & Sharrock (2012). In addition, Pierce (2009) carried out numerical modelling using PFC 3D (Particle Flow Code 3D, Itasca 2014) to study percolation corroborating the shear-induced percolation. Pierce also indicates that, when fines travel with the coarse bed material, they move both laterally and vertically, and where the IMZ narrows near its base, this can lead to stagnation of fines as they percolate closer and closer to the IMZ limit.

Conversely, Power (2012) indicates that it may not be necessary to account for such detailed factors (e.g. shear-induced percolation) at early feasibility study stages, due to the fact that the required input data is rarely available at these stages. Hence, the shear-induced percolation won't be included here, although it should be considered in advanced stage designs.

6.2.4.2 Fines segregation approach in granular materials

Numerous studies have investigated the fines segregation in granular materials related to internal erosion, piping, suffusion and filter design in earth dams. These are reported in standard design manuals such as the Earth & Rock-Fill Dams General Design & Construction Considerations (2004) and Design and Construction of Levees (2000). Research works by Kezdi (1979), Sherard (1979) and Kenney and Lau (1985) make possible the assessment of segregation potential of fines (< 4.75 mm size) from larger particles (>4.75 mm up to 1000 mm).

For instance, if Kezdi's (1979) method is applied in a shear annulus within a draw column, the initial gradation can be divided into a coarse and fine gradation. The key hypothesis of this method is that the segregation of the fines gradation will occur if the ratio D_{15}/d_{85} is higher than 4, where D_{15} is the particle diameter for the 15% of mass passing of the coarse gradation and d_{85} is the particle diameter for the 85% of mass passing of the fine gradation. Here it is necessary to establish the initial gradation, which is assumed to be the block size distribution at the limit between the far and near field, which then allows the calculation of the fine and coarse gradations relative to a specific block size. The segregation potential can then be checked by applying this procedure to several block sizes. It is important to note that this method focuses on fines segregation due to seepage through an earth fill dam (internal erosion in dams), which is not fully comparable to the fines migration in a block cave draw column. However, the fines segregation from a broken ore zone is a dynamic process within the shear bands, involving the continuous downward progression of blocks, including internal movements among blocks and facilitating the migration of fines from the broken ore. Hence, the fines migration in caving is somewhat comparable to the internal erosion in dams. Further studies could allow the use of the Kezdi's method in the fines migration assessment. However at this point, this approach is not considered in the methodology proposed in this work.

6.3 Framework for Empirical Methodology to Estimate the BSD at Drawpoints

The methodology presented in the following sections is built based on four key considerations:

i) Far and near field conditions;

ii) Extrapolation of laboratory 1-D compression and shear test results;

iii) Gravitational flow characteristics of broken rock; and

iv) Fines migration.

6.3.1 Far and near field conditions

Column heights from past caving projects average approximately 210 m (Flores et al. 2004), but are trending towards greater heights approaching 600 m (Woo et al. 2013, Eberhardt et al. 2015). Thus, in developing an empirical method for BSD, consideration needs to be given to differentiating between the *far field* and *near field* stress conditions acting on the broken ore. The *far field* conditions can be represented as broken ore moving uniformly downward towards the drawpoints. A 1-D compression test serves as a practical experimental proxy to represent secondary fragmentation occurring in the far field. In the *near field*, the broken ore experiences variable stress conditions during caving. As previously explained, two different flow mechanics apply to broken ore moving down through the draw column. First, a compressive plug-flow develops in the center of the draw column. This zone can be characterized by *1-D compression* tests in the upper part of the near field, while *isotropic compression* could apply closer to the drawpoints (section 6.3.2.1). Around the outer periphery of the column, shear banding develops, which can be represented experimentally by *simple shear stresses* (Pierce 2009).

The *near field* is limited by a critical height (h_c) which is the height above the drawbell where interactive flow develops. Laubscher (1994) proposed a chart to evaluate the height of interaction zone (HIZ) which depends on the RMR and the minimum spacing of the draw points across the major apex, while Susaeta (2004) indicates that h_c is equivalent to two times the IMZ diameter. Pierce (2009) suggested this height to be 100 to 200 times the mean particle size, which is equivalent to 50 - 100 m assuming an average block size of 0.5. Based on these studies, is it reasonable to define an approximate range of h_c as 50 m to 100 m.

6.3.2 Extrapolation of laboratory compression and shear test results

Analysis of data from laboratory compression and shear testing programs afford the opportunity to use these as analogues for the near and far field loading conditions influencing secondary fragmentation and drawpoint BSD. 1-D compression tests generate fragmentation through splitting and crushing (Chapter 4), while shear tests are associated with shearing, abrasion and corner rounding (section 6.2.3). When comparing compression or shear tests to broken ore materials, scale effects related to specimen size are a key concern. A commonly applied technique to scale geotechnical properties of coarse particle materials (e.g. broken ore) towards small granular samples is based on the parallel gradation method first proposed by Lowe (1964). This technique involves shifting the size distribution curve obtained for a smaller sized shear test to the targeted larger scale (on a semi-log plot). De la Hoz (2007) demonstrated that this technique is suitable for particles sizes such as sands and gravels;

however, other studies have shown that for larger block sizes, scale effects should be accounted for with strength and stiffness generally decreasing with increasing particle size (Frossard et al. 2012).

6.3.2.1 1-D compression tests

As noted above, 1-D compression tests can be used to represent the broken ore fragmentation mechanism in the *far field*. Similarly, the plug-flow zone that develops within the near field can also be simulated as a cross between 1-D (anisotropic) and isotropic compression testing. Pierce (2009) found from numerical modelling results using PFC3D that the IMZ could be characterized by an isotropic condition at a height of 16 d from the base, where d is the diameter of the particles. So, it is feasible to assume that a broken ore zone entering into a plug-flow zone (boundary between the far-field and top of the near field below it) would undergo 1-D compression first and then a stress redistribution to isotropic compression acting on the central plug-flow zone close to the drawpoint. Also, stress reduction occurs in the near field within the plug-flow zone, which can be evaluated using the following equation from Janssen (1985, 2004), also employed in Chapter 3

$$\sigma_v = \frac{R_h \cdot \gamma}{K_o \cdot \tan\phi'}\left(1 - e^{\frac{-K_o \cdot (\tan\phi) \cdot H}{R_h}}\right) \qquad [6.1]$$

Of interest are large 1-D compression tests on rockfill and waste rock with specimen diameters of up to 1 m, as reported by Marsal (1965). These share similar characteristics with broken ore in terms of average particle size and particle shape. Data on uniform size rockfill (diorite) has been collected and analyzed in terms of fragmentation under high confining pressures (Table 6.1). A key consideration to take into account is related to the strength reduction of individual rocks due to size effects. σ_c can be reduced (see Table 6.1) using the following formulation by Yoshinaka et al. (2008):

$$\frac{\sigma_c}{\sigma_{c.0}} = \left(\frac{d_e}{d_{e.o}}\right)^{-k} \tag{6.2}$$

where σ_c is the uniaxial compressive strength associated with an equivalent length $d_e = V^{1/3}$, V is the block volume, and $\sigma_{c.o}$ is the uniaxial compressive strength associated with an arbitrary length $d_{e.o}$ and k is a potential exponent.

Table 6.1: Large 1-D compression tests. Marsal (1965)

Tests list	C_u	σ_v [MPa]	Gs	n_o	n_f	Rock type	σ_c [MPa]	σ_c.o (*) MPa	Part. shape
La Soledad Gravel (Loose)	1.2	3.2	2.41 -2.62	0.51	0.44	Diorite	115.0	60.2	angular
La Soledad Gravel (Dense)	1.2	3.2	2.52	0.44	0.38	Diorite	115.0	60.2	angular
Infiernillo Dam material (No4 - Loose)	3.2	3.2	2.73	0.44	0.38	Diorite	115.0	60.2	angular
Infiernillo Dam material (No4 - Dense)	3.3	3.2	2.73	0.40	0.35	Diorite	115.0	60.2	angular

Cu = D_{60}/D_{10}; Gs = Specific gravity; σ_v = vertical pressure; n_o = Initial porosity; n_f = Final porosity.

For the analysis carried out here, block strengths for the data in Table 6.1 were scaled up to 1 m and a value of k equivalent to 0.25 (as suggested for granite) was applied. This data was combined with 1-D compression test results from Chapter 4 which are presented in Fig.

6.5 to Fig. 6.8 to evaluate D_{80}, D_{65}, D_{50} and D_{25}, respectively. The parameter R is defined below in Equation 6.3, which reflects the size reduction due to fragmentation after an oedometer compression test:

$$R = 1 - \frac{Df}{Di} \tag{6.3}$$

where D_i and D_f are the initial and final diameters for a specific percentage passing. From these charts, it is evident that rockfill data agrees with the 1-D compression test program from Chapter 4 under loose density, which give a measure of confidence in using these small size scale tests to represent broken ore materials from cave mining to evaluate secondary fragmentation.

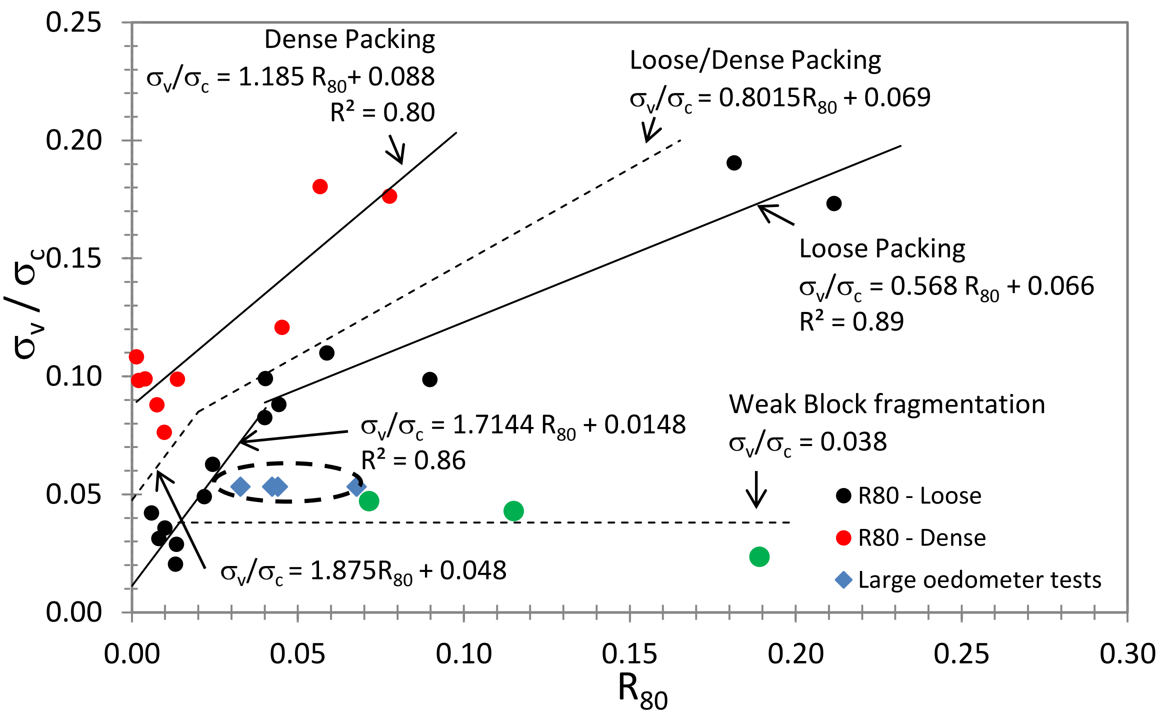

Fig. 6.5: Chart to estimate R_{80}

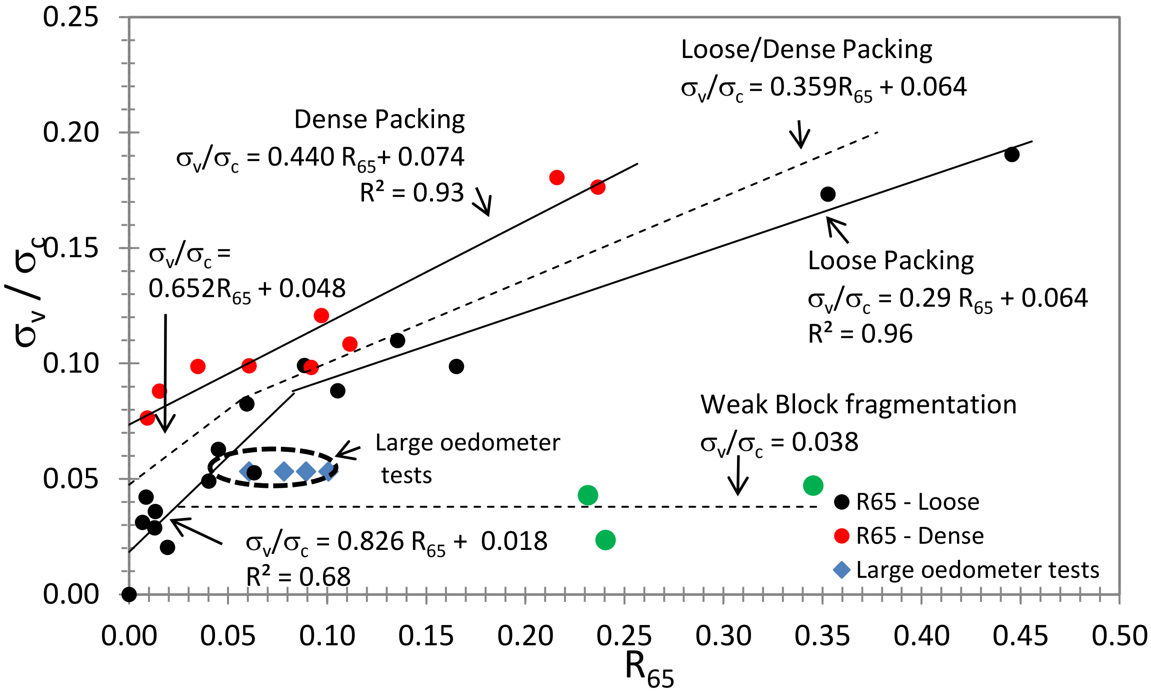

Fig. 6.6: Chart to estimate R_{65}

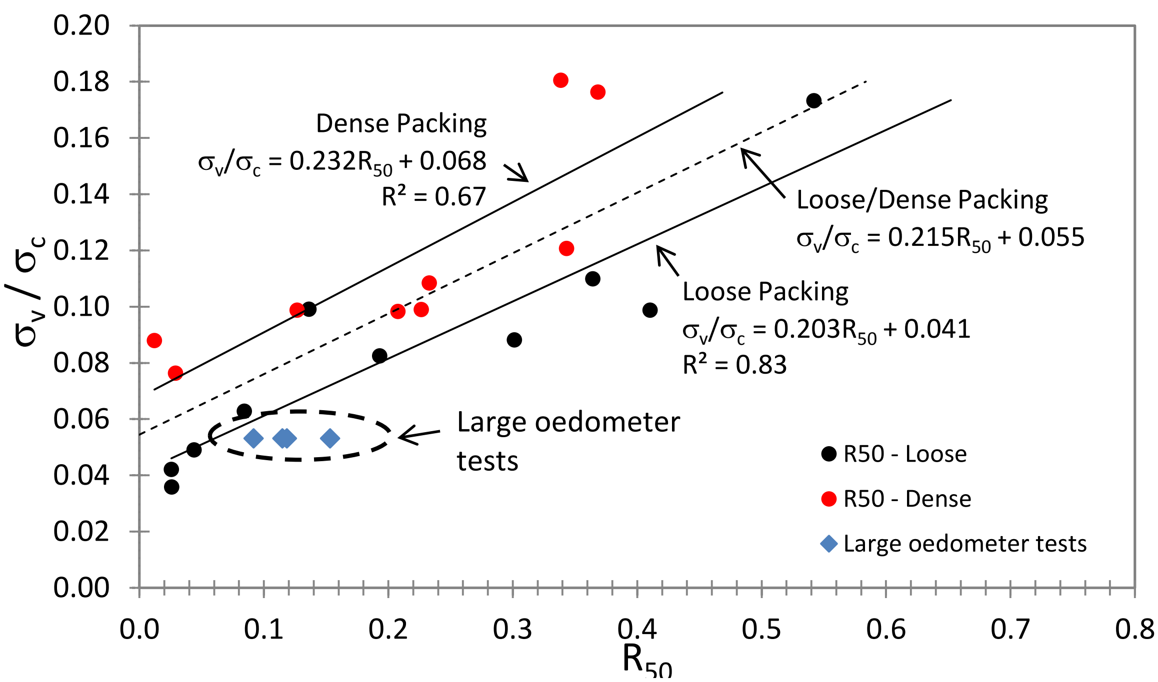

Fig. 6.7: Chart to estimate R_{50}

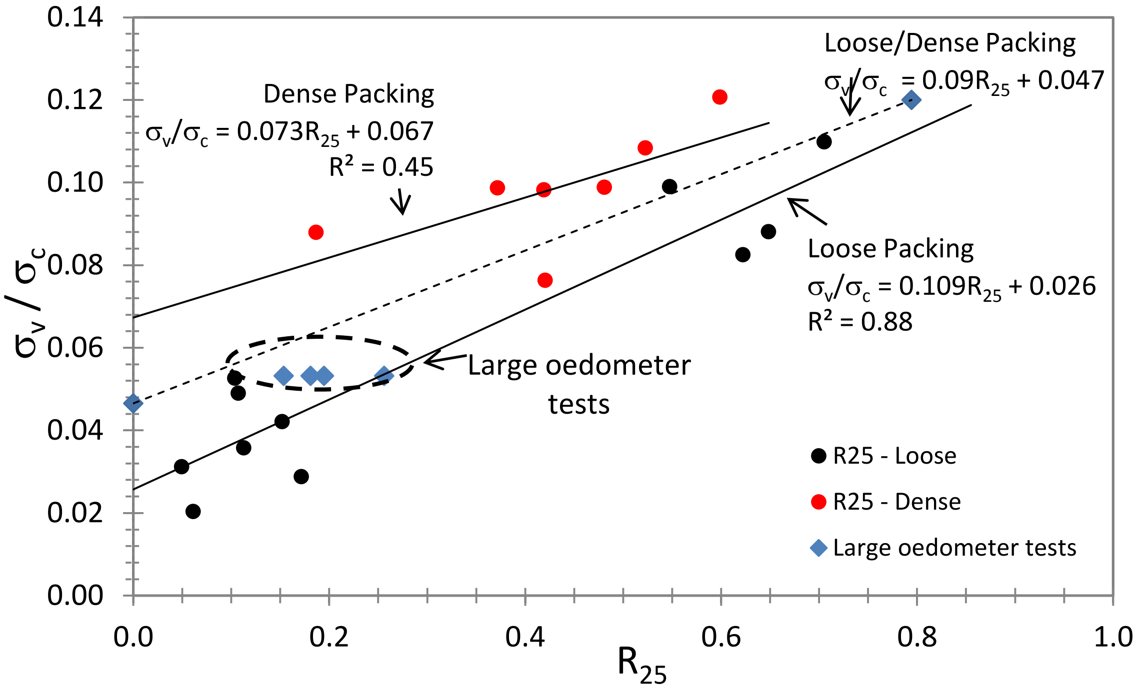

Fig. 6.8: Chart to estimate R_{25}

6.3.2.2 Shear tests

Bridgwater et al. (2003) carried out thorough investigations on mono-size particle samples, varying particle shapes and average particle sizes in ring shear tests. Vertical pressures from 0.15 to 292 kPa and shear strains from 0.9 to 8×10^4 were applied. Based on their results, Bridgwater et al. (2003) were able to propose the following equation to describe the attrition of mono-sized assemblies:

$$W = K_N \left(\frac{(\sigma_N \Gamma^{\phi}}{\sigma_{scs}} \right)^{\beta} \qquad [6.4]$$

where W is the mass fraction (attrition), σ_N is the normal stress, Γ_N is the shear strain, σ_{scs} is the tensile strength, and K_N, ϕ and B are constants.

Although this attrition approach is effective in studying the secondary fragmentation occurring within a shear band, several issues such as high stresses, sample porosity, variable initial size distribution, and particles with defects in terms of veins and small discontinuities weren`t included in their analysis. This represents a key limitation in applying Bridgwater et al.'s (2003) attrition model to broken ore size distribution, as BSD is expected to change with depth, especially under high ore columns, which could over predict the secondary fragmentation within the shear bands. This was noted by Pierce (2009). Despite this concern, it is believed that the Bridgwater' attrition model is sufficient to evaluate the secondary fragmentation within the shear band for the early stage design methodology proposed in section 6.4.

6.3.3 Gravitational flow characteristics of broken rock

One of the key issues regarding the BCF approach as well as by other methodologies is that they do not consider the gravitational flow characteristics of broken rock, which means, for example, that they are not capable to evaluate shear and compression zones separately, which limit their accuracy in secondary fragmentation assessments (section 6.2.2 and 6.2.3) During gravitational flow, the draw column width increases with increasing column height. This topic was discussed extensively by Pierce (2009) who indicated that the Nedderman relationship (equation 6.5) reasonably captures the growth of the ore column, especially for IMZ heights larger than 100-200 mean particle diameters (which for an average block of 0.5 m equates to a column height of 50-100m). The Nedderman relationship is:

$$w = 3.42 \cdot \sqrt{h_{nf}} \qquad [6.5]$$

where w is the column width and h_{nf} is the near-field height. For the pre-feasibility level assessments this work is directed at, the simplicity of this relationship allows it to be easily incorporated into an empirical methodology.

Next, shear band thickness of broken ore materials needs to be considered. Most of the literature cited in section 6.2.3.3 is based on mono-size particles, which differs from typical BSD after primary and secondary fragmentation (Fig. 6.4). Ueda et al. (2012) carried out valuable work on shear bands involving well-graded particulate material. They analyzed nine different gradations as depicted in a through 2-D discrete-element simple shear simulations. These gradations represent broken ore size distributions that are amenable to the application of the *parallel gradation method* (explained later in this section). The authors were able to obtain different shear band thicknesses as a function of the standard deviation of particle size (Fig. 6.9). For mono size gradations, they found similar results as those recommended by Pierce (2009) of 10 times D_{50}. However for gradations of up to $\sigma_d = 0.2$ (equivalent to a Cu = 1.5) the shear band is 15 times D_{50}, while it decreases for σ_d larger than 0.2. Hence, it is feasible to define an approximate relationship of shear band thickness as a function of σ_d as shown in Fig. 6.9b. Interestingly, the results by Ueda et al. (2012) show that under broader gradations, the shear band thickness decreases, explained in part by preferential path generated within the shear band, which share similarities with the finding of Lieou et al. (2014) indicated in section 6.2.3.3.

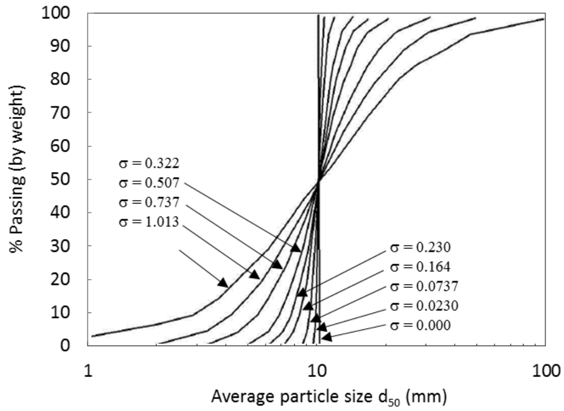

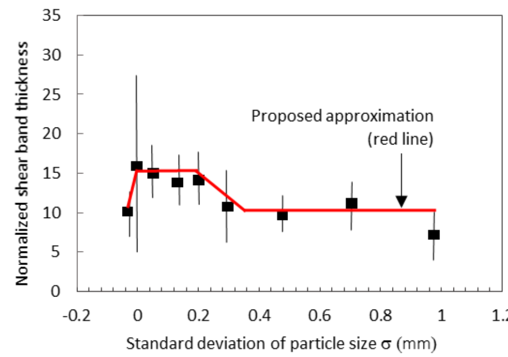

(b)

(a)

Fig. 6.9: Shear band thickness under well graded materials. a) Gradations analyzed; b) shear band thickness relationship. Adapted from Ueda et al. (2012)

6.3.4 Fines migration

Fines migration is the final pillar of the empirical methodology developed to predict BSD at drawpoints. For this, the spontaneous percolation is recommended as discussed in section 6.2.4. Regarding an IMZ, spontaneous percolation can be expected within the shear bands as a fines migration mechanism. Regarding interactive flow, broken ore will experience different responses depending on far field and near field. For the former, the broken ore movement is uniformly downward, lacking shear bands. Thus, it is believed that fines migration wouldn't be significant in the far field. In the latter case, a plug-flow compression zone and an outer shear band annulus occurs simultaneously within a draw column. It is expected that most of the fines will migrate through the shear bands rather than through the plug flow zone.

6.4 Empirical Method for Estimating BSD at Drawpoints

The following procedure has been developed to evaluate the evolution of the BSD as a function of different ore column heights. It aims mainly to be used in a drawzone involving multiple draw columns (i.e., under interactive flow), although single draw columns (i.e., isolated movement zone) can also be analyzed. The underlying methodology considers secondary fragmentation evolving across two main intervals: far and near field. The inputs required by this methodology (Fig. 6.10) are discussed below, together with Fig. 6.11 the procedure for far and near field factors.

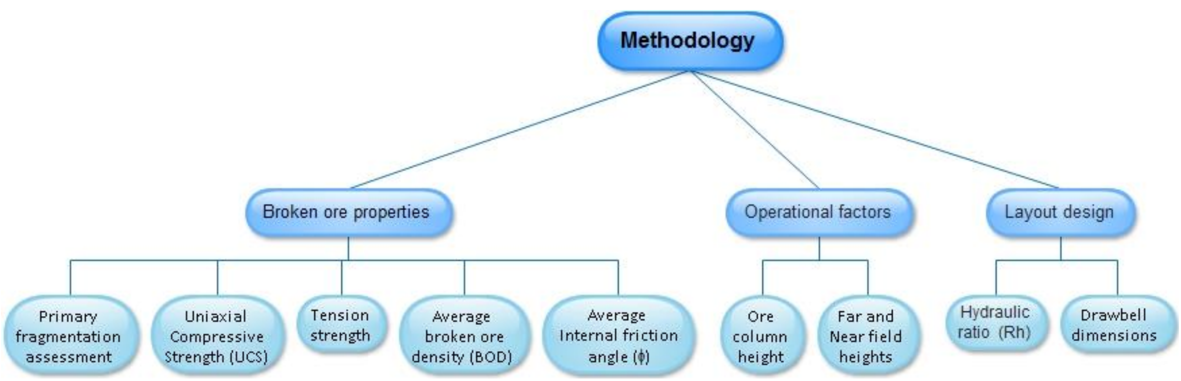

Fig. 6.10 Inputs required by methodology

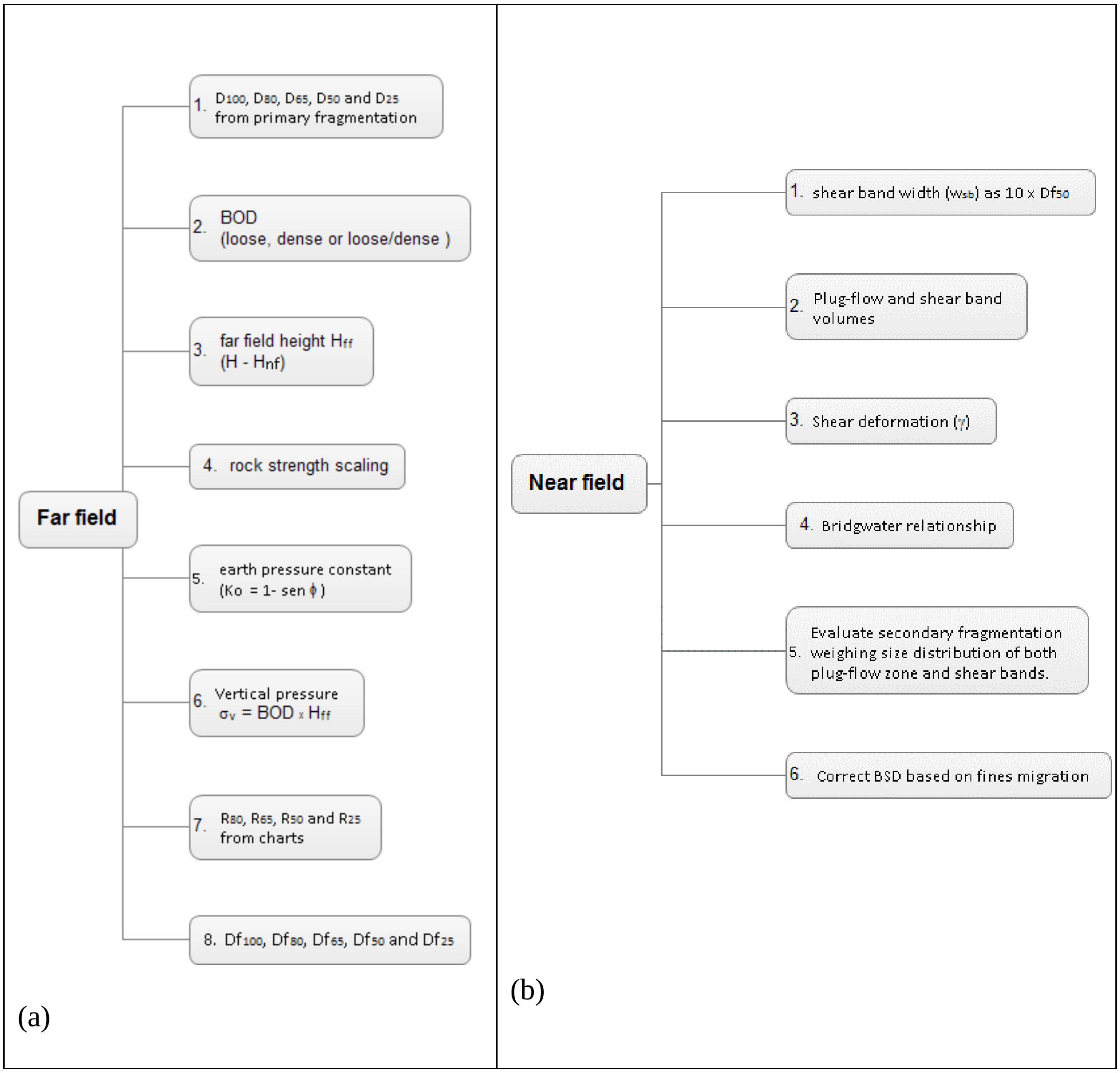

Fig. 6.11: Methodology flow chart. (a) Far field; (b) Near field.

6.4.1 Required inputs

The input parameters required by the methodology are detailed as follow:

1. The *primary fragmentation* (previously depicted in Fig. 6.1), which occurs in the cave back through stress-induced fracturing, represents the initial block size distribution and starting point. Several empirical and numerical approaches to evaluate primary fragmentation

have been developed for this purpose, such as Joints (Villasescusa 1991), JkFrag (Eadie 2003), BCF (Esterhuizen 2005), and FracMan (Dershowitz et al. 1998) amongst others. Each of these require for their input discontinuity data, which is typically derived from borehole televiewer surveys. Examples of primary fragmentation data reported by different authors, ranging from Cu (D_{60}/D_{10}) = 2 - 2.5, is plotted in Fig. 6.4b.

2. *The Uniaxial Compressive Strength (UCS)* is used to evaluate the charts presented in Fig. 6.5 to Fig. 6.8. As introduced in section 6.3.2, the intact rock strength has to be corrected for scale effects. The procedure proposed by Yoshinaka (2008) offers one means to scale intact rock strength to that more representative for the average block size (D_{50}) of the primary fragmentation size distribution.

3. *Tensile strength* is also used in the Bridgwater relationship (section 6.3.2.2). A value of 10% UCS can be assumed.

4. *The Broken Ore Density* (BOD) is required in Fig. 6.5 to Fig. 6.8 and needs to be identified as loose, loose/dense and dense packing state based on the guidelines provided in Chapter 2. In addition, an average value of BOD representing the entire column is needed to evaluate the broken ore (caved rock) overload.

5. *An average inter-block friction angle* (ϕ') along the shear bands is required to evaluate both *stress reduction* using equation 6.1 and *earth pressure constant* K_o = 1- sin ϕ'. Guidelines from Chapter 3 can be used to estimate ϕ'.

6. *Broken ore column height (H) and far & near field limits* are key input parameters that are used to account for the residency time of the ore in the draw column relative to its travel path from the top of the draw column until it reaches the drawpoint. For practical purposes,

the ore column height is measured from the top of the draw column to the top of the drawbell (as depicted in Fig. 6.2 and Fig. 6.3). The near field height (H_{nf}) can be assumed to be between 50 m and 100 m (as discussed in 6.3.1), while the far field height can be obtained as H - H_{nf}.

7. Some parameters related to the *layout design* are required: a) Drawbell geometry is used to evaluate the volumes of shear and compression within a draw column as explained in 6.4.3. b) Hydraulic radius of the drawbell (R_h), which is calculated as area/perimeter, is used in the Janssen' correction (equation 6.1).

6.4.2 Secondary fragmentation initial state – Far field versus near field

For mature operations, where numerous drawpoints are in production and the draw column heights are tall enough for interactive flow, fragmentation depends on a combination of far and near field effects. Evaluation of the broken ore BSD should first be assessed for the far field. This can be directly evaluated based on the charts proposed in Fig. 6.5 to Fig. 6.8. The values for D_{80}, D_{50} and D_{25} can be used to represent the BSD of the broken ore at the boundary between the far and near field. After this transition, the procedure assumes that the broken ore that enters the outer periphery shear bands undergoes re-arrangement due to rotation and shear displacement, promoting fines migration downward to the drawpoints. For practical purposes *spontaneous percolation* can be used to evaluate the broken ore size distribution at the drawpoints.

Near-field conditions apply to either early production where flow occurs through an isolated movement zone (IMZ), or in the case of interactive flow, below the far-field and above the drawpoints. In the near field both a plug-flow compression zone and outer periphery shear bands are present. As discussed in section 6.3.1, the compression zone can be characterized by 1-D compression tests. This requires accounting for a stress reduction due to a preferential vertical stress redistribution (equation 6.1) closer to the drawpoints (section 6.3.2). Due to this stress reduction, it is hypothesized that no additional fragmentation after passing from the far field zone is expected. The charts from Fig. 6.5to Fig. 6.8 can be employed.

In terms of the outer shear bands, Bridgwater's attrition model (6.3.2.2) can be applied. It should be noted that although the Bridgwater model was developed based on low normal stresses, it is assumed here that it can still be used for higher normal stresses acting on the shear bands where a tall draw column and far-field conditions are present. Under a shorter draw column scenario, a smaller amount of fines migration is expected, mainly because a higher amount of fines derived from primary fragmentation and rock-fall impact would yet to have developed. Also, the lower normal stresses in the shear bands would facilitate friction mobilization as opposed to fines generation, as well as the rapid percolation of fines downwards to the drawpoints. This can be evaluated using a *spontaneous percolation* analysis *(*6.2.4.1*)*, and the fines portion weighted together with the BSD. An important consideration is that the amount of fines migration weighted in the final BSD is limited by the broken ore porosity.

6.4.3 Procedure to evaluate the block size distribution at drawpoints

First, the secondary fragmentation in the far field zone should be calculated using the following steps (Fig. 6.11a):

(F1) Use the primary fragmentation curve to estimate D_{100}, D_{80}, D_{65}, D_{50} and D_{25}.

(F2) Determine the BOD and define if the column will be under a loose (1.7 t/m^3), dense (2.6 t/m^3), or loose/dense (2.15 t/m^3) state.

(F3) Estimate the far field height as H minus H_{nf}. A representative value of H_{nf} = 75 m can be assumed (i.e., average between 50 and 100 m).

(F4) Estimate the earth pressure constant using $K_o = 1 - \sin \phi'$.

(F5) Scale the UCS rock strength to account for scale effects using equation 6.4. The rock has to be scaled to the average size (D_{50}) of the primary fragmentation size distribution. Thus, d_e can be equated to D_{50}.

(F6) Estimate the vertical pressure using equation 6.6. Then, obtain the ratio σ_v/σ_c.

$$\sigma_v = BOD \cdot H \qquad [6.6]$$

(F7) Using the ratio σ_v/σ_c as an input, estimate the values of R_{80}, R_{65}, R_{50} and R_{25} from Fig. 6.5 to Fig. 6.8 taking into consideration the BOD state as in step (F2). For higher values of σ_v/σ_c, the correlations can be extrapolated to larger values of R. However, the value of R should be limited to a maximum value of 0.95.

(F8) Using equation 6.3, estimate the BSD at the bottom of the far field based on Df_{100}, Df_{80}, Df_{65}, Df_{50} and Df_{25}

Next, to evaluate the near field zone, the calculation next steps (Fig. 6.11b) are as follows:

(N1) Estimate the shear band width (w_{sb}). Ten times Df_{50} is a reasonable estimation, although Fig. 6.9 could also be considered if a more precise assessment is required.

(N2) Estimate the plug-flow and shear band volumes. Consider that the column width increases by the Nedderman relationship (equation 6.5) from the top of a drawbell up to a column height of 75 m. The total volume of a draw column can be approximated assuming the volume of a truncated cone, where the larger diameter corresponds with the draw column width and the small diameter is equivalent to the drawbell diameter. The outer diameter can be approximated as 10 D_{50}.

(N3) Evaluate the shear deformation (γ) on the broken ore within the shear band as $\gamma = w_{sb} / H_{nf}$, where H_{nf} is the height of the near field draw column. Here is assumed that the shear bands move mainly vertically downwards towards the drawpoints.

(N4) Use equation 6.4 and coefficients from Table 6.2 (Bridgwater relationship) to estimate the BSD of the broken ore after shear deformation within the shear bands. A key consideration is that Bridgwater relationship is built on mono-size particles, which differs from the BSD found at the top of the shear band. Hence, each attrition product is associated to the corresponding size of the broken ore. Also, in equation 6.4, σ_{scs} can be estimated as $0.1\sigma_c$, while σ_n (normal stress of the broken ore within the shear band) is evaluated as an arithmetic average of the normal stress at the beginning and at the end of the shear band (close to drawpoints). σ_n at the top of the shear band can be evaluated using equation 6.7, while σ_n at the bottom of the shear band can be equated as σ_v (using equation 6.1) assuming an isotropic stress field close to drawpoints.

$$\sigma_n = BOD \cdot H_{ff} \cdot K_o \qquad [6.7]$$

Here H_{ff} is the far field height and Ko is the earth lateral pressure constant. It should be noted that stress relief occurs within the plug-flow zone (which can be quantified by Janssen' equation 6.1), in which case no further fragmentation is expected in this zone.

Table 6.2: Bridgwater's coefficients (2003)

Cumulative attrition % initial diameter	K_n	β	ϕ
88	58.6	0.84	0.9
73	48.3	0.85	0.9
63	41	0.98	0.9
53	36.8	0.99	0.9
44	33.4	1	0.9
31	30.9	1.01	0.9
16	16.4	0.94	1
9	10.4	0.86	1.1
3	8.4	0.86	1.1

(N5) The BSD of the broken ore after secondary fragmentation is evaluated after conducting a volume-weight on the size distribution of both the plug-flow zone and shear bands.

(N6) In order to include the fines migration potential, spontaneous percolation (section 6.2.4.1) is considered. This percolation is applied within the shear bands. Hence, this amount of fines is weighed together with the secondary fragmentation curve obtained in (N6). Because the BSD is non-uniform, the average *coarse particle* could be defined between D_{100} and D_{50}, and then, be represented by D_{75}. Thus, the diameter of the percolated fines is $D_{pf} = 0.155\ D_{75}$. Finally, using the BSD at the bottom of the far field before it enters the near field, the D_{pf} can be associated with a percentage of the percolated fines in the shear band, which is then used to volume-weight the percolated fines with the BSD after secondary fragmentation, obtaining the final BSD at the drawpoints.

For the isolated movement zone (IMZ) case, the evaluation of the BSD at the drawpoints can be carried out following the procedure above for the near field zone, with the exception that secondary fragmentation within the plug-flow is expected in this case. For this, the charts from Fig. 6.5 to Fig. 6.8 can be used.

6.5 Methodology Verification and Validation

In this section, the methodology is first tested and verified against different cases involving contrasting rock properties and draw column heights. The verification is used to ensure the implementation of the model is correct, relative to the expected conceptual evolution of the BSD. BSD projections using the methodology are then compared and validated against field data from the El Teniente mine for both fresh dacite and a mix of fresh and weathered dacite.

6.5.1 Verification of BSD at drawpoints under different rock and draw column conditions

In order to verify the capability of this methodology, several representative cases are analyzed as follows. The first case considers a broken ore material under interactive flow and a BSD at the top of the muckpile surface with the following characteristics: D_{100} = 4 m, D_{80} = 1.6 m, D_{65} = 1.3 m, D_{50} = 1 m, D_{25} = 0.8 m and D_{10} = 0.5 m. The UCS of the rock is given as 120 MPa, with a testing diameter of 70 mm for scaling purposes. Other required parameters include: k = 0.2 (representative exponent for hard rocks from equation 6.2), average friction angle = 40° (see Chapter 3); the hydraulic radius R_h is 11.3 m, and the near-field column height, h_{nf} is 75 m. Also, spontaneous percolation is assumed for the fines migration mechanism.

In order to show the evolution of the BSD, from the initial primary fragmentation to the final BSD at the drawpoints, Fig. 6.12 presents the verification results for the case of a 300 m high draw column under loose density (1.7 t/m^3). As expected, the BSD calculated evolves from a narrow to a wide size distribution. First, the BSD is narrow within the far field zone. The far-field broken ore material then enters into the shear bands and plug-flow zone. In the shear band, the material undergoes secondary fragmentation which is evaluated based on Bridgwater's relationship (equation 6.4), while no further significant fragmentation is assumed to occur in the plug-flow zone where the material experiences a stress reduction. Finally, weighting factors are applied to the block size distributions specific to the shear bands, plug-flow zone and fines migration, and a final BSD at the drawpoints can be generated.

The second verification analysis considers the influence of both ore column height and BOD on the BSD arriving at the drawpoints. *Loose density* (e.g. 1.7 t/m^3) and *dense states* (e.g. 2.6 t/m^3) within the draw columns (under interactive flow) are analyzed for draw column heights of 100 m, 300 m and 500 m (Fig. 6.13). Each case assumes the same initial BSD at the top of the muckpile surface (section 6.5.1). A UCS of 150 MPa (sample diameter =70 mm) is assumed in contrast to the 120 MPa value used for the previous case. The resulting BSD evolves towards finer size distributions as the draw column heights increase, as would be expected. The results also highlight that the denser initial state generates higher fragmentation than the loose state. The difference is seen to be quite pronounced for a column height of 500 m.

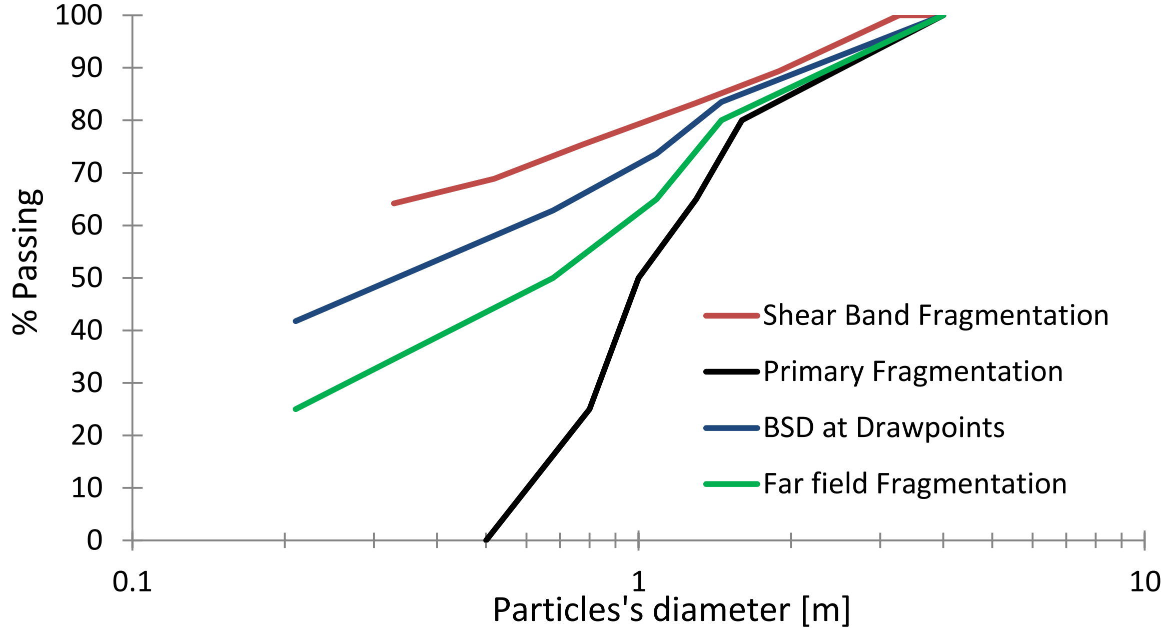

Fig. 6.12: Evolution of block size distribution from primary fragmentation to BSD at drawpoints. Case considers ore column 300 m high and loose density (1.7 t/m^3)

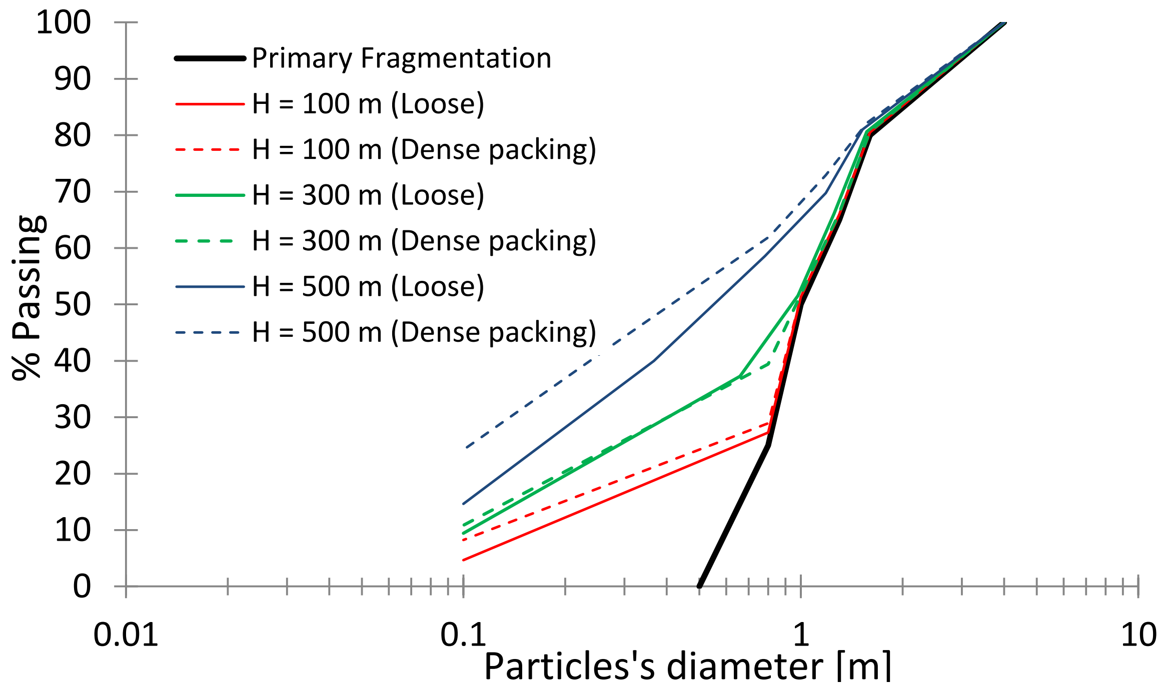

Fig. 6.13: Evolution of BSD under different ore column height and both loose and dense states

Although the loose state correlations are associated with higher fragmentation relative to the dense state in Fig. 6.5 to Fig. 6.8 the density is also directly proportional to the stresses acting on the broken ore (σ_v, σ_n). This more directly affects the secondary fragmentation assessment, which explains why dense states generate more fragmentation than loose states.

A sensitivity analysis was conducted considering the same input data as the previous verification analysis. The first of these examined the influence of varying UCS values for the intact rock: 150, 110 and 70 MPa. The resulting BSD are plotted in Fig. 6.14 where it is possible to observe that finer BSD correspond with lower UCS values of the rock. The inter-block friction angle was also analyzed as it conditions the earth lateral pressure K_o (section 6.4.1) as well as the vertical pressure close to the drawpoints based on the Janssen equation (6.3.2.1). Three values of ϕ' were considered: 30º, 40º and 50º. The results can be seen in Fig. 6.15, which show that ϕ' affects the BSD at the drawpoints only slightly.

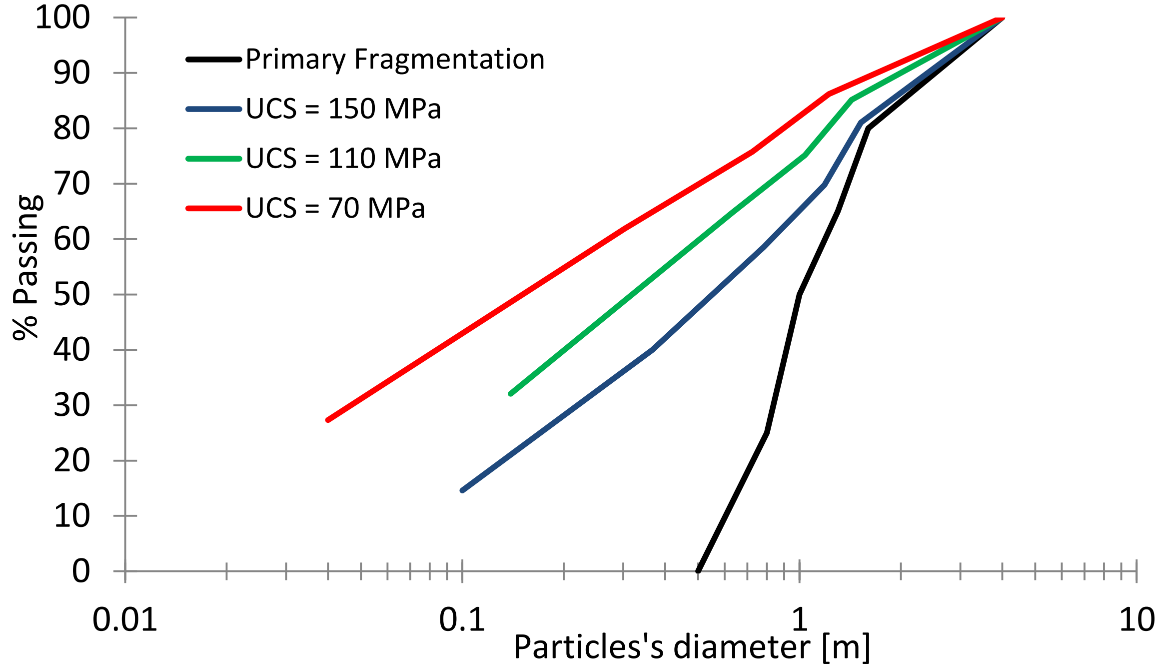

Fig. 6.14: Influence of compressive strength on BSD at drawpoints predictions. H = 500m

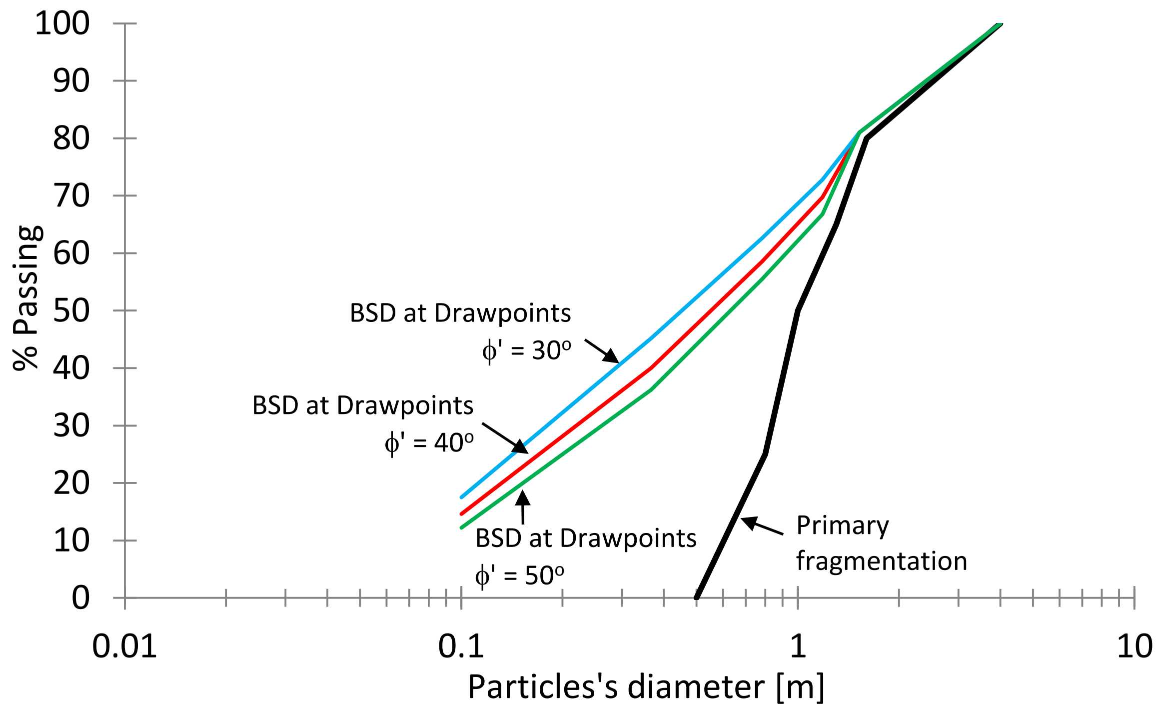

Fig. 6.15: Influence of ϕ' in BSD at drawpoints assessment

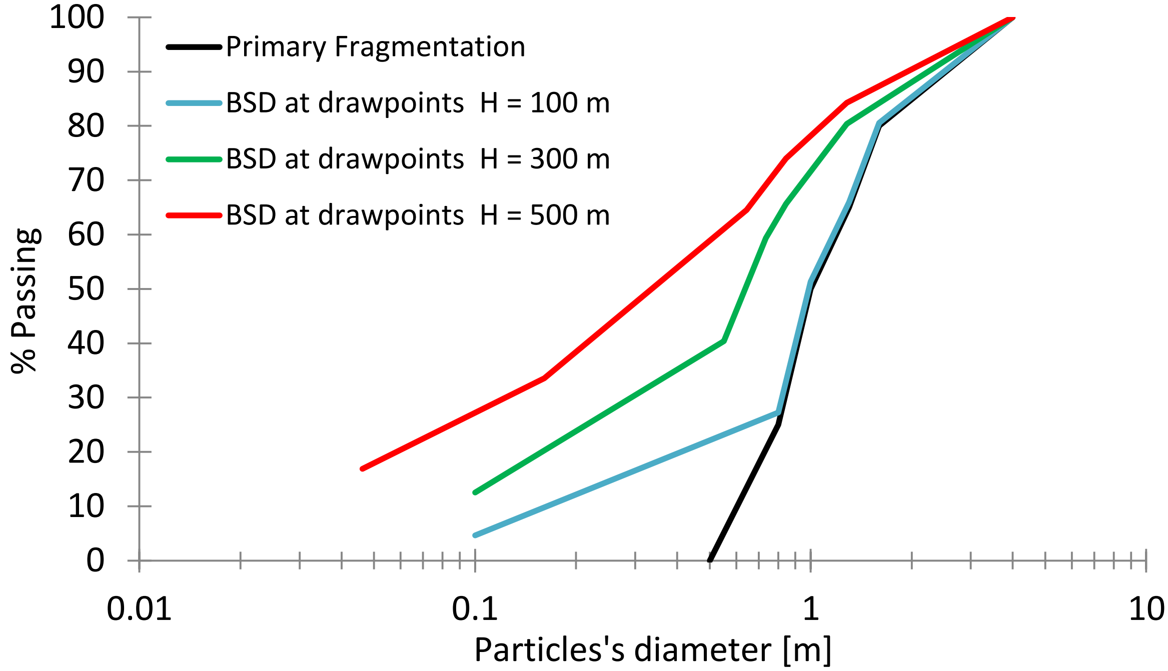

Fig. 6.16: Influence of large weak blocks undergoing fragmentation

Finally, the methodology developed also recognizes the potential fragmentation of large weak blocks surrounded by smaller but stronger blocks, as previously analyzed in Chapters 4 and 5. The verification scenario modelled to investigate this considers a subset of large blocks with a reduced UCS of 50% of the smaller blocks making up the matrix. The same input data was used as in the second verification analysis, with the exception of the exponent k, which was assumed here to be 0.3. Three draw columns heights of 100, 300 and 500 m are studied. Also, using Fig. 6.5 and Fig. 6.6, a limit of σ_v/UCS = 0.038 can be considered for fragmentation of the large blocks. Fig. 6.16 shows the results obtained, for which a significant decrease of D_{80} is clearly noticed for draw column heights of 300 and 500 m.

Summarizing, *primary fragmentation, draw column height* (H) and *rock strength (UCS) scaled to in situ block sizes,* conditions the shape of the broken ore size distribution within a draw column and at the drawpoints. Also, two additional factors also control the block size reduction via secondary fragmentation: *shear* deformation (γ) and *shear band thickness* (w_{sb}). Within the methodology developed her, γ is a sensitive parameter to take into account, which depends strongly on w_{sb}. The latter experiences a reduction according to the relationship of 10 D_{50}, with D_{50} decreasing as the broken ore approaches the drawpoints. This reduction works well for non-weathered and hard rocks. However, under weak and weathered rock conditions (e.g UCS < 50 MPa) D_{50} will undergo a high reduction, decreasing significantly the shear band thickness, affecting strongly the weighting of both shear bands and plug-flow zone. Thus in terms of verification, this methodology should be employed only for strong and medium strength rocks.

6.5.2 Methodology validation

In order to validate the effectiveness of the methodology developed, an analysis was carried out and compared with in situ block size distribution data from the El Teniente caving operation in Chile (see Hurtado & Brzovic 2013; Brzovic et al. 2014, Vallejos et al. 2014, Brzovic 2015). The data collected correspond to 5 different zones at the mine, where each zone is comprised of several draw columns under interactive flow, without air gap development and under a maximum draw column height of 150 m. The data can be divided into two rock types: one that involves predominantly strong rocks, and one that is a mixture of strong and weak rocks. The strong rocks were classified as having an approximate UCS of 133 MPa, and involves mostly dacite and dolerite (associated to k = 0.2 from equation 6.2).

An important consideration is that the strong rocks were preconditioned by means of hydraulic fracturing (to increase its in situ fragmentation). The weak rocks encountered at El Teniente were heterogeneous; a representative value of UCS = 30 MPa was assigned. Also, an exponent k = 0.28 as recommendation by Yoshinaka et al. (2008) for highly weathered granite (k = 0.27-0.29) is selected. Rock strength data was obtained from Vallejos et al. (2014) and Brzovic et al. (2014).

The drawpoint BSD data was mapped by means of visual observation for different draw column heights. In order to assign primary fragmentation curves for the analysis, representative drawpoint BSD during early extraction were used. For each draw column height, an h_{nf} = 75m was assumed, together with a draw column diameter of D = 45 m (i.e., R_h = D/4 = 11.3 m) and an equivalent drawbell diameter of 15 m. A broken ore density (BOD) of 1.8 t/m^3 was assumed based on representative field values reported by Brzovic (2015). Hence, a loose state condition was assigned using the charts in Fig. 6.5 to Fig. 6.8. Drawpoint observations suggest significant moisture conditions can be found in the zones analyzed. Although water won't affect the strength of stronger rocks, it could affect the weaker weathered rocks. In Chapter 5, is was found that the UCS can decrease by 70% due to moisture conditions. Thus, a strength reduction of 85% is considered here for the analysis of the mixed strong and weak rocks case.

6.5.2.1 Validation - Strong rock zones

Zones 1 to 3 represent lithology units associated largely with dacite. Table 6.3 lists the most important rock and draw column properties. The mapped drawpoint BSD from each zone is compared with that predicted using the methodology developed here. Results are shown in Fig. 6.17 to Fig. 6.19. As can be observed, the predicted value is located between the mapped drawpoint BSD and the primary fragmentation curve. It should be noted that the mapped in-situ values don't show significant fragmentation due to low stresses and high rock strengths that limit fragmentation in the far field zone. The low stresses in the near field also cause negligible fragmentation within the shear bands. Thus, for low draw column heights the fragmentation occurs only by means of attrition in the shear bands, dictated by the Bridgwater relationships.

Table 6.3: Summary for rock and draw column properties (zone 1 to 5)

Zone	BOD (t/m^3)	ϕ º	K_o	k (eq. 6-4)	σ_c (Intact) MPa	σ_c scaled (D_{80}) MPa	σ_c scaled (D_{65} MPa)	σ_c scaled (D_{50}) MPa	H ore column (m)
1	1.8	48 (1)	0.26	0.2 (2)	133	76.4	79.7	84.2	150
2	1.8	48 (1)	0.26	0.2 (2)	133	76.6	79.5	83.3	150
3	1.8	48 (1)	0.26	0.2(2)	133	75.6	80.8	85.8	150
4	1.8	39 (3)	0.37	0.24(4)	81.5	26	26.8	28.8	75
5	1.8	39(3)	0.37	0.24 (4)	81.5	25.8	26.5	28.6	75

(1) Obtained based on methodology from Chapter 3; (2) Average value of k recommended by Yoshinaka et al. (2008) for strong rocks ; (3) Average arithmetic value between 48º and 30º. (4) Average value between 0.2 (strong rock) and 0.28 (weathered rock).

6.5.2.2 Validation - Mixture of strong and weak rock zones

Zones 4 and 5 are composed of a mix of fresh and weathered dacite. Table 6.3 details the most important rock and draw column properties. The main assumption used here is that a UCS = 81.5 MPa was assigned, taken as the average of the fresh rock (133 MPa) and weathered rock (30 MPa). As can be seen in Fig. 6.20 and Fig. 6.21 the predicted curves reproduce the mapped drawpoint BSD data with a high precision.

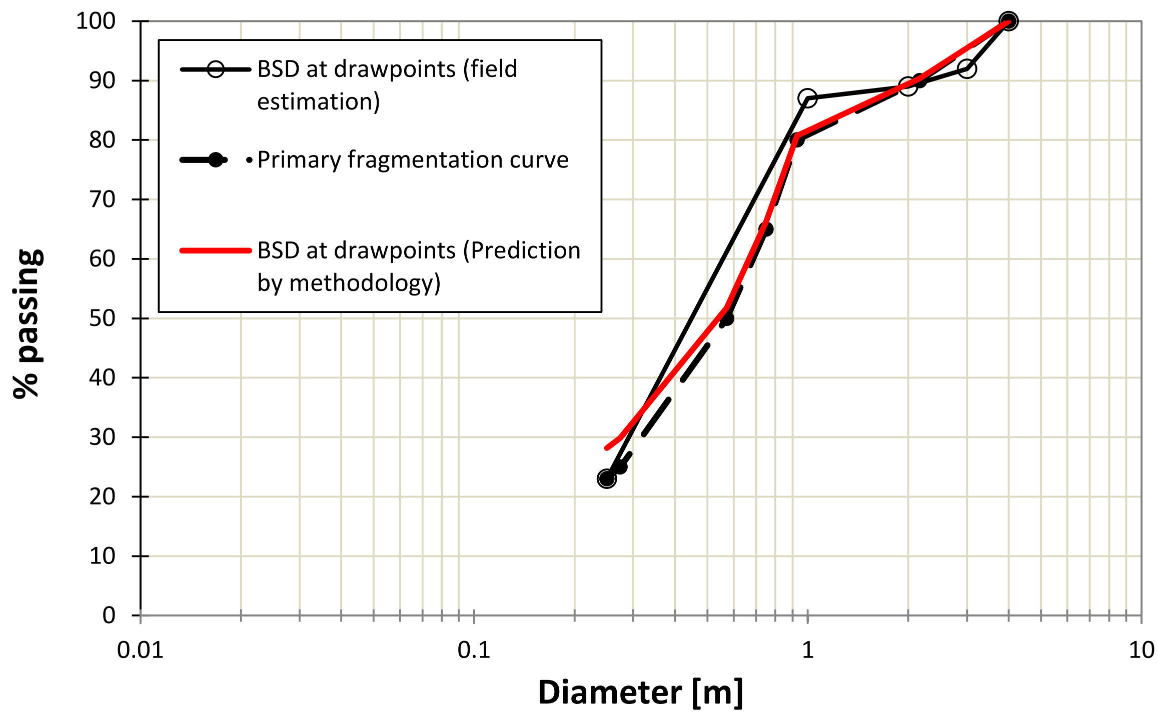

Fig. 6.17: BSD at drawpoints. Strong rock. Zone 1

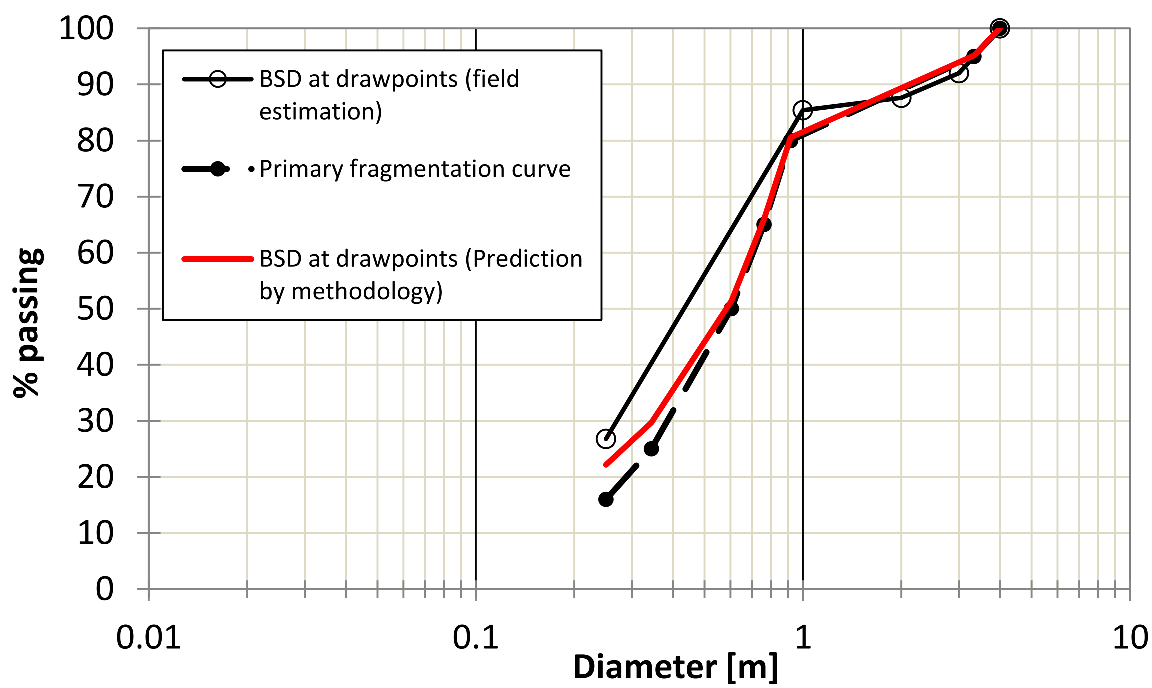

Fig. 6.18: BSD at drawpoints. Strong rock. Zone 2

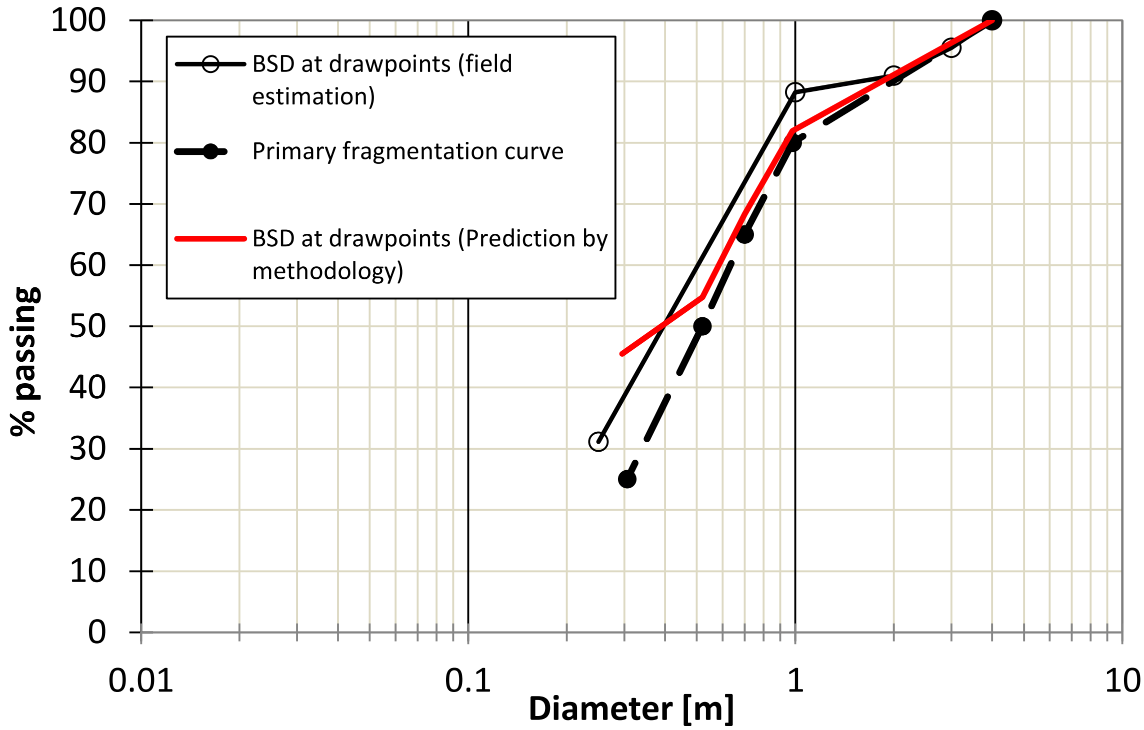

Fig. 6.19: BSD at drawpoints. Strong rock. Zone 3.

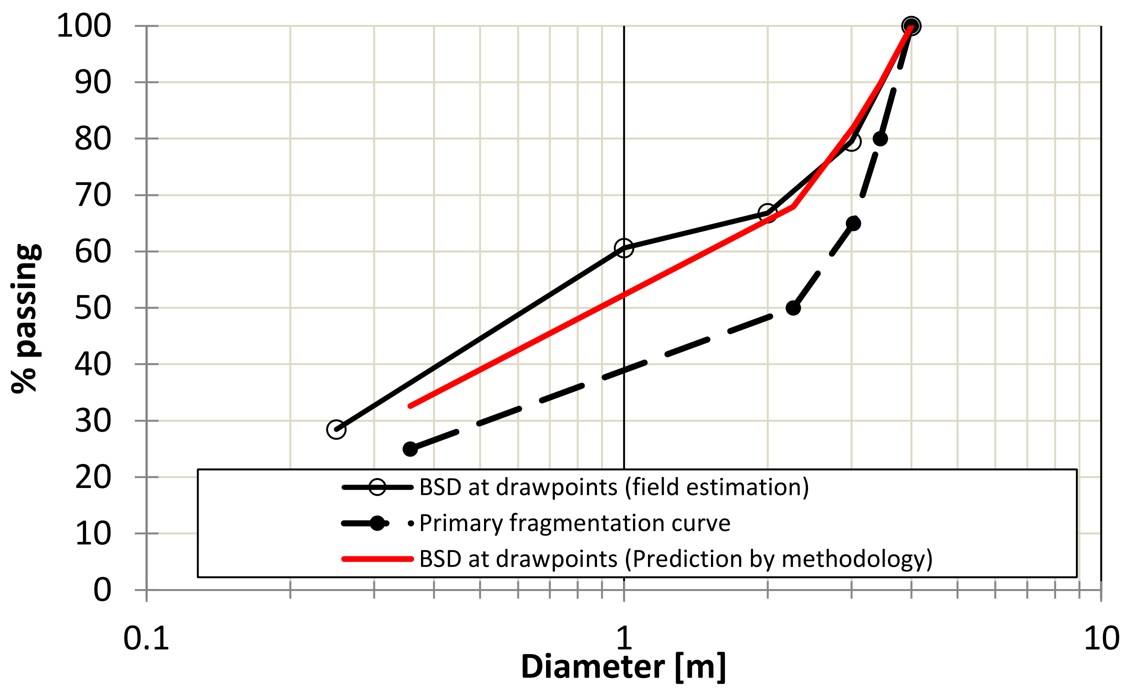

Fig. 6.20: BSD at drawpoints. Zone 4

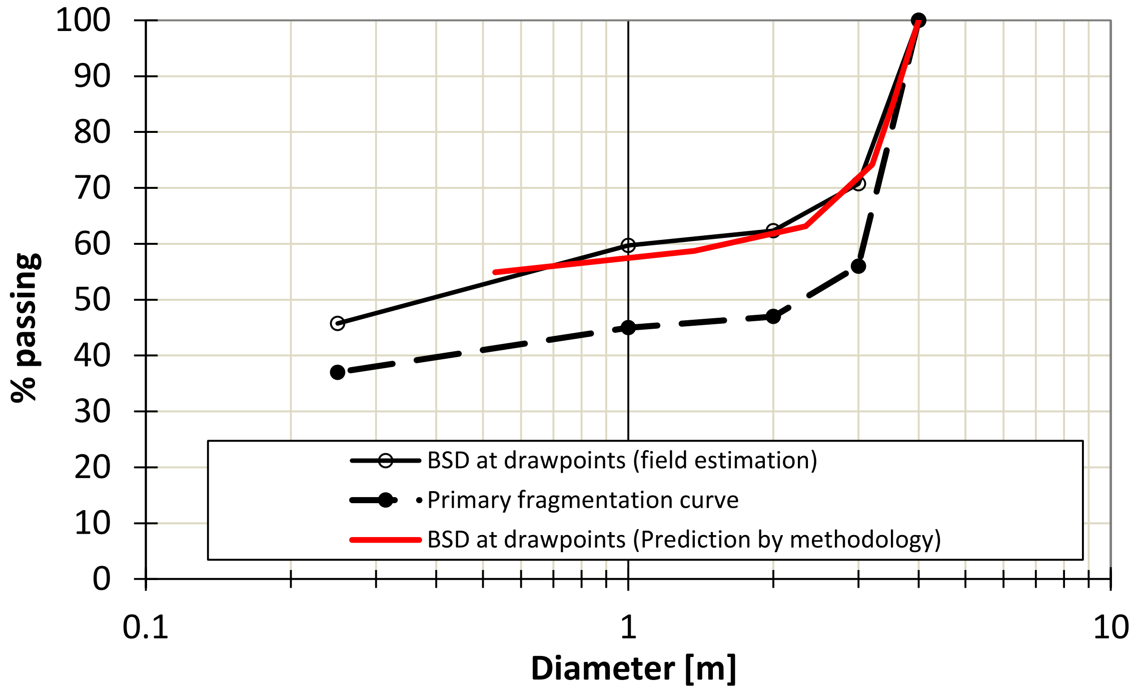

Fig. 6.21: BSD at drawpoints. Zone 5.

6.5.3 Discussion of methodology limitations

The methodology presented in this chapter has been able to reasonably reproduce the evolution of the BSD from the top of a draw column down to the drawpoints where it is extracted. The BSD is expected to be finer for higher draw columns and weaker rocks. The drawpoint BSD predictions at drawpoints also rotate around the largest block size (D_{100}) which is in agreement with the more advanced design methodology by Pierce (2009).

Another relevant case is that of larger weaker blocks mixed in a matrix of stronger smaller blocks. This was analyzed experimentally based on 1-D compression tests presented in Chapter 4. It is believed that this broken ore condition could be more and more relevant as a number of new block caving projects are being designed in more massive rock (i.e., coarser in situ fragmentation). Due to the presence of veins and non-persistent joints, larger blocks can be expected to have strengths that are half the intact UCS of the rock. Thus, additional tests, like those carried out in Chapter 4, are highly recommended to further improve the relationships of σ_v/σ_c versus R as in Fig. 6.5 to Fig. 6.8. Numerical modelling based on approaches such as FEM-DEM (e.g. Vyazmensky 2008) or the PFC-based synthetic rock mass (Pierce et al. 2007) can also be very useful to study this topic in more detail. In addition, this study could be extended to shear tests (e.g., annular ring shear tests) in order to constrain the Bridgwater relationships (2003). Regarding the Bridgwater relationships, it is necessary to develop new correlations that account for non-uniform particulate materials with defects (veins and small discontinuities) to represent more realistic broken ore materials. In the case of mixtures of equal amounts of strong and weak blocks (as was the case for zones 4 and 5 from El Teniente), the average UCS between the strong and weak rocks appears to work well. However, this assumption should be applied with caution while further comprehensives studies can be used to corroborate and/or improve this hypothesis.

Regarding Fig. 6.12 several outcomes can be discussed. First, fragmentation in terms of splitting is observed in both the far field and shear band zones. D_{80} decreases in both zones. Also, a significant amount of fines is generated which influences the percolation and shear band fragmentation, which in turn depends directly on the BSD after the far field fragmentation. These outcomes emphasize the importance of the far field fragmentation in the overall drawpoint BSD. The strength of this methodology in predicting fines makes it quite useful as an input for mineral processing investigations, which is not a capability of other approaches such as BCF.

Regarding block properties, the aspect ratio (AR) was studied in Chapter 4, where it was found that the block shape is not a critical factor for AR between 1 and 1.67. It is believed that larger aspect ratios could favor block splitting, but at the same time, broken ore could also experience preferential flow by elongated blocks as noted in Chapter 2. The influence of AR in both secondary fragmentation and gravitational flow are topics which deserve further investigation. Veins and small discontinuities within blocks is also a topic discussed in Chapter 4. Although this factor is covered by equation 6.2 in this methodology, it would be of value to update the relationships from Fig. 6.5 to Fig. 6.8 to account for block defects. This theme is currently being investigated.

Although this methodology aims to be used for early stage feasibility and design, additional factors which influences secondary fragmentation (see Chapter 5) such as: air gap thickness, cushioning, block strength degradation under confined stresses, time-dependent and segregation by large blocks due to a surface cone, shear-induced percolation, and others, should be further investigated to improve the drawpoint BSD assessments obtained. Further validation is currently ongoing, which will allow for improved predictions of drawpoint BSD.

6.6 Summary and Key Findings

The evolution of block size distribution (BSD) within a draw column during block cave mining plays an important role in controlling the gravitational flow, secondary fragmentation, and fines migration of the broken ore. These are central to preparing a reliable feasibility assessment for a potential caving operation. However, there is a scarcity of procedures for assessing secondary fragmentation and its influence on BSD, especially at the pre-feasibility level. Recent efforts have focussed more on the use of advanced numerical modelling for which the level of detail required is more suitable for advanced feasibility and engineering design stages. In addition, the current approaches to assess secondary fragmentation need to be updated to consider new mechanistric understanding such as *Pierce's gravitational flow model*, and new *laboratory testing analogues* (Chapter 4) together with consideration of both far and near field effects. These factors were considered here in the development of a new empirical alternative to evaluating secondary fragmentation and drawpoint BSD, with focus on how the block size distribution evolves from the top of a draw column to the drawpoints where the ore is extracted.

The simple methodology to evaluate drawpoint BSD was developed to target early stage design (conceptual, pre-feasibility and feasibility). This approach is built on four main pillars: i) *far and near field conditions*, ii) *laboratory testing* (1-D compression and shear tests) as an analogue for secondary fragmentation, iii) *Pierce' gravitational flow model,* and iv) *fines migration*. Preliminary analysis using this methodology suggests that the BSD evolves from a uniform primary fragmentation gradation to a well-graded size distribution at the drawpoints, which corroborates field data of drawpoint BSD published by different authors.

Key input for determining drawpoint BSD begins with the primary fragmentation, which represents the starting point for the analysis. Other critical input include: draw *column height* (H), *rock strength (UCS) scaled to the in situ block size*, *shear band thickness* and *shear* deformation (γ). Thus, these factors must be defined carefully when using this methodology.

Other less sensitive input parameters include: broken ore density (BOD) and inter-block friction angle (ϕ'). This methodology has been tested against BSD data from the El Teniente mine in Chile, and performed reasonably well for strong rock types, as well as on mixtures of different strength broken ore. Special attention must be placed on using reliable data especially regarding primary fragmentation curves, rock strength and rock strength reduced for larger block sizes in order to obtain acceptable results. The main advantages of this methodology against others approaches to evaluate BSD at drawpoints are:

- It allows the evolution of the BSD to be constrained by the largest block size observed in preliminary drawpoint production data. Also, the procedures developed predict a finer drawpoint BSD for higher ore columns and weaker rocks, as would be expected.
- It considers the influence of both the far and near field zones. This allows fragmentation to be assessed under different stress fields and laboratory analogues (e.g. 1-D compression for the far field and plug flow compression zones, and ring shear tests for the peripheral shear bands).

However, this methodology, does not consider several factors believed to affect the BSD at drawpoints such as rock-fall impact following primary fragmentation, draw rate, and shear-induced percolation among others. Based on this, the use of this methodology is recommended for feasibility and early stage design studies. The simplicity of the methodology helps to reduce uncertainties regarding estimations of BSD required for optimizing layout design by using it in parallel with existing industry standard tools like BCF to evaluate drawpoint BSD. For more advanced engineering design stages, Pierce's REBOP methodology is highly recommended.

Chapter 7: Summary and Conclusions

Mass mining, specifically block caving, is experiencing a global growth in importance as new large, lower grade ore bodies are discovered and developed. With the block caving method, block caving fragmentation take place when the rock mass fractures and breaks into smaller fragments (caved rock). Although reliable fragmentation predictions are fundamental to allow efficient engineering design, the final stage in the block caving fragmentation process, referred as secondary fragmentation, is not well understood. As such, a need to undertake a comprehensive investigation aimed to develops standard guidelines to evaluate secondary fragmentation during block caving was identified. Thus, the secondary fragmentation process has been thoroughly studied in this thesis, focused mostly on how the geotechnical properties of broken ore affect this fragmentation process.

7.1 Chapter Summaries

7.1.1 Chapter 2: Broken ore density distribution within a draw column during block caving

Broken ore density (BOD) is a critical geotechnical parameter in block cave mine planning. It is acknowledged that ore column density decreases (and swell factor increases) at the shear bands within a draw column and at the drawpoint due to the development of a loosening zone generated by ore extraction. The broken ore in the draw column also potentially experiences stress and density heterogeneities throughout, depending on the block properties (e.g., shape, aspect ratio and size distribution). Other important factors include air gap thickness, draw rate and draw sequence. In addition, the blocks undergo grinding and breakage (e.g., secondary fragmentation), which increases with draw column height. This generates more rounded block shapes and smaller particles, enabling different block shape configurations and finer broken ore size distributions. These smaller particles migrate downwards into the draw column, increasing the BOD at drawpoints

Hence, a conceptual framework on the broken ore density within draw columns during block caving is proposed in this in order to take into consideration these factors as well as the huge difference of swell factor in cave mines found in the literature. This chapter also includes correlations of coarse granular soils, large 1-D compression test data and findings from rock fill dams and mine waste rock dump studies available in order to evaluate the BOD for early stage mine planning design.

7.1.2 Chapter 3: Inter-block friction angle of broken ore applied to gravitational flow in block caving

This chapter presents a methodology to evaluate the inter-block friction angle (ϕ') on broken ore materials based on empirical shear tests on rockfill and waste rock materials, under both isolated movement zone and interactive flow. This chapter concludes that ϕ' varies along a draw column and it could reach values higher than 60^{o} under low confining stresses and strong broken ore, but lower than 30^{o} under higher stresses and weak broken ore. Hence, this work provides a new approach for assessing the inter-block friction angle for early level studies of large block caving projects.

7.1.3 Chapter 4: Secondary fragmentation and hang-up potential in the compression zone of a draw column during block cave mining

This chapter details a detailed experimental study examining secondary fragmentation and hang-up potential during block caving, relative to an isolated movement zone. The laboratory program consisted of 74 small-scale one-dimensional compression tests designed to simulate broken ore (caved rock) moving down through the compression zone (plug-flow zone) of a draw column. More than 5,000 concrete cuboids were fabricated and tested as a proxy for broken ore, carefully controlling their size, aspect ratio and intrinsic strengths. A subset of these were embedded with a small, non-persistent discontinuity, controlling their length, orientation and thickness in order to examine the role of small joints and veining on secondary fragmentation processes. Broken ore packing density was also studied and controlled during testing.

The results indicate that size distribution and aspect ratio were less important variables than packing density, confining pressure (i.e., column height), and intrinsic block strength. In addition, the orientation and thickness of small discontinuities present in the blocks was shown to play a significant role in promoting secondary fragmentation. Based on these results, several empirical relationships are presented to provide pre-feasibility and feasibility-level estimates of secondary fragmentation size distributions, together with hang-up potential related to oversize blocks.

7.1.4 Chapter 5: Factors affecting secondary fragmentation during block caving

Although several variables regarding secondary fragmentation are associated with early stage layout design (e.g. column height, rock strength, inter-block friction angle, near and far field zones and shear band thickness), a number of additional variables can significantly affect secondary fragmentation depending on the characteristics of each block cave project. These include: air gap thickness, BOD, segregation by large blocks due to surface cone, broken ore strength heterogeneity, block strength damage and crushing under high confining stresses, water within draw columns and cushioning. In this work, each of those factors were studied independently in order to consider them in secondary fragmentation assessments under feasibility and advanced engineering stages. Special emphasis was given to rock strength reduction due to moisture conditions and large overload stresses, as well as to the role of fines within draw columns, which are believed to control most of the factors developed in this work.

7.1.5 Chapter 6: Evolution of broken ore size distribution in a draw column during block cave mining

This chapter investigates the evolution of block size distribution (BSD) within a draw column during block cave mining. BSD plays an important role in controlling the gravitational flow, secondary fragmentation, and fines migration in the broken ore - which are all fundamental to preparing a reliable feasibility assessment for a potential caving operation. However, there is a marked lack of procedures for assessing secondary fragmentation and its influence on BSD, especially at the pre-feasibility level. Recent efforts have focussed more on the use of advanced numerical modelling for which the level of detail required is more suitable for advanced feasibility and mine design stages. To complement these, this chapter presents a simple to use empirical method to estimate BSD that has been developed based on laboratory and field data reported in the literature. The method accounts for a combination of secondary fragmentation processes (e.g. block impact, attrition and comminution) together with fines migration under both isolated and interactive flow. In this chapter, this model is tested against field data from the El Teniente mine in Chile to both calibrate it and determine its limitations. The resulting procedure provides an improved means for assessing secondary fragmentation and hang-up potential for pre-feasibility and feasibility level studies of large block caving projects.

7.2 Conclusions and Key Contribution

The key contribution of this work is the development of a new approach to evaluate secondary fragmentation and block size distribution (BSD) at drawpoints for early-stage feasibility and engineering design purposes, focused on how the BSD evolves from the top of a draw column to the drawpoints. This methodology is built on four main pillars: *Far and near field conditions*, *laboratory testing* (1-D compression and annular ring shear tests), *Pierce' gravitational flow model* and *fines migration*. The two main advantages compared to other methodologies are: 1) It allows the evolution of the BSD to rotate around the largest block, which is observed in typical field BSD data. Furthermore, the predicted BSD at drawpoints are finer for higher ore columns and weaker rocks as expected. 2) It considers the near and far field zone approach. This allows the assessment of fragmentation in the broken ore under different stress fields (e.g. 1-D compression in the far field and shear tests within the shear bands). This methodology has been tested against BSD data from the El Teniente mine (Chile), resulting in satisfactory predictions under strong rocks, as well as on mixtures of different broken ore strength, with further validations are ongoing in order to enhance its capabilities. The main conclusions of this thesis, relative to the research objectives, are as follow.

i. A conceptual framework has been proposed to classify Broken Ore Density (BOD) within a draw column. Three broken ore packing states have been defined: *Dense (tidy)*, *Loose (untidy)* and a *hybrid Loose/Dense* packing, which cover the large variation in swell factors reported by different block caving operations. Guidelines to evaluate the BOD within a draw column are proposed where the role of the broken ore initial arrangement at the top of the muckpile surface to reach each of these packing states is highlighted.

ii. The inter-block friction angle (ϕ') in broken ore materials during block caving has been addressed and a methodology was developed based on a theoretical background from soil mechanics in order to evaluate ϕ' along the outer periphery (shear bands) within a draw column.

iii. A comprehensive experimental laboratory testing program on 1-D compression tests was carried out, and then, three predictive charts were created to evaluate secondary fragmentation on broken ore within the plug flow zone in a draw column.

iv. Seven factors believed to significantly affect secondary fragmentation during feasibility and advanced engineering assessments were addressed: Air gap thickness, broken ore density (BOD), segregation by large blocks due to surface cone, block strength heterogeneity, block strength damage and crushing under high confining stresses, water within draw columns, and cushioning. Each of these factors can greatly contribute to secondary fragmentation assessments, although they will be triggered under certain conditions. Hence several guidelines have been developed for each factor in order to improve secondary fragmentation analysis during block caving.

v. A simple user-friendly methodology to evaluate block size distribution at drawpoints at early-stage engineering design (conceptual and feasibility stage) is presented which considers the role of both near and far field influencing secondary fragmentation, Pierce's gravitational flow model and fines migration. This methodology has been tested against field data from El Teniente mine (Chile), resulting in satisfactory predictions under strong rocks as well as on mixtures of strong and weak broken ore materials, but it is not able to predict reliable secondary fragmentation on weak rocks.

Chapter 8: Recommendations for Further Investigations

8.1 Numerical Modelling Applied to Rockfall Impact Fragmentation on Muckpile Surface

As discussed along this thesis, single blocks impacting the muckpile surface could undergo fragmentation or disintegration, and then, be associated with the block size distribution (BSD) for each block. This BSD is strongly dependent on air gap height, rock mass (discontinuities orientations) and muckpile surface conditions (even or sloped surface). Numerical modelling could strongly support further studies on this theme, which will allow current approaches to evaluate secondary fragmentation and BSD at drawpoints to be adjusted.

8.2 Extend Bridgwater et al's Equations to Non-Uniform Size Distributions

In agreement with the recommendations by Pierce (2009), the empirical study of Bridgwater *et al.* (2003) associated to particle's fragmentation under an annular ring shear tests is limited to uniform particles and should be expanded to well graded BSD. Artificial concrete particles, such as those employed in Chapter 4, are recommended as a testing material for further empirical tests while Finite Element-Discrete Element Method modelling (FEM-DEM) could strongly complement this study.

8.3 Numerical Modelling on Influence of Block's Veins and Small Discontinuities on Secondary Fragmentation

Veins and small discontinuities found within individual blocks have proven to have a significant influence on secondary fragmentation in both the far and near fields. An extension of the laboratory tests carried out in Chapter 4 and numerical models (FEM-DEM approach) would allow this topic to be examined in detail. This will help to develop additional relationships, such as those provided in Chapter 4 and 6, to evaluate secondary fragmentation in both plug-flow zone and far field.

8.4 Numerical and Empirical Analysis on Shear Band Thickness

As noted in Chapter 6, shear band thickness is decisive regarding the amount of fragmentation generated in the near field and it is dependent on how wide is the size distribution of broken ore within shear bands. Thus, more empirical and numerical analysis examining the relationship between shear band thickness and D_{50} are highly required, similar to those conducted by Ueda et al. (2012).

8.5 Further Laboratory Testing Program on Strength Reduction Due to Size Scaling

Rock strength in terms of UCS has to be scaled to real block sizes, which in turn has a critical influence in the secondary fragmentation. Despite the contribution by Yoshinaka et al. (2008) in detailing a potential relationship of strength and block size, more efforts need to be carried out in order to better characterize the exponent “k” (Chapter 6). Thus, more laboratory testing programs on uniaxial compressive strength under series of specimens of 30 to 200 mm diameter are highly recommended to execute in order to build more reliable scale effect relationships

8.6 Numerical Modelling on Mixtures of Strong and Weak Blocks

The fragmentation of strong and weak blocks mixtures need to be further studied. As discussed in Chapter 5, several parameters and factors such as confining pressure, block shape, broken ore density, and the *weak/strong strength ratio* should be considered. Hence, it would allow the characterisation of key factors governing secondary fragmentation when mixtures of strong and weak blocks occur in a draw column. Experimental studies, based on artificial concrete particles (Chapter 4), as well as numerical models (FEM-DEM approach) are recommended for further research.

8.7 Time-Dependency

The travel time of broken ore material from the top of a draw column to drawpoints could extend to any period between months up to several years. Then, the broken ore could be affected by a fragmentation component we can call *time-dependence.* This topic potentially represents a major issue because future columns heights are being planned in excess of 500 m (Hancock 2013, Flores 2014, and Eberhardt et al., 2015). Unfortunately, no studies from mining engineering or from other related disciplines are available to quantify the amount of additional secondary fragmentation due to a *time effect.* In order to carry out a comprehensive study regarding the time-dependency on secondary fragmentation during block caving, an empirical 1-D compression test program consisting of crushable particulate materials and discrete element modelling could be undertaken. Then, different set of tests on variable test time could be evaluated. This investigation can be supported by valuable background on rockfill compressibility (Oldecop & Alonso 2001, 2007). The time-dependency of secondary fragmentation within shear bands could also be studied by means of empirical tests or numerical modelling (e.g. ring shear tests or discrete element modelling) under different test times.

References

ASTM D854 – 14 Standard Test Methods for Specific Gravity of Soil Solids by Water Pycnometer

ASTM D3080 / D3080M – 11 Standard test method for direct shear test of soils under consolidated drained conditions

ASTM D4253 – 00 Standard test methods for maximum index density and unit weight of soils using a vibratory table

ASTM D4254 – 00 Standard test methods for minimum index density and unit weight of soils and calculation of relative density

ASTM D5731-08 Standard test method for determination of the point load strength index of rock and application to rock strength classifications

ASTM D6467 – 13. Standard test method for torsional ring shear test to determine drained residual shear strength of cohesive soils

ASTM D6528 – 07. Standard test method for consolidated undrained direct simple shear testing of cohesive soils

ASTM D7012 – 14 Standard test methods for compressive strength and elastic moduli of intact rock core specimens under varying states of stress and temperatures

ASTM D7181 - 11 Method for consolidated drained triaxial compression test for soils

ASTM D7608 – 10. Standard test method for torsional ring shear test to determine drained fully softened shear strength and nonlinear strength envelope of cohesive soils (using normally consolidated specimen) for slopes with no preexisting shear surfaces

Alcalde F, Bustamante M, Aguayo A (2008) Estimation of remaining broken material at division Andina. In Proceedings of the 5th International Conference and Exhibition on Mass Mining. Luleå, Sweden; pp. 179-189

Alejano L, González J, Muralha J (2012) Comparison of different techniques of tilt testing and basic friction angle variability assessment. Rock Mech Rock Eng, 45:1023–1035

Ampadu SK, Tatsuoka F (1993) A hollow cylinder torsional simple shear apparatus capable of a wide range of shear strain measurement. Geotech Test J, 16: 3–17

Baker J, Kudrolli A (2010) Maximum and minimum stable random packings of platonic solids. Phys Rev E 82, 061304

Bardet JP (1994) Observations on the effects of particle rotations on the failure of idealized granular materials. Mech Mater, 18: 159-182

Barrera V, Valderrama C, Lara P, Arancibia E, Báez F, Molina E (2014) Caving propagation and dilution control through the pre-conditioning technology. In Proceedings of the 3rd International Symposium on Block and Sublevel Caving, Santiago, Chile; pp. 532-537

Barton N, Lien R, Lunde J (1974) Engineering classification of rock masses for the design of tunnel support. Rock Mech 6(4):189–236

Barton N, Kjaernsli B (1981) Shear strength of rockfill. J Geotech Eng Div, 107: 873-889

Barton N (2013) Shear strength criteria for rock, rock joints, rockfill and rock masses: problems and some solutions. J Rock Mech Geotech Eng, 5:249–261

Bauer E (2009) Hypoplastic modelling of moisture-sensitive weathered rockfill materials. Acta Geotech, 4:261–272

Baxter GW, Behringer RP, Fagert T, Johnson GA (1989) Pattern formation in flowing sand. Phys Rev Lett, 62: 2825 – 2829

Baxter GW, Behringer RP (1990) Cellular automata models of granular flow. Phys Rev A 42, 1017-1020

Becker E, Chan CK, Seed HB (1972) Strength and deformation characteristics of rockfill materials in plane strain and triaxial compression tests. Report No TE-72-3. Dept. of Civil Engineering, University of California, Berkeley, USA

Behn G, Brzovic A (1997) Determinación gravimétrica de la densidad del material quebrado remanente del cráter Teniente. VIII Chilean Geological Conference, Antofagasta, Chile (in Spanish)

Biarez J, Hicher PY (1994) Elementary mechanics of soil behaviour: Saturated remoulded soils. A. A. Balkema, Rotterdam, NE

Blanks RF, McNamara CC (1935) Mass concrete tests in large cylinders. J Am. Concr. Inst, 31:280–303

Börzsönyi T, Szabó B, Törös G, Wegner S, Török J, Somfai E, Bien T, Stannarius R (2012) Orientational order and alignment of elongated particles induced by shear. Phys Rev Lett, 108, 228302

Börzsönyi T, Stannarius R (2013) Granular materials composed of shape-anisotropic grains. Soft Matter 9: 7401-7418

Botha J, Watson S, Arkadius T, Samosir E (2008) Simulation applications at pt Freeport Indonesia's DOZ/ESZ block cave mine. In proceedings of the 5th international conference and exhibition on mass mining, Luleå, Sweden; pp. 237-246

Bridgwater J, Cooke, MH, Scott AM (1978) Inter-particle percolation: equipment development and mean percolation velocities. T I Chem Eng. 56: 157-167

Bridgwater J, Utsumi R, Zhang Z, Tuladhar T (2003) Particle attrition due to shearing – The effects of stress, strain and particle shape. Chem Eng Sci, 58: 4649-4665.

Brown ET (2007) Block caving geomechanics. 2nd edn. Indooroopilly: Julius Kruttschnitt Mineral Research Centre. ISBN 978-0-98003622-0-6. Queensland, Australia

Brzovic A, Villaescusa E (2007) Rock mass characterization and assessment of block-forming geological discontinuities during caving of primary copper ore at the El Teniente mine, Chile. Int J Rock Mech Min Sci, 44: 565-583

Brzovic A, Hurtado JA (2013) Fragmentation measurements to validate effect of rock mass preconditioning at The El Teniente Mine, Chile. Proc. of the 3rd Int. Seminar on Geology for the Mining Industry. Santiago, Chile

Brzovic A, Schachter P, de los Santos C, Vallejos J, Mas Ivars D (2014) Characterization and synthetic simulations to determine rock mass behaviour at the el Teniente mine, Chile. Part I. Proceedings of the 3rd International Symposium on Block and Sublevel Caving, Santiago, Chile; pp. 171-178

Brzovic A (2015). Personal communication

Brzovic A, Gonzalez R (2015) Rock mass disassembly observed during caving at the El Teniente mine, Chile. In Proceedings of the 4th International Seminar on Geology for the Mining Industry, GEOMIN2015, Antofagasta, Chile

Butcher RJ, Thin IGT (2007). The inputs and choices for predicting fragmentation in block cave projects. In Proceedings 1st International Symposium on Block and Sub-level Caving, Southern African Institute of Mining and Metallurgy, Johannesburg, South Africa, pp. 35–49

Castro R (2006) Study of the mechanisms of granular flow for block caving, Ph.D thesis, University of Queensland, Brisbane, Australia

Castro R, Gonzales F, Arancibia E (2009). Development of a gravity flow numerical model for the evaluation of drawpoint spacing for block/panel caving. J S Afr Inst Min Metall 109: 393-400

Castro R, Vargas R, De la Huerta F (2012) Determination of drawpoint spacing in panel caving: a case study at the El Teniente Mine. J S Afr Inst Min Metall, 112: 871-876

Castro R, Fuenzalida M, Lund F (2014) Experimental study of gravity flow under confined conditions. Int J Rock Mech Min Sci, 67: 164–169

Chambon G, Schmittbuhl J, Corfdir A (2006) Frictional response of a thick gouge core: 1. Mechanical measurements and microstructures. J Geophys Res, 111, B09308

Charles JA, Watts KS (1980) The influence of confining pressure on the shear strength of compacted rockfill, Géotechnique 30: 353-367

Chen X, Zhang J, Li Z (2014) Shear behaviour of a geogrid-reinforced coarse-grained soil based on large-scale triaxial tests. Geotext Geomembranes 42: 312-328

Cheng YM, Liu ZN, Song WD, Au SK (2009) Laboratory test and particle flow simulation of silos problem with nonhomogeneous materials. J Geotech Geoenviron, 135: 1754-1761

Cheon D, Jeon S, Park C, Song W, Park E (2011) Characterization of brittle failure using physical model experiments under polyaxial stress conditions. Int J Rock Mech Min Sci, 48: 152–160

Chitombo GP (2010) Cave mining - 16 years after Laubscher's 1994 paper 'Cave mining - state of the art'. In Proceedings of the Second International Symposium on Block and Sublevel Caving, WA, Australia, pp. 45-61

Cleary P, Sawley M (2002) DEM modelling of industrial granular flows: 3D case studies and the effect of particle shape on hopper discharge. Appl Math Model, 26: 89-111

Codelco (2011) Estimación de curvas de fragmentación primaria y secundaria para el primer nivel de explotación – Mina Chuquicamata subterránea. Confidential Report (in Spanish)

Contreras L (2011) Comportamiento friccionante de materiales granulares gruesos. M.Sc thesis, Department of Civil Engineering, University of Chile, Santiago, Chile (in Spanish)

Coop MR, Sorensen KK, Bodas Freitas T, Georgoutsos G (2004) Particle breakage during shearing of a carbonate sand. Géotechnique, 54: 157-163

Corbella E, Zini R (1988) – Manuale dei marmi, pietre, graniti. Vol I: Guida Tecnica – Vallardi Editore, Italy

Cundall. P., Mukundakrishnan B. and Lorig. L (2000). REBOP (Rapid Emulator Based on PFC3D) Formulation and User‘S Guide, Itasca Consulting Group, Inc., Report to the International Caving Study, ICG00-099-7-20

Darlington W, Ranjith G, Choi SK (2011) The effect of specimen size on strength and other properties in laboratory testing of rock and rock-like cementitious brittle materials. Rock Mech Rock Eng, 44:513–529

De La Hoz K (2007) Estimación de los parámetros de resistencia al corte en suelos granulares gruesos. M.Sc. thesis, Department of Civil Engineering, University of Chile, Santiago, Chile (in Spanish)

De Mello VFB (1977) Reflections on design decisions of practical significance to embankment dams. Géotechnique 27: 279-355

Dershowitz W, Lee G, Geier, J, LaPointe PR (1998) FracMan: Interactive discrete feature data analysis geometric modelling and exploration simulation, User documentation, Golder Associates, Seattle, WA, USA

Dessureault S., Scoble M., Rubio E. (2000). Simulating Block Cave Secondary Breakage — An Application of Information and Operations Management Tools in Mass Mining Systems. In Proceedings of the 3th International Conference and Exhibition on Mass Mining. Brisbane, Australia, pp. 893-896

D'Espessailles N, Dorador L, Pastén C (2014) Particle breakage in blasting sands from a mining tunnel under simple shear stresses. In Proceedings of the IV South-American Young Geotechnical Engineering Conference. Bogotá, Colombia (in Spanish)

Desrues J, Hammad W (1989). Shear banding dependency on mean pressure level in sand. Int. Workshop on Numerical Methods for Localisation and Bifurcation of Granular Bodies. Gdansk, Poland

Diering T (2000) PC-BC: A block cave design and draw control system. In Proceedings of the 4th International Conference and Exhibition on Mass Mining, Brisbane, Australia; pp. 469- 484

Dodds JS (2003) Particle shape and stiffness - Effects on soil behavior. M.Sc. thesis, Georgia Institute of Technology, Atlanta, GA, USA

Dolipas RS (2000) Rock mechanics as applied in philex block cave operations. In Proceedings of the 3th International Conference and Exhibition on Mass Mining, Brisbane, Australia pp. 395-404

Dorador L (2010) Análisis experimental de las metodologías de curvas homotéticas y corte en la evaluación de propiedades geotécnicas de suelos gruesos. M.Sc. thesis, Department of Civil Engineering, University of Chile, Santiago, Chile (in Spanish)

Dorador L, Besio G (2013) Some considerations about geotechnical characterization on soils with oversize. In Proceeding of 5th International Young Geotechnical Engineering Conference - 5iYGEC'13, Paris; pp. 407-410

Dorador L, Eberhardt E, Elmo D, Aguayo A (2014) Assessment of broken ore density variations in a block cave draw column as a function of fragment size distributions and fines migration. In Proceedings of the 3rd International Symposium on Block and Sublevel Caving, Santiago; pp. 109-117

Dorador L, Eberhardt E, Elmo D (2015) Influence of block strength and veining on secondary fragmentation related to block caving. In Proceedings, 13th International Congress of Rock Mechanics: Innovations in Applied and Theoretical Rock Mechanics, ISBN 978-1-926872-25-4, Paper 806

Dorren LKA (2003) A review of rockfall mechanics and modelling approaches. Progr Phys Geogr, 27:69–87

Douglas, K. J. (2002) The shear strength of rock masses. Ph.D thesis, School of Civil and Environmental Engineering, The University of New South Wales, Sydney, Australia

Duncan JM, Chang CY (1970) Nonlinear analysis of stress and strain in soils. J Soil Mech Found Div, 96: 1629-1653

Eadie B (2003). A framework for modeling fragmentation in block caving. Ph.D thesis. University of Queensland. Brisbane, Australia

Eberhardt E, Woo K, Stead D, Elmo D (2015) Keynote Paper – Transitioning from open pit to underground mass mining: meeting the rock engineering challenges of going deeper. In Proceedings, 13th International Congress of Rock Mechanics: Innovations in Applied and Theoretical Rock Mechanics, Montreal. Paper 896, pp. 1-14

Einav I (2007) Breakage mechanics. Part I: Theory. J Mech Phys Solids, 55: 1274-1297

Elfahal MM, Krauthammer T, Ohno T, Beppu M, Mindess S (2005) Size effect for normal strength concrete cylinders subjected to axial impact. Int J Impact Eng, 31: 461–481

Encina V. (2015). Personal communication

Esterhuizen GS (1994) A program to predict block cave fragmentation. User's Guide. BCFV2.1

Esterhuizen GS, Rachmad L, Potapov A (2004) Investigation of swell factor in a block cave draw column. In Proceedings of the 4th International Conference and Exhibition on Mass Mining, Santiago, Chile; pp. 215-219

Esterhuizen GS (2005) A program to predict block cave fragmentation. User's Guide. BCFV3.05

Esterhuizen, GS, Karacan, CO (2008) A methodology for determining gob permeability distributions and its application to reservoir modeling of coal mine longwalls. National Inst. for Occupational Safety and Health, Pittsburgh, PA, USA

Fityus A, Giacomini A, O. Buzzi (2013) The significance of geology for the morphology of potentially unstable rocks. Eng Geol, 162: 43–52

Fityus A, Giacomini A, Thoeni K (2015) The Influence of Shape on the Inherent Rolling Potential of Loose Rocks. Engineering Geology for Society and Territory – Vol. 2: 2045-2048

Flores G, Karzulovic A, Brown ET (2004) Current practices and trends in cave mining. In Proceedings of the 4th International Conference and Exhibition on Mass Mining, Santiago, Chile; pp. 83-90

Flores G (2014) Keynote Paper - Future challenges and why cave mining must change. In Proceedings of the 3rd International Symposium on Block and Sublevel Caving, Santiago, Chile. pp. 23–52

Fragaszy R, Su W, Siddiqi F (1990) Effects of oversize particles on the density of clean granular soils, Geotech Test J, 13: 106-114

Frossard E, Hu W, Dano C, Hicher PY (2012) Rockfill shear strength evaluation: a rational method based on size effects. Géotechnique 62: 415-428

Fuenzalida MA, Garza-Cruz T, Pierce M, Andrieux P (2014) Application of a methodology for secondary fragmentation prediction in cave mines. Proceedings of the 3rd International Symposium on Block and Sublevel Caving, Santiago, Chile; pp. 318-327

Fukumoto T (1992) Particle breakage characteristics in granular soils. Soils Found, 32: 26-40

Gehle C, Kutter HK (2003) Breakage and shear behaviour of intermittent rock joints. Int J Rock Mech Min Sci, 40: 687–700

Ghadiri M, Ning Z, Kenter SJ, Puik E (2000) Attrition of granular solids in a shear cell. Chem Eng Sci, 55: 5445–5456

Ghazvinian A, Sarfarazi V, Schubert W, Blumel M (2012) A study of the failure mechanism of planar non-persistent open joints using PFC2D. Rock Mech Rock Eng, 45: 677–693

Giacomini A, Buzzi O, Renard B, Giani GP (2009) Experimental studies on fragmentation of rockfalls on impact with rock surfaces. Int. J. Rock Mech. Min. Sci, 46: 708–715

Gilbride L, Free K, Kehrman R (2005) Modeling block cave subsidence at the Molycorp, inc., Questa mine-a case study. The 40th U.S. Symposium on Rock Mechanics, Anchorage, AK, USA

Glazer SN, Townsend P (2008). The application of seismic monitoring to the future Lift 2 block cave at Palabora mining company. In Proceedings of the 5th International Conference and Exhibition on Mass Mining, Lulea, Sweden; pp. 919-930

Gonzalez-Carbonell P, Duplancic P, Thin I (2012) A generic overview of the interaction of a block cave draw strategy and cave monitoring. In 6th International Conference and Exhibition on Mass Mining, Sudbury, Canada

Grasselli G, Egger P (2003) Constitutive law for the shear strength of rock joints based on three-dimensional surface parameters. Int J Rock Mech Min Sci, 40: 25–40

Gu DX, Tamblyn W, Lamb I, Ramsey N (2008) Effect of weathering on strength and modulus of basalt and siltstone. In Proceeding of 42nd US Symposium on Rock Mechanics, San Francisco, CA, USA.

Gupta AS, Seshagiri Rao K (2000) Weathering effects on the strength and deformational behaviour of crystalline rocks under uniaxial compression state. Eng Geol, 56: 257–274

Hakami E, Larsson E (1996) Aperture measurements and flow experiments on a single natural fracture. Int J Rock Mech Min Sci, 33: 395–404

Hamrin H (2001) Underground mining methods and applications. Underground Mining Methods: Engineering Fundamentals and International Case Studies (eds WA Hustrulid and RL Bullock), 1: 3–14. Society for Mining, Metallurgy and Exploration: Littleton, Colorado.

Hancock W, Weatherley D, Chitombo G (2012) Modeling the gravity flow of rock using the discrete element method. In 6th International Conference and Exhibition on Mass Mining, Sudbury, Canada

Hancock W (2013) Gravity flow of rock in caving mines: Numerical modelling of isolated, interactive and non-ideal draw. Ph.D thesis. University of Queensland, Brisbane, Australia

Hardin B (1985) Crushing of soil particles. J Geotech Eng, 111: 1177-1192

Hasan A, Alshibli K (2012) Three dimensional fabric evolution of sheared sand. Granul Matter, 14: 469–482

Hashim MHM, Sharrock G, Saydam S, (2008) A review of particle percolation in mining. 1st Southern Hemisphere International Rock Mechanics Symposium. Perth, Australia; pp. 273-284

Hashim MHM, Sharrock GB (2012). Dimensionless percolation rate of particles in block caving mines. In Proceedings of the 6th international Conference and Exhibition on Mass Mining, Sudbury, Canada

Hoek E, Brown ET (1980) Underground excavation in rock. The Institution of Mining and Metallurgy, London; 527 pp

Hong ES, Kwon TH, Cho GC (2015). Observation of the degradation characteristics and scale of unevenness on three-dimensional artificial rock joint surfaces subjected to shear. Rock Mech Rock Eng 49: 3-17

Horii H, Nemat-Nasser S (1986). Brittle failure in compression: splitting, faulting and brittle-ductile transition. Philos Trans A Math Phys Eng, 319: 337–374

Howson M (2004) Estimation of geotechnical variables for mass mining. In Proceedings of 4th International Conference and Exhibition on Mass Mining. Santiago, Chile; pp. 44-48

Hungr O, Dawson R, Kent A, Campbell D, Morgenstern NR (2002) Rapid flow slides of coal-mine waste in British Columbia, Canada, in Evans, S.G., and DeGraff, J.V., eds., Catastrophic landslides: Effects, occurrence, and mechanisms. Geological Society of America Reviews in Engineering Geology, Vol. XV. Boulder, CO, USA

Hustrulid W (2000) Method selection for large-scale underground mining. In Proceedings of the 3th International Conference and Exhibition on Mass Mining. Brisbane, Australia, pp. 29-56

Hyodo M, Hyde AFL, Aramaki N, Nakata Y (2002). Undrained monotonic and cyclic shear behaviour of sand under low and high confining stresses. Soils Found, 42: 63-76

Indraratna B, Ionescu D, Christie HD (1998) Shear behavior of railway ballast based on large-scale triaxial tests. J Geotech Geoenviron, 124: 439-449

Indraratna B, Tennakoon N, Nimbalkar S, Rujikiatkamjorn C (2013) Behaviour of clay-fouled ballast under drained triaxial testing. Geotechnique, 63: 410–419

Isabel A (2016) Personal communication

Itasca (2014) PFC3D ver. 5.0, Itasca Consulting Group, Inc., Minneapolis, MN, USA

Jakubec J, Clayton R, Guest A (2012) Mudrush risk evaluation. In Proceedings of the 6th International Conference and Exhibition on Mass Mining, Subdury, Canada

Jaky J (1948) Pressure in silos. 2nd International conference in soil mechanics and foundation engineering, London, UK; Vol. 1, pp 103-107

Janssen H (1895) Versuche über getreidedruck in silozellen. Zeitschrift Des Vereines Deutscher Ingenieure; Vol. 39, pp 1045-1049 (In German)

Janssen H (2004) Experiments regarding grain pressure in silos. In Proceedings of the 4th International Conference and Exhibition on Mass Mining. Santiago, Chile; pp.293 – 300

Julin D (1992) Block Caving. Chapter 20.3, SME Mining Engineering Handbook, Hartman H. (ed) Society for mining, metallurgy and exploration. Littleton, CO, USA, pp 1815-1836

Kalenchuk KS, Diederichs MS, McKinnon S (2006) Characterizing block geometry in jointed rock masses. Int J Rock Mech Min Sci, 43: 1212-1225

Kapur PC, Pande D, Fuerstenau DW (1997). Analysis of single-particle breakage by impact grinding. Int J Miner Process 49: 223-236

Kenney T, Lau D (1985). Internal stability of granular filters. Can Geotech J, 22: 215–225

Kezdi A (1979) Soil physics – selected topics. Elsevier Scientific Publishing Co., Amsterdam, NE

Khanal M, Schubert W, Tomas J. (2008). Compression and impact loading experiments of high strength spherical composites. Int J Miner Process 86: 104–113

Khola N (2015) Correlations for shear-induced percolation in granular shear flows. M. Sc. Thesis. Purdue University, USA

Khono M, Maeda H (2012) Relationship between point load strength index and uniaxial compressive strength of hydrothermally altered soft rocks. Int. J. Rock Mech. Min. Sci, 50: 147–157

Kim YS, Kim BT (2008) Prediction of relative crest settlement of concrete-faced rockfill dams analyzed using an artificial neural network model. Comput Geotech 35: 313–322

Kojovic T (2010) Application of the hybrid model to RWD. Subproject Report submitted to MMT2 Secondary Fragmentation Project

Kvapil R (1965) Gravity flow of granular materials in hoppers and bins, Int J Rock Mech Min Sci, 2: 35-41

Kvapil R (2004) Gravity flow in sublevel and panel caving – A common sense approach, Luleå University of Technology Press, Luleå, 152 pp

Lafarge Inc. (North America, 2014), http://www.lafarge-na.com

Laubscher D (1994) Cave mining – The state of the art. J S Afr Inst Min Metall, 94:279-293

Laubscher D (2000) Block caving manual. Prepared for the International Caving Study Phase 1. University of Queensland, Australia

Laubscher D, Jakubec J (2001) The MRMR rock mass classification for jointed rock masses. In: Hustrulid WA, Bullock RL, eds. Underground mining methods: Engineering fundamentals and international case studies. Littleton, CO: Society for Mining, Metallurgy, and Exploration, Inc., pp. 475–481

Laubscher D (2003) Cave Mining Handbook. De Beers, Johannesburg, South Africa.

Lee Y (1986) Strength and deformation characteristic of rockfill. Ph.D thesis, Asian Institute of Technology, Thailand

Leleu SL, Valdes JR (2007) Experimental study on the influence of mineral composition on sand crushing. Geotechnique, 57: 313-317

Leonardi CR, Owen DRJ, Feng YT, Ferguson WJ (2008) Computational modelling fines migration in block caving operations. In Proceedings of the 5th International Conference and Exhibition on Mass Mining, Lulea, Sweden; pp. 1063-1072

Leps T (1970) Review of shearing strength of rockfill. J Soil Mech Found Div, 96: 1159-1170

Lieou C, Elbanna A, Carlson J (2014). Grain fragmentation in sheared granular flow: Weakening effects, energy dissipation, and strain localization. Phys Rev E 89, 022203

Lighthall PC, Sellars CD, Burton WD (1985). Design of waste dumps with flow-through rock drains. Proceedings of the 9th Annual British Columbia Mine Reclamation Symposium, Kamloops, BC, Canada

Linero S, Palma C, Apablaza R (2007) Geotechnical characterization of waste material in very high dumps with large scale triaxial testing. In Proceedings of the International Symposium on Rock Stability in Open Pit Mining and Civil Engineering, Perth, Australia; pp . 59-76

Lorig L, Pierce M (2000) Methodology and guidelines for numerical modelling of undercut and extraction level behaviour in caving mines. Itasca Consulting Group Inc, Report to International Caving Study

Lowe J (1964) Shear strength of coarse embankment dam materials. Proceedings 8th International Congress on Large Dams, Edinburgh, UK; vol.3, pp. 745-761

Luzzani L, Coop MR (2002). On the relationship between particle breakage and the critical state of sands. Soils Found, 42: 71–82

Mairs K, Abe S (2011) Breaking up: comminution mechanisms in sheared simulated fault gouge. Pure Appl Geophys, 168: 2277–2288

Maranha Das Neves E, Veiga Pinto A (1989) Collapse of rockfill. In Proceedings of the 12th International Conference on Soil Mechanics and Foundation Engineering, Rio de Janeiro, Brazil; Vol 1: pp. 735-738

Marsal RJ, Moreno E, Nunez A, Cuellar R, Moreno R (1965) Research on the behavior of the granular material and rockfill samples. Electricity Federal Commission (CFE), Mexico

Marsal RJ (1967) Large scale testing of rockfill materials. J Soil Mech Found Div, 93: 27-43

Marsal RJ (1973) Mechanical properties of rockfill. In Embankment-Dam Engineering: Casagrande Volume, Wiley, New York, USA

Martin RA (1966) The effect of moisture on the compressive and tensile strength on a variety of rock materials. M.Sc. thesis. Missouri University of Science and Technology, MO, USA

Mas Ivars D, Pierce M, Darcel C, Reyes-Montes J, Potyondy D, Young RP (2011) The synthetic rock mass approach for jointed rock mass modelling. Int J Rock Mech Min Sci: 48:219–44

Matsushima T, Saomoto H, Tsubokawa Y, Yamada Y (2003) Grain rotation versus continuum rotation during shear deformation of granular assembly. Soils Found, 43: 95–106

McCarter MK (Ed.) (1985) Design of non-impounding mine waste dumps. Society of Mining Engineers, 216 pp

McDowell, GR, Bolton M, D, Robertson D (1996) The fractal crushing of granular materials. J Mech Phys Solids, 44: 2079-2102

Melo F, Vivanco F, Fuentes C, Apablaza V (2008) Kinematic model for quasi static granular displacements in block caving: dilatancy effect on drawbody shapes. Int J Rock Mech Min Sci, 5: 248–59

Millan J, Brzovic A (2013) Cave modeling and material flow estimation in Block I, Esmeralda mine, El Teniente deposit. 3th International Seminar on Geology for Mining Industry, Santiago, Chile

Miura, N, Yamanouchi T (1975) Effect of water on the behavior of a quartz-rich sand under high stresses. Soils Found, 15: 23-34

Mohamed A, Gutierrez M (2010) Comprehensive study of the effects of rolling resistance on the stress-strain and strain localization behavior of granular materials. Granul Matter, 12: 527-541

Montecino N (2011) Modelo de mezcla de fragmentación secundaria en minería de block/panel caving. M.Sc thesis. University of Chile, Chile (in Spanish)

Moss A, Russell F, Jones C (2004) Caving and fragmentation at Palabora: Prediction to production. In Proceedings of the 4th International Conference and Exhibition on Mass Mining. Santiago, Chile; pp. 585-590

Moss A (2011) An introduction to block and panel caving. Global Metals & Mining Conference. Hollywood, FL, USA

Muller P, Tomas J (2013) Investigation on the compression behavior of tetrahedral Agglomerates. Granul Matter 15: 863–872

Munson, DE, Benzley SE (1980) Analytic subsidence model using void-volume distribution functions. The 21st U.S. Symposium on Rock Mechanics, Rolla, MO, USA

Naderian AR, Williams DJ (1996) Simulation of open-cut coal mine back-fill behaviour. In Proceedings of National Symposium on the Use of Recycled Materials in Engineering Construction, Sydney, Australia; pp. 17-22

Naderian A (1997) Characterisation of behaviour of open-cut coal mine back-fill. Ph.D thesis, University of Queensland, Brisbane, Australia

Nedderman RM (1995). The use of the kinematic model to predict the development of the stagnant zone boundary in the batch discharge of a bunker, Chem Eng Sci, 50: 959-965

Nichols RS (1986) Rock segregation in waste dumps. In Proceedings of the International Symposium on Flow-Through Rock Drains, Cranbrook, BC, Canada

Ngidi SN, Pretorius DD (2011) Impact of poor fragmentation on cave management. In proceeding of 6th Southern African Base Metals Conference. Phalaborwa, South Africa; pp. 111-122

Oldecop LA, Alonso, EE (2001) A model for rockfill compressibility. Geotechnique 51: 127–139

Oldecop LA, Alonso EE (2007) Theoretical investigation of the time-dependent behaviour of rockfill. Geotechnique 57: 289–301

Otuonye FO (2000). Drawpoint design in caving and stoping mines. In Proceedings of the 3th International Conference and Exhibition on Mass Mining, Brisbane, Australia; pp. 569-573

Palma C, Linero S, Apablaza R (2009) Geotechnical characterization of waste material in very high dumps with large scale triaxial and odometer testing. In Proceedings of the 3rd South-American Conference of Young Geotechnical Engineers. Córdoba, Argentina (in Spanish)

Pappas DM, Vallejo LE (1997) The settlement and degradation of nondurable shales associated with coal mine waste embankments. Int J Rock Mech Min Sci, 34, paper No. 241

Parkin AK (1977) The compression of rockfill. Aust. Geomech. J, 7: 33-39

Penswick DP (1997) Technical Note: The Palabora high reach rig. J South Afr Inst Min Metall, 97: 69-72

Pfeiffer T, Bowen T (1989) Computer simulation of rockfalls. Bull Assoc Eng Geol, 26:135–145

Pierce M, Mas Ivars D, Cundall P, Potyondy D (2007) A synthetic rock mass model for jointed rock. In Eberhardt et al. (Eds.), Proceedings of the 1st Canada–US Rock Mechanics Symposium, Vancouver, Canada. Taylor & Francis, London, pp. 341–349

Pierce M (2009). A model for gravity flow of fragmented rock in block caving mines. Ph.D thesis, University of Queensland, Brisbane, Australia

Pierce M, Weatherley DK, Kojovic T (2010) A hybrid methodology for secondary fragmentation prediction in cave mines. In Proceedings, 2nd International Symposium on Block and Sublevel Caving, Perth, Australia, pp. 567-581

Piteau Associates Engineering ltd (1991) Mined rock and overburden piles: investigation and design manual, interim guidelines. Prepared for ministry of Energy and mines, Victoria, BC, Canada

Power G (2012) Optimizing caving recovery using comparative draw planning strategies and PGCA flow modelling software. In Proceedings of the 6th International Conference and Exhibition on Mass Mining. Subdury, Canada

Prakoso WA, Kulhawy FH (2011) Effects of testing conditions on intact rock strength and variability. Geotech Geol Eng, 29:101–111

Rahal DC (2008) Draw control in block caving using mixed integer linear programming. Ph.D thesis, University of Queensland, Brisbane, Australia

Rashidi-Nejad F, Suorineni F, Asi B (2014). Open pit or block caving? A numerical ranking method for selection. Presented at A Southern African Silver Anniversary 2014 SOMP Annual Meeting, Johannesburg, South Africa

Rice J (2006) Heating and weakening of faults during earthquake slip. J Geophys Res, Vol. 111, B05311

Riquelme J, Dorador L (2014) Metodología para determinar densidades máxima y mínima en suelos granulares gruesos a partir de ensayos de laboratorio de escala reducida. VIII Chilean Geotechnical Conference. Santiago, Chile (in Spanish)

Ritchie A (1963) Evaluation of rockfall and its control. Highway Research Record, 17: 13-28.

Rockfield Software (2009) ELFEN Version 4.3.3, Swansea, UK

Rogers S, Elmo D, Webb G, Catalan A (2010). A discrete fracture network based approach to defining in situ, primary and secondary fragmentation distributions for the Cadia East panel cave. In Proceedings of the 2nd International Symposium on Block and Sublevel Caving, Perth, Australia

Ross IT, Van As A (2012) Major hazards associated with block caving. In 6th International Conference and Exhibition on Mass Mining, Sudbury, Canada

Rubio E, Cáceres C, Scoble M (2004) Towards an integrated approach to block cave planning. In Proceedings of the 4th International Conference and Exhibition on Mass Mining, Santiago, Chile; pp. 128-134

Ruiz-Carulla R, Coromina J, Mavrouli O (2015) A methodology to obtain the block size distribution of fragmental rockfall deposits. Landslides 12: 815-825

Rustan A (2000) Gravity flow of broken rock – what is known and unknown. In Proceedings of the 3th International Conference and Exhibition on Mass Mining, Brisbane, Australia; pp. 557-567

Sadrekarimi A, Olson SM (2010) Particle damage and crushing observed in ring shear tests on sands. Can Geotech J, 47: 497-515

Sagong M, Bobet A (2002) Coalescence of multiple flaws in a rock-model material in uniaxial compression. Int J Rock Mech Min Sci, 39: 229–241

Samadani A, Pradhan A, Kudrolli A (1999) Size segregation of granular matter in silo discharges. Physical Review E 60, 7203

Sammis C, King G, Biegel R (1987) The kinematics of gouge deformation. Pageoph 125: 777–812

Santamarina JC, Cho GC (2004) Soil behaviour: The role of particle shape. In Proceedings Skempton Conference, London, UK

Schall P, Van Hecke M (2010) Shear bands in matter with granularity. Annu Rev Fluid Mech 42: 67–88

Seidel J, Haberfield C (2002) Laboratory testing of concrete-rock joints in constant normal stiffness direct shear. Geotech Test J, Vol. 25, No. 4. Paper ID GTJ200210416_254

Sharrock GB, Hashim MHM (2009) Disturbed gravity flow in block caving. The 43rd U.S. Symposium on Rock Mechanics, Asheville, NC, USA

Sharrock GB, Beck D, Capes GW, Brunton I (2012) Applying coupled newtonian cellular automata - Discontinuum finite element models to simulate propagation of Ridgeway Deeps Block Cave. In 6th International Conference and Exhibition on Mass Mining, Sudbury, Canada

Sherard JL (1979) Sinkholes in dams of coarse, broadly graded soils. In Proceedings of the13th International Congress on Large Dams, New Delhi, India, vol. 2, pp. 25-35

Siddiqi FH (1984) Strength evaluation of cohesionless soils with oversize particles, Ph.D. thesis, University of California Davis, USA

Sielamowicz I, Blonski S, Kowalewski T (2005) Optical technique DPIV in measurements of granular material flows, Part 1 of 3—plane hoppers. Chem Eng Sci, 60: 589-598

Singh M, Lakshmi V, Srivastava LP (2015) Effect of pre-loading with tensile stress on laboratory UCS of a synthetic rock. Rock Mech Rock Eng, 48: 53–60

Sowers GF, Williams, RC, Wallace TS (1965) Compressibility of broken rock and settlement of rockfills. In Proceedings of the 6th International Conference Soil Mechanics. Foundation Engineering, Montreal Vol. 2; pp. 561–565

Srikant A, Nicholas D, Rachmad L (2004) Visual estimation of fragment size distribution in the DOZ block cave. In Proceedings of the 4th International Conference and Exhibition on Mass Mining, Santiago, Chile; pp. 286-290

Susaeta A (2004) Theory of gravity flow (part 1). In Proceedings of the 4th International Conference and Exhibition on Mass Mining, Santiago, Chile; pp. 167-178

Susaeta A, Rubio E, Pais G (2008). Dilution behaviour at Codelco panel cave mines. In Proceedings of the 5th International Conference and Exhibition on Mass Mining, Luleå University of technology, Sweden; pp. 167-178

Symons IF (1970) The effect of size and shape of specimen upon the unconfined compressive strength of cement-stabilized materials. Mag Concrete Res, 22:45–50

Tejchman J (2000) Behaviour of granular bodies in induced shear zones. Granul Matter 2:77-96

Tengattini A, Das A, Nguyen GD, Viggiani G, Hall SA, Einav I (2014) A thermomechanical constitutive model for cemented granular materials with quantifiable internal variables Part I—Theory. J Mech Phys Solids, 70: 281–296

Tsoungui O, Vallet D, Charmet JC (1999) Numerical model of crushing of grains inside two-dimensional granular materials. Powder Technol, 105: 190–198

Ueda T, Matsushima T, Yamada Y (2012) DEM simulation of the shear strength and shear band development of well-graded granular materials. Proceedings of the Fifth

International Symposium on Deformation Characteristics of Geomaterials, IS-Seoul, Vol. 1, pp.520-525

Uhle RJ (1986) A statistical analysis of rockfill data—Shear strength and deformation parameters with respect to particle size: M.Sc. thesis, Colorado State University, CO, USA

U.S. Army Eng. Manual (2000) Design and construction of levees, EM 1110-2-1913, available from:

<http://www.publications.usace.army.mil/Portals/76/Publications/EngineerManuals/EM_1110-2-1913.pdf>

U.S. Army Eng. Manual (2004) Earth & rock-fill dams general design & construction considerations, EM 1110-2-2300, available from:

<www.publications.usace.army.mil/Portals/76/Publications/EngineerManuals/EM_1110-2-2300.pdf>

Valdes JR, Leleu SL (2008) Influence of mineral composition on the simple shear response of sands: Experimental study. J Geotech Geoenviron, 134: 1820-1824

Valenzuela L, Bard E, Campana J, Anabalon ME (2008) High waste rock dumps—Challenges and developments. In Proceeding of the First International Seminar on the Management of Rock Dumps, Perth, Australia; pp. 65-78

Vallejos J, Suzuki K, Brzovic A. Mas Ivars D (2014). Characterization and synthetic simulations to determine rock mass behaviour at the El Teniente mine, Chile. Part II.

Proceedings of the 3rd International Symposium on Block and Sublevel Caving, Santiago, Chile; pp. 179-188

Vallejo L, Chik Z, Lobo-Guerrero S (2011) Force chains and the fragmentation of granular materials. In proceedings of 14th Pan-Am CGS Geotechnical Conference. Toronto, Canada

Van As A, Van Hout GJ (2008) Implications of widely spaced drawpoints, In Proceedings of the 5th International Conference and Exhibition on Mass Mining, Luleå, Sweden; pp. 147–154

Van Hout, G, Allen S, Breed M, Singleton J, (2004) Status of draw control practice and waste Management at Cullinan diamond mine. In Proceedings of the 4th International Conference and Exhibition on Mass Mining, Santiago, Chile; pp. 491-497

Vardoulakis I (1980) Shear band inclination and shear modulus in biaxial tests. Int J Numer Anal Meth Geomech, 4: 103-119

Verdugo R, Ubilla J (2004). Geotechnical analysis of gravity flow during block caving. In Proceedings of the 4th International Conference and Exhibition on Mass Mining, Santiago, Chile; pp. 195–200

Verma D, Kainthola A, Singh TN, Thareja R (2014) Influence of water content on geotechnical properties of deccan basalt, Maharashtra, India. Int Res J Geol Min, 4: 122-132

Villaescusa EC (1991) A three dimensional model of rock jointing. Ph.D thesis, University of Queensland, Brisbane, Australia

Vivanco F, Watt T, Melo F (2011) The 3D shape of the loosening zone above multiple draw points in block caving through plasticity model with a dilation front. Int J Rock Mech Min Sci, 48, 406-411

Vyazmensky A (2008) Numerical modelling of surface subsidence associated with block cave mining using a finite element/discrete element approach. Ph.D thesis, Simon Fraser University, BC, Canada

Wang JJ, Qiu ZF, Deng WJ, Zhang HP (2016) Effects of mudstone particle content on shear strength of a crushed sandstone–mudstone particle mixture. Mar Georesour Geotec, 34: 395-402

Wang Y, Tonon F (2009) Discrete element modeling of impact fragmentation in rock fall analysis. In Proceedings of the the 43rd U.S. Symposium on Rock Mechanics, Asheville, NC, USA; paper 153

Wang Y, Tonon F (2012) Discrete element modeling of drop tests. Rock Mech Rock Eng, 45: 863–869

Waters AJ, Drescher A (2000) Modeling plug flow in bins-hoppers. Powder Technol, 113: 168–175

Watson GR (1993) Flow patterns in flat bottomed silos. Ph.D thesis, University of Edinburgh, UK

Weatherley D (2010). Six monthly technical report, sub-project frag 1: Fundamentals of caving fragmentation, University of Queensland, Brisbane, Australia. Report to the Mass Mining Technology 2 Project, March

Wegner S, Stannarius R, Boese A, Rose G, Szabo B, Somfai E, Börzsönyi T (2014) Effects of grain shape on packing and dilatancy of sheared granular materials. Soft Matter, 10, 5157

Wellman E, Annavarapu S, Pratt RW, Nicholas D (2012) Prediction of fragmentation in block cave mine design – an update of the Core2Frag Program. In 6th International Conference and Exhibition on Mass Mining, Sudbury, Canada

Wijewickreme D, Sriskandakumar S, Byrne P (2005) Cyclic loading response of loose air-pluviated Fraser River sand for validation of numerical models simulating centrifuge tests. Can Geotech J, 42: 550–561

Williams DJ (2000) Assessment of embankment parameters. In slope stability in surface mining. Edited by Hustrulid WA, McCarter MK, and van Zyl DJA, Littleton, CO: SME

Williams DJ, Currey NA (2004) Innovative mine site rehabilitation in a semi-arid climate. In: C D Shackelford, In Proceedings of the Eleventh Tailings and Mine Waste Conference. Tailings and Mine Waste '04, Vail, CO, USA; pp. 383-391

Woo KS, Eberhardt E, Elmo E, Stead D (2013) Empirical investigation and characterization of surface subsidence related to block cave mining. Int J Rock Mech Min Sci, 61: 31-42

Wood DM, Maeda K (2008) Changing grading of soil: effect on critical states. Acta Geotech, 3: 3-14

Yoshida T, Tatsuoka F, Siddiquee M (1994). Shear banding in sands observed in plane strain compression. Localisation and Bifurcation Theory for Soils and Rocks. Eds.: R. Chambon, J. Desrues and I. Vardoulakis, Balkema, Rotterdam; pp. 165-181

Yoshinaka R, Osada M, Park H, Sasaki T, Sasaki K (2008) Practical determination of mechanical design parameters of intact rock considering scale effect. Eng Geol, 96: 173–186.

Appendix A: Laboratory testing results (Chapter 4 and 5)

Stress - strain relationship

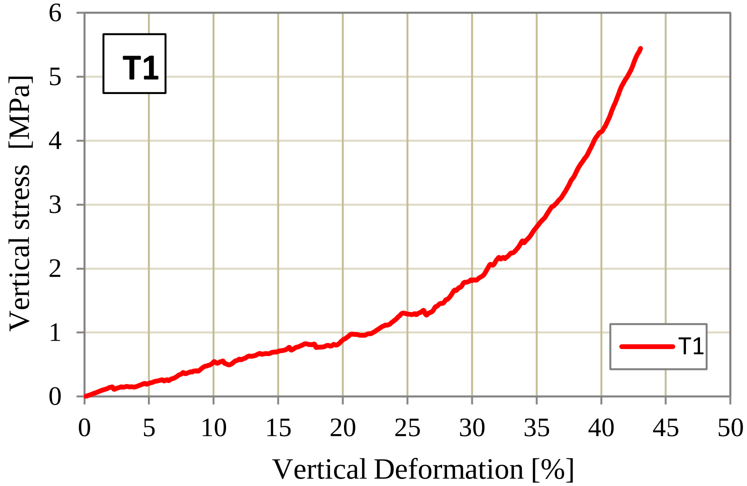

Post - gradation curve

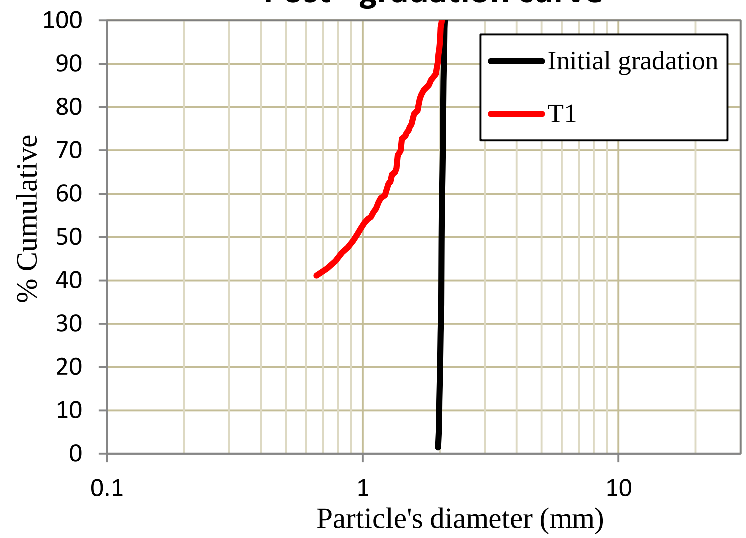

Plan view after testing

(Mould diameter = 10 cm)

Particles after testing

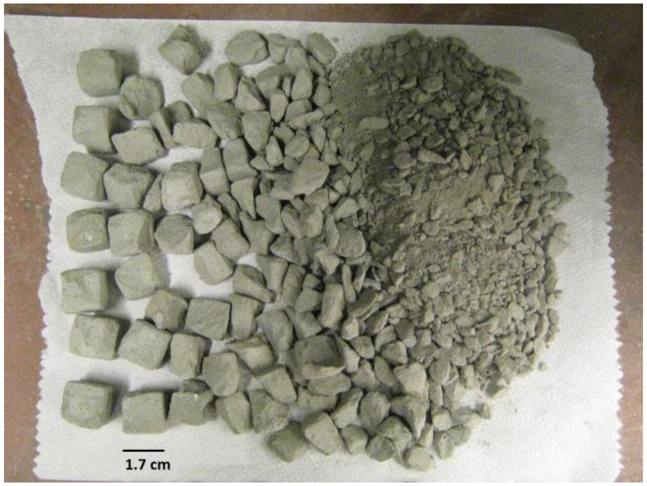

Stress - strain relationship

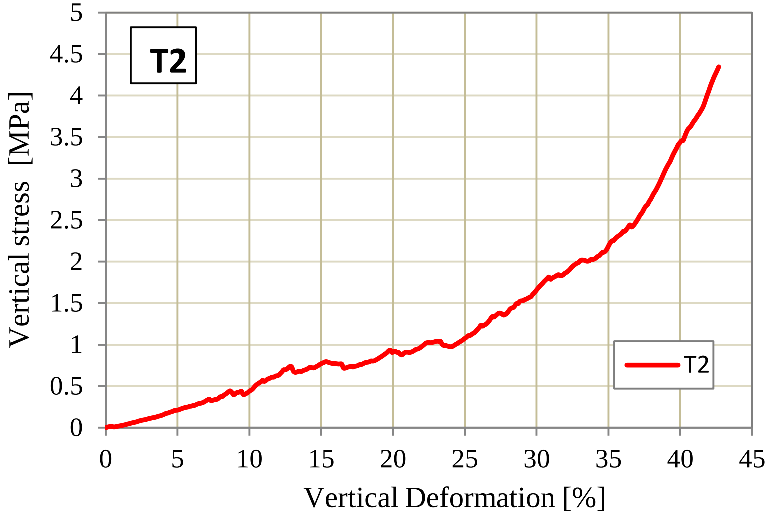

Post - gradation curve

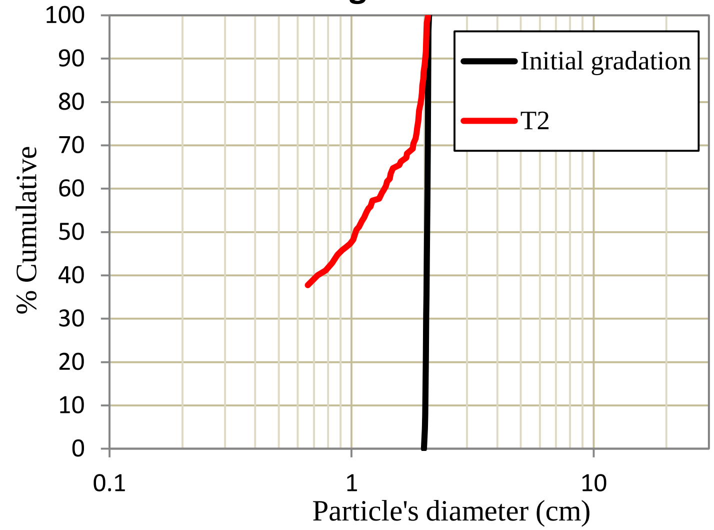

Plan view after testing

(Mould diameter = 10 cm)

Particles after testing

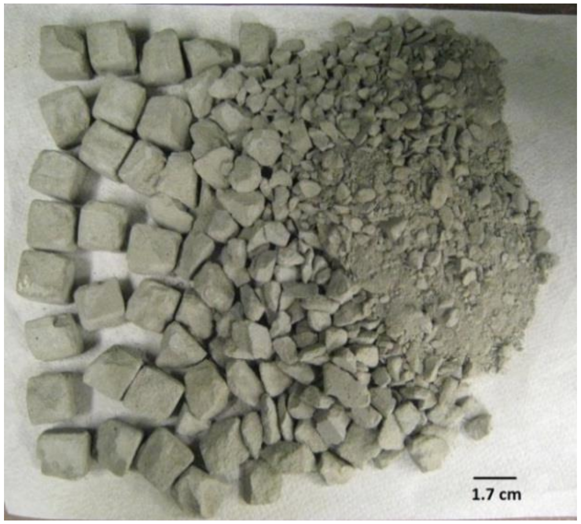

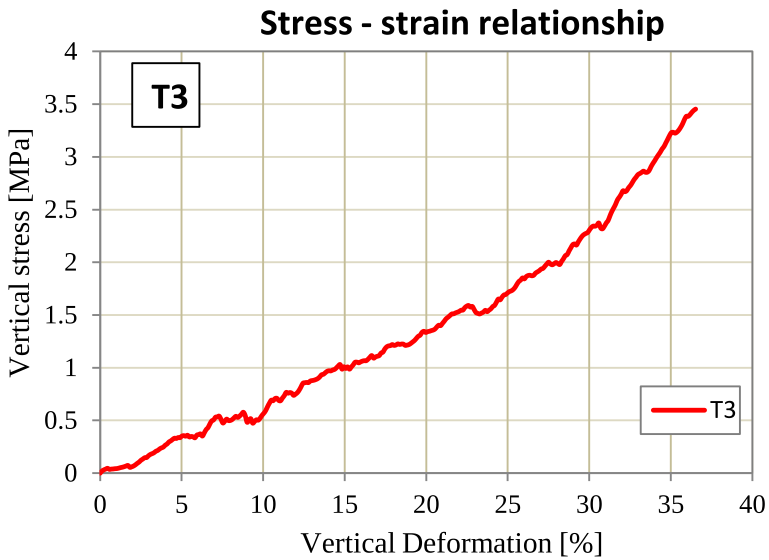

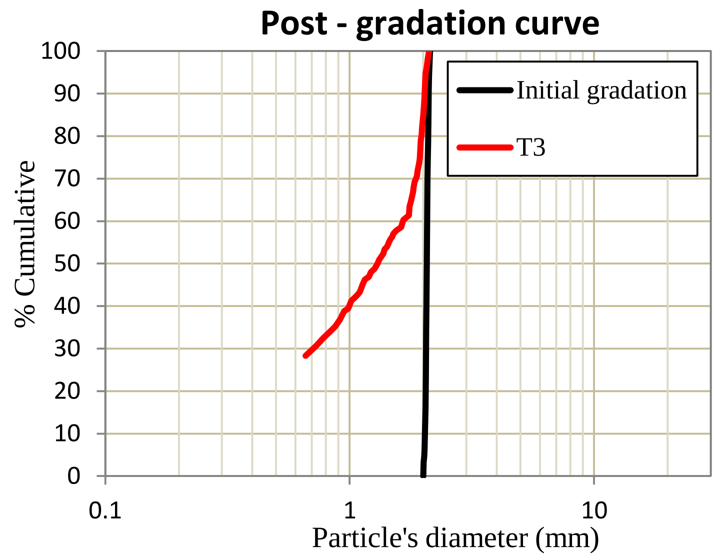

Plan view after testing

(Mould diameter = 10 cm)

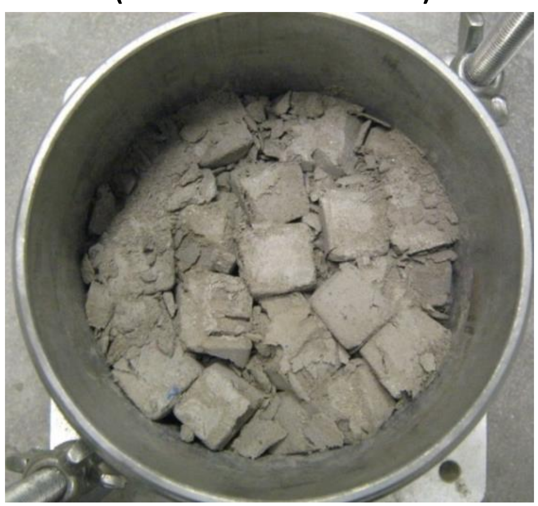

Particles after testing

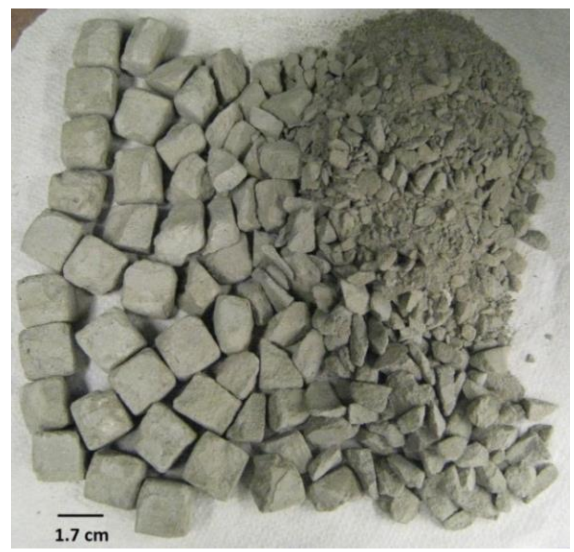

Stress - strain relationship

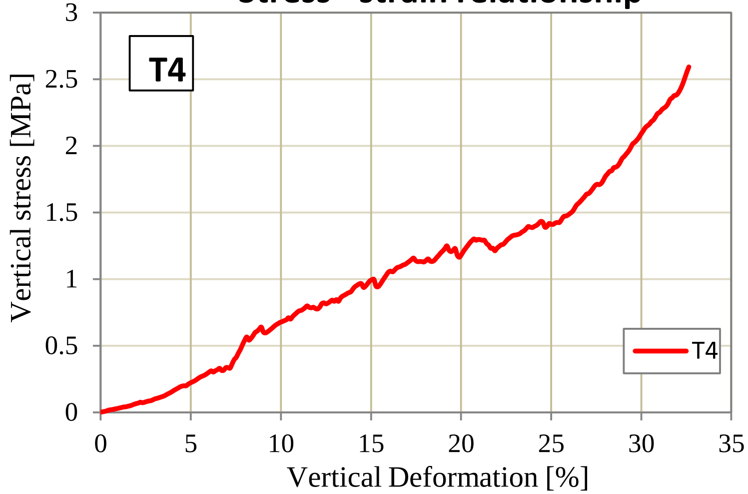

Post - gradation curve

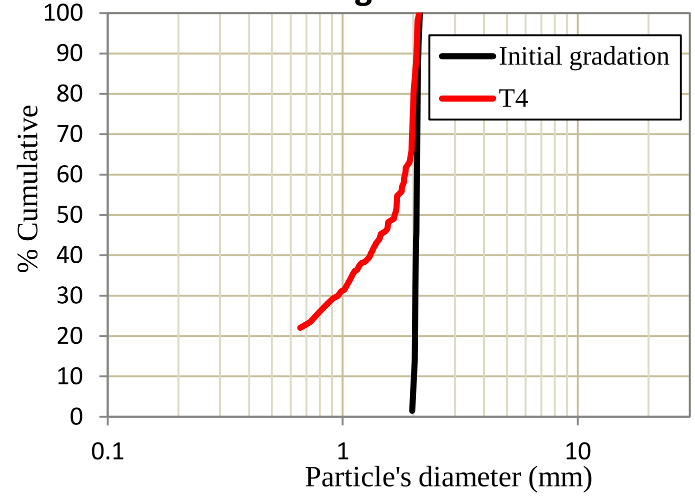

Plan view after testing
(Mould diameter = 10 cm)

Particles after testing

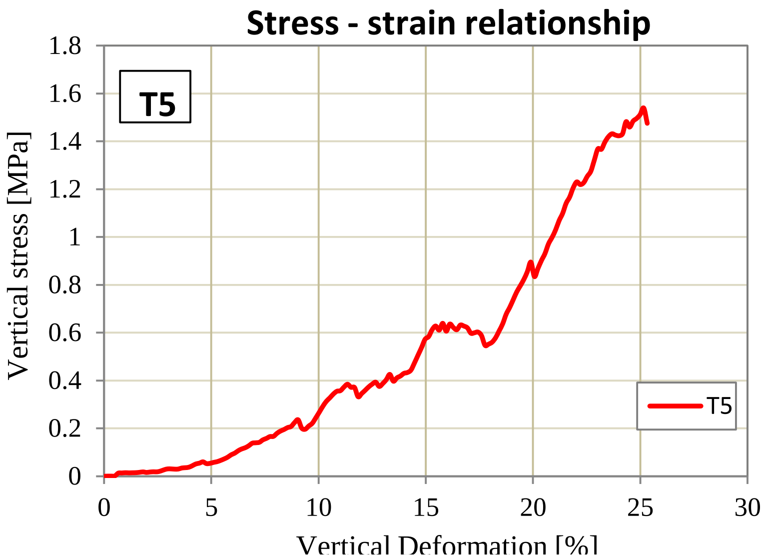
Stress - strain relationship
T5
Vertical stress [MPa]
Vertical Deformation [%]
T5

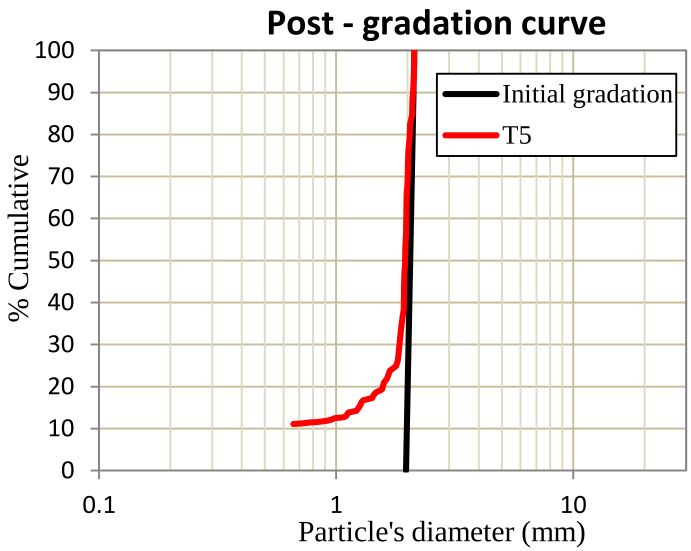
Post - gradation curve
% Cumulative
Particle's diameter (mm)
Initial gradation
T5

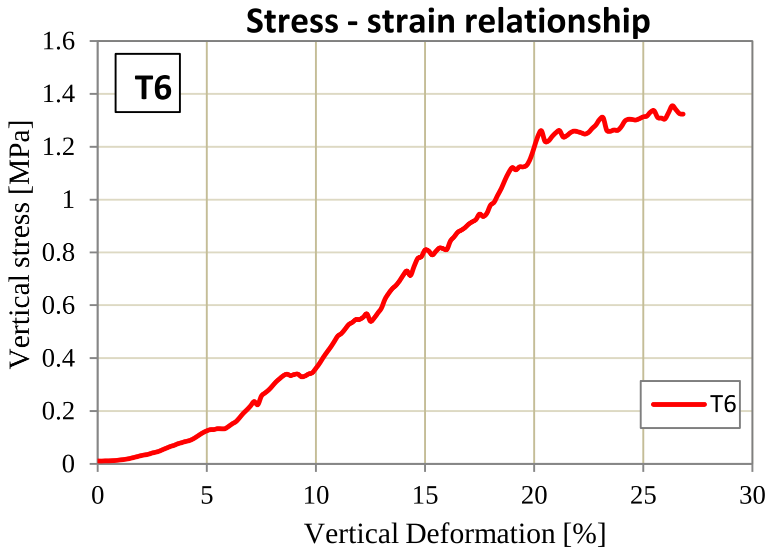
Stress - strain relationship
T6
Vertical stress [MPa]
1.6
1.4
1.2
1
0.8
0.6
0.4
0.2
0
0
5
10
15
20
25
30
Vertical Deformation [%]
T6

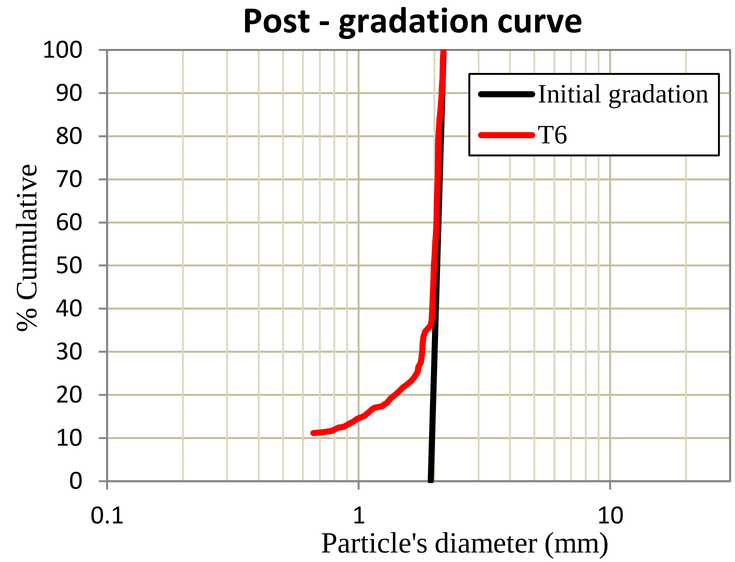
Post - gradation curve
% Cumulative
100
90
80
70
60
50
40
30
20
10
0
0.1
1
10
Particle's diameter (mm)
Initial gradation
T6

Stress - strain relationship

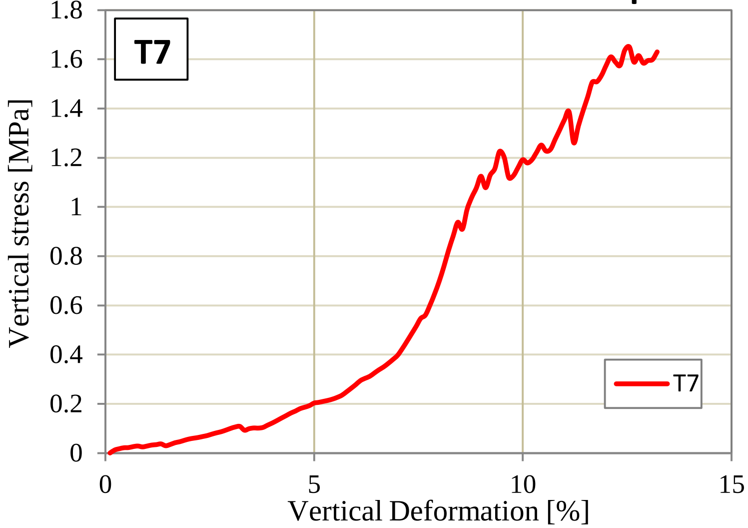

Post - gradation curve

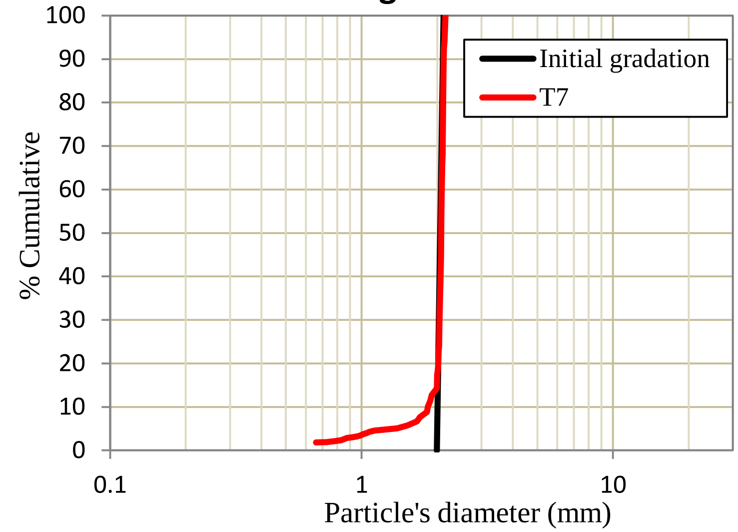

Plan view after testing

(Mould diameter = 10 cm)

Particles after testing

Stress - strain relationship

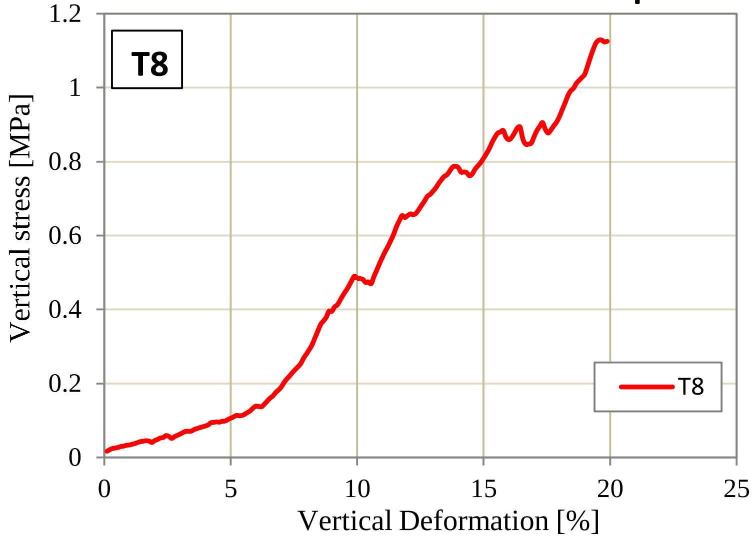

Post - gradation curve

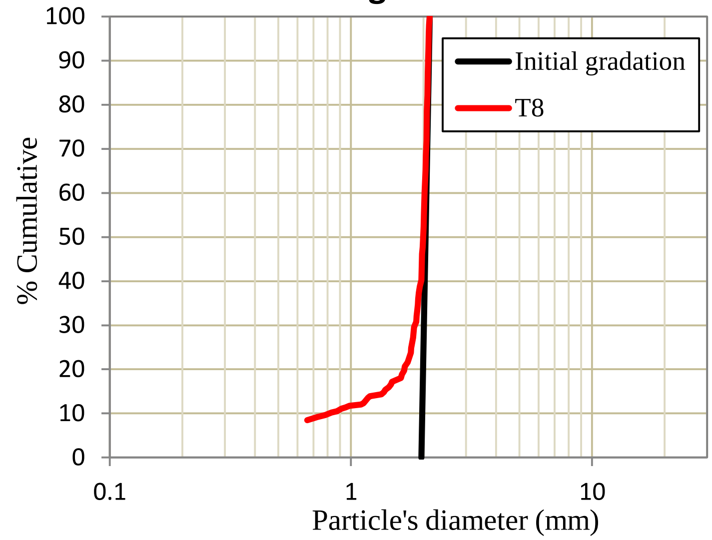

Plan view after testing

(Mould diameter = 10 cm)

Particles after testing

Stress - strain relationship

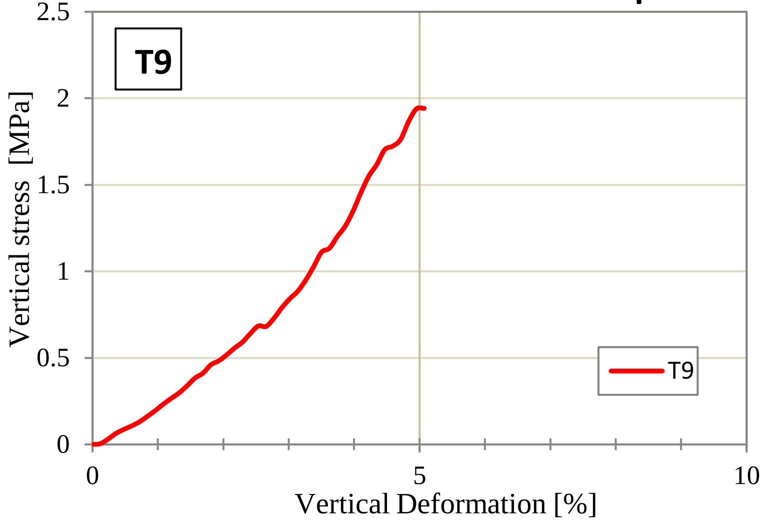

Post - gradation curve

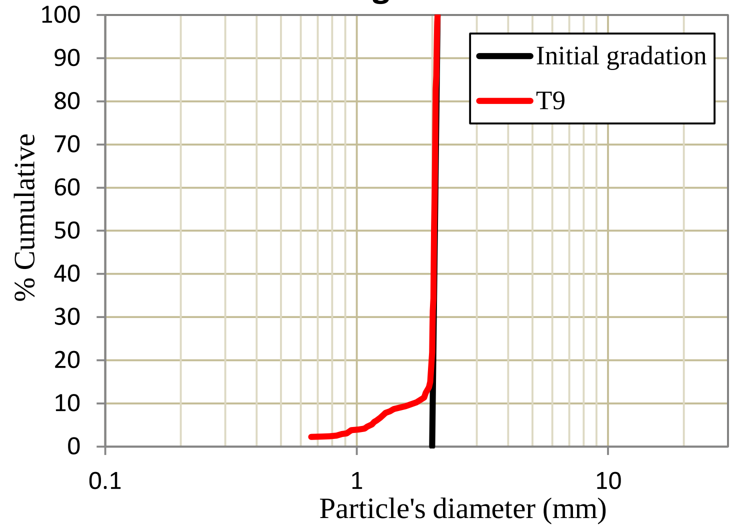

Plan view after testing

(Mould diameter = 10 cm)

Particles after testing

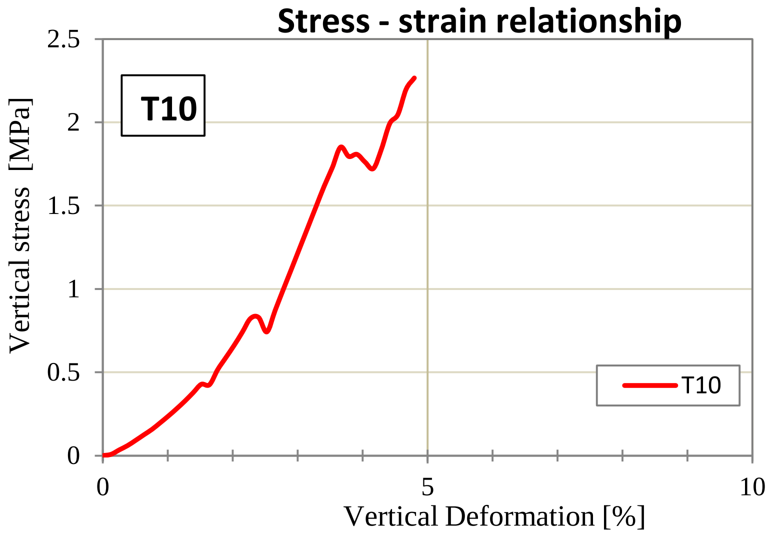

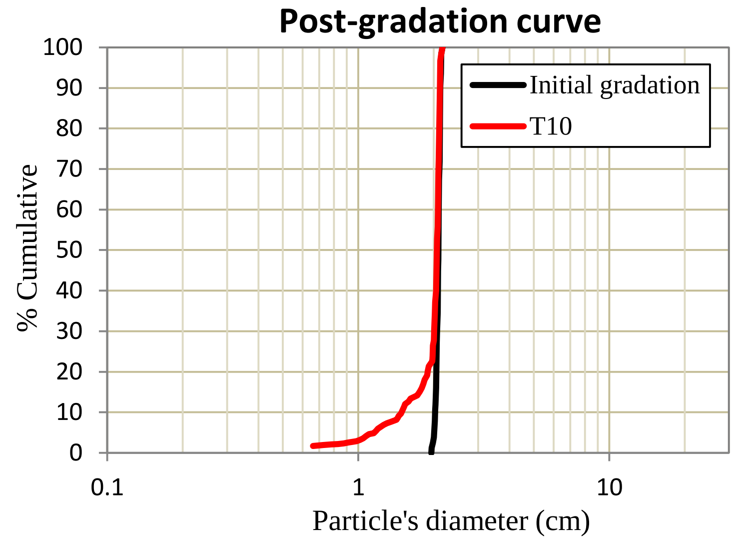

Plan view after testing

(Mould diameter = 10 cm)

Particles after testing

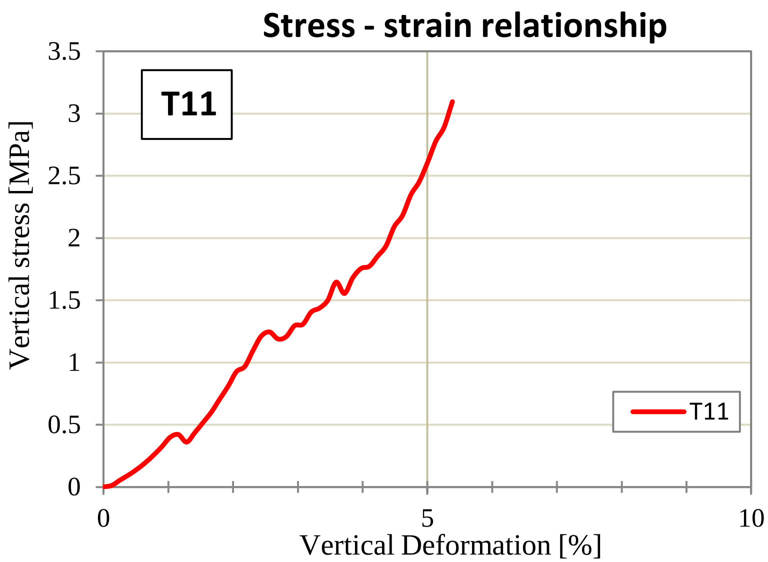

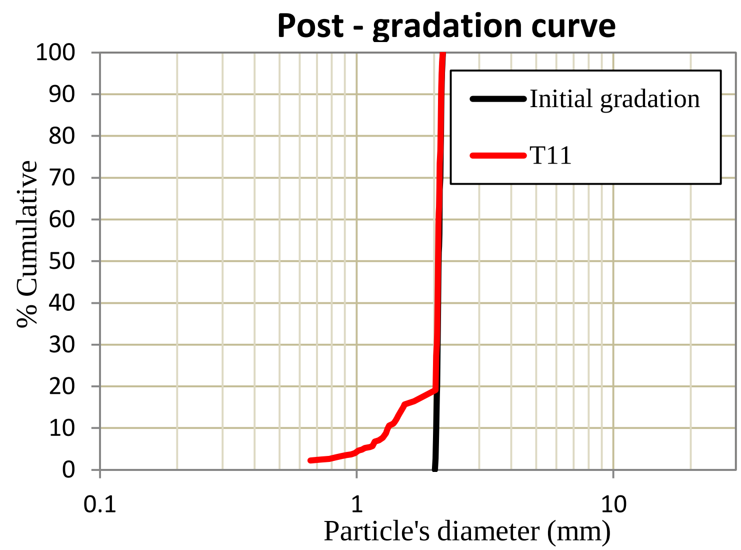

Plan view after testing

(Mould diameter = 10 cm)

Particles after testing

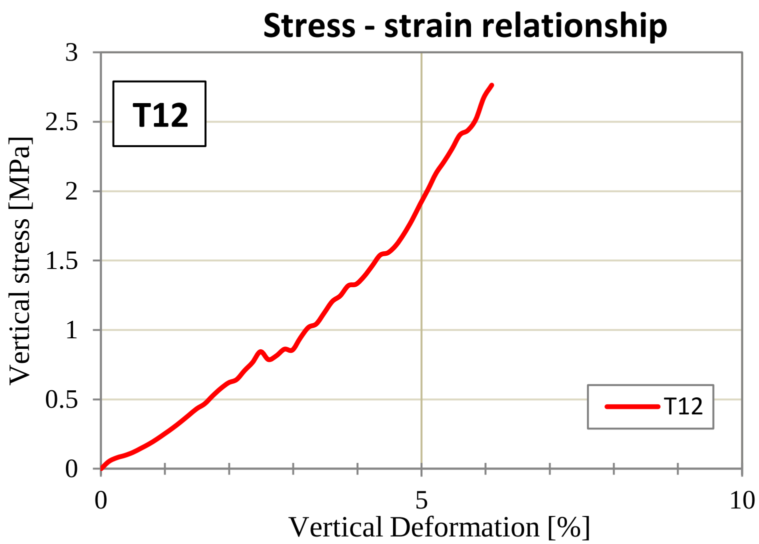

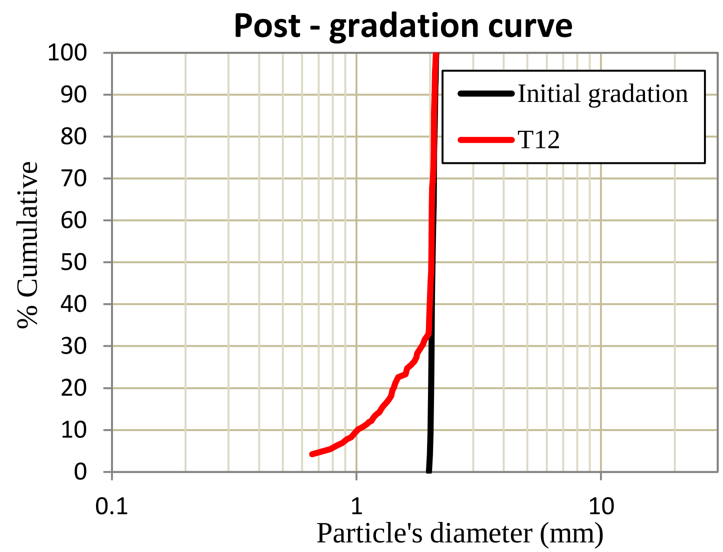

Plan view after testing

(Mould diameter = 10 cm)

Particles after testing

Stress - strain relationship

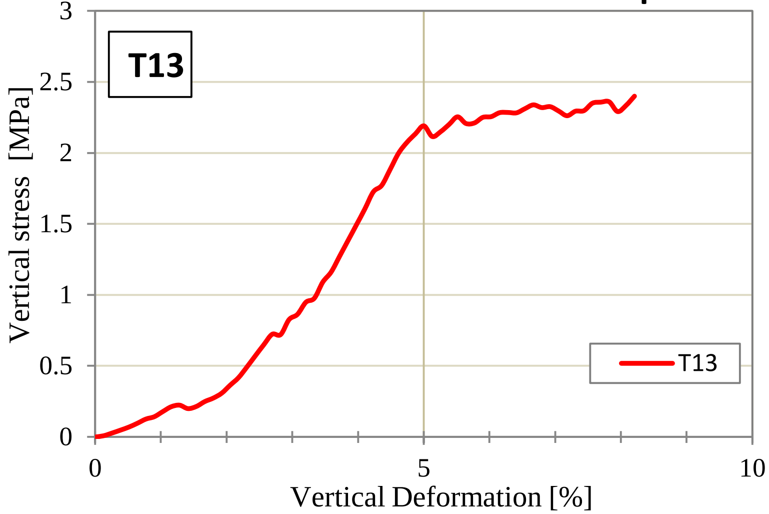

Post - gradation curve

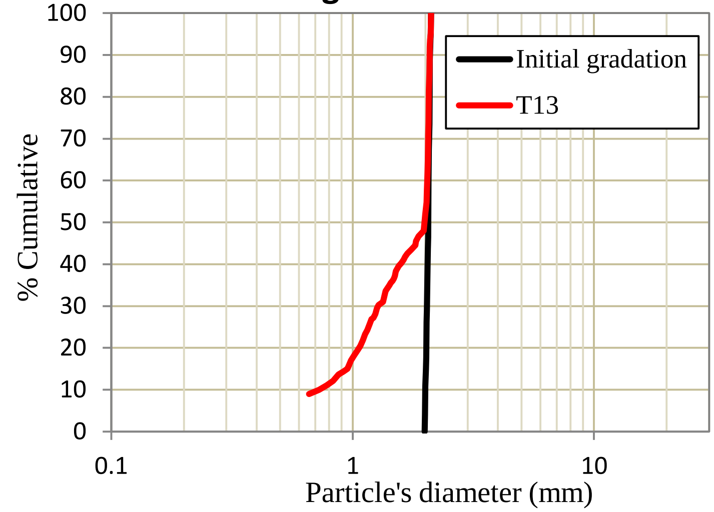

Plan view after testing

(Mould diameter = 10 cm)

Particles after testing

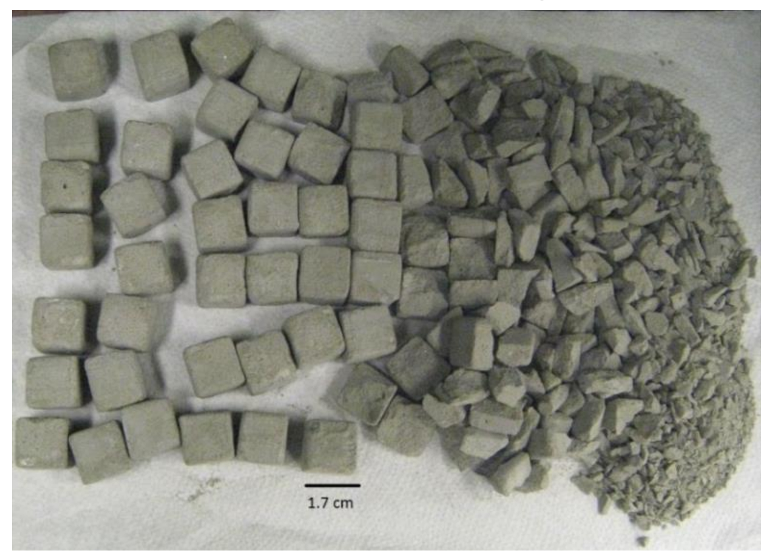

Stress - strain relationship

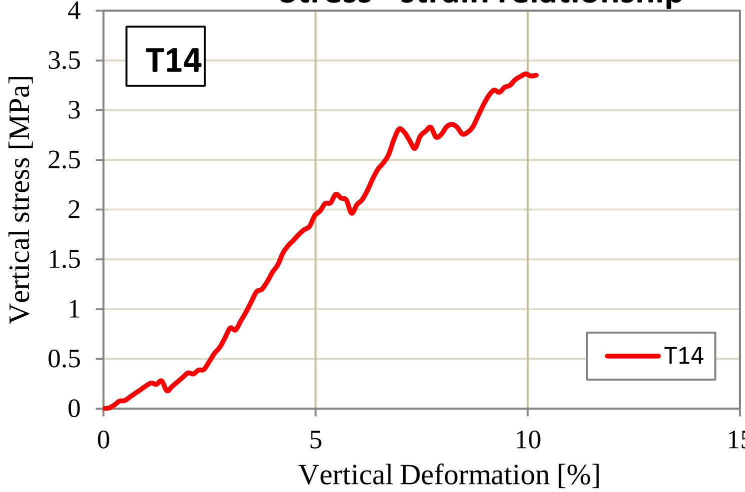

Post - gradation curve

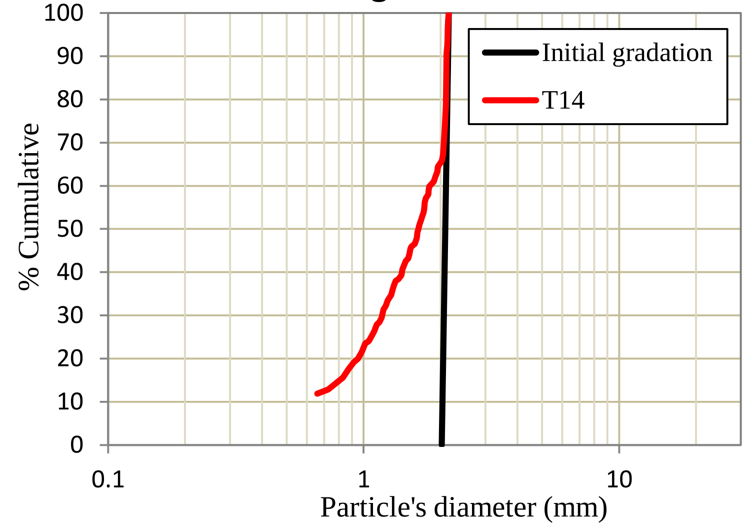

Plan view after testing

(Mould diameter = 10 cm)

Particles after testing

Stress - strain relationship

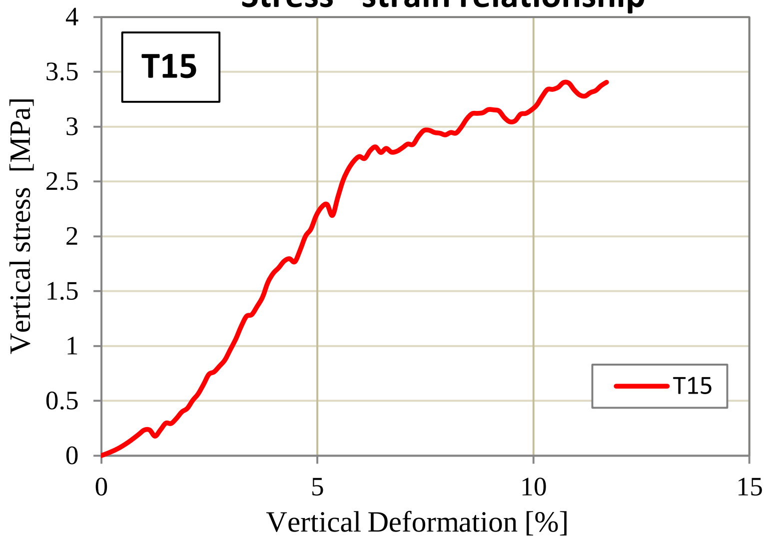

Post - gradation curve

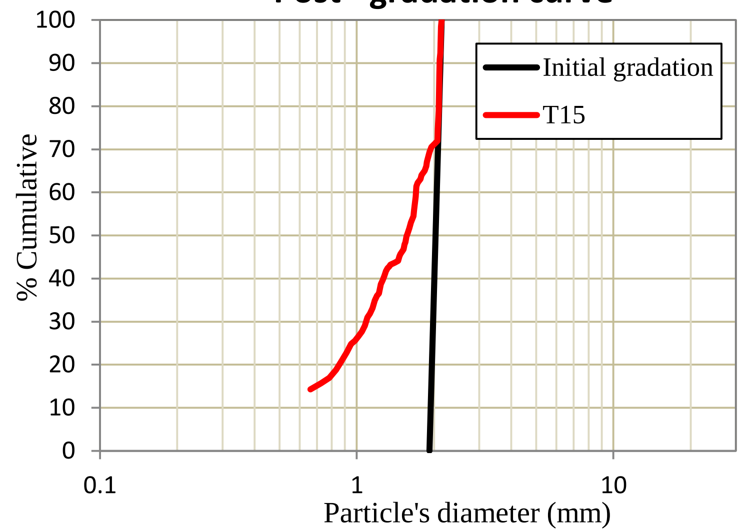

Plan view after testing

(Mould diameter = 10 cm)

Particles after testing

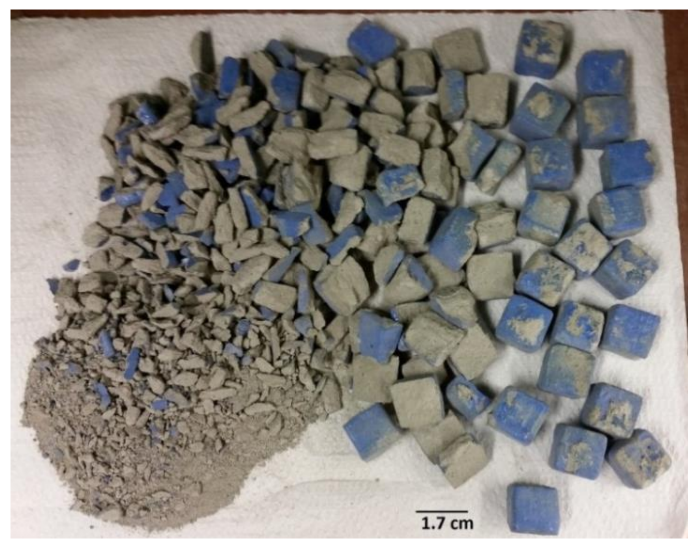

Stress - strain relationship

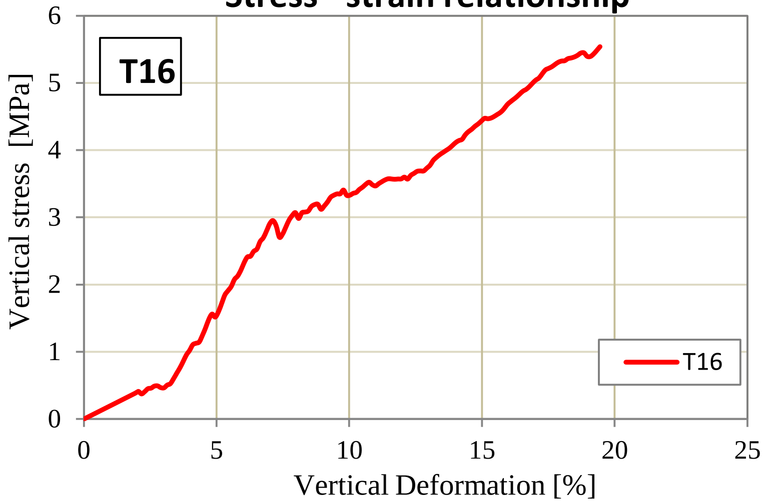

Post - gradation curve

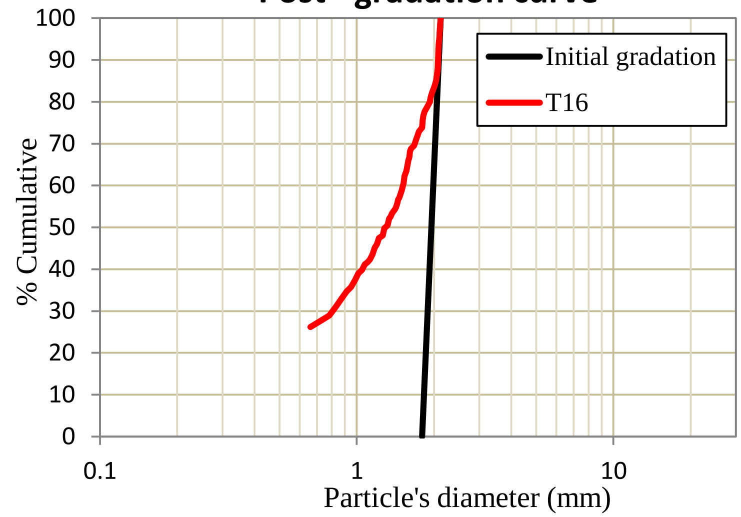

Plan view after testing

(Mould diameter = 10 cm)

Particles after testing

Stress - strain relationship

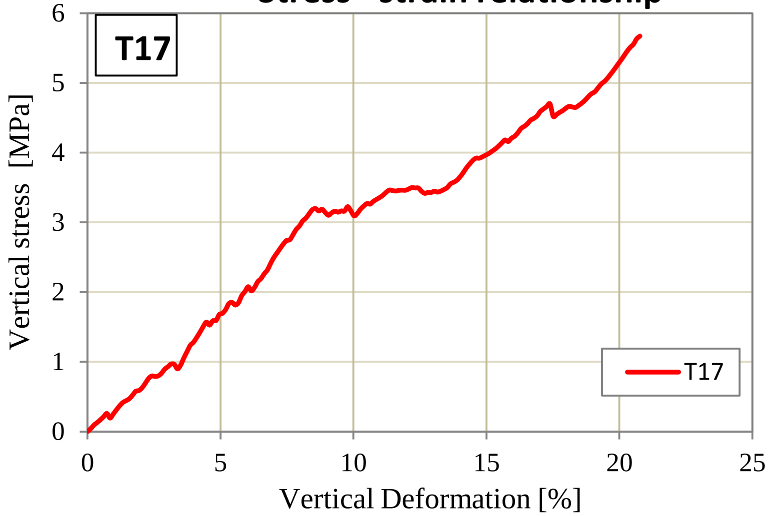

Post-gradation curve

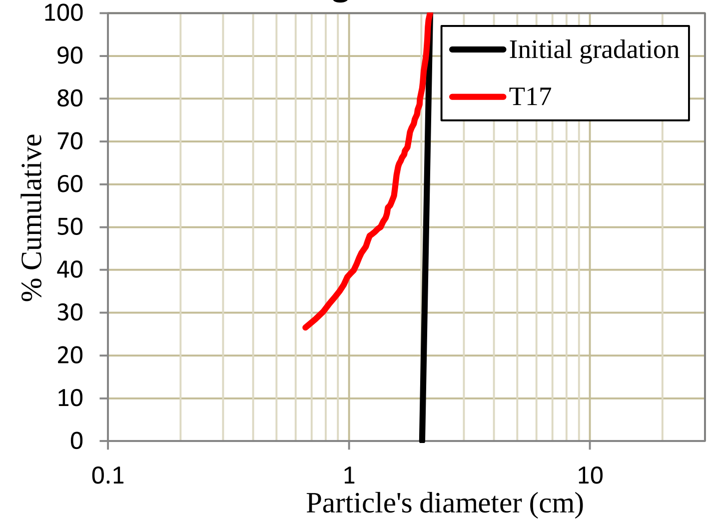

Plan view after testing

(Mould diameter = 10 cm)

Particles after testing

Stress - strain relationship

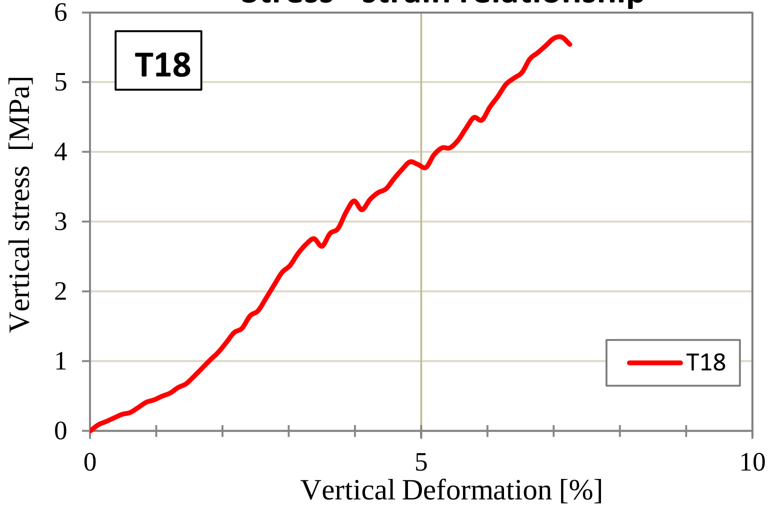

Post - gradation curve

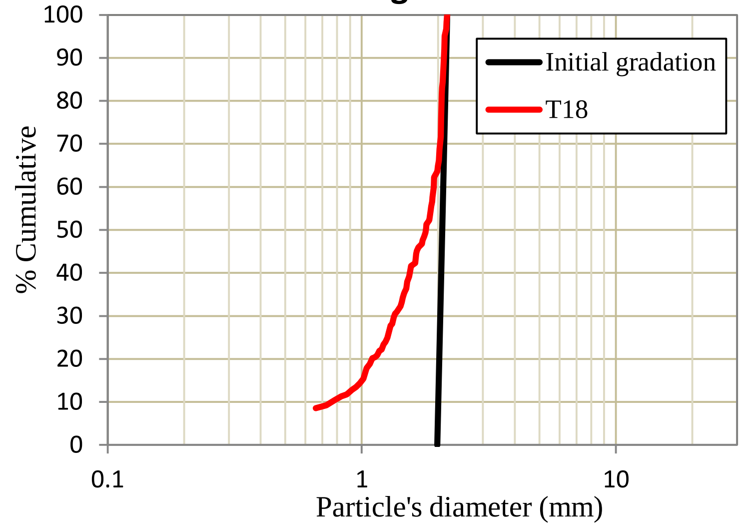

Plan view after testing

(Mould diameter = 10 cm)

Particles after testing

Stress - strain relationship

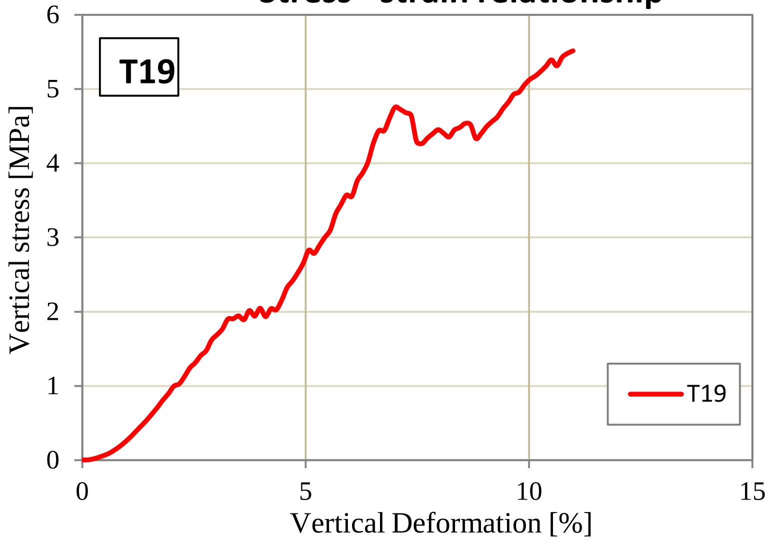

Post - gradation curve

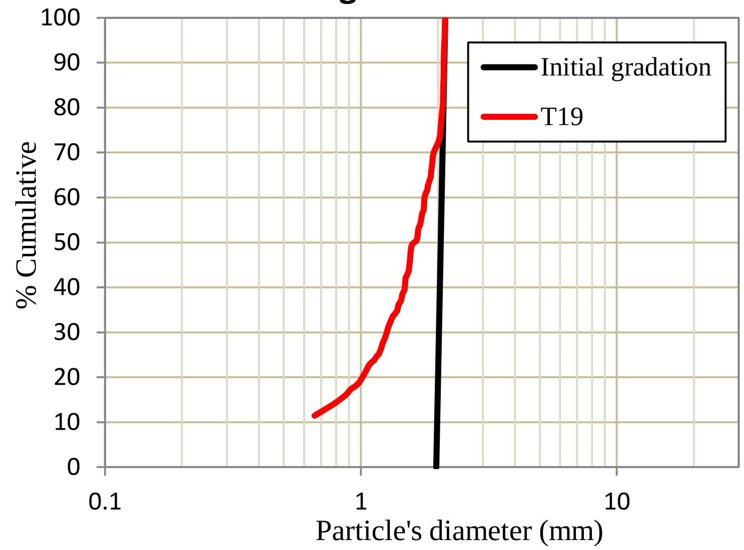

Plan view after testing

(Mould diameter = 10 cm)

Particles after testing

Stress - strain relationship

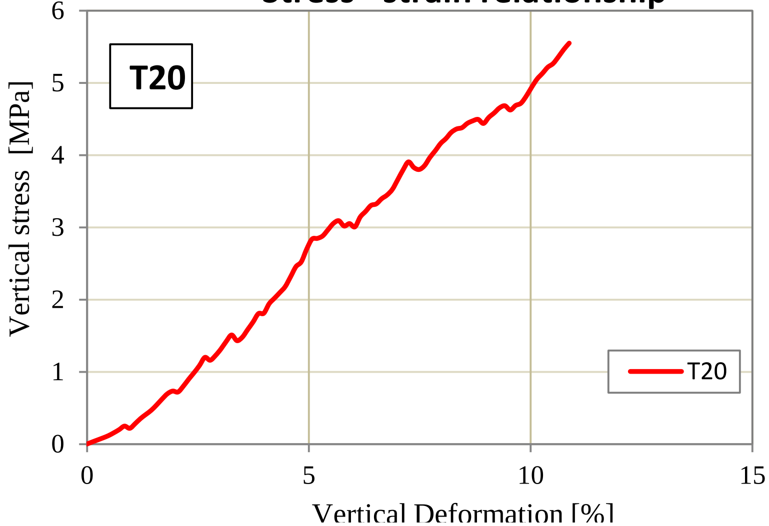

Post - gradation curve

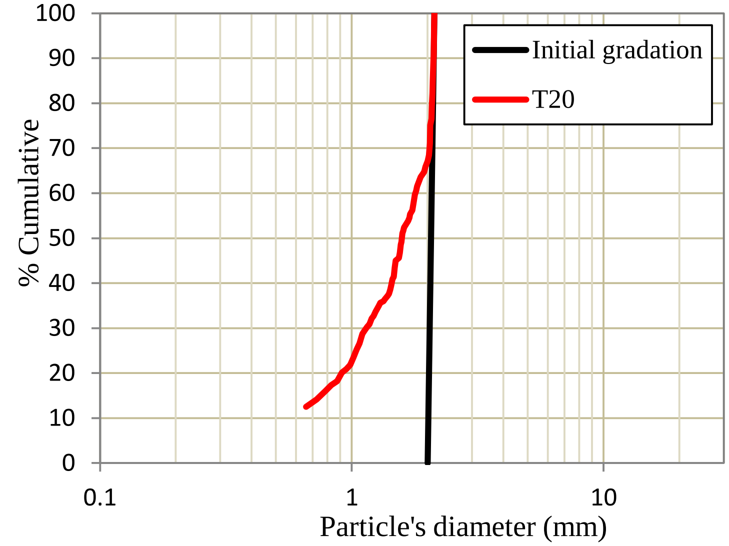

Particles after testing

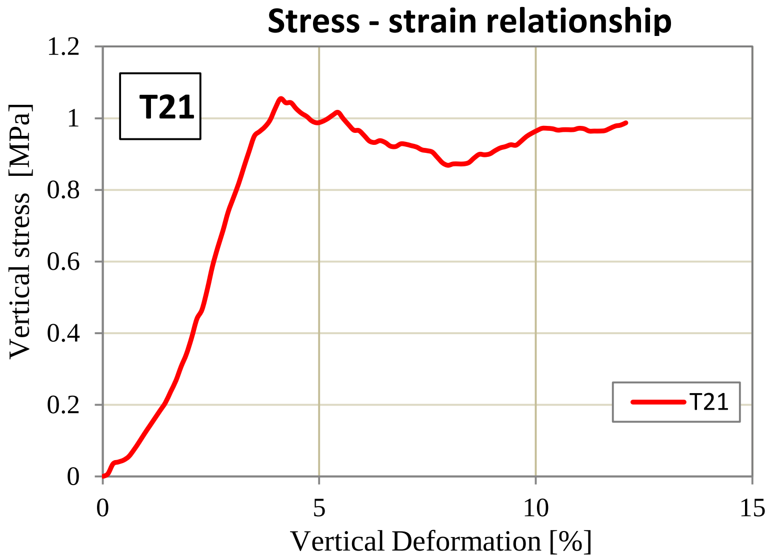

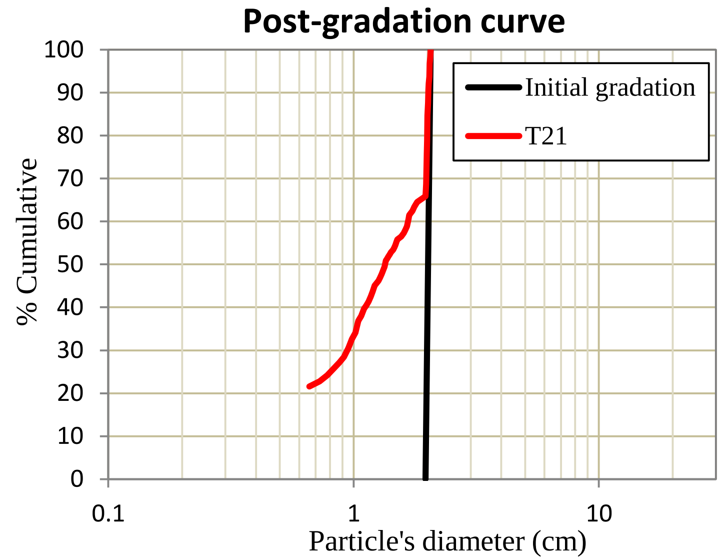

Particles before testing

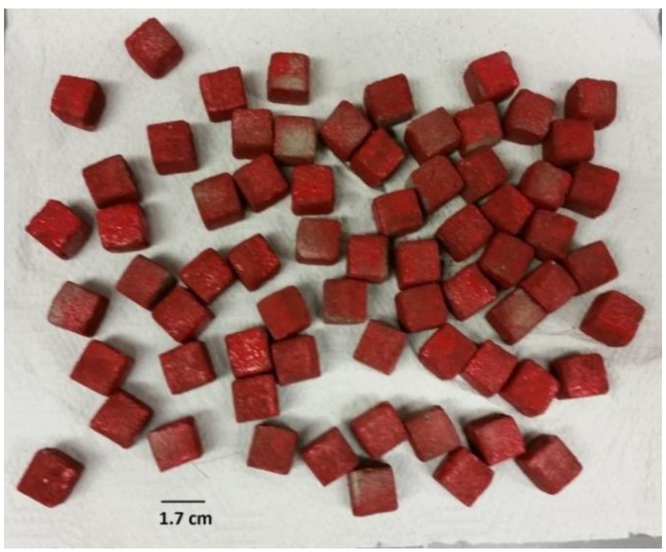

Particles after testing

Stress - strain relationship

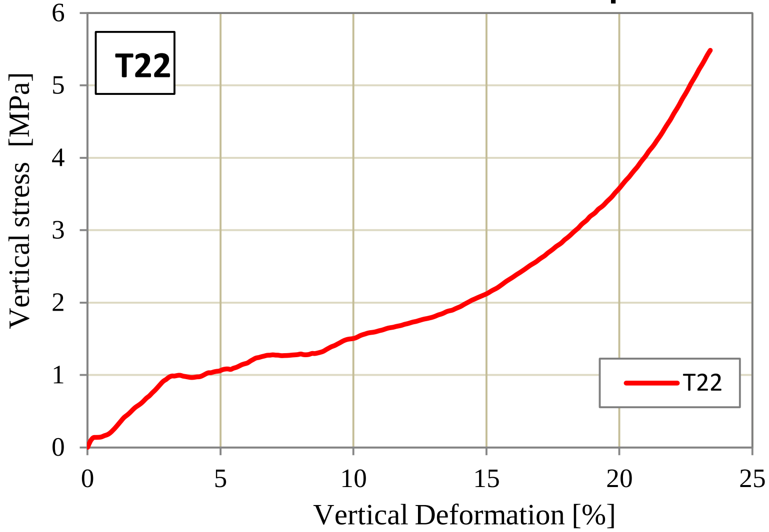

Post-gradation curve

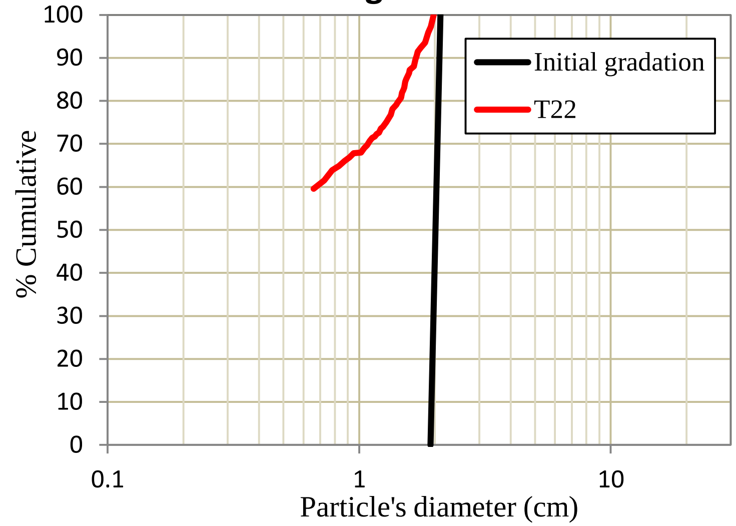

Particles before testing

Particles after testing

Stress - strain relationship

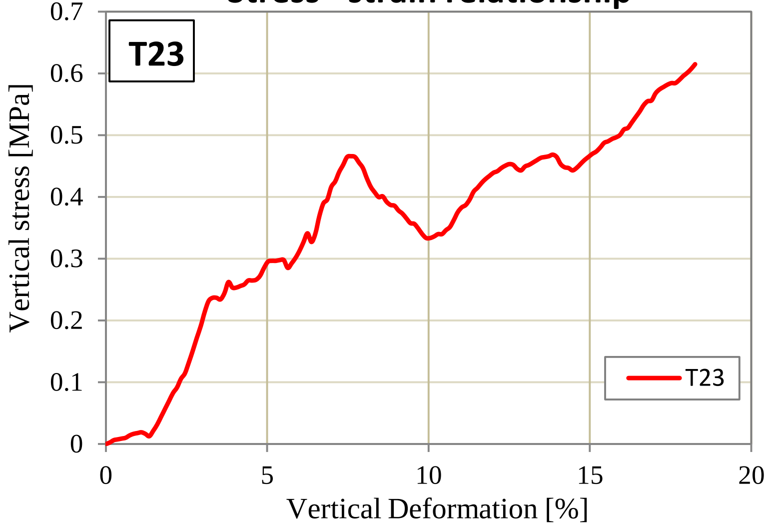

Post - gradation curve

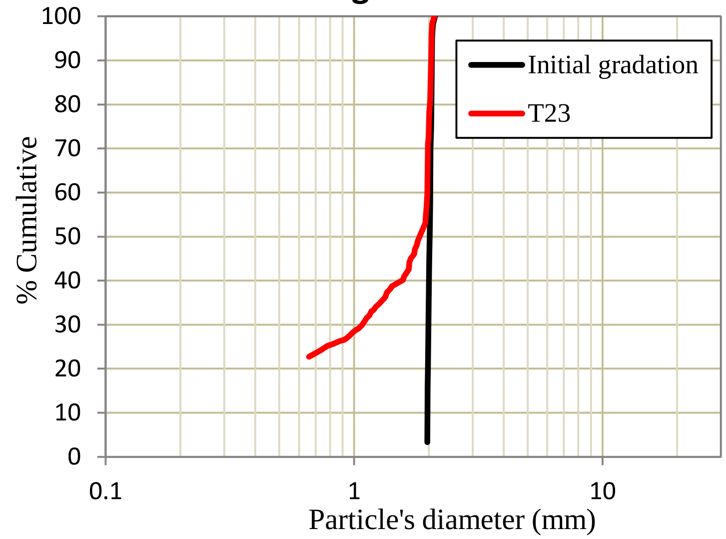

Particles after testing

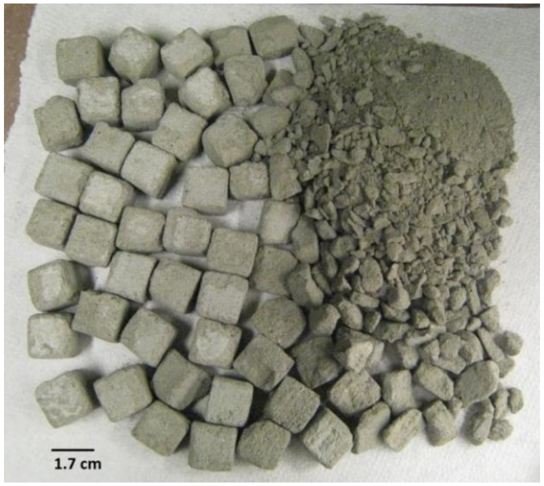

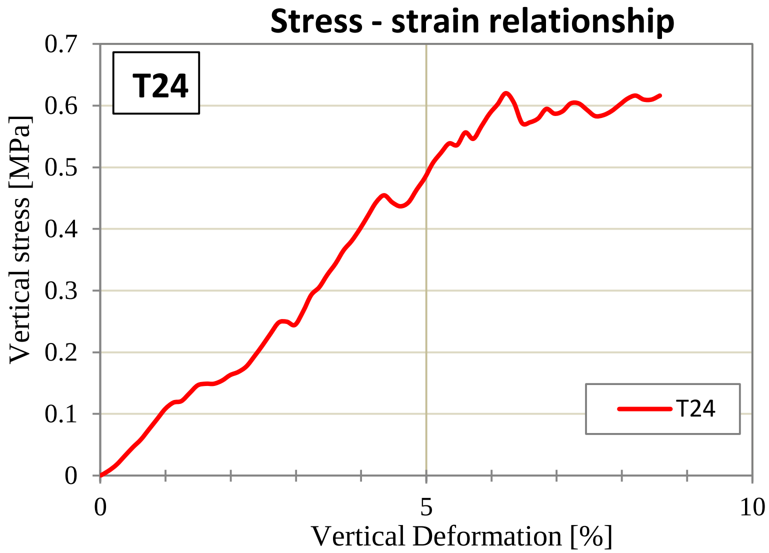

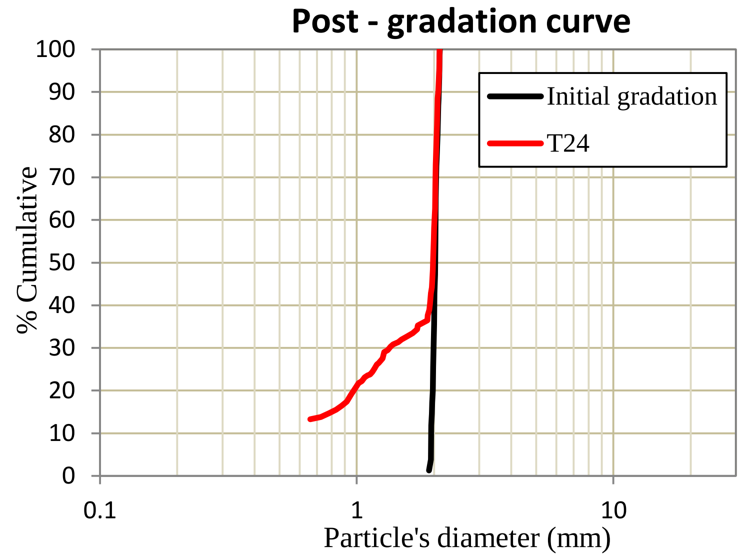

Plan view after testing

(Mould diameter = 10 cm)

Particles after testing

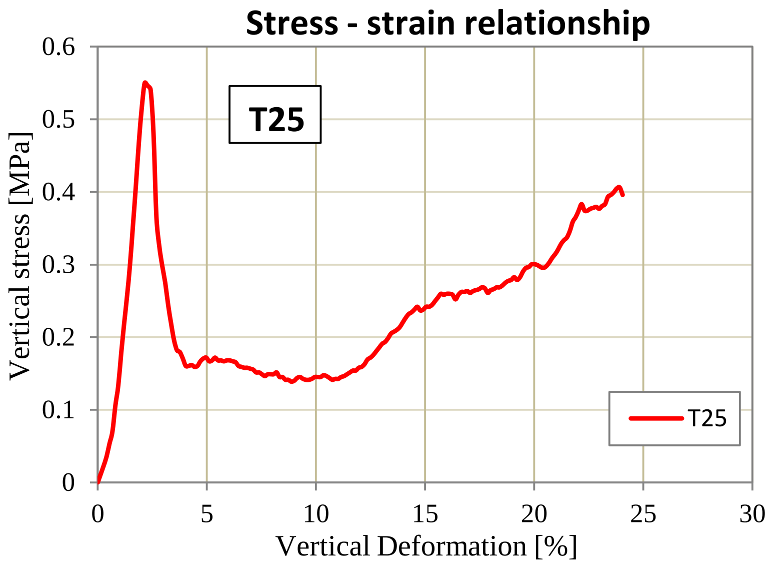

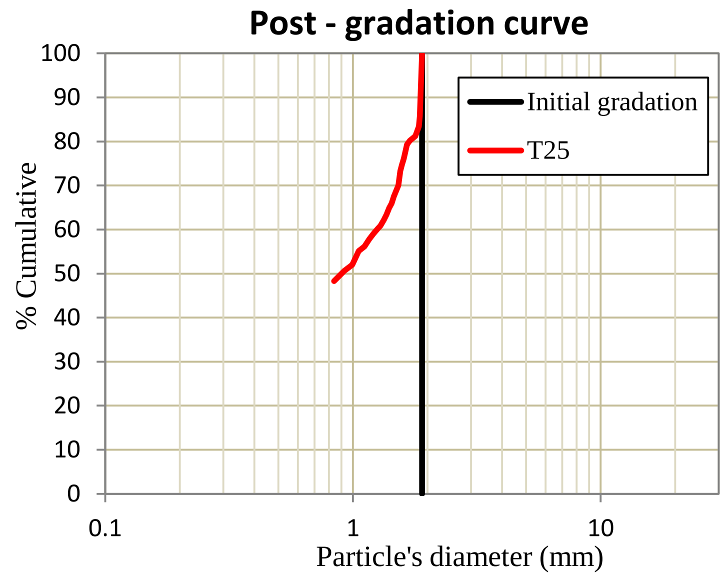

Particles after testing

Stress - strain relationship

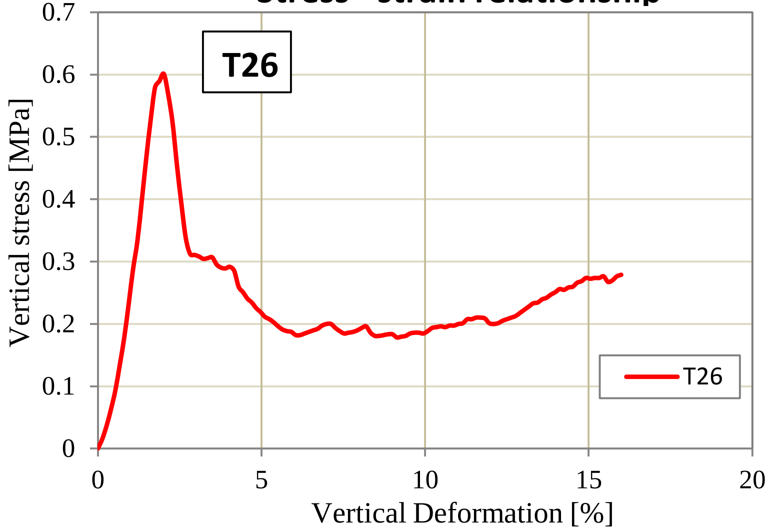

Post - gradation curve

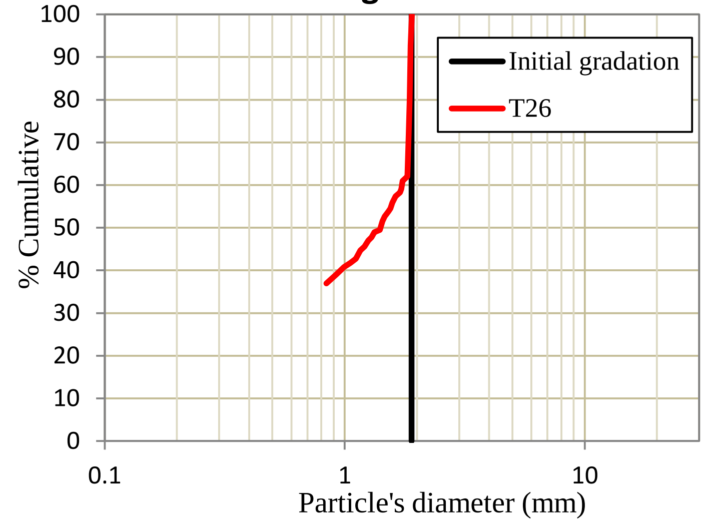

Particles after testing

Stress - strain relationship

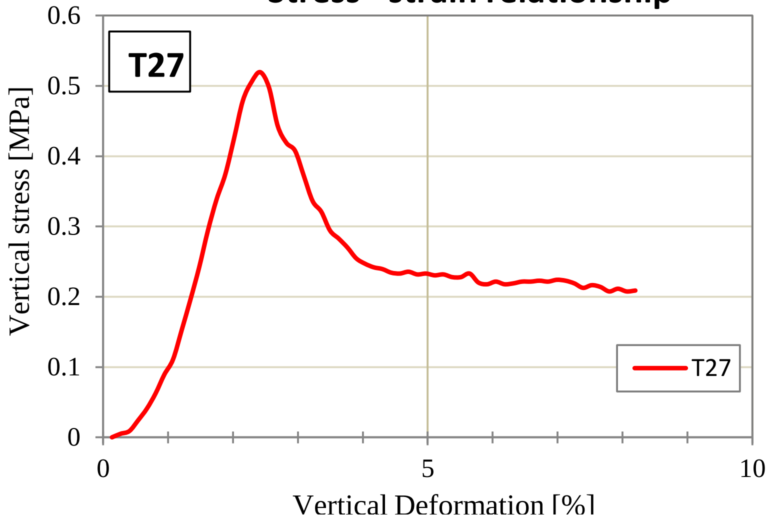

Post - gradation curve

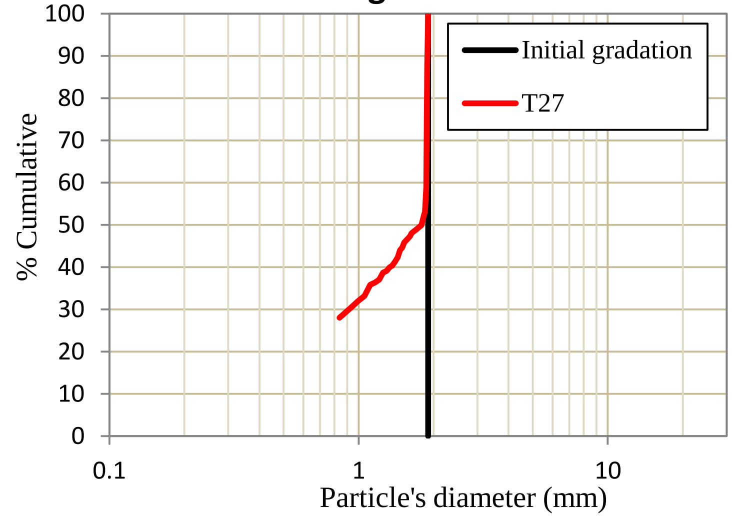

Particles after testing

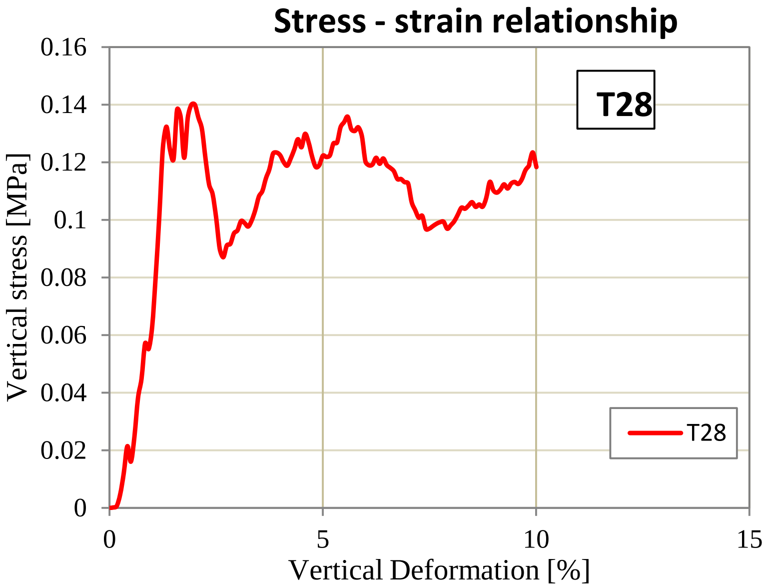

Stress - strain relationship
T28
Vertical stress [MPa]
0.16
0.14
0.12
0.1
0.08
0.06
0.04
0.02
0
0
5
10
15
Vertical Deformation [%]
T28

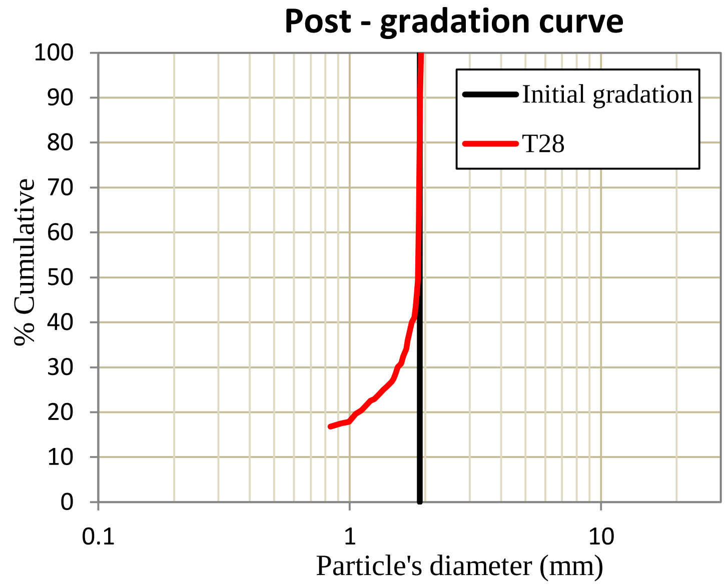

Post - gradation curve
Initial gradation
T28
% Cumulative
100
90
80
70
60
50
40
30
20
10
0
0.1
1
10
Particle's diameter (mm)

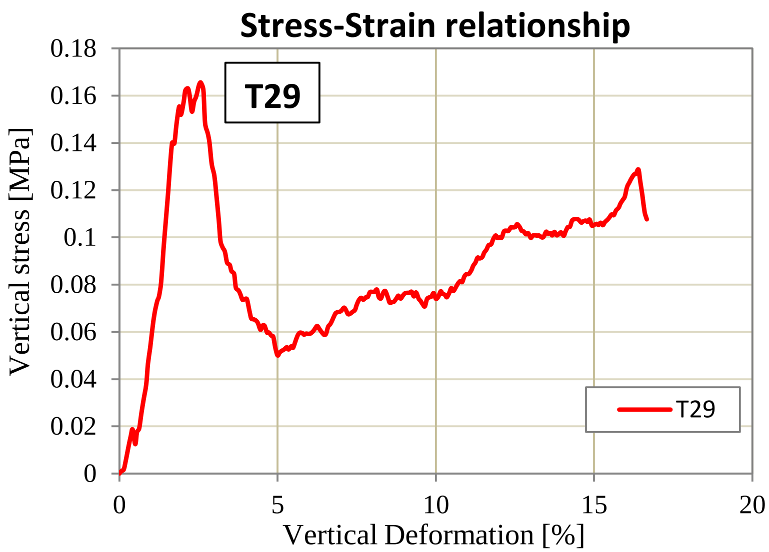
Stress-Strain relationship
T29
Vertical stress [MPa]
0.18
0.16
0.14
0.12
0.1
0.08
0.06
0.04
0.02
0
0
5
10
15
20
Vertical Deformation [%]
T29

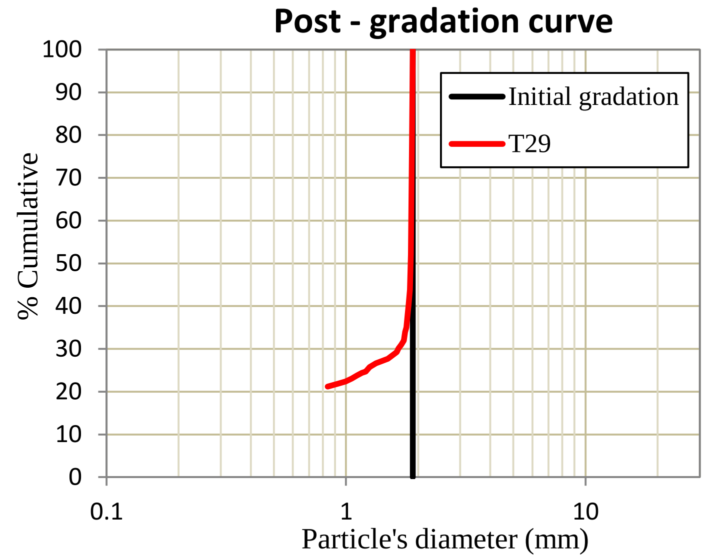
Post - gradation curve
% Cumulative
100
90
80
70
60
50
40
30
20
10
0
0.1
1
10
Particle's diameter (mm)
Initial gradation
T29

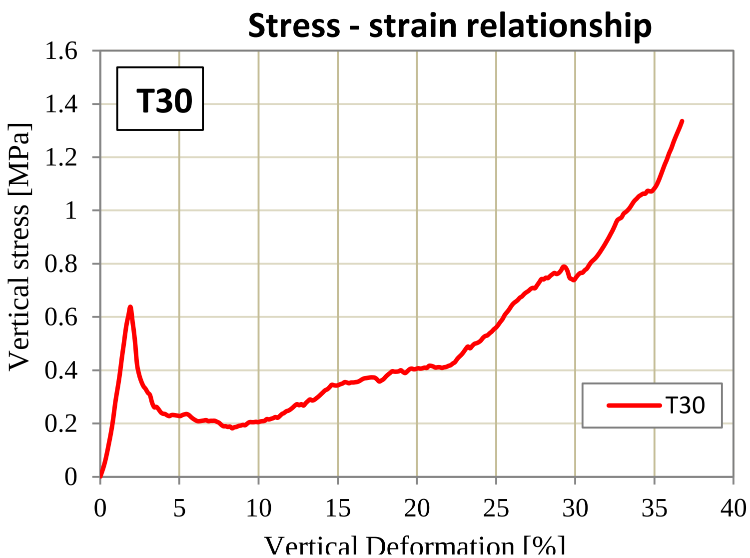

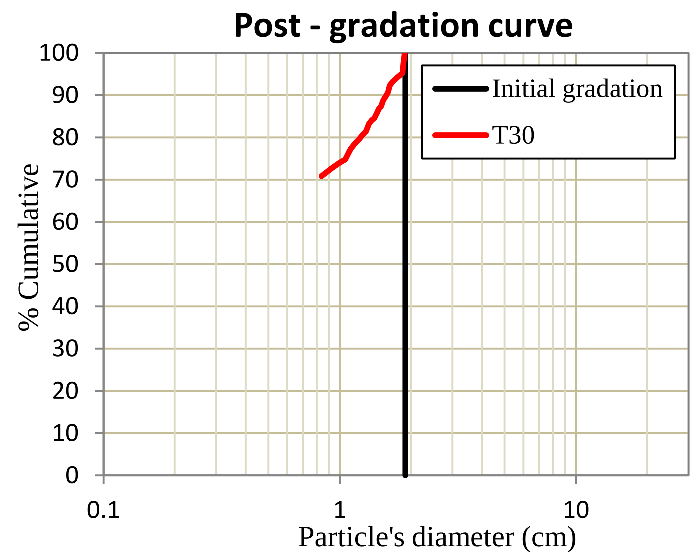

Plan view after testing

(Mould diameter = 10 cm)

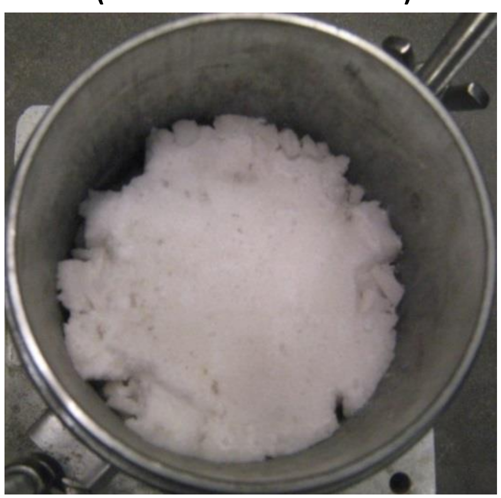

Particles after testing

Stress - strain relationship

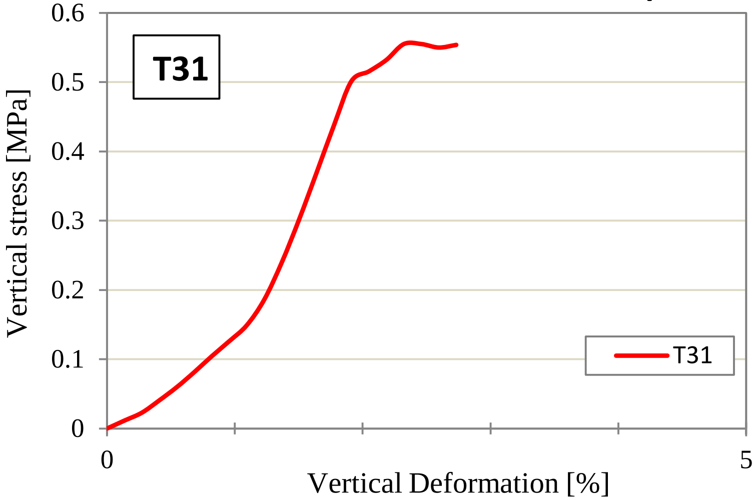

Post - gradation curve

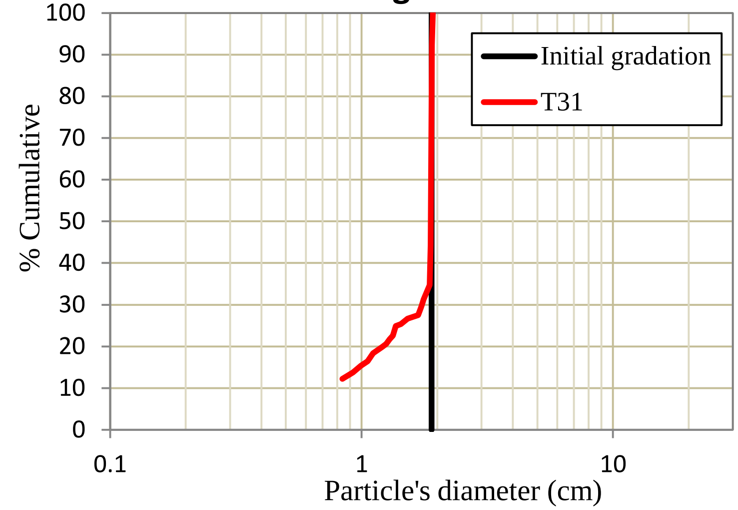

Plan view after testing

(Mould diameter = 10 cm)

Particles after testing

Stress - strain relationship

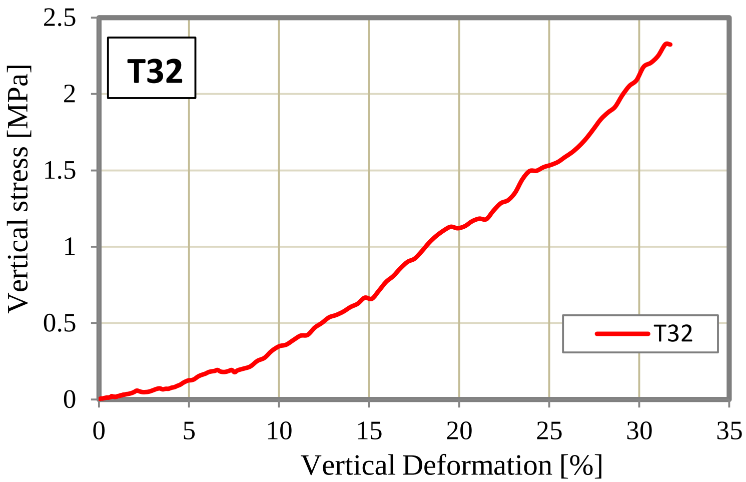

Post - gradation curve

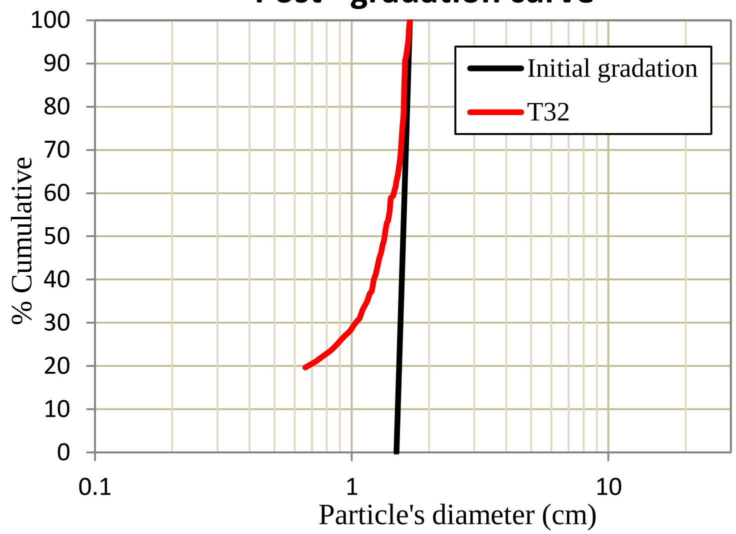

Plan view after testing

(Mould diameter = 10 cm)

Particles after testing

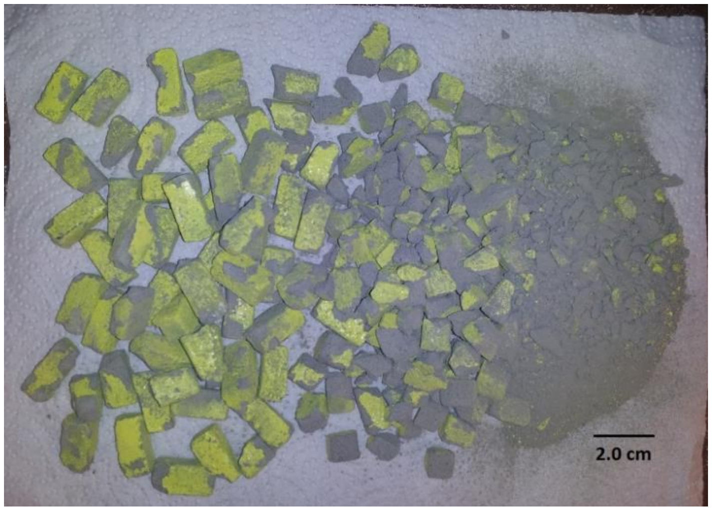

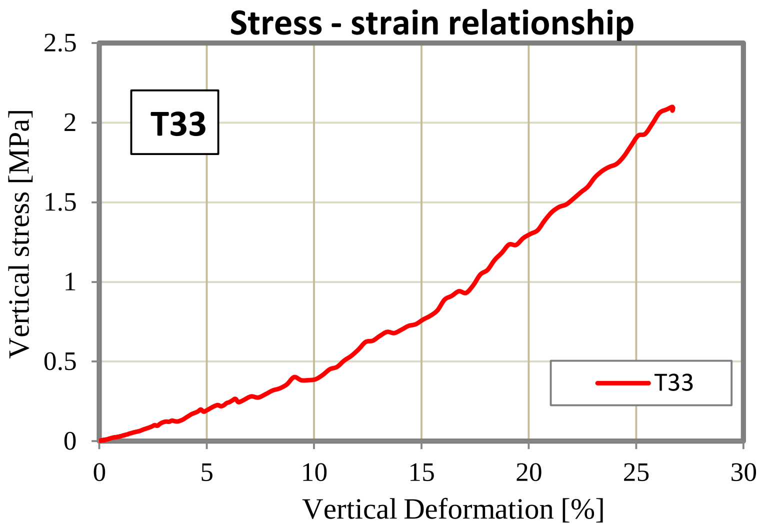

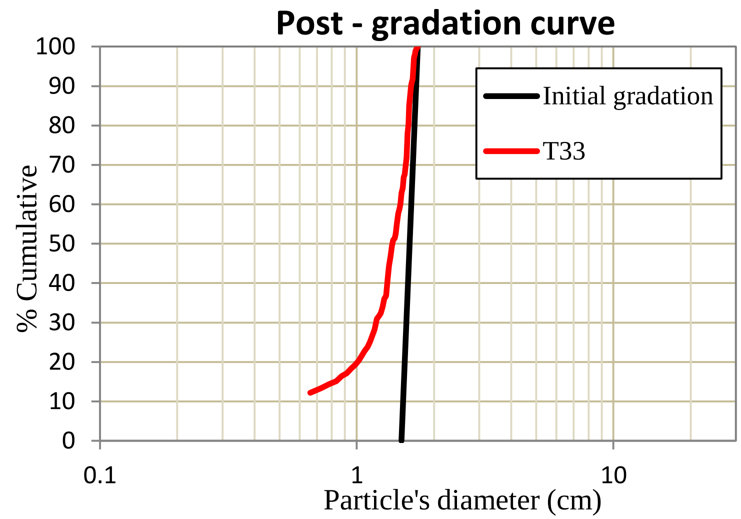

Plan view after testing

(Mould diameter = 10 cm)

Particles after testing

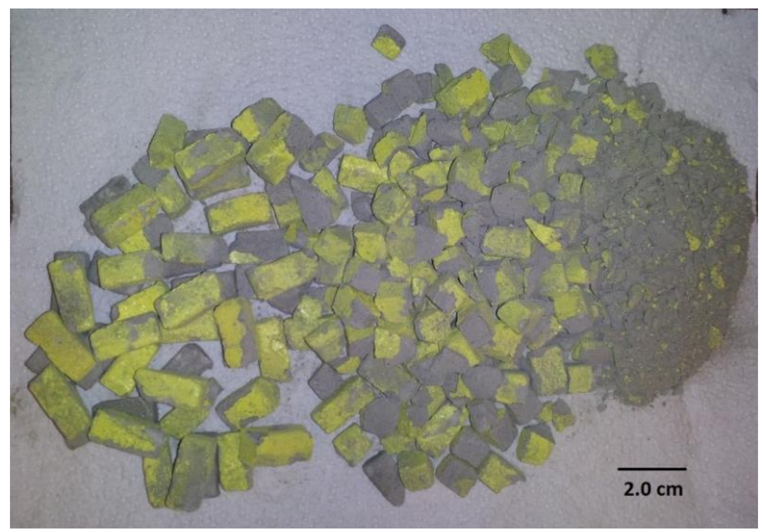

Stress - strain relationship

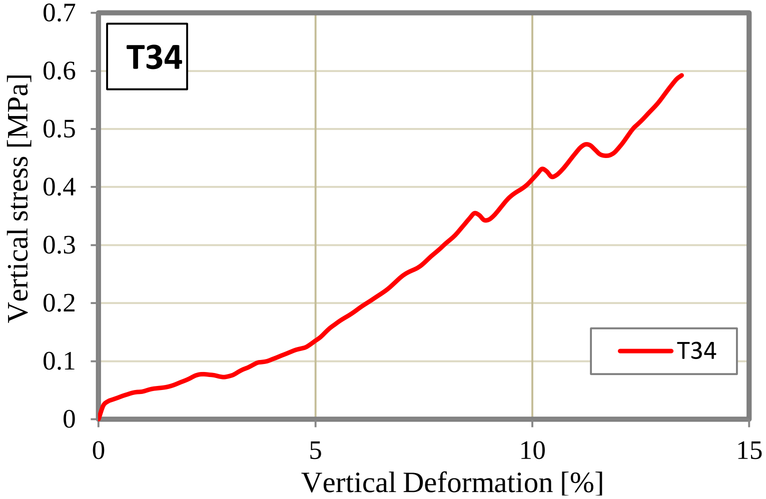

Post-gradation curve

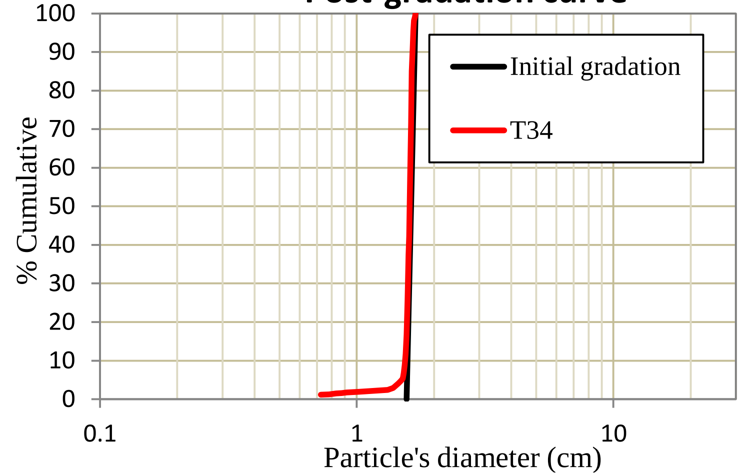

Plan view after testing

(Mould diameter = 10 cm)

Particles after testing

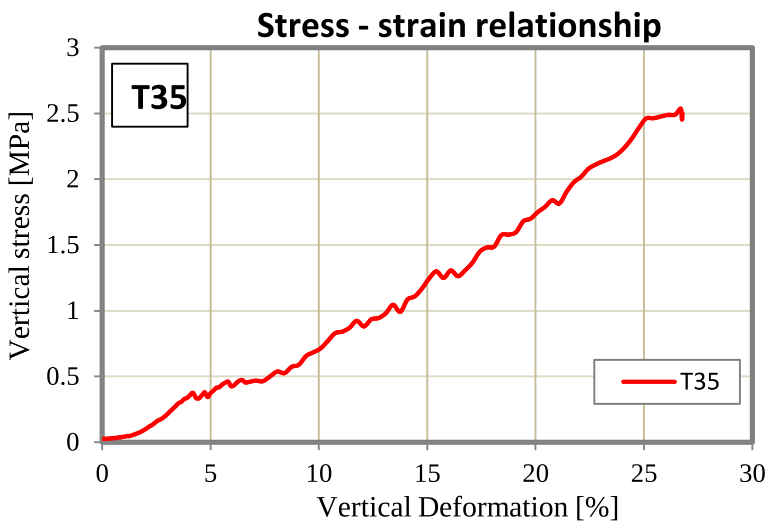

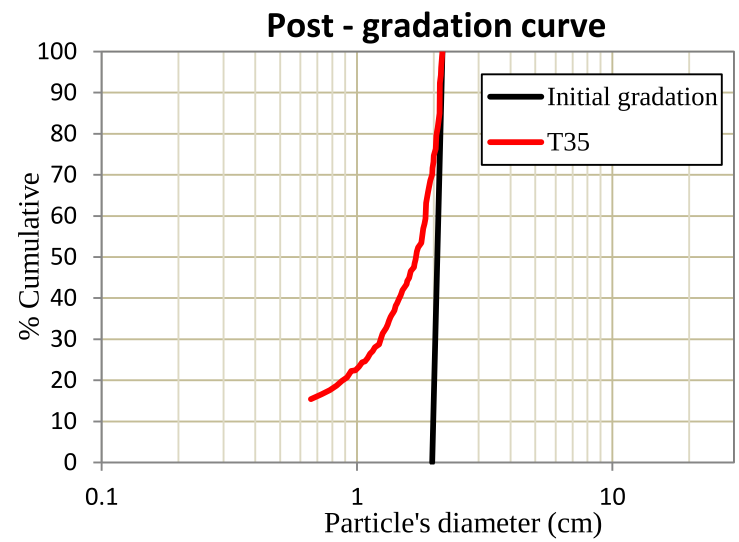

Plan view after testing

(Mould diameter = 10 cm)

Particles after testing

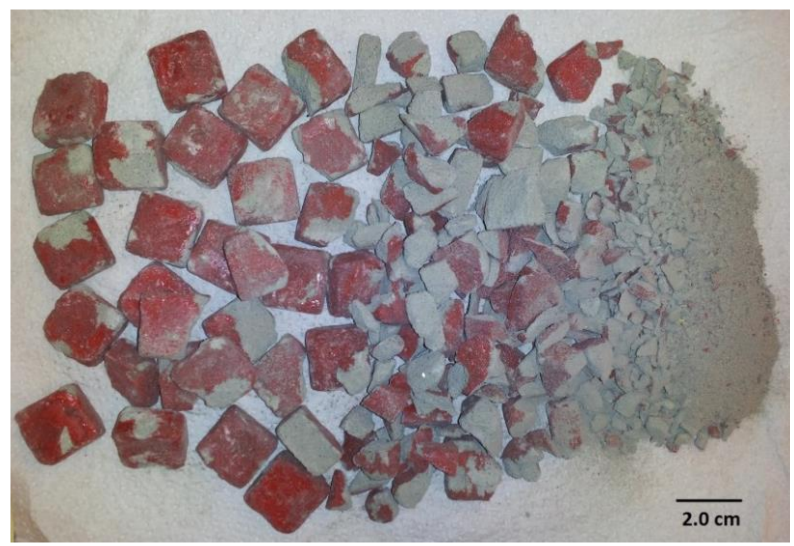

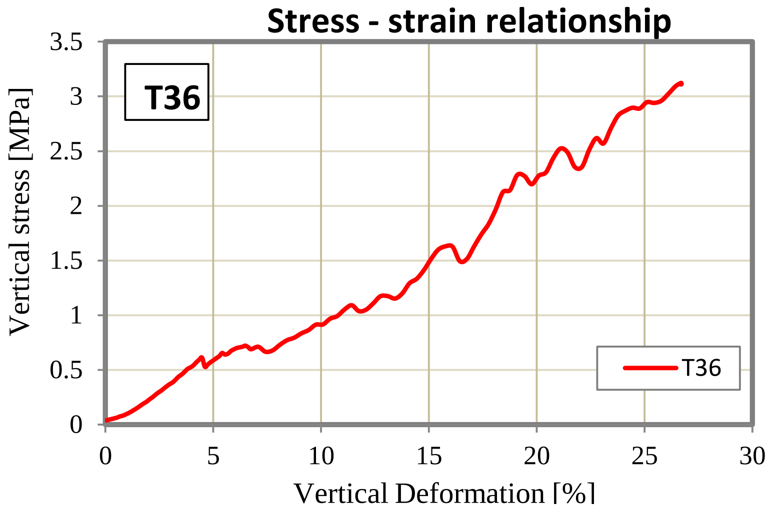

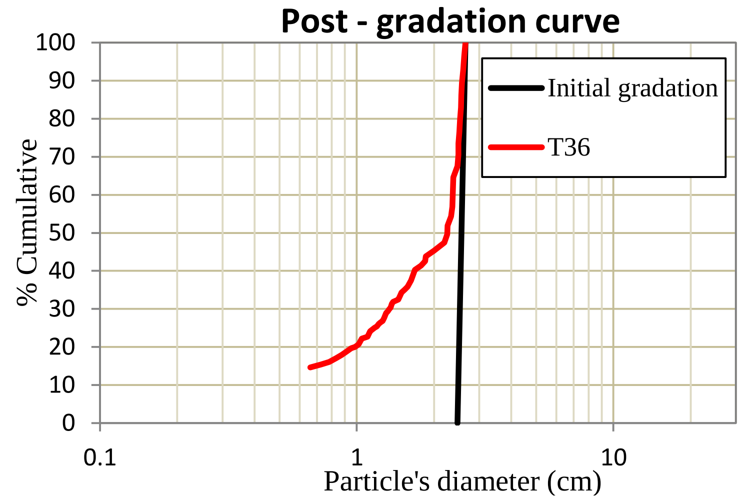

Plan view after testing

(Mould diameter = 10 cm)

Particles after testing

Stress - strain relationship

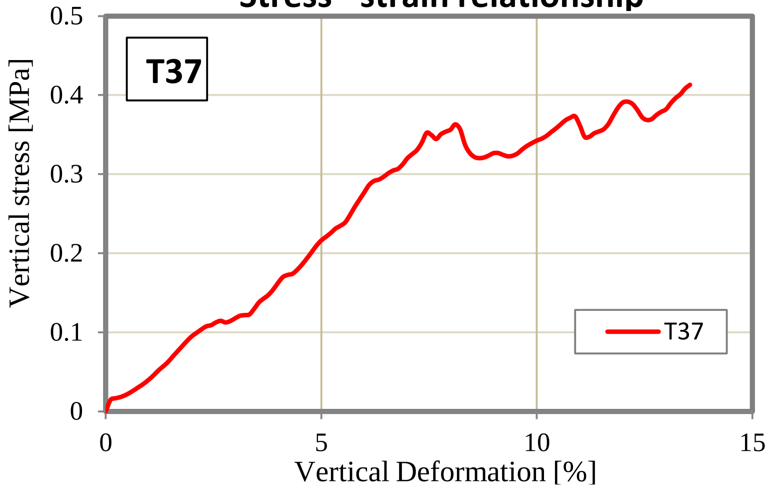

Post-gradation curve

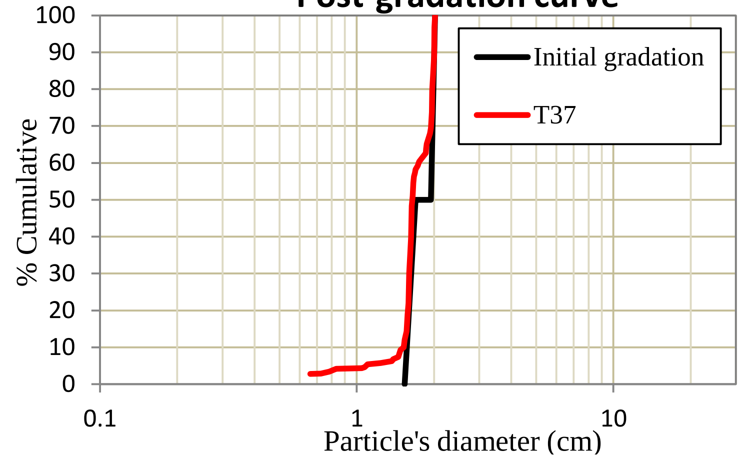

Plan view after testing

(Mould diameter = 10 cm)

Particles after testing

Stress - strain relationship

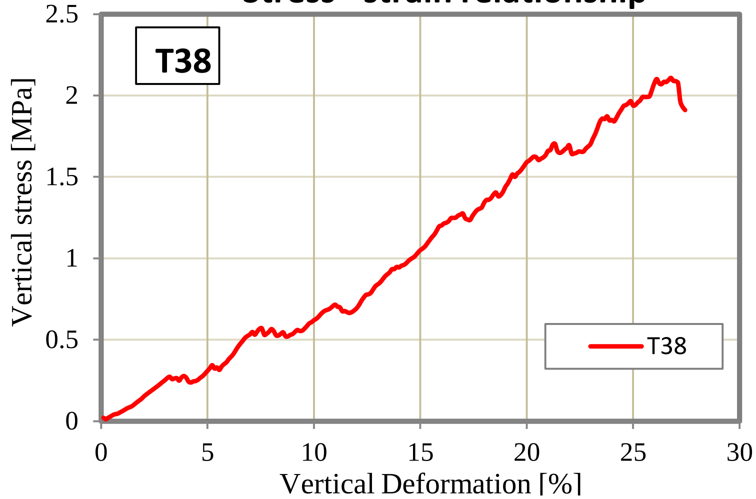

Post - gradation curve

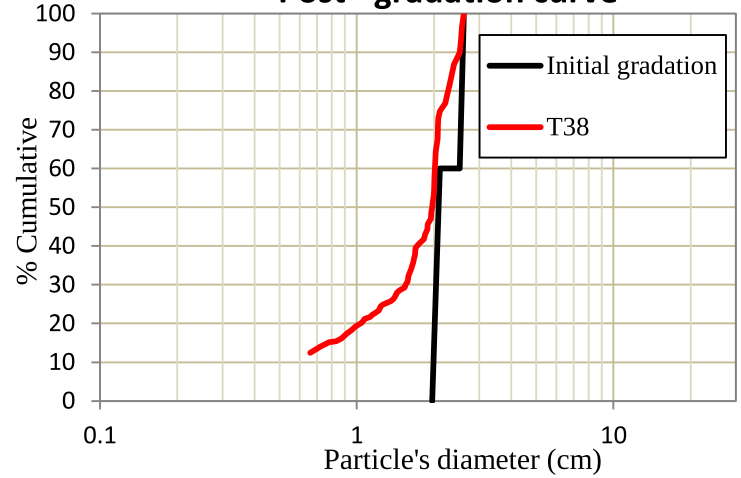

Plan view after testing

(Mould diameter = 10 cm)

Particles after testing

Stress - strain relationship

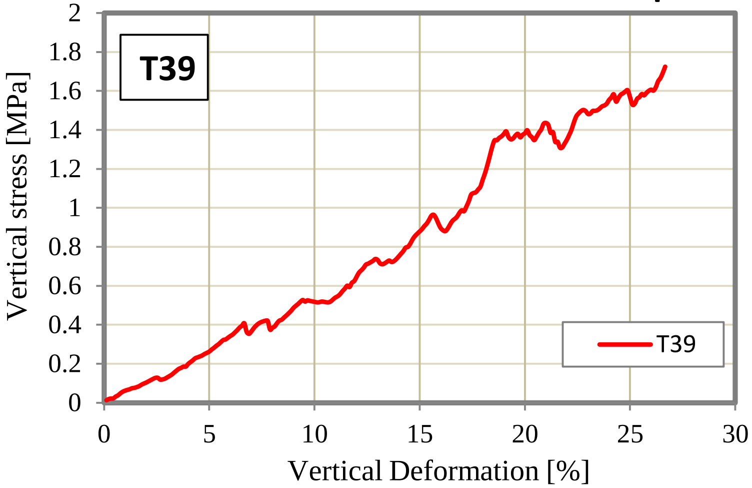

Post - gradation curve

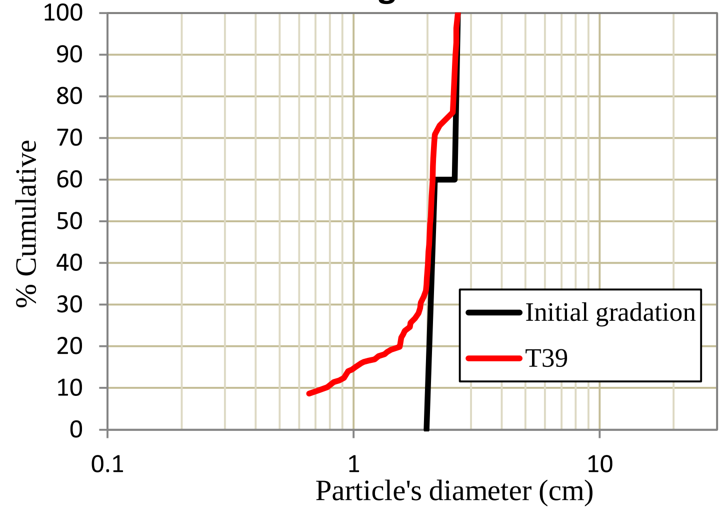

Plan view after testing

(Mould diameter = 10 cm)

Particles after testing

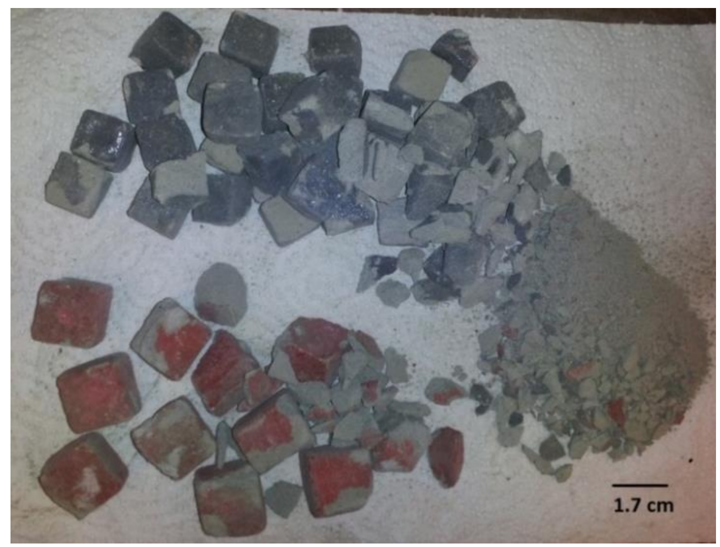

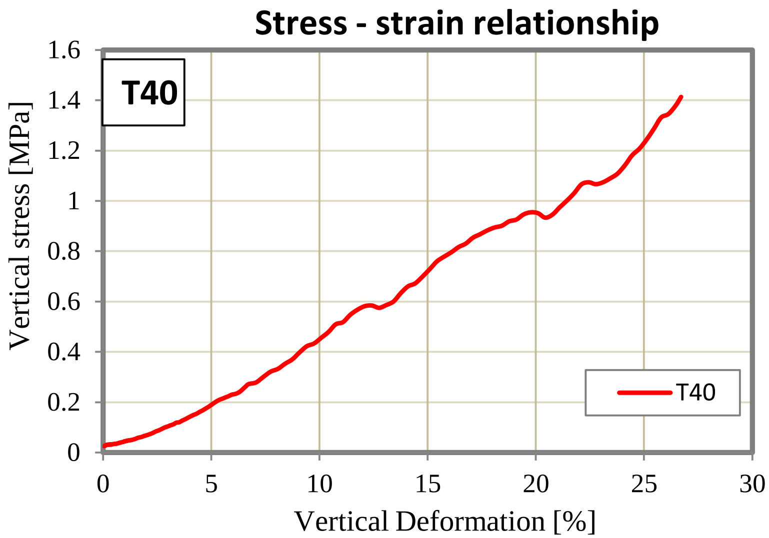

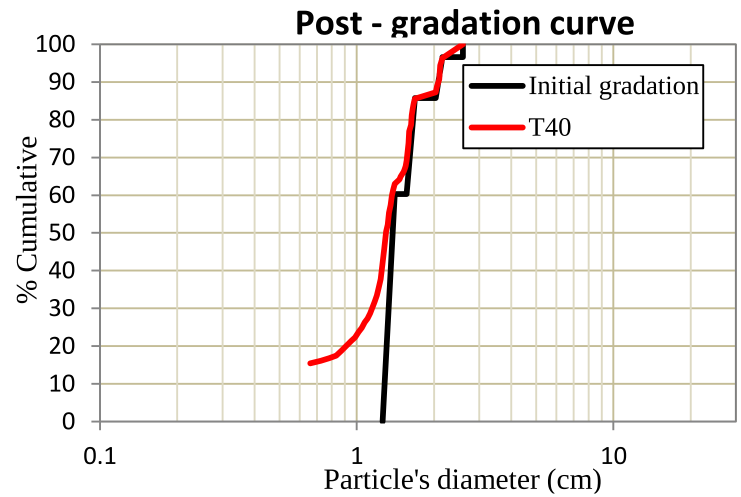

Particles before testing

Particles after testing

Stress - strain relationship

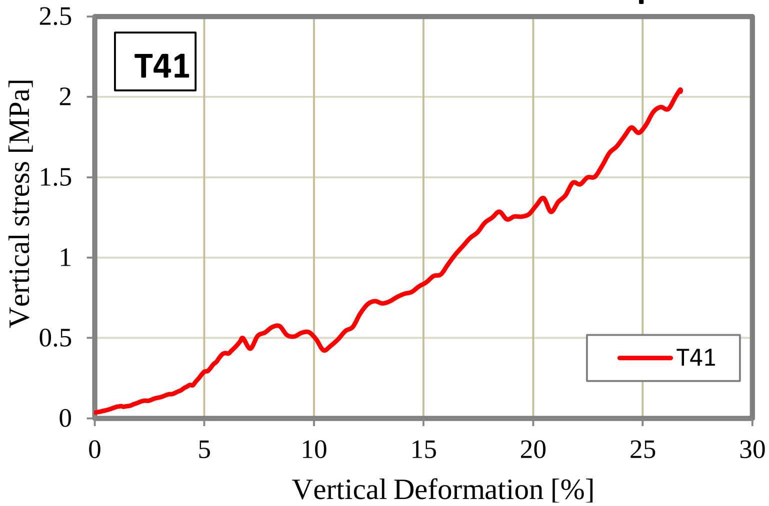

Post - gradation curve

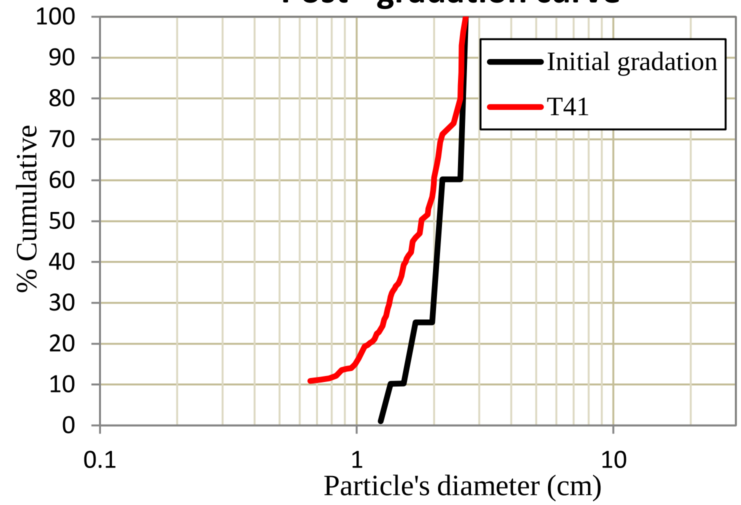

Particles before testing

Particles after testing

Stress - strain relationship

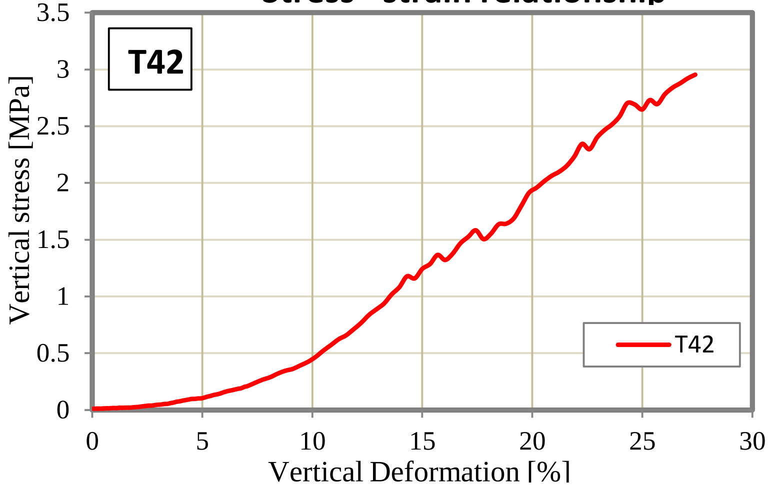

Post-gradation curve

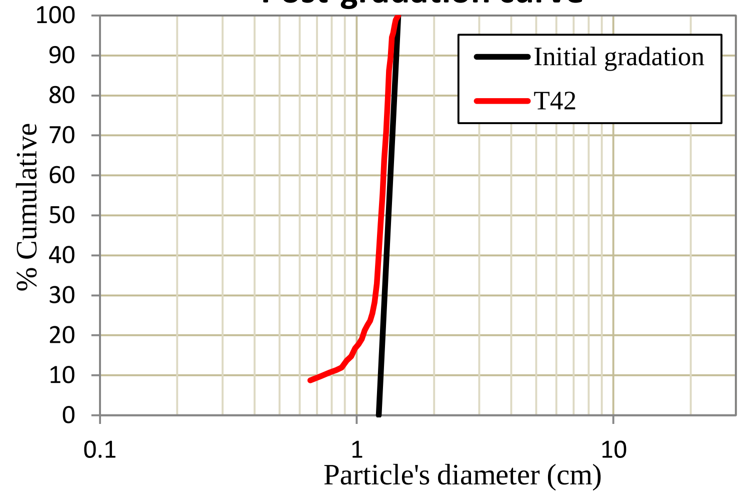

Plan view after testing

(Mould diameter = 10 cm)

Particles after testing

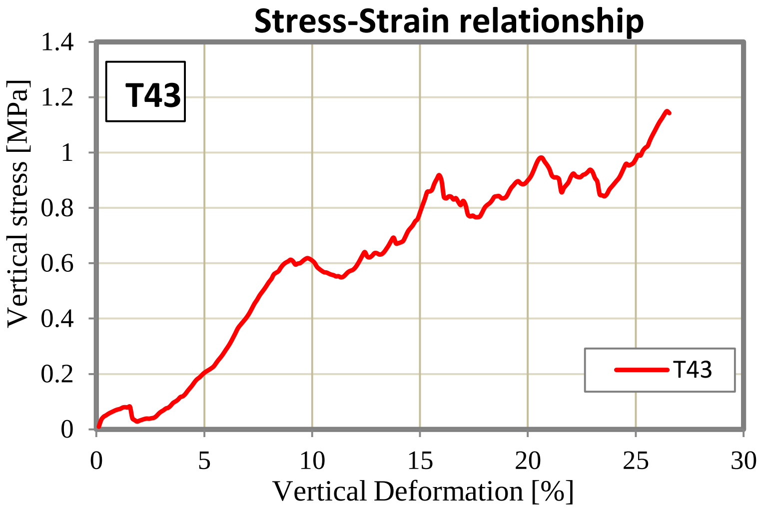

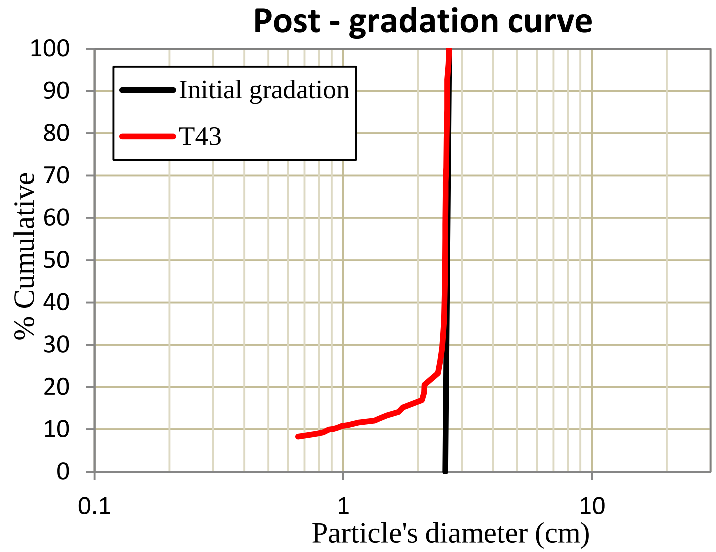

Plan view after testing

(Mould diameter = 10 cm)

Particles after testing

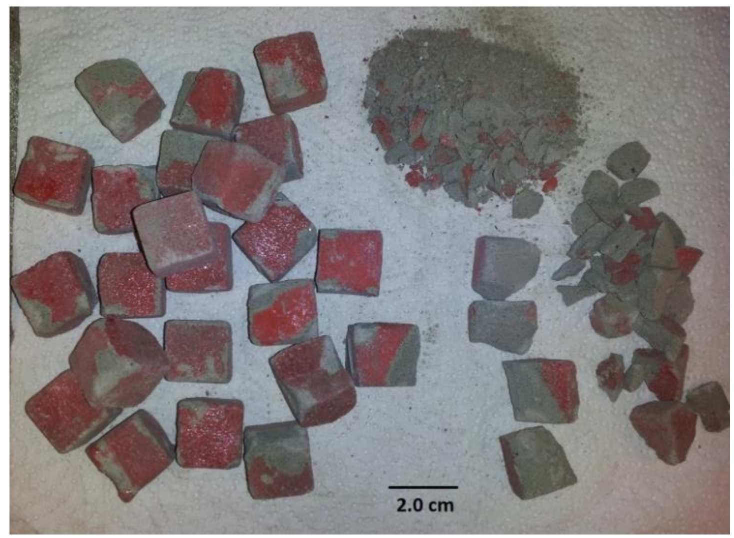

Stress - strain relationship

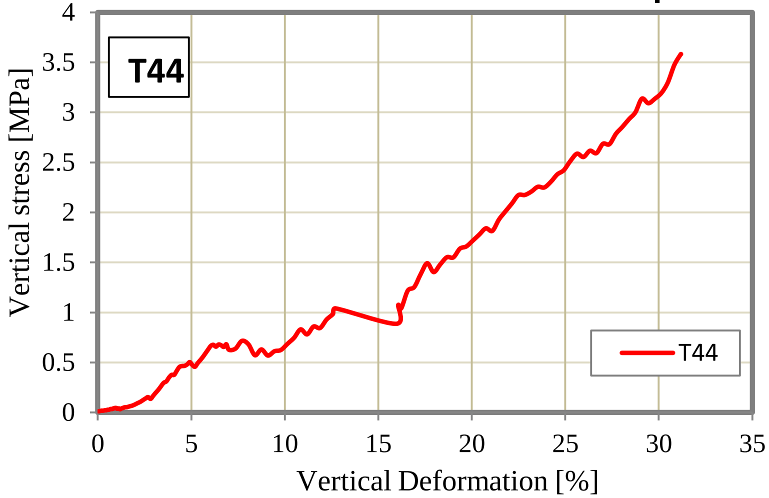

Post-gradation curve

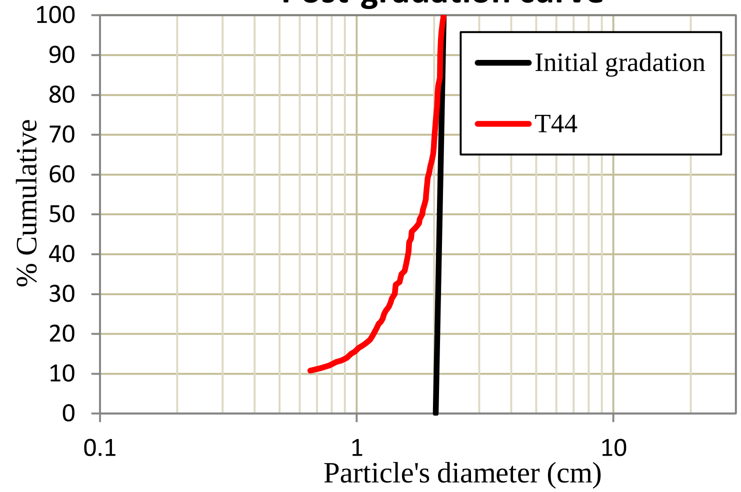

Plan view after testing

(Mould diameter = 10 cm)

Particles after testing

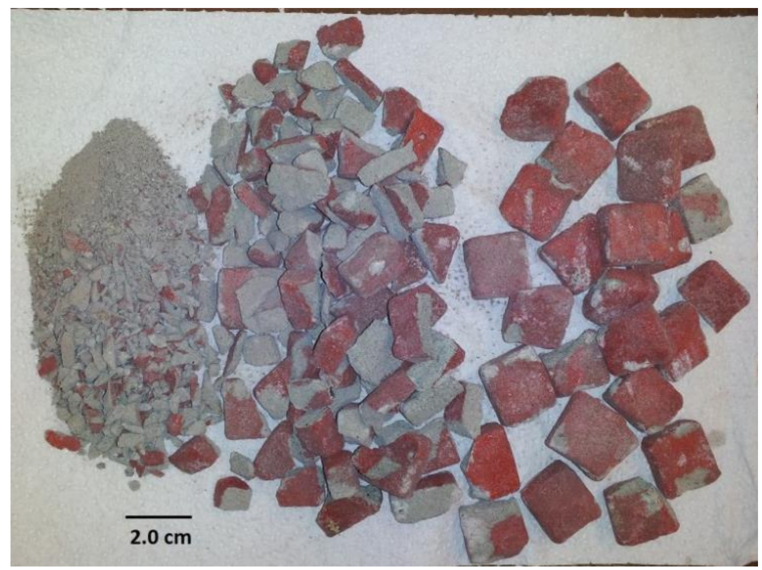

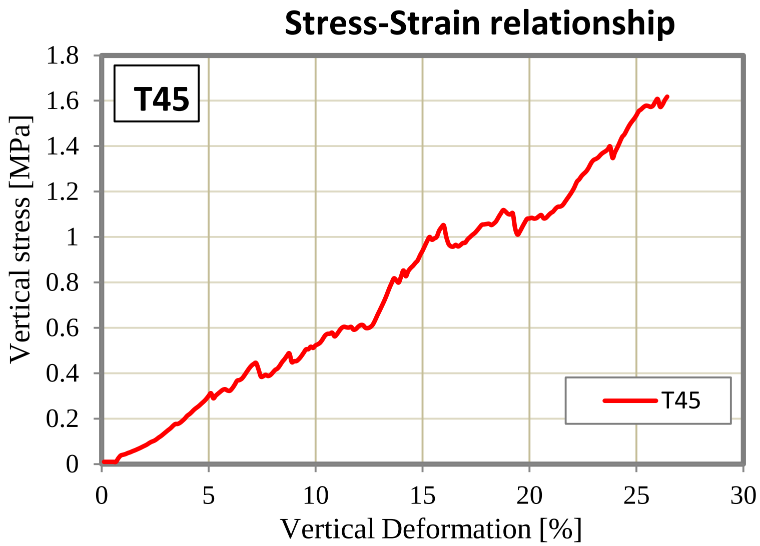

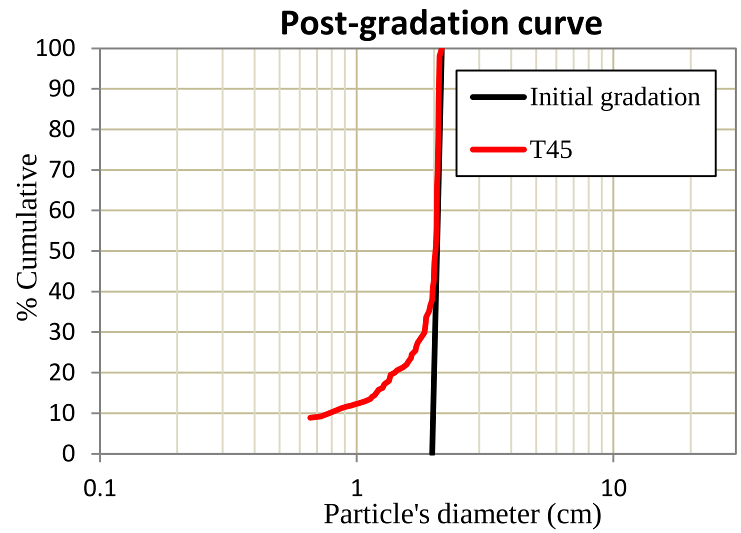

Plan view after testing

(Mould diameter = 10 cm)

Particles after testing

Stress-Strain relationship

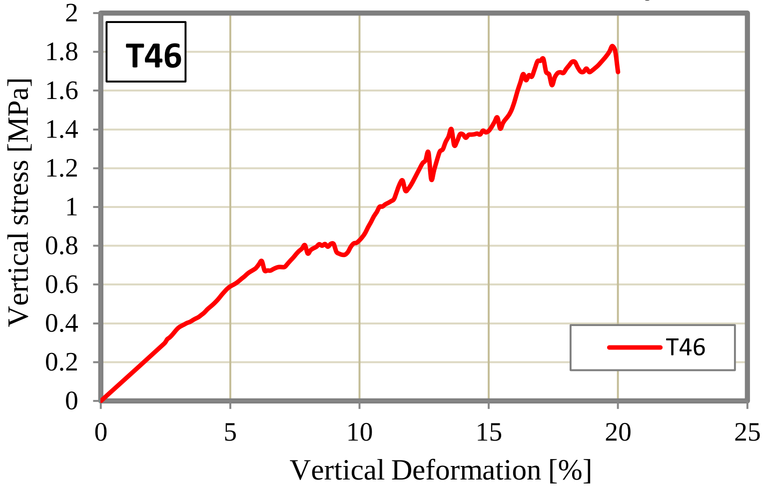

Post-gradation curve

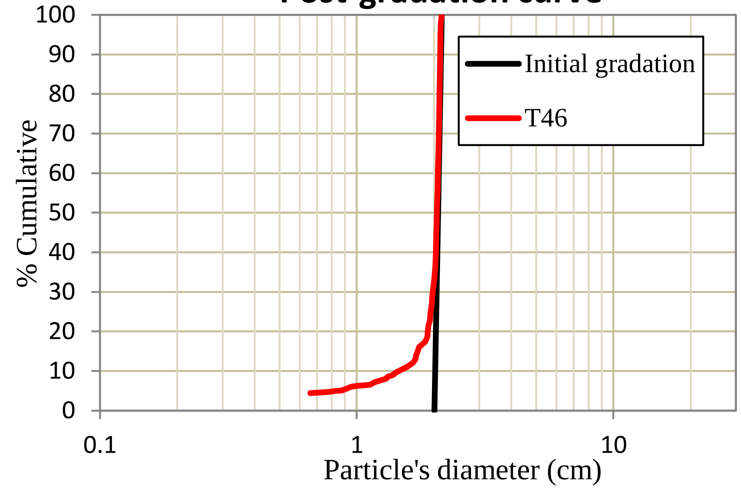

Plan view after testing

(Mould diameter = 10 cm)

Particles after testing

Stress - strain relationship

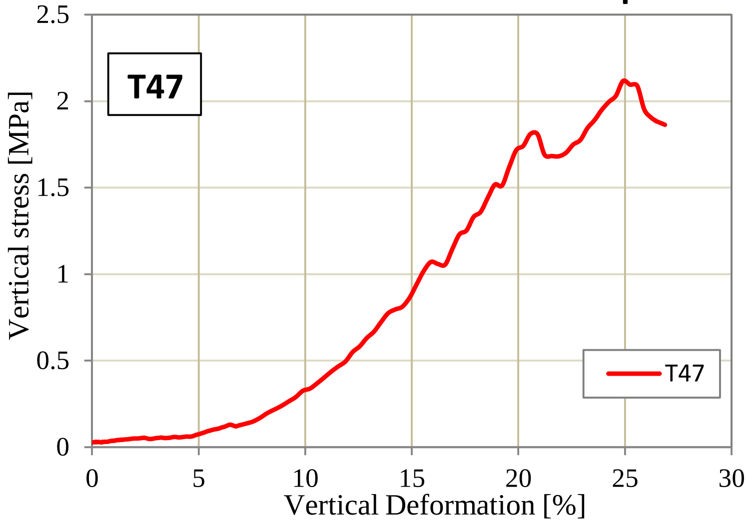

Post-gradation curve

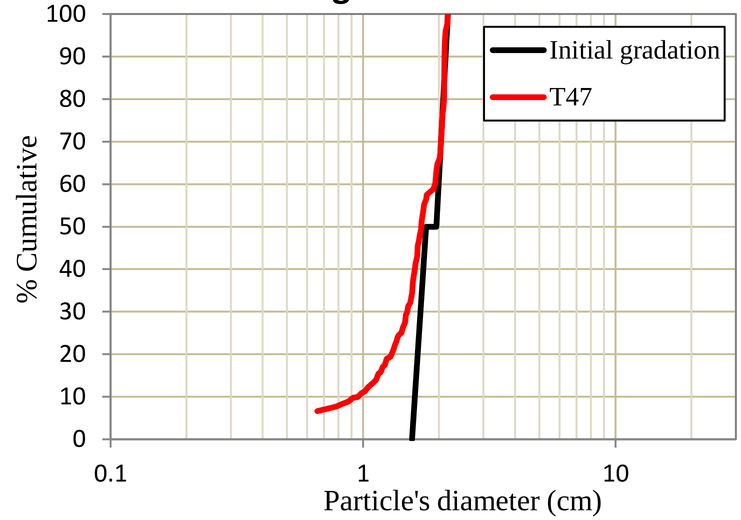

Plan view after testing

(Mould diameter = 10 cm)

Particles after testing

Stress - strain relationship

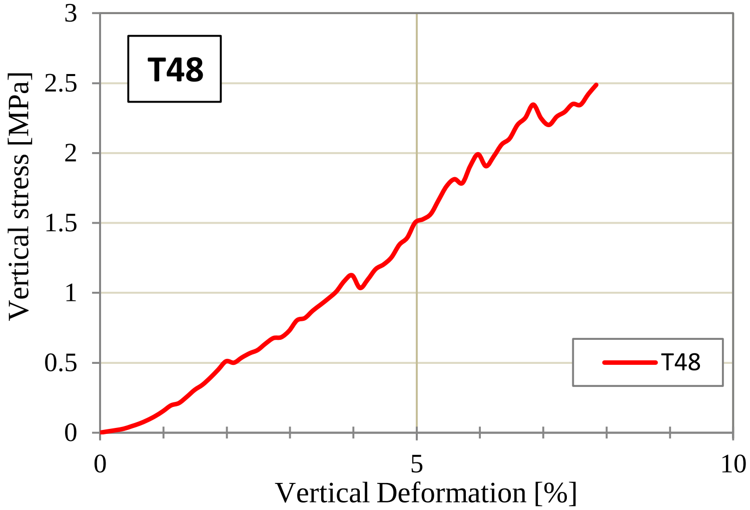

Post - gradation curve

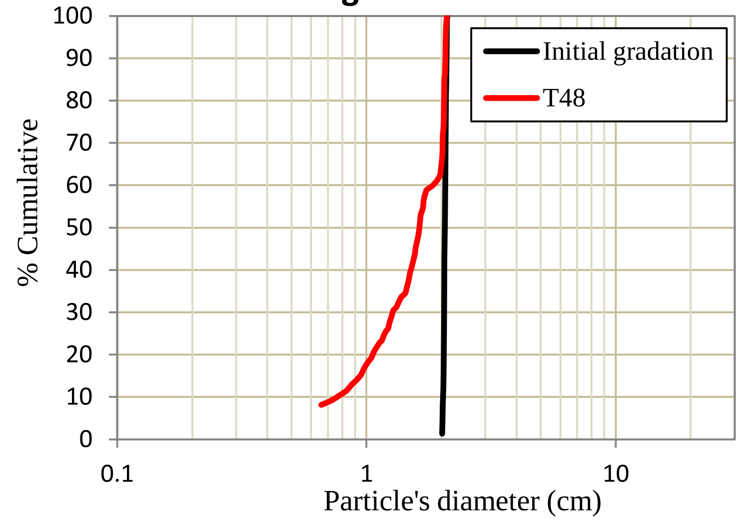

Plan view after testing

(Mould diameter = 10 cm)

Particles after testing

Stress - strain relationship

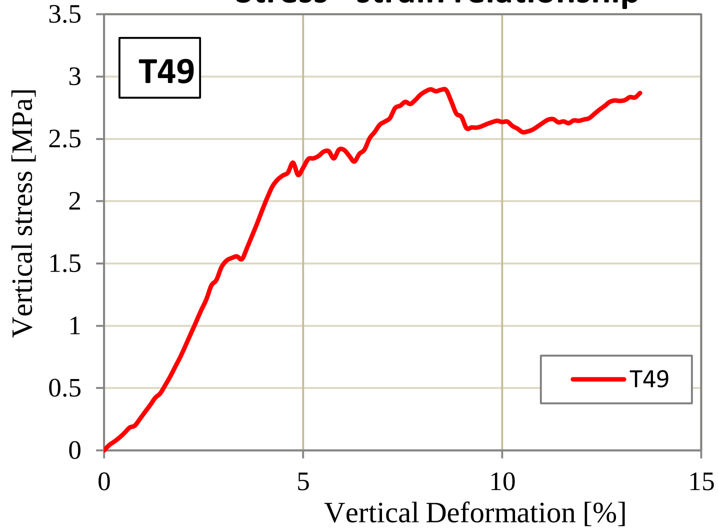

Post - gradation curve

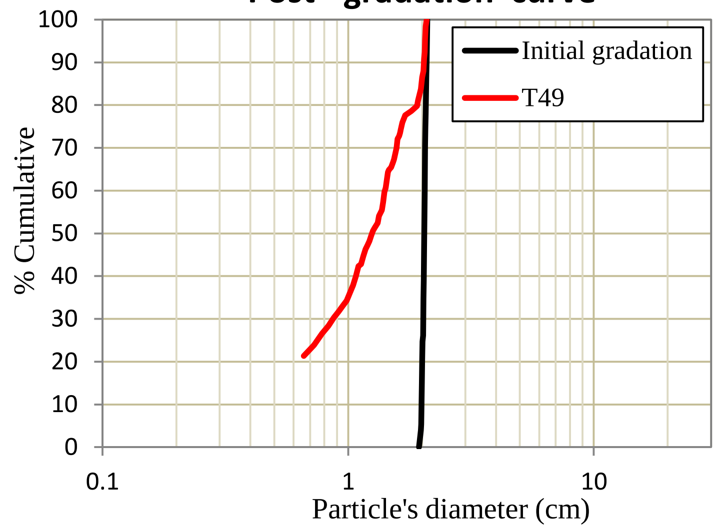

Plan view after testing

(Mould diameter = 10 cm)

Particles after testing

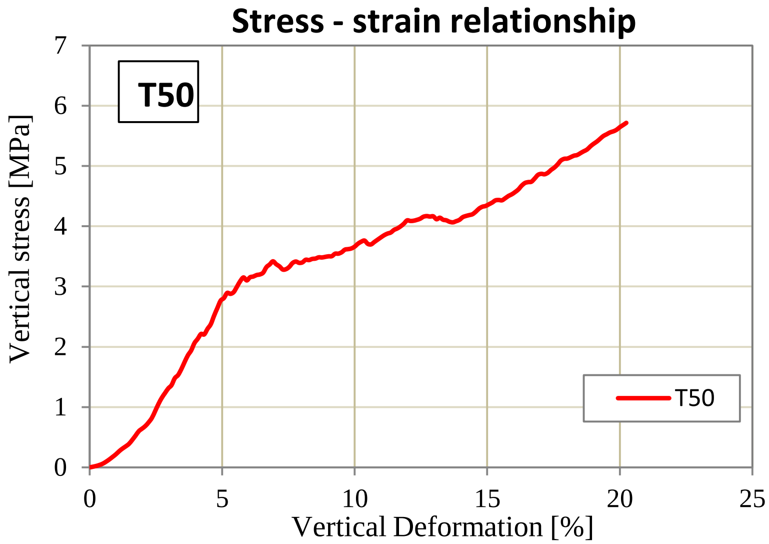

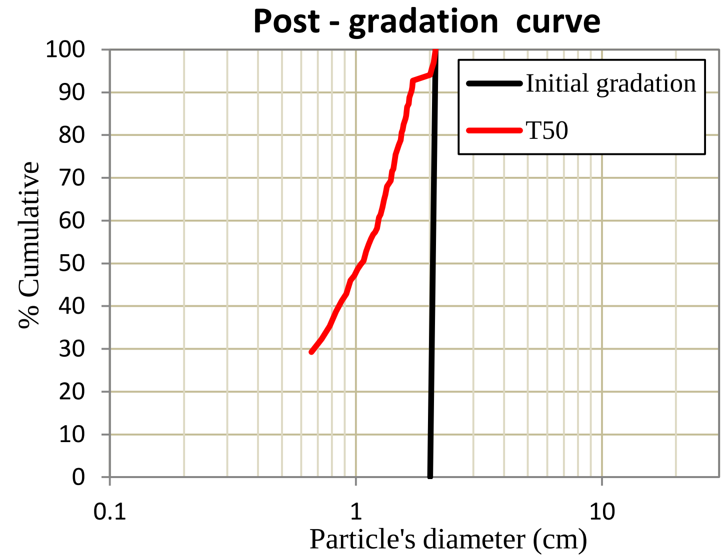

Plan view after testing

(Mould diameter = 10 cm)

Particles after testing

Stress - strain relationship

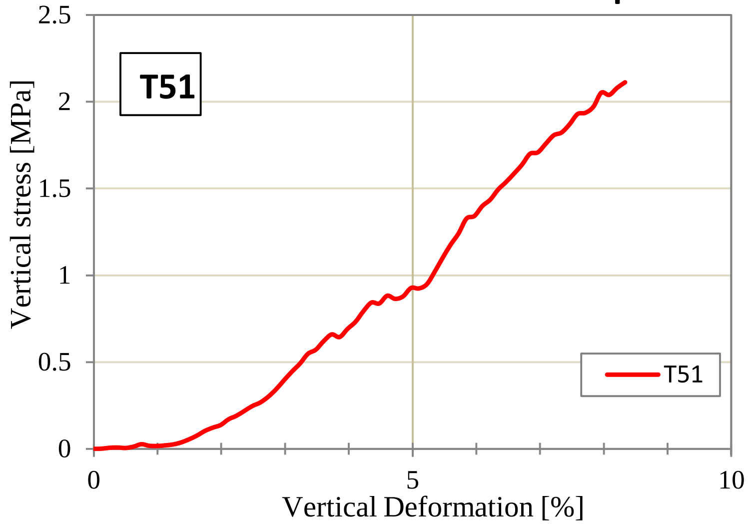

Post - gradation curve

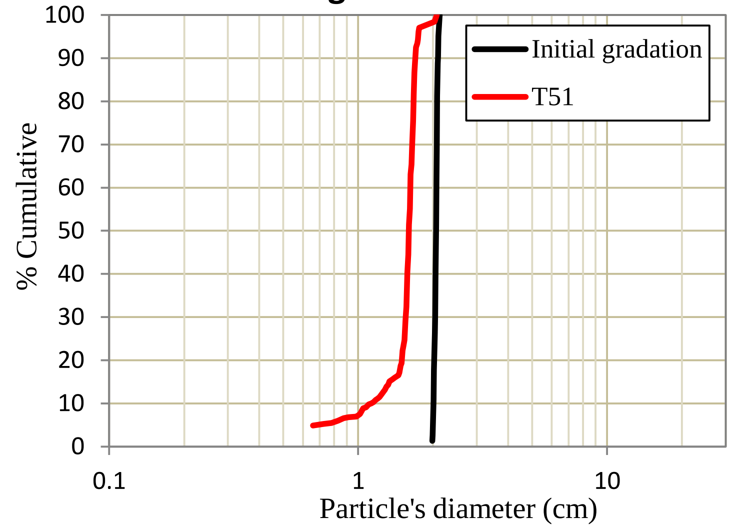

Plan view after testing

(Mould diameter = 10 cm)

Particles after testing

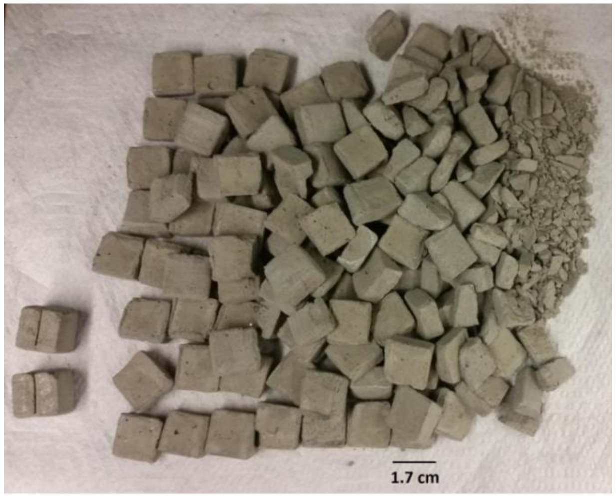

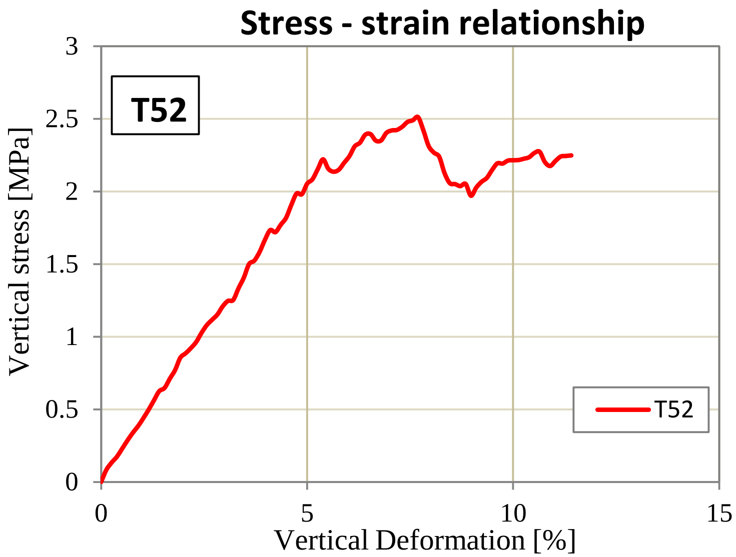

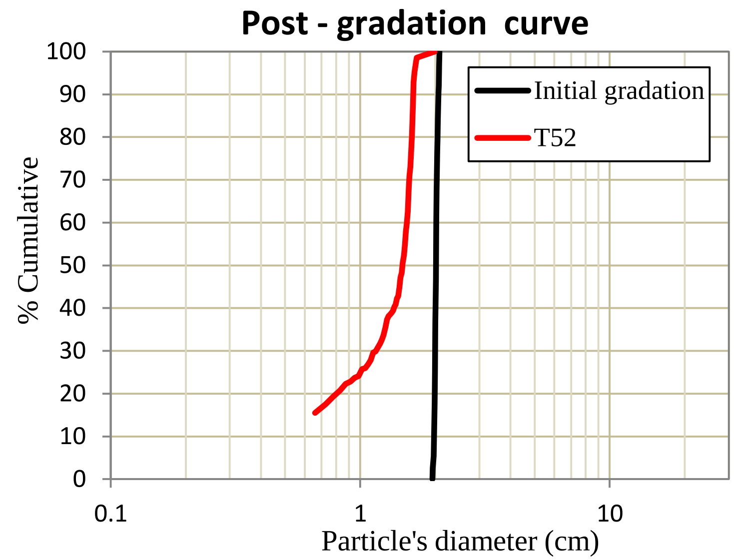

Plan view after testing

(Mould diameter = 10 cm)

Particles after testing

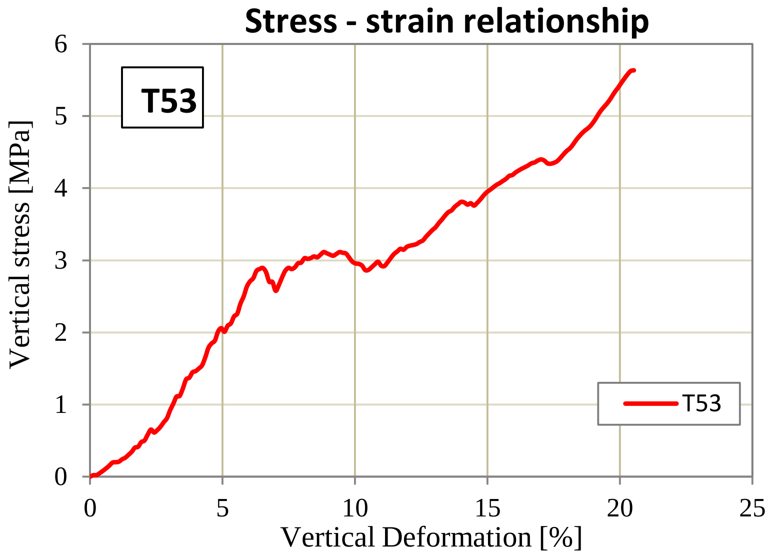

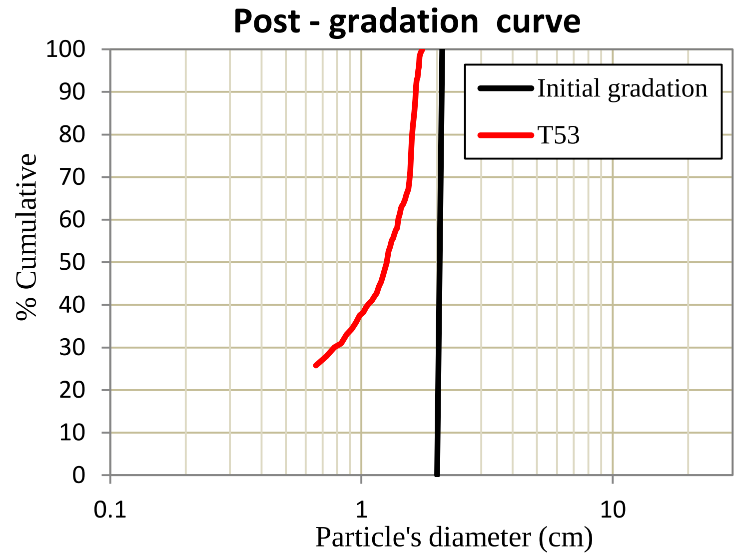

Plan view after testing

(Mould diameter = 10 cm)

Particles after testing

Stress - strain relationship

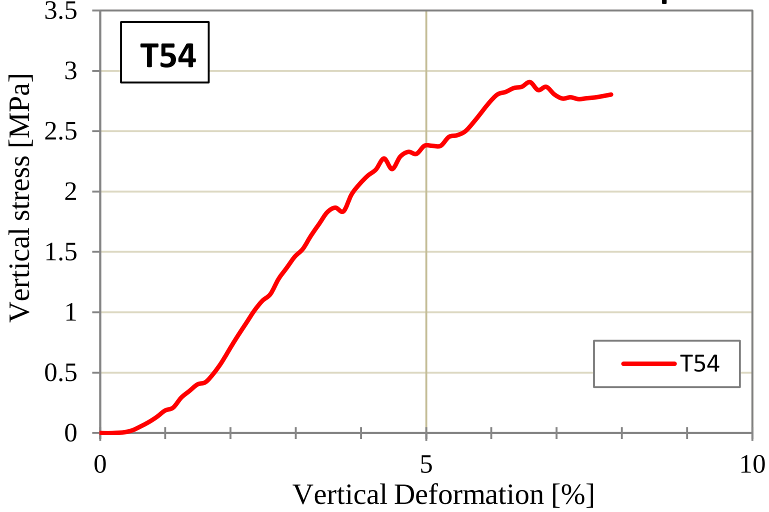

Post - gradation curve

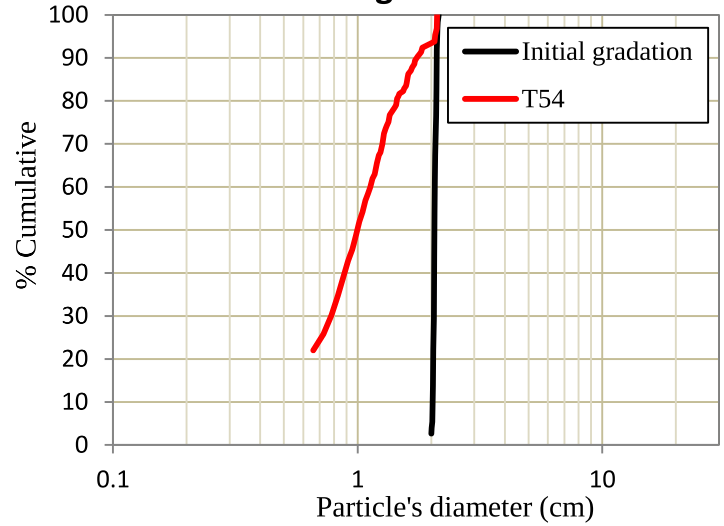

Plan view after testing

(Mould diameter = 10 cm)

Particles after testing

Stress - strain relationship

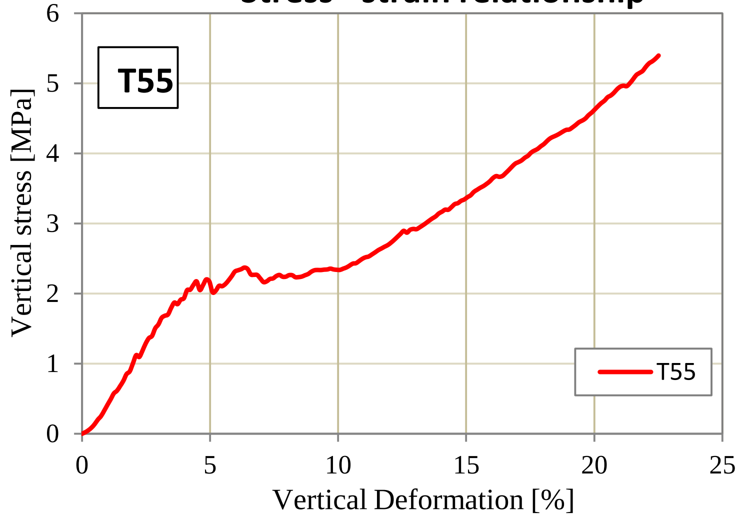

Post - gradation curve

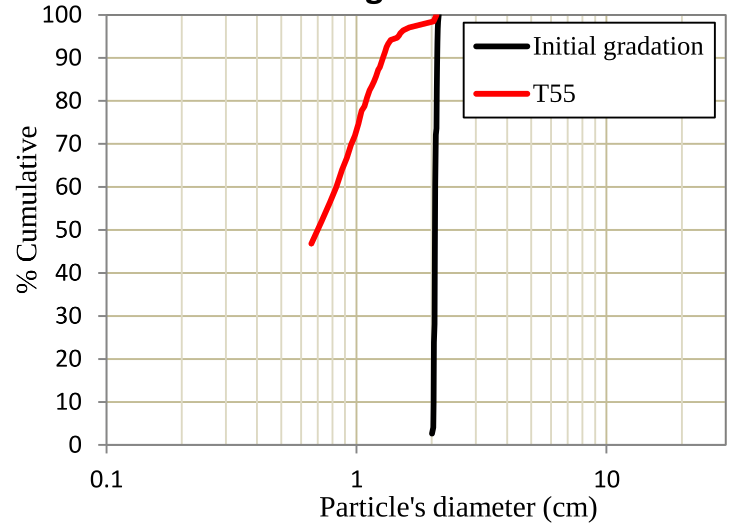

Plan view after testing

(Mould diameter = 10 cm)

Particles after testing

Stress - strain relationship

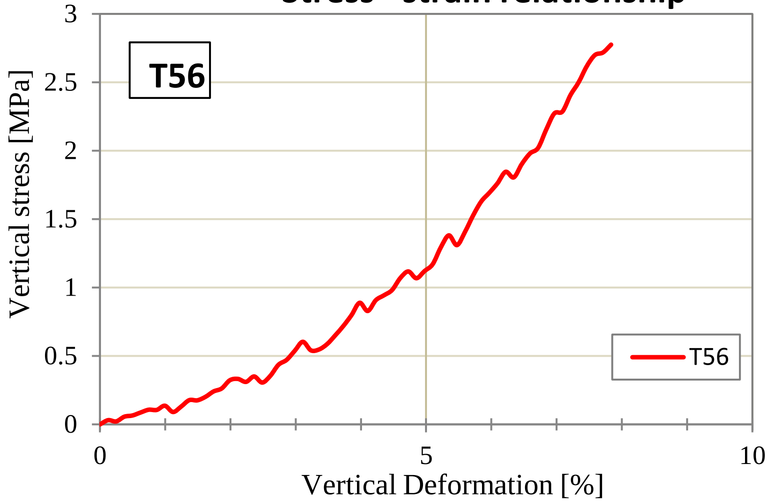

Post - gradation curve

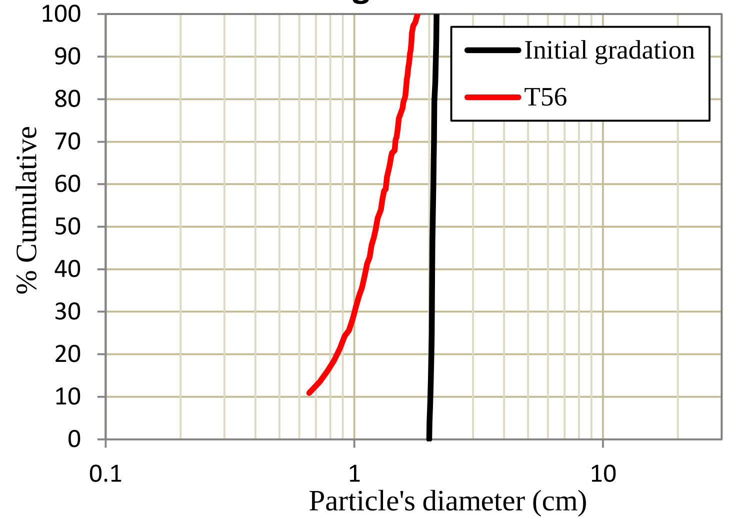

Plan view after testing

(Mould diameter = 10 cm)

Particles after testing

Stress - strain relationship

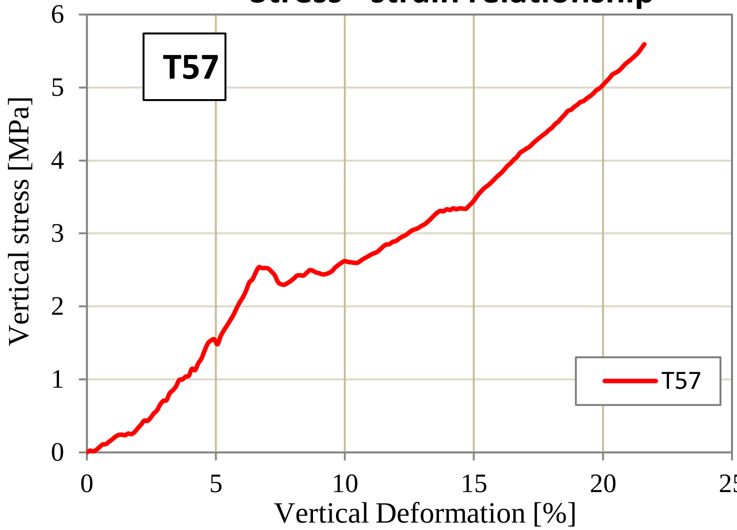

Post - gradation curve

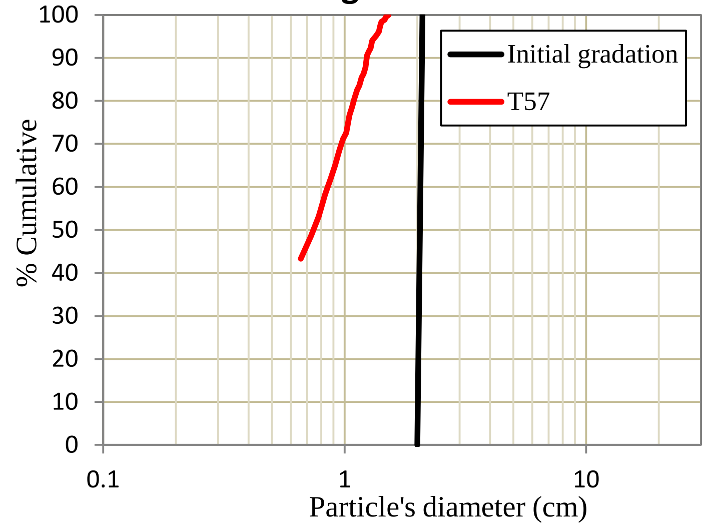

Plan view after testing

(Mould diameter = 10 cm)

Particles after testing

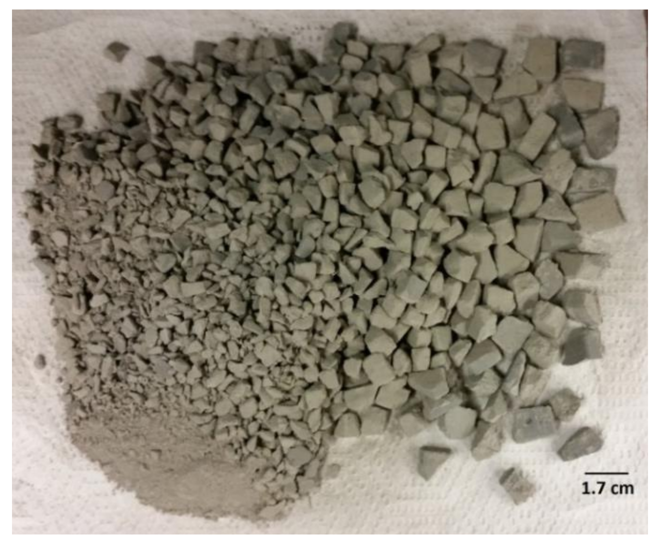

Stress - strain relationship

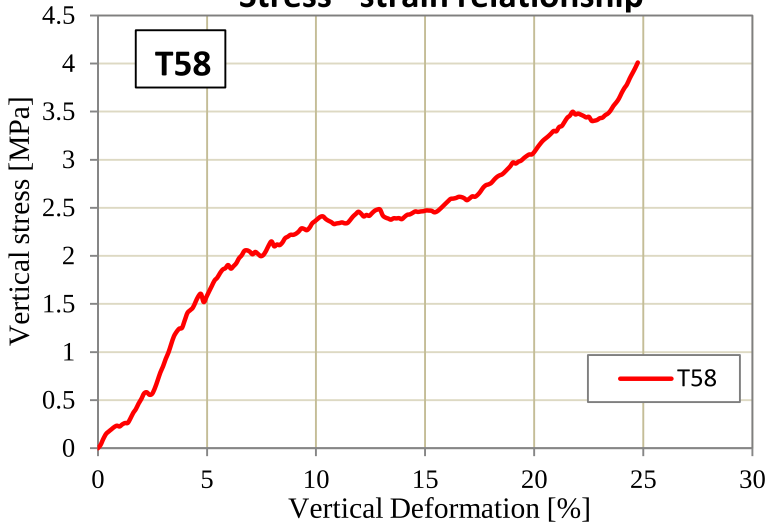

Post - gradation curve

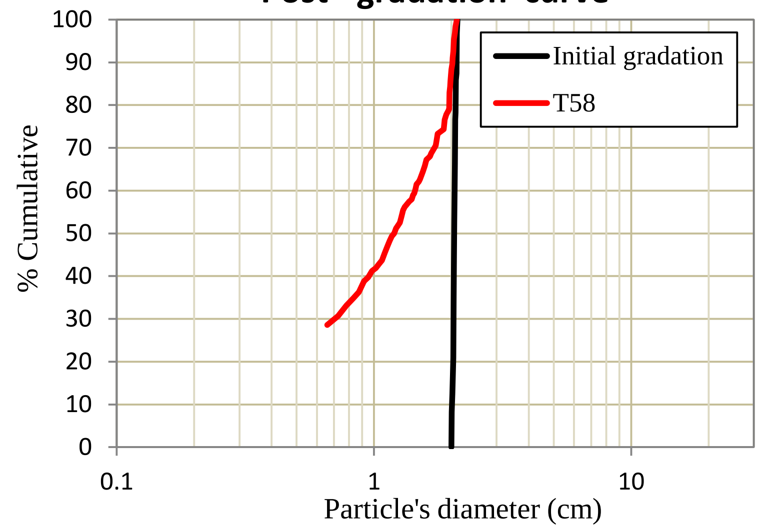

Plan view after testing

Particles after testing

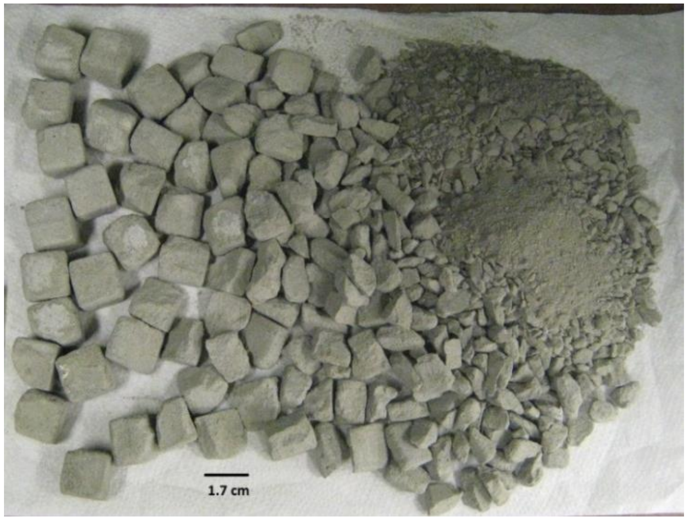

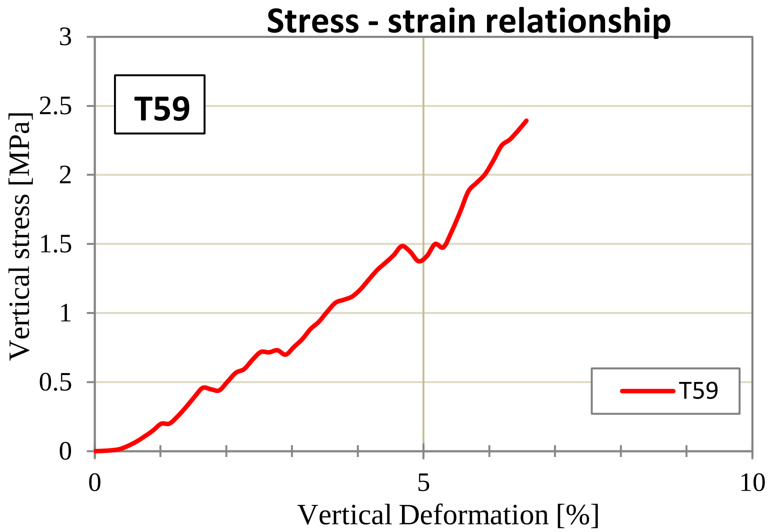

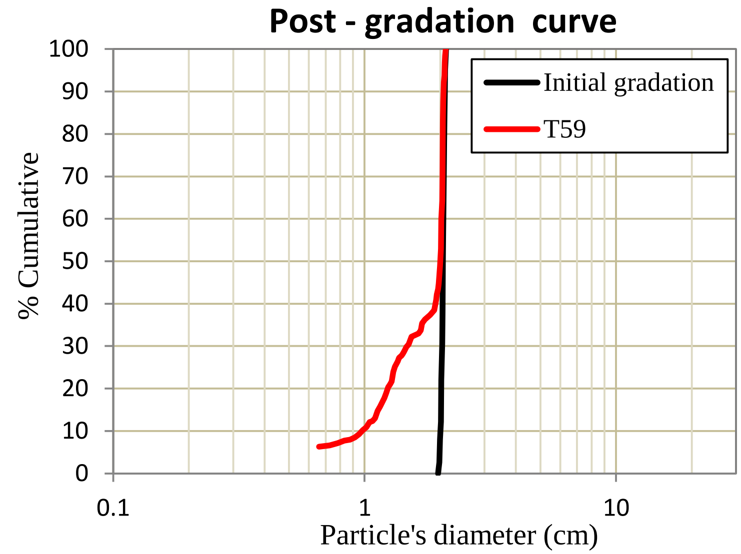

Plan view after testing

(Mould diameter = 10 cm)

Particles after testing

Stress - strain relationship

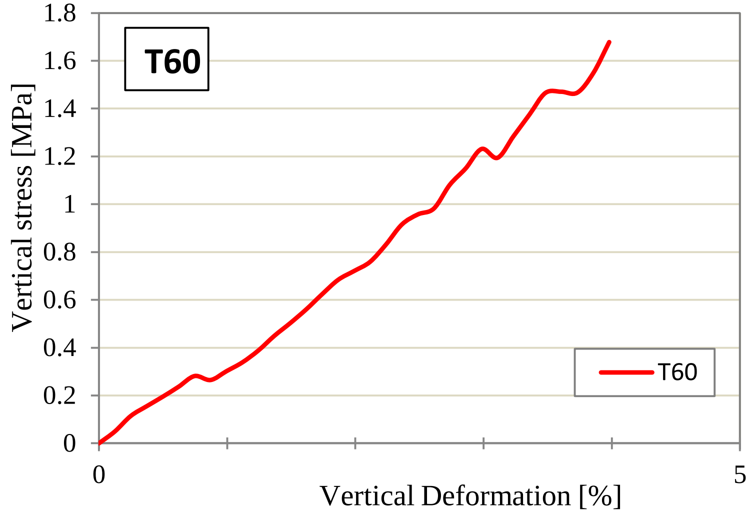

Post - gradation curve

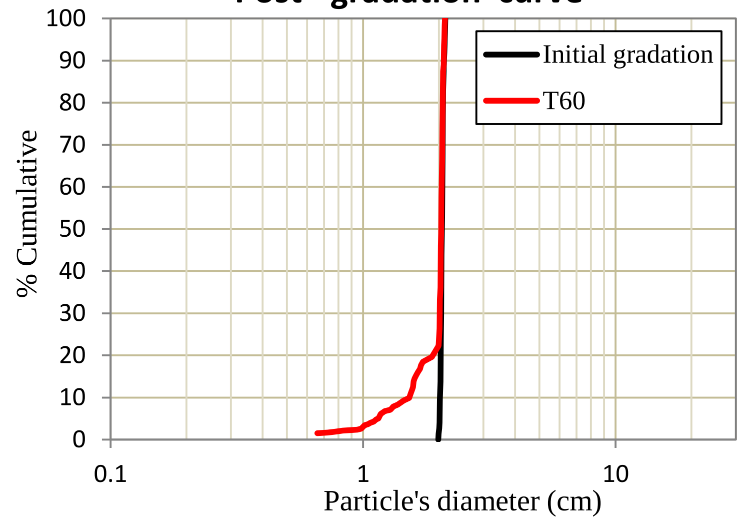

Plan view after testing

(Mould diameter = 10 cm)

Particles after testing

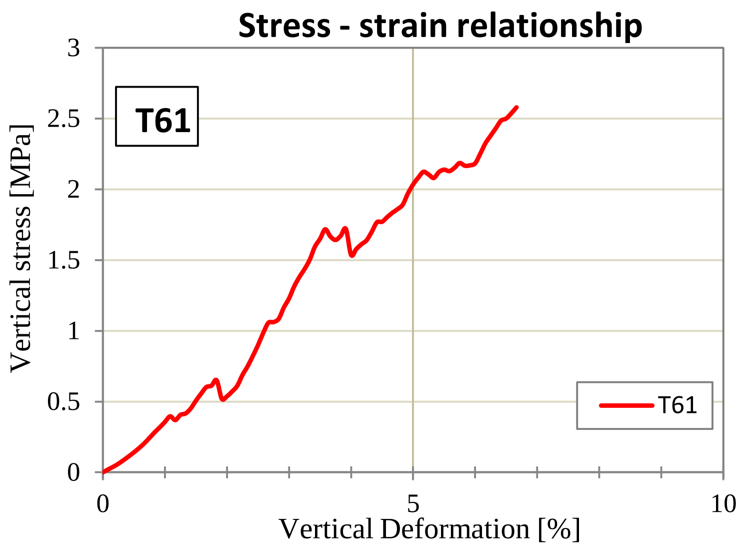

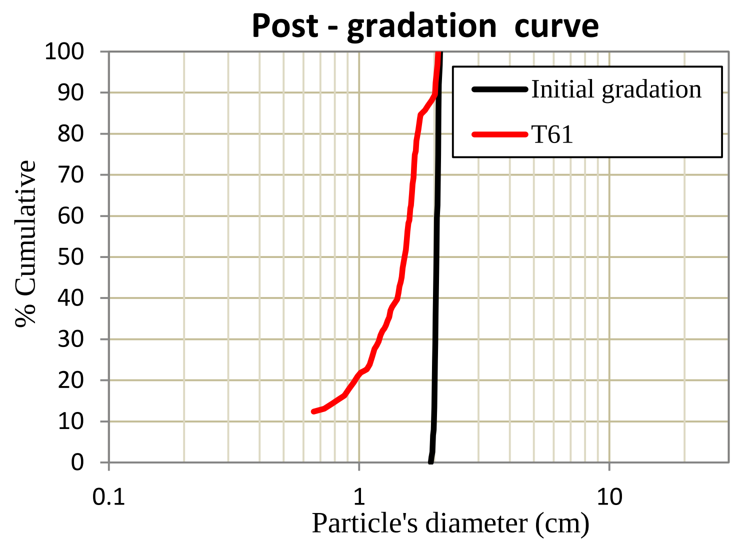

Plan view after testing

(Mould diameter = 10 cm)

Particles after testing

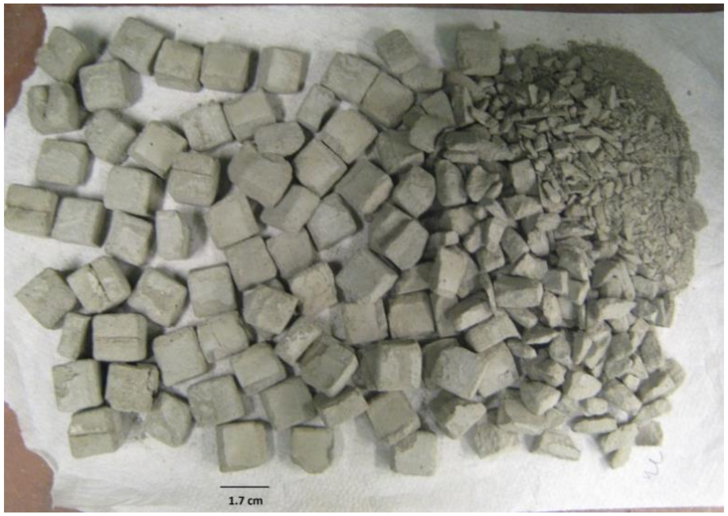

Stress - strain relationship

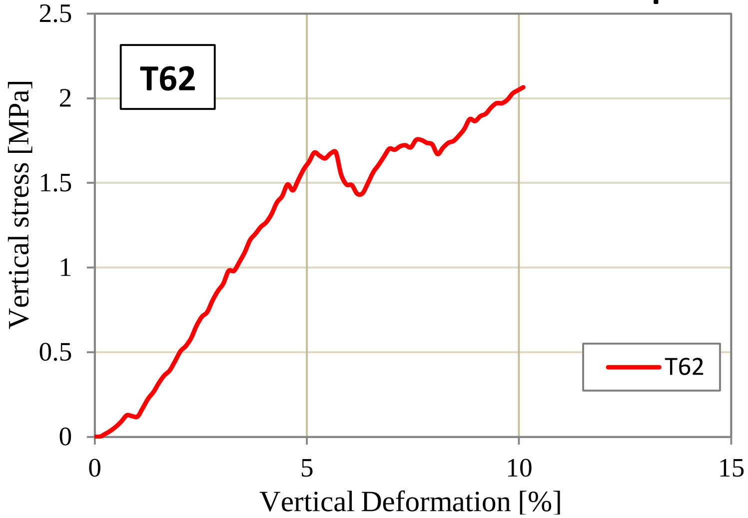

Post - gradation curve

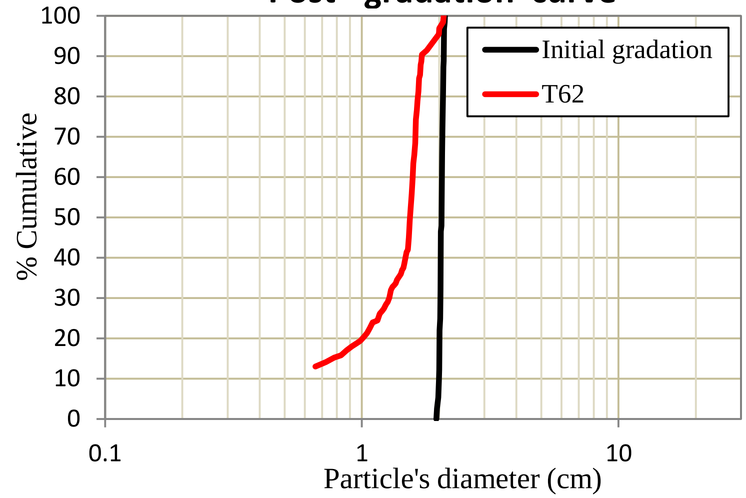

Plan view after testing

(Mould diameter = 10 cm)

Particles after testing

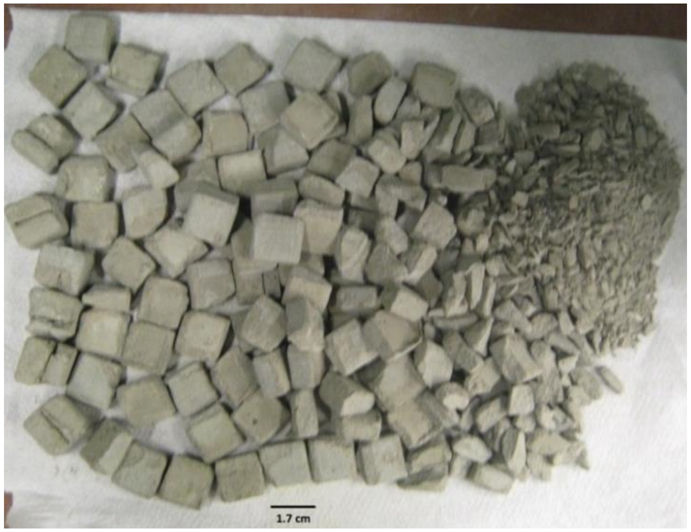

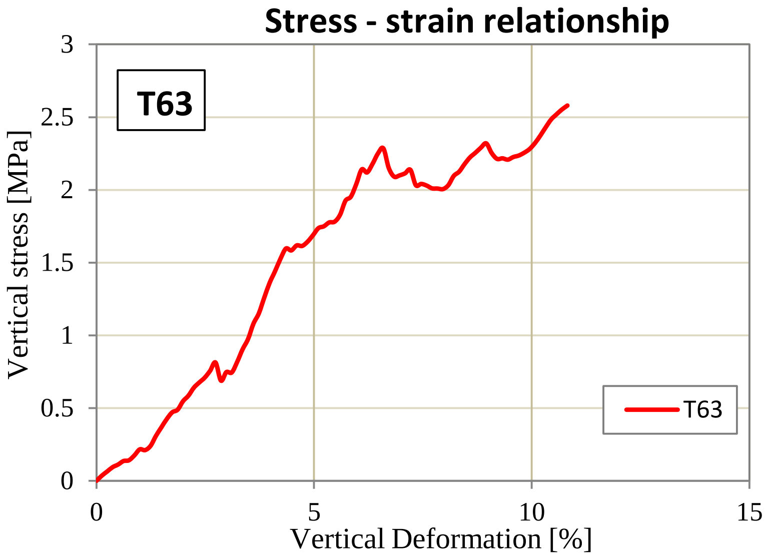

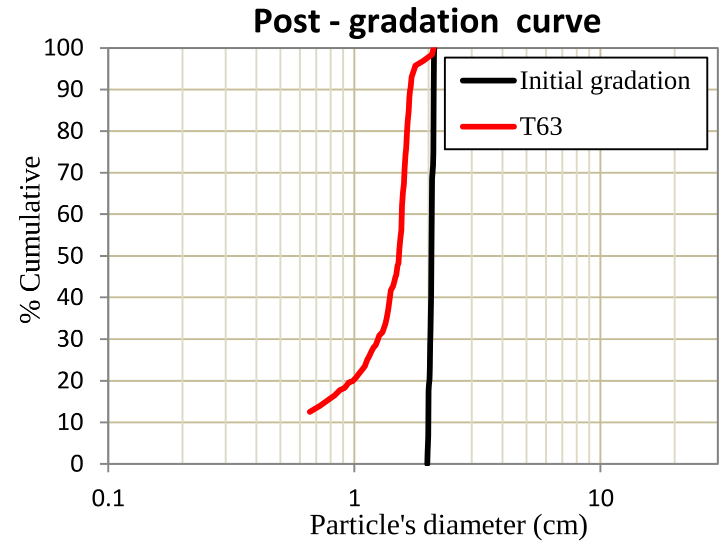

Particles after testing

Stress - strain relationship

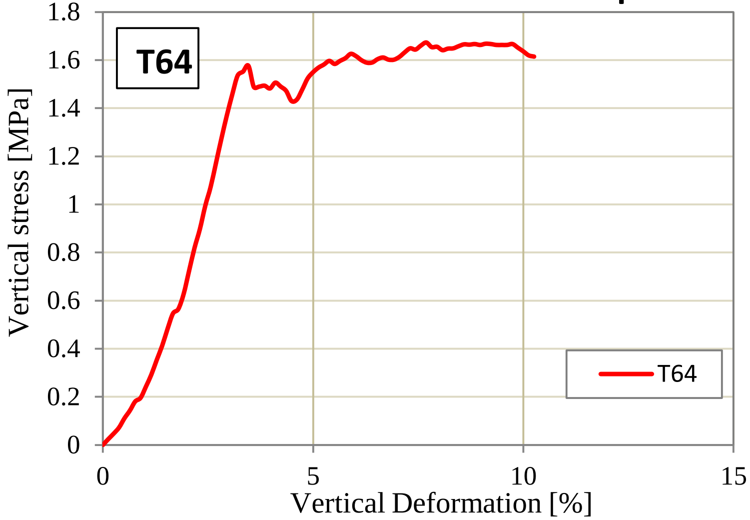

Post - gradation curve

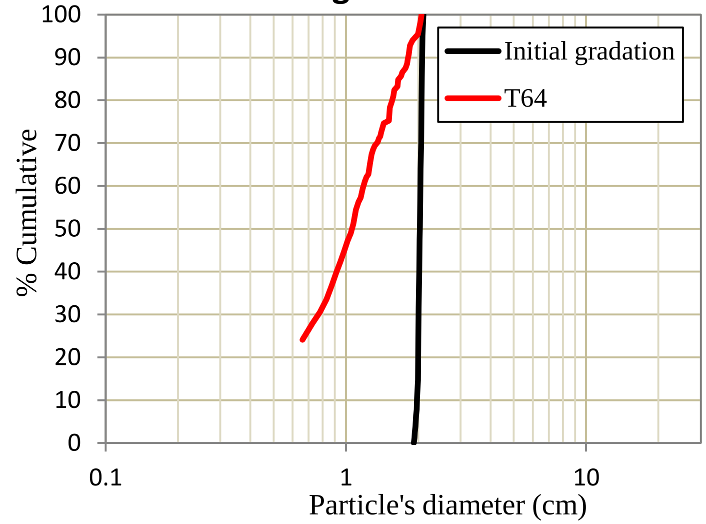

Plan view after testing

(Mould diameter = 10 cm)

Particles after testing

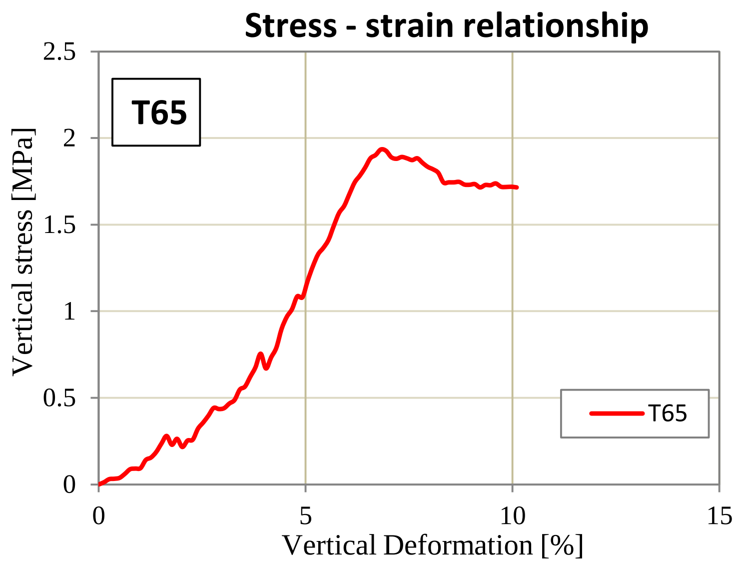

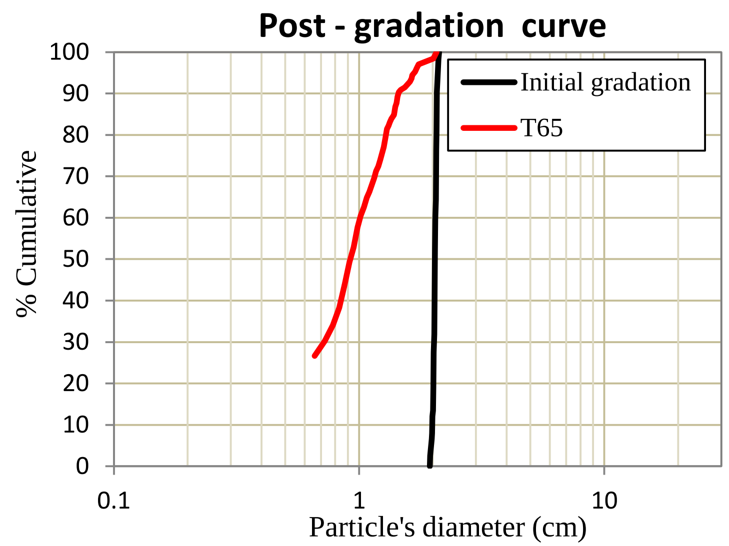

Plan view after testing

(Mould diameter = 10 cm)

Particles after testing

Stress-Strain curve

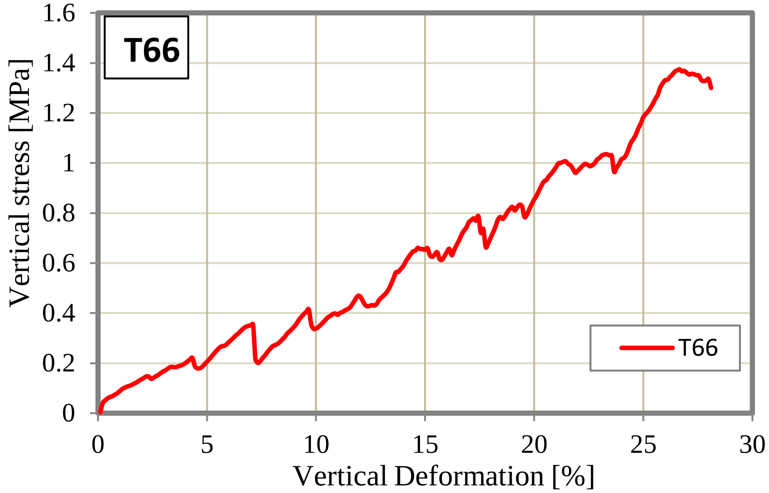

Post - gradation curve

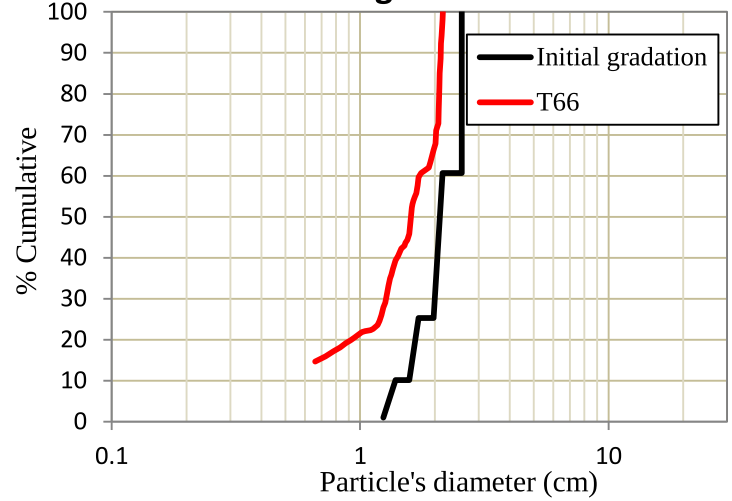

Plan view after testing

(Mould diameter = 10 cm)

Particles after testing

Stress - strain relationship

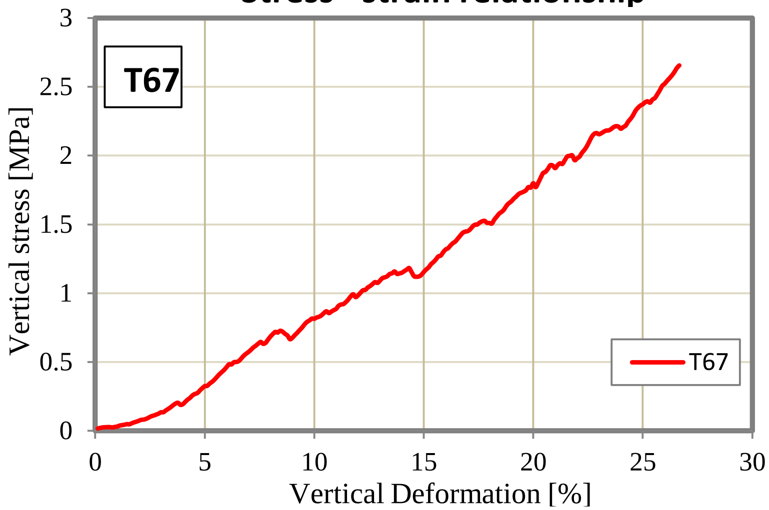

Post - gradation curve

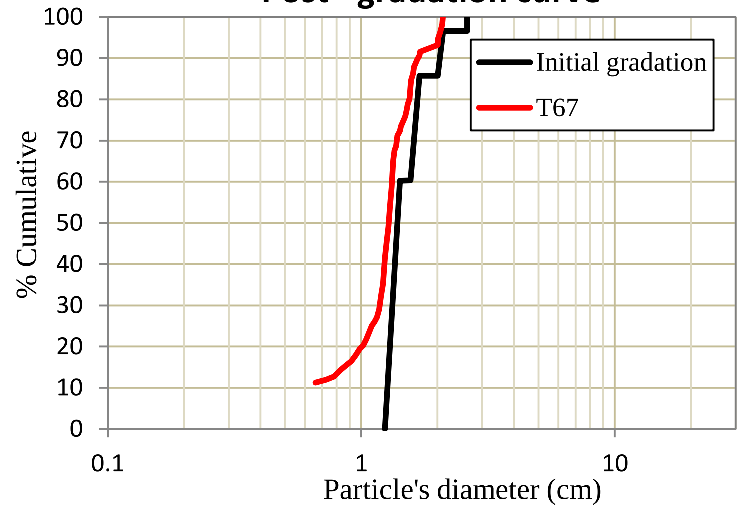

Plan view after testing

(Mould diameter = 10 cm)

Particles after testing

Stress - strain relationship

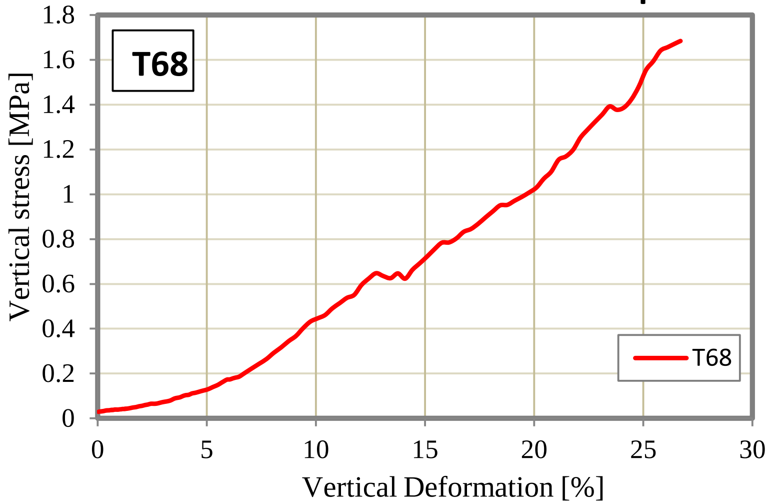

Post - gradation curve

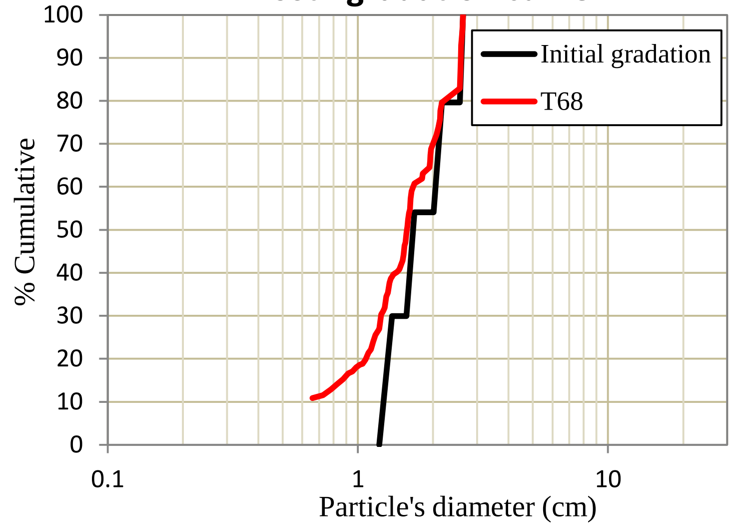

Plan view after testing

(Mould diameter = 10 cm)

Particles after testing

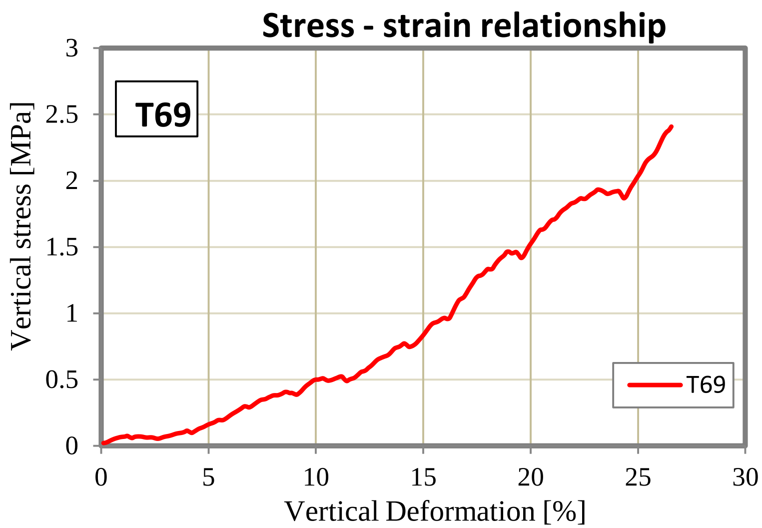

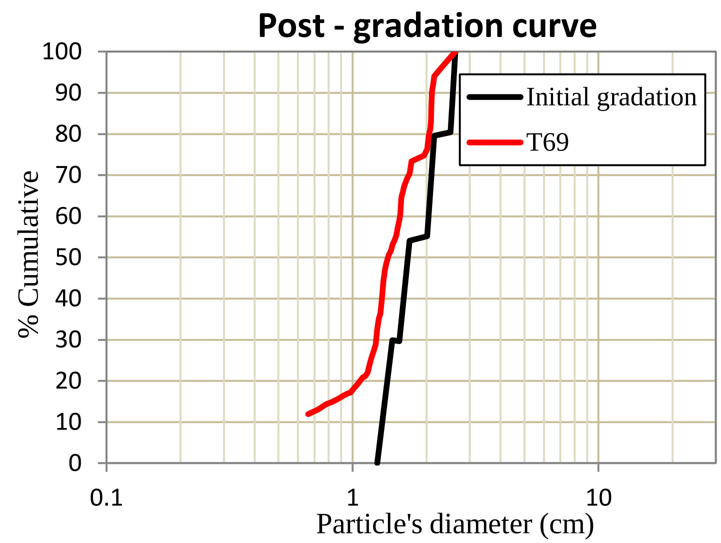

Plan view after testing

(Mould diameter = 10 cm)

Particles after testing

Stress - strain relationship

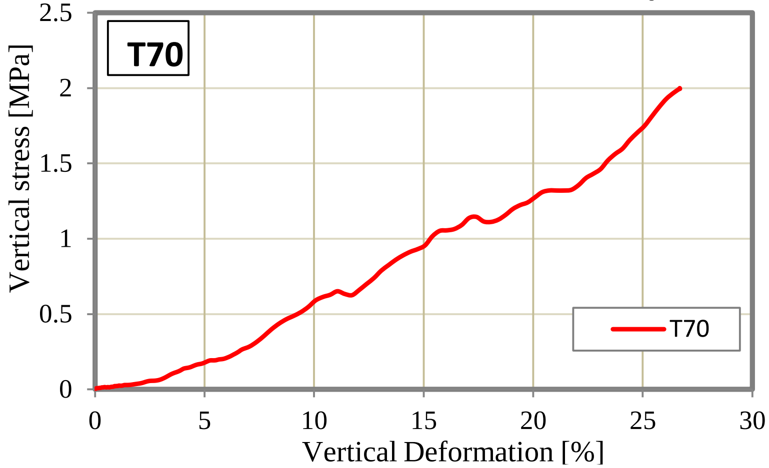

Post-gradation curve

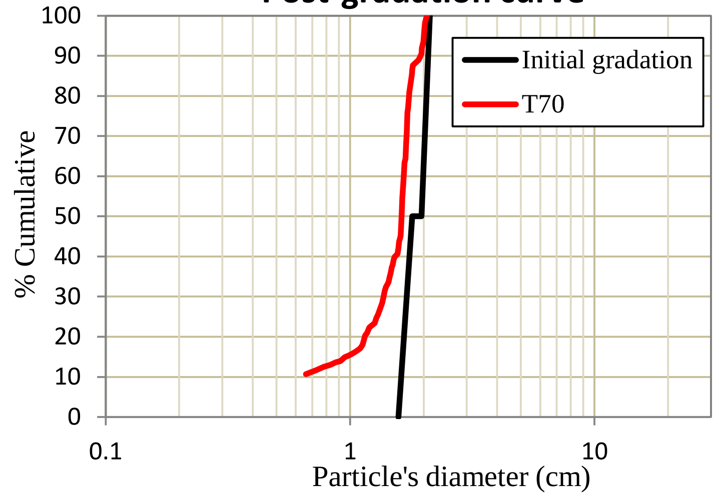

Plan view after testing

(Mould diameter = 10 cm)

Particles after testing

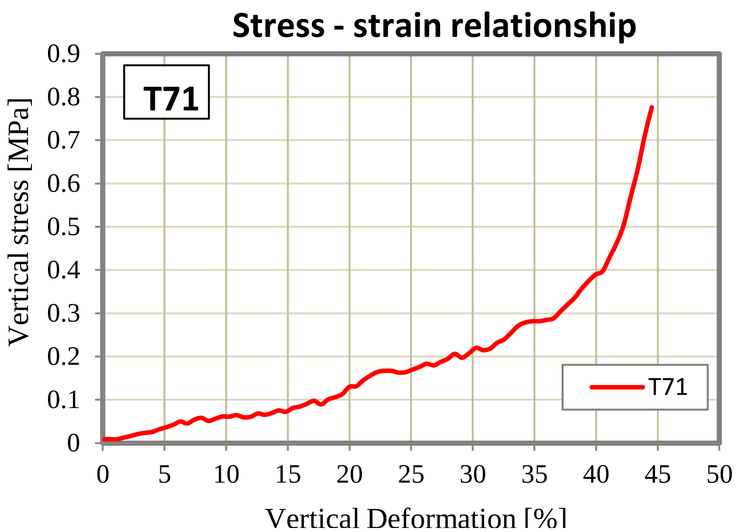
Stress - strain relationship
T71
Vertical stress [MPa]
Vertical Deformation [%]
0.9
0.8
0.7
0.6
0.5
0.4
0.3
0.2
0.1
0
0
5
10
15
20
25
30
35
40
45
50
T71

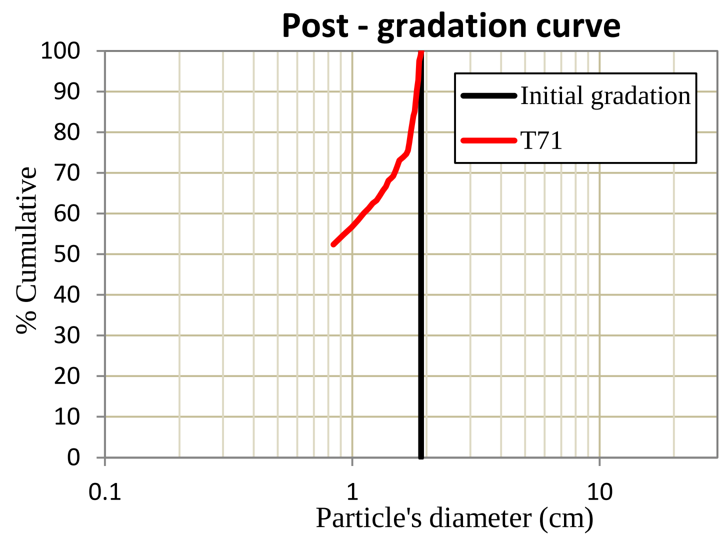
Post - gradation curve
% Cumulative
Particle's diameter (cm)
100
90
80
70
60
50
40
30
20
10
0
0.1
1
10
Initial gradation
T71

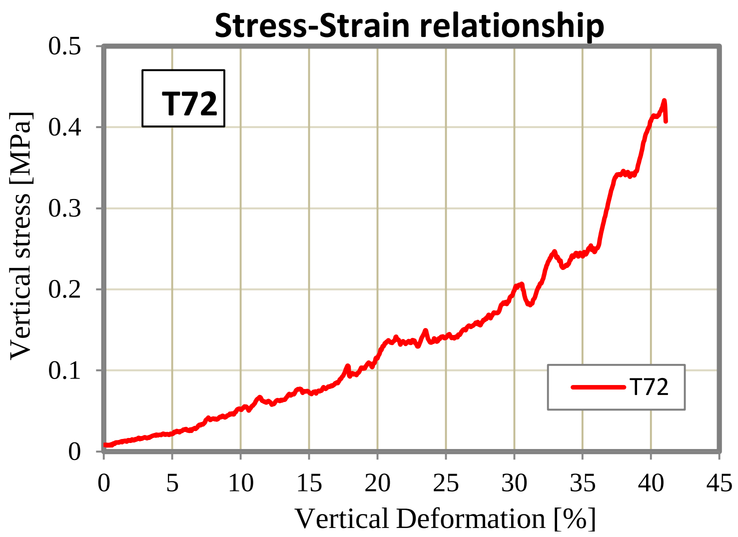
Stress-Strain relationship
T72
Vertical stress [MPa]
0.5
0.4
0.3
0.2
0.1
0
0
5
10
15
20
25
30
35
40
45
Vertical Deformation [%]
T72

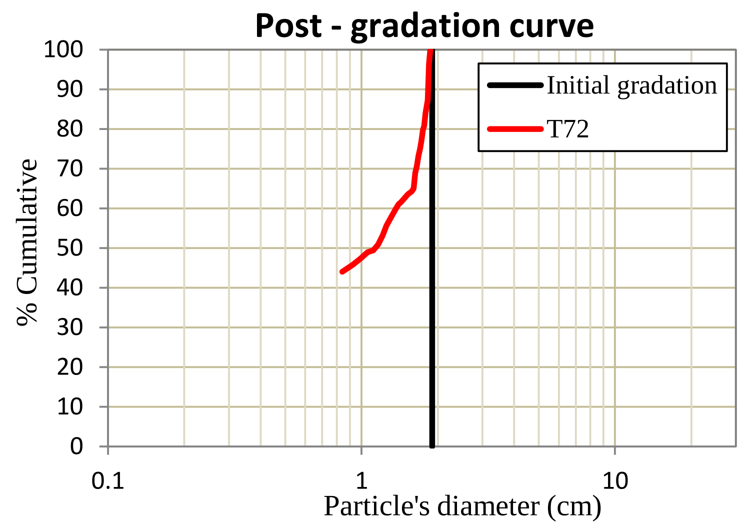
Post - gradation curve
% Cumulative
100
90
80
70
60
50
40
30
20
10
0
0.1
1
10
Particle's diameter (cm)
Initial gradation
T72

Stress - strain relationship

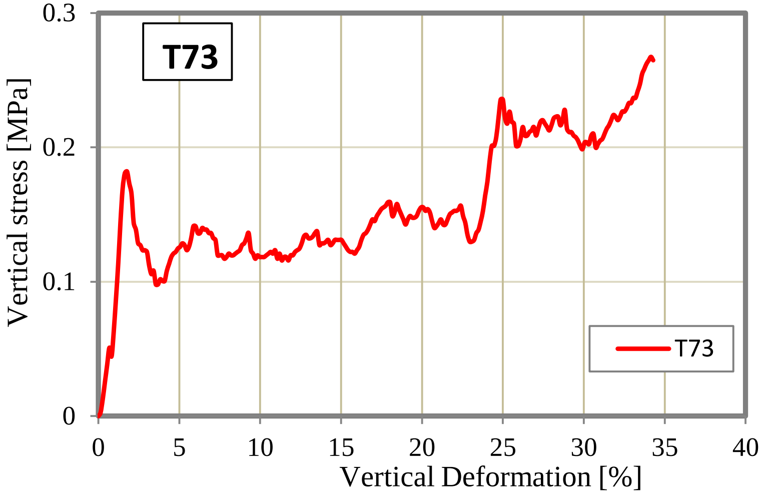

Post - gradation curve

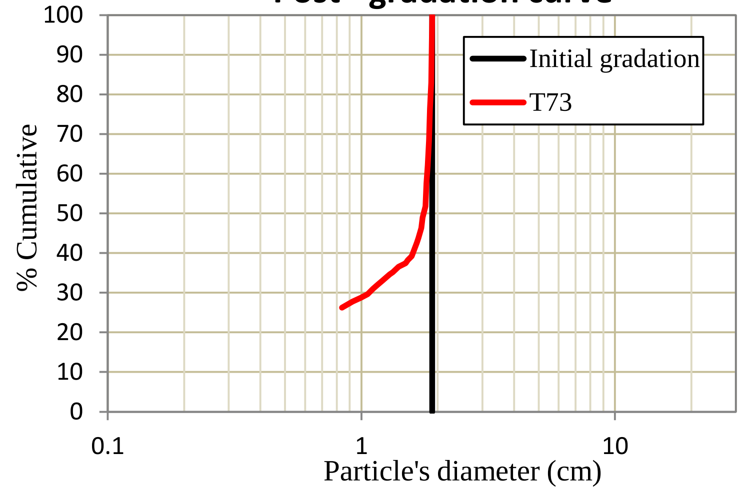

Plan view after testing

(Mould diameter = 10 cm)

Particles after testing

Stress - strain relationship

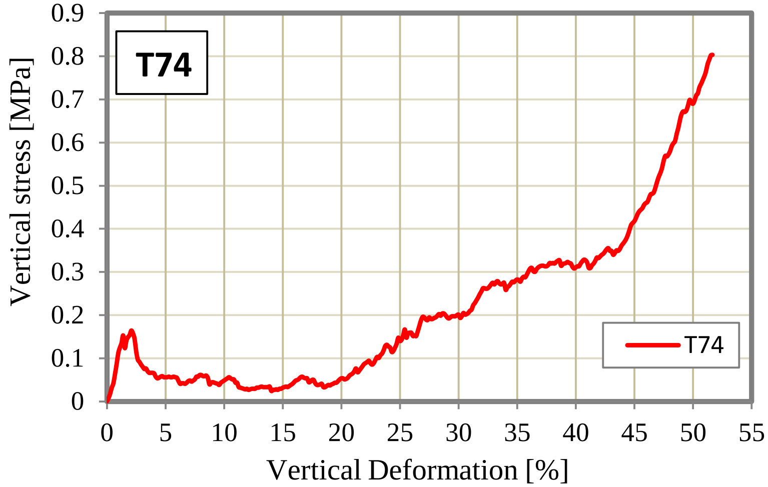

Post - gradation curve

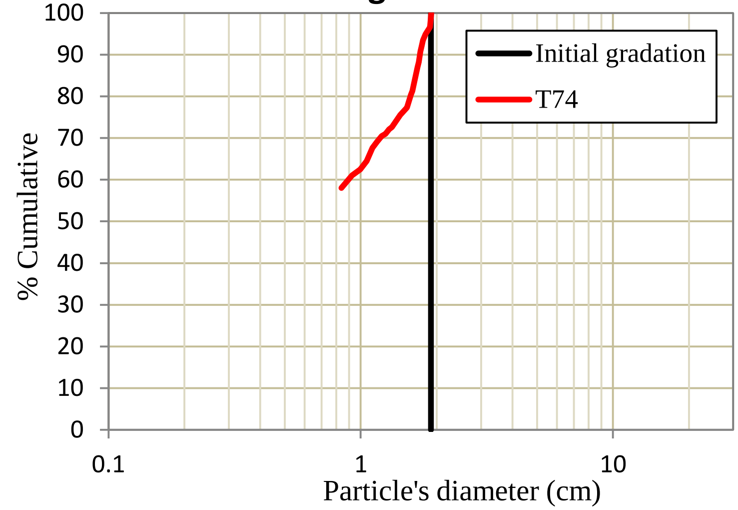

Plan view after testing

(Mould diameter = 10 cm)

Particles after testing